

Improving hand prosthesis control with advanced single-finger proportional decoding and robotic shared control

Présentée le 30 juin 2023

Faculté des sciences et techniques de l'ingénieur
Chaire Fondation Bertarelli en neuro-ingénierie translationnelle
Programme doctoral en génie électrique

pour l'obtention du grade de Docteur ès Sciences

par

Vincent Alexandre MENDEZ

Acceptée sur proposition du jury

Prof. S. Lacour, présidente du jury
Prof. S. Micera, directeur de thèse
Prof. K. Nazarpour, rapporteur
Prof. N. Thakor, rapporteur
Prof. M. Shoaran, rapporteuse

Acknowledgements

When I started my Ph.D. I didn't know what an adventure it would be. They were possibly the most stimulating years of my life, but also the toughest. As a freshly graduated master's student, I started with innocence, full of hope and motivation. I learned a tremendous amount during these 4 years, about my thesis subject of course but also about myself. I believe I am a more accomplished person than before, scientifically speaking as well as personally. The path was not always easy, I had to overcome doubts, losses of motivation and the feeling of being drowned in an ocean of tasks to prove to myself that I deserve to be where I am today. A great number of people played a role in the realization of this work, and I must thank them for helping me to get here.

Firstly, I would like to warmly thank Prof. Silvestro Micera; without him, nothing would have been possible. After my Master's thesis, he trusted me in my difficult beginnings to be accepted into a doctoral school, during these 4 years he reassured me when I saw no solutions to the problems I encountered and finally gave me the necessary independence to pursue my vision while guiding me throughout my thesis.

Then, I would like to thank Dr. Fiorenzo Artoni for his guidance starting from the master's thesis and still guiding me now, and for all the scientific discussions and paper sheets used to discuss new ideas.

I had the luck to arrive in a wonderful environment created and shaped by Prof. Silvestro Micera, the TNE lab. After all these years, I can say that the TNE lab is the best research environment I could have imagined. Many thanks to all the past and current brilliant and talented persons who shaped my Ph.D. journey. These people are not just colleagues anymore; they are also friends. I am also grateful to all the students I supervised at the TNE who helped me to explore new ideas throughout these 4 years.

A great part of this work would not have been possible without Prof. Aude Billard and her laboratory where I spent a substantial amount of time collaborating with the Ph.D. students there.

On a more personal note, I would like to thank my family for their unconditional support over the years, which has shaped me into the person I am today. There are also all my friends (from the lab and outside) who are an important part of my life. The time spent together was truly one of the main drives to keep my motivation until the end.

Finally, I would like to thank the president of my jury Prof. Stéphanie Lacour, as well as the experts Prof. Mahsa Shoaran, Prof. Nitish Thakor, and Prof. Kianoush Nazarpour for taking the time to review my thesis and for their insightful comments and inputs.

Abstract

Upper limb amputation significantly impacts daily activities and diminishes the quality of life for those affected. The aspiration to replace a lost hand with a functional substitute has deep historical roots. People have sought prosthetic limbs for aesthetic, professional, or personal independence purposes. Indeed, the hand is an essential part of the body and a powerful tool, and its loss can lead to significant physical and emotional challenges.

After hand loss, basic daily tasks can become challenging and people with upper limb amputation have limited options to regain some dexterity. Over the years, researchers have been working on creating robotic prosthetic hands (RPHs) that now match the size and weight of a human hand. Today, RPHs can execute single-finger movements and reproduce grasps used in most situations, as well as non-grasp-related motions. However, despite the growing complexity of these devices, the control strategy has remained the same, and RPHs continue to be seen as basic tools.

This thesis presents research on single-finger proportional control for RPHs, a strategy close to the natural way we control our hands. I investigate different aspects of EMG decoding using deep learning techniques and integrating such decoding with robotic automation to tackle the inherent limitations of surface EMG decoding.

I begin by presenting the existing solutions for patients with trans-radial amputation and describe EMG decoding in the framework of RPHs. Focusing specifically on the potential and existing limitations of their primary components, I also offer insights into the future development of various elements and the overall field of RPH advancement.

In the second chapter, I investigate the potential of deep learning for single-finger proportional control, characterize a new medium-density EMG system, explore EMG data augmentation using a generative adversarial network, and propose an easy-to-use real-time model calibration framework to bridge the gap between lab experiments and home-based applications.

Finally, I explore the advantages of implementing shared control approaches that combine proportional single-finger decoding and robotic automation to improve the control of RPHs. This includes the development of a compliant robotic controller to improve grasp robustness and an autonomous controller for in-hand object manipulation.

This thesis contributes to the improvement of RPH control with a biomimetic decoding approach, aiming to improve the intuitiveness, dexterity, and adoption of RPHs by individuals with trans-radial amputation by offering more accessible, effective, and user-friendly solutions.

Keywords: robotic prosthetic hand, EMG, deep learning, CNN, proportional control, shared control, robotic automation

Résumé

L'amputation d'un membre supérieur a un impact significatif sur les activités quotidiennes et diminue la qualité de vie des personnes concernées. L'aspiration à remplacer une main perdue par un substitut fonctionnel a des racines historiques profondes. Des personnes ont cherché à obtenir des prothèses à des fins esthétiques, professionnelles ou d'indépendance personnelle. En effet, la main est une partie essentielle du corps et un outil puissant, et sa perte peut entraîner des difficultés physiques et émotionnelles considérables.

Après la perte de la main, les tâches quotidiennes de base peuvent devenir difficiles et les personnes amputées d'un membre supérieur ont peu d'options pour retrouver une certaine dextérité. Au fil des années, les chercheurs ont travaillé à la création de prothèses de main robotisées (PMR) qui ont désormais la taille et le poids d'une main humaine. Aujourd'hui, les mains prothétiques robotisées peuvent exécuter les mouvements de chaque doigt indépendamment et reproduire les mouvements de préhension utilisés dans la plupart des situations, ainsi que des mouvements non liés à la préhension. Cependant, malgré la complexité croissante de ces dispositifs, la stratégie de contrôle est restée la même et les PMRs continuent d'être considérés comme des outils basiques.

Cette thèse présente une recherche sur le contrôle proportionnel de chaque doigt pour les PMRs, une stratégie proche de la manière naturelle dont nous contrôlons nos mains. J'étudie différents aspects du décodage EMG en utilisant des techniques d'apprentissage profond et en intégrant ce décodage à l'automatisation robotique pour s'attaquer aux limites inhérentes au décodage EMG de surface.

Je commence par présenter les solutions existantes pour les patients souffrant d'amputation transradiale et je décris le décodage EMG dans le cadre des PMRs. En me concentrant spécifiquement sur le potentiel et les limites actuelles de leurs principaux composants, j'offre également un aperçu du développement futur de divers éléments et du domaine général de l'avancement des PMRs.

Dans le deuxième chapitre, j'étudie le potentiel de l'apprentissage profond pour le contrôle proportionnel de chaque doigt, je caractérise un nouveau système EMG de densité moyenne, j'explore l'augmentation des données EMG à l'aide de réseaux antagonistes génératifs et je propose un cadre de calibration de modèle en temps réel facile à utiliser pour combler le fossé

entre les expériences de laboratoire et les applications à domicile.

Enfin, j’explore les avantages de la mise en œuvre d’approches de contrôle partagées qui combinent le décodage proportionnel de chaque doigt et l’automatisation robotique pour améliorer le contrôle des PMRs. Cela inclut le développement d’un contrôleur robotique pour améliorer la robustesse de la saisie et d’un contrôleur autonome pour la manipulation d’objets dans la main.

Cette thèse contribue à l’amélioration du contrôle des PMRs grâce à une approche de décodage biomimétique, visant à améliorer l’intuitivité, la dextérité et l’adoption des PMRs par les personnes souffrant d’amputation trans-radiale en offrant des solutions plus accessibles, plus efficaces et plus facile à utiliser.

Mots-Clés : main prothétique robotisée, EMG, apprentissage profond, CNN, contrôle proportionnel, contrôle partagé, automatisation robotique.

Contents

Acknowledgements	i
Abstract (English/Français)	iii
List of Figures	xi
List of Tables	xv
1 Introduction	1
1.0 Abstract	2
1.1 Introduction	2
1.2 Robotic Hands	3
1.2.1 Existing Robotic Prosthetic Hands	5
1.2.2 Perspectives	7
1.3 Interfaces with the Neuromuscular System	7
1.3.1 Taxonomy of Existing Interfaces	7
1.3.2 Perspectives	10
1.4 Motor Control	10
1.4.1 Decoding Algorithms	11
1.4.2 Shared Control to Help Motor Decoding	13
1.4.3 Decoding Motor Intention via Implanted Electrodes	14
1.4.4 Perspectives	15
1.5 Restoring Sensory Feedback	16
1.5.1 Sensors for Proprioception	16
1.5.2 Tactile Sensors	18
1.5.3 Sensory Architectures	18
1.5.4 Sensory Feedback	19
1.5.5 Perspectives	22
1.5.5.1 Embedded sensorization	22
1.5.5.2 Improved stimulation strategies	22
1.5.5.3 New computational architectures	23
1.6 Performance Assessment	23
1.7 Conclusion	28
1.8 References	29
	vii

2	EMG Decoding	43
2.1	Deep Learning with Convolutional Neural Network for Proportional Control of Finger Movements	43
2.1.0	Abstract	44
2.1.1	Introduction	44
2.1.2	Methods	45
2.1.3	Results	48
2.1.4	Discussion	49
2.1.4	Conclusion	50
2.1.5	References	50
2.2	A novel medium-density EMG system for prosthetic hand control	53
2.2.0	Abstract	54
2.2.1	Introduction	54
2.2.2	Methods	57
2.2.3	Results	61
2.2.4	Discussion	65
2.2.4	References	66
2.3	EMG Data Augmentation for Grasp Classification Using Generative Adversarial Networks	70
2.3.0	Abstract	71
2.3.1	Introduction	71
2.3.2	Methods	72
2.3.3	Results	73
2.3.4	Discussion	75
2.3.4	Conclusion	76
2.3.5	References	76
2.4	Optimizing setup and usability for potential home-based applications	78
2.4.1	Simple finger angle acquisition with markerless angle extraction	78
2.4.2	Transfer Learning to reduce calibration time	83
2.4.3	A framework to train deep models in real-time for wrist and finger proportional control	86
3	Shared Control	89
3.1	Robotic Automation to Improve Grasp Robustness	89
3.1.0	Abstract	90
3.1.1	Introduction	90
3.1.2	Results	91
3.1.3	Discussion	100
3.1.3	Methods	103
3.1.4	References	111
3.2	Robotic Automation to Perform In-Hand Object Manipulation	114
3.2.0	Abstract	115

3.2.1	Introduction	116
3.2.2	Methods	119
3.2.3	Results	129
3.2.4	Discussion	135
3.2.4	Conclusion	138
3.2.5	References	139
4	Future Perspectives for the Control of RPHs	141
4.1	EMG Decoding: Increase performance and reduce computational cost	141
4.2	Shared Control: Robotic automation for an improved tool or towards hand replacement?	143
4.3	Integration of a complete system for long-term use	144
5	General Conclusion	147
A	Supplementary Material	151
	Curriculum Vitae	177

List of Figures

Figure 1.1	Examples of functioning hand replacement.	4
Figure 1.2	A neural interface and the target area for somatosensory feedback.	20
Figure 1.3	Examples of available assessment tools.	26
Figure 2.1.1	Training paradigm difference between STD approach and Deep learning.	46
Figure 2.1.2	Illustration of the movements present in the EMG recordings.	46
Figure 2.1.3	Architecture of the best model.	48
Figure 2.1.4	Boxplots of the test loss over all sessions for the best model with RAW, FFT and STD conditions.	49
Figure 2.1.5	Barplot of the test loss per subject for the best model with RAW, FFT and STD conditions.	49
Figure 2.1.6	Plot of the predicted angles (orange) vs. target angles of the test set.	49
Figure 2.2.1	Picture of the MD-EMG system. It consists of 64 monopolar electrodes placed around the forearm of the subjects.	57
Figure 2.2.2	Model optimization pipeline.	58
Figure 2.2.3	Genetic Algorithm results.	62
Figure 2.2.4	Boxplot of the finger-averaged coefficient of determination (R^2) on the testing set obtained from models with the lowest validation loss.	62
Figure 2.2.5	Single-finger performance in each condition.	62
Figure 2.2.6	Virtual hand and predicted scaled finger angles on unseen data from a representative LD-EMG recording.	63
Figure 2.2.7	Virtual hand and predicted scaled finger angles on unseen data from a representative MD-EMG recording.	63
Figure 2.2.8	Finger-averaged R^2 between recording-specific model architecture (A) and the average of all other architectures (B).	64
Figure 2.2.9	Model architecture overview.	65
Figure 2.3.1	Distribution of features extracted from EMG signal (true) and synthetic data (generated) for one channel and all classes with the whole train set.	74
Figure 2.3.2	Two first components extracted from PCA on the EMG signal of one channel for all classes with the whole train set.	74

Figure 2.3.3	Boxplots of the accuracy obtained for the three conditions with (A) one repetition of the movements, (B) two repetitions and (C) the whole train set.	74
Figure 2.3.4	Evolution of the accuracy with respect to the number of samples used during training for the three conditions with (A) one repetition of the movements, (B) two repetitions and (C) the whole train set.	75
Figure 2.3.5	(Left) Evolution of the accuracy with respect to the number of samples used during training for the three conditions with all channels on the whole train set. (Right) Boxplots of the accuracy obtained for the three conditions Generated and combined accuracy values are obtained with the optimal amount of generated data.	75
Figure 2.4.1	illustration of the wrist and finger angles obtained from MediaPipe.	80
Figure 2.4.2	(Left) Position of IMUs to extract the wrist pronation/supination and flexion/extension angles. (Right) Normalized angles extracted from IMUs and MediaPipe.	80
Figure 2.4.3	Plot of the predicted finger angles from EMG signals (Blue) vs. target angles obtained from MediaPipe (orange) on the test set.	82
Figure 2.4.4	Plot of the predicted wrist angles from EMG signals (Blue) vs. target angles obtained from MediaPipe (orange) on the test set.	83
Figure 2.4.5	Illustration of the task performed by the subjects with the robotic hand.	84
Figure 2.4.6	Mean coefficient of determination (R^2) obtained for each of the degrees of freedom decoded.	84
Figure 2.4.7	Architecture of the real-time training framework.	87
Figure 3.1.1	Experimental Setup and Subjects.	92
Figure 3.1.2	Analysis of online prediction performance of the MLP.	94
Figure 3.1.3	Shared control in virtual environment, setup and results.	95
Figure 3.1.4	Shared Control results in virtual environment cont'd.	97
Figure 3.1.5	Shared control in physical environment, setup and results.	99
Figure 3.1.6	EMG analysis with and without shared control.	102
Figure 3.2.1	List of shared control conditions.	118
Figure 3.2.2	An example of tracking target angle in the first experiment.	119
Figure 3.2.3	Overview of the experimental setup.	120
Figure 3.2.4	An example of one experiment run.	123
Figure 3.2.5	Summary of the experimental protocol.	124

Figure 3.2.6	Block diagram of robot hand control with state machines of the (shoulder) EMG-robot interface.	126
Figure 3.2.7	Performance of two shoulder decoders with the robotic hand fixed.	129
Figure 3.2.8	Average EMG validation loss during calibration of the finger decoder across subjects (N = 8), throughout the three experimental sessions	130
Figure 3.2.9	Virtual hand and predicted scaled joint flexion on the validation set of a representative recording for fingers and shoulder.	131
Figure 3.2.10	All collected data from all 8 participants.	132
Figure 3.2.11	Performance progress of all subjects and all control conditions over 3 sessions (3 days).	133
Figure 3.2.12	Performance of all shared controller conditions across all subjects and sessions.	134
Figure 3.2.13	Median completion time (left) and mean failed attempts (right) for each pair of sub-tasks and shared control condition.	135

List of Tables

Table 1.1	Maternity levels of different technologies.	8
Table 1.2	Sensor types and encoding strategies used in milestone publications on bidirectional hand prostheses.	17
Table 1.3	Clinical assessments for transradial amputees using robotic prosthetic hands.	24
Table 2.4.1	Result of the robotic hand task.	85
Table 2.4.2	Result of the robotic hand task with the real-time framework after 3 minutes and 30 seconds of data acquisition	87

1 Introduction

This thesis explores different ways to enhance the control of robotic prosthetic hands (RPHs). To provide a comprehensive context, the following literature review aims at giving the reader a broader overview of the field synthesizing the different aspects related to improving RPHs and situating the control dimension within a larger, overarching challenge.

The content of this chapter is the postprint from the article Mendez, Iberite et al., “Current Solutions and Future Trends for Robotic Prosthetic Hands.” Published in *Annual Reviews of Control, Robotics, and Autonomous Systems*, 2021, pp. 595–627.

Find the published article here: <https://doi.org/10.1146/annurev-control-071020-104336>

Personal contributions as co-first author: Writing different chapters as well as designing the related figures and tables.

Current Solutions and Future Trends for Robotic Prosthetic Hands

Vincent Mendez,^{1,*} Francesco Iberite,^{2,*} Solaiman Shokur,^{1,†} and Silvestro Micera^{1,2,†}

¹Center for Neuroprosthetics and Institute of Bioengineering, École Polytechnique Fédérale de Lausanne, 1202 Genève, Switzerland; email: silvestro.micera@epfl.ch

²BioRobotics Institute and Department of Excellence in Robotics and AI, Scuola Superiore Sant'Anna, 56127 Pisa, Italy

*These authors contributed equally to this article

†These authors contributed equally to this article

Keywords

hand, prosthesis, neuroprostheses, sensory feedback, electromyography, EMG

Abstract

The desire for functional replacement of a missing hand is an ancient one. Historically, humans have replaced a missing limb with a prosthesis for cosmetic, vocational, or personal autonomy reasons. The hand is a powerful tool, and its loss causes severe physical and often mental debilitation. Technological advancements have allowed the development of increasingly effective artificial hands, which can improve the quality of life of people who suffered a hand amputation. Here, we review the state of the art of robotic prosthetic hands (RPHs), with particular attention to the potential and current limits of their main building blocks: the hand itself, approaches to decoding voluntary commands and controlling the hand, and systems and methods for providing sensory feedback to the user. We also briefly describe existing approaches to characterizing the performance of subjects using RPHs for grasping tasks and provide perspectives on the future of different components and the overall field of RPH development.

1. INTRODUCTION

Decades of research on robotic prosthetic hands (RPHs) have led to a paradoxical situation: On the one hand, the development of novel RPHs is among the most exciting fields of robotics (Piazza 2019), but on the other hand, the vast majority of amputee patients still use technologies that have changed little in almost half a century. However, this apparent discrepancy might seem less surprising when considering the immense challenge of developing a prosthetic that can mimic the functions of a hand. Indeed, the hand has one of the largest sensory representations in the brain, and grasping is among the most complex coordination tasks (1); the hand has both the highest density of mechanoreceptors in the human body (see the sidebar titled Skin Mechanoreceptors) and the largest number of degrees of freedom (DOFs); and the hand permits people to both experience the surrounding world and shape it.

The skin has four types of mechanoreceptors, which are sensitive to different stimuli and therefore involved in different sensory functions: Merkel disks (which sense skin indentation, fine touch, and texture perception), Ruffini capsules (which sense skin stretch), Pacinian corpuscles (which sense vibration), and Meissner corpuscles (which sense dynamic deformation and slipperiness). Merkel disks and Ruffini capsules are slow-adapting receptors, meaning that they fire continuously during tactile stimuli, with a firing rate related to the pressure applied in their receptive field. Pacinian corpuscles and Meissner corpuscles are fast-adapting receptors that respond mostly to changes in applied pressure or brief stimuli.

The challenges are multiple and intricate, and they can be overcome only by combining advanced mechatronic solutions for dexterous and highly sensorized robotic hands with new approaches for robust and effective interfaces with users' nervous systems to allow seamless natural-artificial integration. As such, several viable solutions can emerge from this multidimensional optimization problem.

Tremendous efforts have been made in the past 20 years on the quest for an RPH that is easy to wear, comfortable, and intuitive to control. The design of such a device can be considered a compromise among dexterity, robustness, and usability (2). In the past 5 years, another aspect has been proposed by researchers as an essential milestone: sensorization. Indeed, feedback systems can increase both the acceptability and the performance of the new generation of RPHs (3–5).

This review summarizes the main achievements in this field. In particular, after providing an overview of the existing neuroprostheses and their characteristics, we focus on four central aspects: (a) stable interfaces that enable a new connection with the nervous system to record neural signals and stimulate neural structures, (b) algorithmic strategies for decoding motor intentions, (c) RPH sensorization plus encoding strategies to convey somatosensory feedback, and (d) assessment methods to measure the efficacy of a given strategy or technology. Throughout the review, we keep a patient-centered perspective and ask ourselves, Does a novel approach significantly improve the subjects' quality of life? Is it easy to learn and natural to use? And does it improve their independence? On a technical aspect, our goal is to provide a critical view of the most advanced technologies and a perspective on future implementations of RPHs.

2. ROBOTIC HANDS

Following a limb amputation, three solutions are generally considered: passive cosmetic limbs (**Figure 1a**); mechanical hands, often with hooks (**Figure 1b**); and RPHs (**Figure 1c–g**). In a survey of below-elbow amputees from Sweden, the United Kingdom, and Canada (6), 53% of the respondents wore a cosmetic prosthesis, 13% used a hook, 4% used a cable hand, and 30% used a myoelectric RPH. Despite encouraging results in the late 1990s (7), hand transplantation (**Figure 1h**) encountered significant surgical and clinical difficulties (rejection

and immunosuppression); it has therefore been tested in only a few patients and is not yet considered one of the available options.



Figure 1 Examples of functioning hand replacement. (a) A personalized cosmetic hand solution (ITOP, Italy) provides a natural look. Photos reproduced with permission from ITOP and Procosil. (b) A body-powered prosthetic solution (Ottobock, Germany) is a common approach for people with an upper-limb amputation. Photo reproduced with permission from Ottobock. (c) An sEMG-based pattern recognition system (Gen2, Coapt, USA) allows grasp classification. Photo reproduced with courtesy of Coapt LLC, www.coaptengineering.com. (d) sEMG control and extracellular stimulation via an implanted FINE were used to convey sensory feedback for home-use applications. The implant was stable for more than five years, and home-use electrical stimulation for sensory feedback was investigated for up to 13 days (115). Pannel adapted from reference 115 (CC BY-SA 4.0). (e) Fully implanted myoelectric sensors provide stronger and more reliable signals that do not change with arm positioning, socket rotation, or sweating (106). Pannel adapted with permission from reference (106). (f) Six-DOF prosthetic hand control (i-Limb Ultra, Össur, Iceland) uses threshold-based sEMG control and cocontraction to switch between grasps. (g) Sensory feedback conveyed via intraneural TIMEs enables the encoding of objects' shape and stiffness (5). Pannel reproduced with permission © 2014 Lifehand 2 / Patrizia Tocci. (h) Hand transplantation is a promising technique which has not yet become a standard procedure due to several surgical and clinical difficulties. Pannel adapted with permission from reference (Bernardon et al. 2015).

Abbreviations: DOF, degree of freedom; FINE, flat interface nerve electrode; RPNI, regenerative peripheral nerve interface; sEMG, surface electromyography; TIME, transverse intrafascicular multichannel electrode.

The cosmetic solution is often used for the most distal amputations (e.g., fingers) but is not adapted for patients with a transradial amputation given the dramatic loss of functionality. Body-powered mechanical hooks, mainly with one-DOF control, are popular solutions thanks to their low price, light weight, and easy maintenance. This type of prosthesis is also well suited for high-intensity work due to the control robustness. Also, because the subject must move their shoulder to open and close the hook, these systems have inherent proprioception feedback (8). However, one of the major limitations of the hook solution is the low level of dexterity and nonanthropomorphic appearance. Body-powered hands have solved the anthropomorphic aspect while keeping the robustness of body-powered solutions (9). For example, Baril et al. (10) developed a programmable body-powered hand that can perform different grasp types using a mechanical selector that blocks the closing of one or more fingers. Nevertheless, this solution has its drawback as well: Because of their low mechanical efficiency, body-powered prostheses require large amounts of energy (from 33 N for a hook to 131 N for a hand) to produce a relatively low pinch force (15 N) (11). This could explain their high rejection rate by patients, which ranges between 16% and 66% depending on the survey and time period (12).

Here, we concentrate on RPHs because they potentially offer the most versatile, natural, and power-efficient replacement for amputated hands and could become the default solution for patients. We investigate the challenges in existing RPHs, considering both commercially available solutions (**Supplemental Table 1**) and those in the research phase (**Supplemental Table 2**).

Mimicking the biomechanics of a hand is not easy. Early prototypes (13) succeeded in designing fingers with skeleton-like structures, but biomimetic actuation was only recently properly implemented using muscle-like actuators (14). The challenge for RPH developers is to embed actuators, sensors, and electronic components into a prosthesis with the same size and weight as the replaced hand (13, 15, 16). Major system integration and miniaturization is necessary before these systems could be used by amputee patients.

Instead, underactuation is a widespread approach to simplify the mechanics while keeping reasonable dexterity. An underactuated system is one where the number of degrees of actuation (DOAs) is smaller than the number of DOFs (see $DOA/DOF < 1$ in **Supplemental Tables 1** and **2**). The passive (nonactuated) DOFs are exploited to adapt to the surface in contact, as suggested by the concept of morphological computation (17), and to enable a self-adjusting grip without the need to control each articulation. These systems reduce the number of motors needed in the RPH and therefore its complexity, weight, and price.

2.1 Existing RPHs

Numerous commercially available RPH solutions use underactuated mechanisms (**Supplemental Table 1**), including the Michelangelo prosthetic hand (Ottobock, Germany), the i-Limb Ultra (Össur, Iceland), the bebionic hand (Ottobock), and the VINCENTevolution 3 (Vincent Systems, Germany). Despite remarkable advances, there is still arguably a trade-off

between dexterity and weight in these solutions, with companies usually emphasizing one aspect or the other.

Many research groups are currently working on innovative solutions to tackle the dexterity/weight dilemma (18), such as the use of a monolithic 3D-printed soft material (19) or mechanical solutions to implement finger synergies via clutches (20). For example, Jing et al. (18) proposed an anthropomorphic RPH using only three motors that could achieve 13 grasp types while weighing only approximately 130 g.

The price of RPHs is an additional limiting factor for broader adoption by patients. With most advanced solutions costing \$10,000–20,000, many researchers advocate for cheaper solutions, particularly for emerging countries (e.g., 21).

Open source RPHs are an exciting alternative to dramatically reduce the cost of development and distribution. One particularly interesting aspect of such hands is simplified maintenance and repairs (using, e.g., 3D printing) that do not rely on specific suppliers. For example, Open Bionics (United Kingdom) commercializes solutions for transradial amputees (e.g., the medically certified Hero Arm) but also provides the source files for some of their designs, and e-NABLE (<https://enablingthefuture.org>) reports 8,000 recipients of their prosthetics, which were built by volunteers around the world. Open source RPHs also enable users to alter the design to meet their unique needs; for example, the Galileo Hand (22) allows easy customization of the types of movements and number of electromyography (EMG) electrodes.

Researchers are also working on better mechanical solutions to improve RPH dexterity. An underactuated hand prosthesis designed by Abayasiri et al. (23) has finger abduction and adduction to enable it to grasp larger objects, and an adaptive prosthetic hand designed by Yong et al. (24) adds DOFs in the palm with movable metacarpals. The Karlsruhe Institute of Technology (KIT) prosthetic hand (25) has an embedded camera and real-time object recognition, enabling the hand to be preshaped. Pneumatic artificial muscle (26) permits the development of light, compact solutions. Finally, biomimetic actuation is used for muscle-like actuators (14).

In addition to the hardware aspect, there are also innovations in RPH control and sensorization. Low-level controllers use information about the state of the device and eventually activate the actuation to meet the desired state imposed by the user's intentions. The choice of the state variable has a strong influence on how the device works. Position or speed can be read through encoders of each joint and controlled; these are straightforward approaches that have been used broadly in robotic applications. When the interaction of the hand with the external environment is of interest, more advanced control systems are implemented, such as torque or impedance control. Both approaches measure the force applied by the actuator, controlling it directly in the first case and simulating compliance in the second. Advanced control strategies enable complex manipulation and smoother gestures at the expense of a bulkier mechanical structure and a more complex control system. Therefore, enabling more sophisticated control requires integrated force and position sensors, which have been previously developed mainly to close the robotic control loop (27).

In summary, low-cost and light hands have flourished over the last few years. The race to simplify designs and reduce costs through 3D printing should not impact the dexterity of RPHs. For now, underactuated mechanisms are the best solution for RPHs and innovative designs based on synergy mechanisms or friction, the latter of which can help increase the number of DOAs without increasing the number of motors.

2.2. Perspectives

While rigid architectures are still the norm, there has been recent interest in the development of flexible systems that inherently permit safe robot–human interaction (28). Instead of using a rigid structure with mechanical joints, the compliant structures in soft designs enable them to bend continuously in any part. Since seminal work by Hirose & Ma (29), there have been several attempts to develop soft underactuated hand prostheses (30) and soft body-powered devices (8). These architectures combine the advantages of simple actuation with the performance of an adaptable hand. Recent studies have proved that soft manipulators could match the performance of rigid systems in many applications (31). Further investigations are necessary to determine whether soft architectures are viable solutions for larger use.

Innovative actuations systems such as McKibben pneumatic muscles, granular jamming (32), and electro-conjugate fluid (33), which are strongly tied to soft robotic devices, are another interesting direction. Soft RPHs have the advantage of exploiting the structure to embed and eventually improve sensorization, safety, and efficiency (e.g., 34). These systems are at the early stage and need massive integration before being deployed in portable devices.

3. INTERFACES WITH THE NEUROMUSCULAR SYSTEM

Decades of work on robotic prosthetics have led to numerous invasive and noninvasive solutions for interfacing with the body (for a review, see Yoshida 2017) (**Table 1**). Here, we describe existing technologies and outline the ones we consider the most promising for the future.

3.1 Taxonomy of the existing interfaces

To classify and evaluate the quality of an interface, selectivity—defined as the ability to record from a specific location within the nerve—is the most straightforward metric. Both spatial and temporal selectivity are important, naturally, as they enable better motor decoding and more localized sensory feedback. Electrode invasiveness, by contrast, is categorized into two large classes, surface electrodes and implanted electrodes, the latter of which includes extraneural (i.e., around the nerve) (35, 36), intraneural (i.e., through the nerve) (5), and regenerative approaches (where the nerve regrows inside the electrode) (37; for reviews, see 38, 39). Invasiveness is often seen as a trade-off to selectivity, with the observation that higher selectivity comes at the cost of greater invasiveness (40). While this relationship continues to be true to a large extent, two amendments are necessary: First, there are a multitude of other

dimensions to consider, and second, recent results are suggesting that the relationship might not be the same in the motor and the sensory domains. We detail both aspects here.

Table 1 Maturity levels of different technologies

Technology	Most widespread	Mature, home use	Cutting edge, laboratory use	Future directions
Interface	Body harness ^c	sEMG ^a iEMG (50) ^a Vibrotactile interface (176) ^b TENS ^b FINEs (135) ^b Osseointegration (137) ^c	HD-sEMG (177) ^a Regenerative electrodes (37) ^a TIMEs (5, 41) ^b LIFEs (42) ^b Sieve electrodes (178) ^b Utah Array (112) ^c	Noninvasive intraneural stimulation (ultrasound) ^b Soft neurotechnology (47) ^b
Motor decoding	Body power Threshold-based sEMG	EMG-based pattern recognition (e.g., Ottobock Myo Plus, Coapt Gen2)	Simultaneous single-finger classification (74) Linear regression and shared control (78)	Advanced control using regenerative peripheral nerve interfaces (37) Deep learning for single-finger proportional control
Sensory feedback	No feedback	Vibrotactile haptic feedback (128) Touch contact (137) Position (135)	Neuromorphic (61) Texture (60) Object stiffness (5) Multimodal (position and tactile) (63) Biomimetic stimulation (61)	Temperature feedback Proprioception
Sensorization	No skin	Force sensors (measuring motor current) Sensorized fingertips (e.g., bebionic)	Asynchronously coded electronic skin (124)	Soft embedded sensors (114) Bioinspired flexible organic artificial afferent nerve (121)

Abbreviations: EMG, electromyography; FINE, flat interface nerve electrode; HD-sEMG, high-density surface electromyography; iEMG, intramuscular EMG; LIFE, longitudinal intrafascicular electrode; sEMG, surface electromyography; TENS, transcutaneous electrical nerve stimulation; TIME; transverse intrafascicular multichannel electrode.

^aMotor interface.

^bSensory interface.

^cBoth motor and sensory interface.

Beyond the selectivity of an interface, it is crucial to consider its reach and level of discrimination. For example, transverse intrafascicular multichannel electrodes (TIMEs) (41) and longitudinal intrafascicular electrodes (LIFEs) (42) can have a very similar selectivity, but TIMEs reach a more substantial proportion of the nerve and therefore can infer more information about the whole signal. Comparing muscle stimulation with different electrodes,

Badia et al. (43) showed that a TIME could target three muscles, whereas they could not activate more than one muscle with a LIFE. Spatial discrimination of neural signals from nontarget signals is influenced not only by the electrode's invasiveness (how close it is to the source) but also by its geometry (e.g., a spherical point source targets a small volume), electrode material, and configuration (e.g., a cylindrical electrode better discriminates the axons perpendicular to the main axis) (44).

Signal quality and stability are also important aspects that have been extensively studied. Work in this area has included interventions to improve the device–tissue interfaces [e.g., electrode coating (45) or a hollow glass cone that permits the ingrowth of cortical neurites in the electrodes (46)], electrode impedance, and filtering processes to increase the signal-to-noise ratio. The recording stability depends on biocompatibility, the electrode's robustness (resistance to physical manipulation), and the stability of the contact between the interface and neural tissue. Significant efforts toward soft and implantable electrodes (47) have been made in order to reduce insertion trauma and physical mismatches between neural tissues and implantable interfaces. Finally, properly anchoring the electrodes with the neural tissues is also essential to maintain a steady recording or stimulation site over time. This is particularly important in the sensory domain, where the stability of the elicited sensation is paramount for continuous use.

Finally, practicalities such as the cost of the technology and the difficulty of the implant must be considered. As such, an implantation procedure based on a known surgical procedure (48) has a better chance to be accepted and adopted by surgeons. The use of existing devices, materials, and mature technologies is also a way to reduce costs and risks. An example of such strategy is the use of Utah Arrays, which use well-established electrodes for brain recording, to interface with the peripheral nervous system.

For motor decoding, surface EMG (sEMG) approaches are by far the most widely used technique to date. Recent implementations using a large number of electrodes [termed high-density sEMG (HD-sEMG) (49)] have shown unprecedented results in term of accuracy and decoding robustness (for details, see Section 4). Implanted EMG (iEMG) has shown higher performance and stability than sEMG on the continuous control of three DOFs (50). However, studies have found no statistical difference in different electrodes' ability to differentiate among 12 types of grasps (51). Neural interfaces with the peripheral nerves have also shown promising results on grasp classification with TIMEs (52) and proportional control with a Utah Slanted Electrode Array (53). However, the development of real-time control and sensory feedback stimulation is still at an early stage (52, 53) and will need further investigation.

In the sensory domain, there is no current consensus for noninvasive approaches. Tactile feedback using vibrotactile (54, 55), mechanotactile (56), or sensory substitution [e.g., audio (57)] has been proposed. Transcutaneous electrical nerve stimulation (TENS) is a viable noninvasive approach to induce close to natural sensation with amputee patients (58, 59). However, as detailed elsewhere in this review, current solutions using implanted electrodes (particularly intraneural interfaces) have shown levels of sensory recovery far superior to those of noninvasive approaches. This is true from a functional point of view [e.g., the

possibility to encode texture (60) or shapes and stiffness (5)], phenomenologically [patients perceive the feedback as close to natural (61)], and in terms of cognitive load (62).

3.2. Perspectives

The challenges for future interfaces that can provide the necessary read/write bandwidth to use RPHs in a natural fashion are immense. We argue that the motor and sensory domains raise different problems. Indeed, the stimulation being close to the target is mandatory with current technologies, and therefore the best solutions are the most invasive ones. In the motor domain, it is possible to decompose the signal if we have enough sources (even noninvasive sources, as with sEMG). As shown in Section 4, machine learning techniques can help infer information from noninvasive interfaces.

On the sensory level, the currently implantable electrodes are the most promising solution. However, the main advancement so far has been for the tactile modality, while the use of other modalities for proprioception has been obtained via a nonhomologous approach based on intraneural stimulation combined with the delivery of homologous tactile feedback via indirectly targeted intraneural electrical stimulation (63).

Temperature sensation is another limit. Temperature is mediated through A δ fibers (for cold) and C fibers (for warmth). Given the very small size of these fibers (C fibers are 20–100 times smaller than A β fibers), it is not possible to target them using existing state-of-the-art electrodes (41). Future electrodes with even higher levels of selectivity might be able to target A δ and C fibers. Sensory remapping (64) can be another viable solution to simulate temperature feedback on a different part of the body using a temperature display.

4. MOTOR CONTROL

Despite the advances in techniques for voluntary motor decoding and the increased sophistication of the available RPHs, body-powered prostheses are still the most robust control approach. The mechanism of these devices is based on a cable actuated by movements of the shoulder to control one DOF. The vast majority of commercially available RPHs use simple threshold-based sEMG decoding over a few surface electrodes and also generally control one DOF (65); in some cases, the RPH provides more DOFs, but this comes at the cost of a nonintuitive command scheme. These systems also offer no possibility to control several DOFs at the same time. The current situation is, therefore, increasingly sophisticated RPH mechanics with unchanged control strategies. As such, patients often abandon myoelectric prostheses, in part because the small functional improvement does not justify their price and complexity (12, 66).

Here, we describe recent advances in control strategies in terms of decoding type (classification or continuous control) and functional achievement (e.g., number of DOFs, grasping, or single-finger decoding) and compare them with the classical direct control approach. Section 4.1 details different algorithmic approaches to decode motor functions,

with an emphasis on sEMG; Section 4.2 discusses the addition of robotic automation to improve grasp robustness; Section 4.3 compares implanted methods to extract the user's intentions; and finally, Section 4.4 presents a perspective on the broader adoption of these techniques by patients. **Table 1** includes the different decoding strategies and their level of maturity.

4.1. Decoding Algorithms

The clinical standard for RPH control is based on the use of two sEMG channels, with the electrodes placed superficially on antagonist muscles. The envelope of the signal is extracted so that the user can control the closing and opening of the RPH by modulating the amplitude of their muscle contraction. When the amplitude exceeds a certain threshold, the RPH will move depending on which muscle was activated. Companies are offering more DOFs, using cocontraction to cycle through different types of grasps (e.g., Ottobock's Michelangelo hand). However, this type of control is highly nonintuitive and gives only low dexterity to the user. An alternative to this direct control approach is based on pattern recognition methods, extracting hand-crafted features to characterize the signal in a discriminative way (e.g., the signal root mean square, wavelength, and zero crossing) and classify the type of grasp intended by the user. This solution has become robust enough to reach the market (the Coapt system and Ottobock's Myo Plus). Using 2–12 bipolar sEMG electrodes makes it possible to obtain good classification rates for different kinds of grasps, with 90–95% accuracy for 4–12 classes and up to 75% for 50 classes (67–71).

Using a similar electrode disposition and classification method, other groups showed the possibility of decoding single-finger movement using the classification of flexion or extension (72, 73). Recently, Bhagwat & Mukherji (74) showed single- and multifinger classification of 15 different movements with 99.79% accuracy. Researchers are also working on proportional control instead of classification, which makes it possible to decode several DOFs (e.g., wrist and finger movements) simultaneously and proportionally (75, 76). This type of control offers continuous position control. Several studies have also shown that single-finger proportional control is feasible, with good results (77, 78).

As an alternative, nonbiomimetic EMG decoders have been developed that rely on the subject learning inverse maps to relate motor outputs to arbitrary control variables (79). Using an abstract decoding cursor control space, subjects can learn to modulate their EMG activity to reach different targets arranged in a center-out task in order to trigger various grasping movements (80). Dyson et al. (81) recently validated these results on amputee participants; they showed that after training, the difficulty of the tasks could be increased, improving the possibilities for robotic hand control.

With only a few electrodes placed on muscles of interest, the accurate positioning of the electrodes requires anatomical knowledge; indeed, the type of amputation (congenital or traumatic), the surgical procedure, and the time since amputation (82) could influence the muscle anatomy and make the placement of the electrode tedious and specific to individual subjects. Moreover, a small shift in electrode placement can disrupt the pattern recognition

algorithm (83). To tackle these issues, several authors have proposed HD-sEMG as an alternative solution, which consists of a grid of closely spaced electrodes. The large number of electrodes allows information to be recorded from a large part of the subject's forearm.

HD-sEMG signals offer high spatial resolution, and recorded signals can be interpreted as spatial images of EMG activity. Using this image representation of EMG data, HD-sEMG is robust to small electrode shifts (84). Boschmann & Platzner (84) used a structural similarity index, borrowed from the computer vision field, on HD-sEMG images combined with a simple one-against-one nearest-neighbor classifier to decode wrist and hand motions. Similarly, Stango et al. (85) used a variogram of images (a measure of the degree of spatial correlation, used mainly in geostatistics) to classify wrist movements. Both groups showed that their methods, which use spatial information from the images, performed better or similarly to the classic feature extraction approach. Moreover, their strategies improved the robustness to electrode shift and electrode number. The use of several spatially close electrodes makes it possible to decompose the EMG signal into its constituent motor unit action potential (49, 86). Kapelner et al. (87) investigated this approach, decomposing EMG signals to extract motor unit activity from forearm muscles during wrist motions. Recently, Dai & Hu (88) showed that an approach consisting of finger joint angle estimation, combining classification for finger selection with EMG decomposition into motor unit activity, outperforms a standard amplitude-based approach.

We observe a paradigm shift from feature engineering to feature learning using raw data as input for deep neural networks. Studies have shown that combining this deep learning approach with HD-sEMG offers better performance than hand-crafted features in both grasp classification (89) and simultaneous single-finger and wrist movement classification (90). Deep learning has also shown good results with a smaller number of electrodes for grasp classification (71) and regression of arm or wrist motions (91, 92).

This approach permits both high dexterity and robustness, with unprecedented performance. However, one of the major difficulties of the deep learning approach is that it requires an extensive data set for training. For example, the deep learning used for the ImageNet challenge in 2012 used 1.2 million images for training on 1,000 categories (93). In the context of hand gesture recognition, generating tens of thousands of examples for a subject is not a viable option.

A possible solution could use domain adaptation [often called transfer learning in the EMG literature (94, 95)], by leveraging data acquired from several subjects to enhance and accelerate training for a new user. Indeed, the aim is to use information from a database of several source domains and adapt it to a target domain (the end user) with a small number of samples. Authors generally apply deep domain adaptation (domain adaptation combined with deep learning) by pretraining a deep neural network and fine-tuning it with a few repetitions of movements by a target subject. The main idea is that gathering the recordings of several participants can meet the necessary conditions to learn a general mapping of all users' sEMG signals.

Using this idea, Côté-Allard et al. (96) showed that their deep model was able to learn the features and significantly enhance the performance of deep networks on out-of-sample gestures. Using HD-sEMG and deep learning, Du et al. (97) also showed an unsupervised deep domain adaptation method that incrementally learns from data during a new session without explicit calibration of gestures. Consequently, deep learning offers a particularly attractive context from which to develop deep domain adaptation algorithms to leverage interuser data. This approach can increase decoding performance, improve robustness to electrode shift, and reduce the number of repetitions needed during training (98).

As seen in this section, the search for new EMG decoding algorithms that go beyond threshold-based detection is an active field of research. Phinyomark & Scheme (99) and Khamparia & Singh (100) have reviewed recent research in EMG pattern recognition methods.

Machine learning in the field of computer vision and object recognition has shown outstanding results using deep learning and is already used commercially by many companies. Some deep learning algorithms based on a pretrained network are now usable without any fine-tuning (e.g., self-driving cars). However, bio-signals are intrinsically different from images and need adaptation. More important, the amount of labeled EMG data available to effectively train deep networks might not be sufficient to capture the evolution of the signal over time (electrode displacement, skin impedance changes, etc.). Therefore, if model architectures and data processing are tailored for bio-signal applications and take into consideration signal evolution with time, deep learning can become a solution for more robust motor intention decoding.

4.2. Shared Control to Help Motor Decoding

The ultimate goal of RPH control is to be as close as possible to controlling a natural hand. Therefore, an ideal control needs to be intuitive and continuous over individual fingers and wrist movements. Increasing the number of DOFs and developing proportional control will increase dexterity for prosthesis users but will inevitably reduce the overall robustness of the decoder. Since reliability is one of the main factors for upper-limb prosthesis users (101), this is a significant issue for the commercialization of more dexterous control schemes.

One possible solution to improve decoding robustness is to add robotic automation of some portion of the motor command. Shared-control strategies between a subject and a smart robotic hand have been reported for automated preshaping and grasping (102), grip force adjustment (103), slip detection, and hand closing (104). In the context of single-finger proportional control, Zhuang et al. (78) proposed a shared-control strategy to increase grasp robustness (avoiding accidental drops), by maximizing the number of contacts between the RPH and an object while allowing the user to maintain full autonomy over decisions about grasping and releasing, grasp preshaping, and non-grasp-related motions. These strategies allow both freedom during single-finger control and robustness during a grasp event (78) and can perform more dexterous movements that cannot be decoded based on EMG alone. However, they necessitate many DOAs (e.g., active control of each phalanx to reposition the

fingers around an object), which is still a significant challenge in terms of motor miniaturization, power consumption, and cost.

4.3. Decoding Motor Intention via Implanted Electrodes

Surface electrodes cannot precisely record the signal from deep muscles; to overcome this issue, several groups have focused on iEMG electrodes. This technique is more invasive but allows one to record EMG signals (50) uncorrelated from the underlying musculature and avoids the daily placement of electrodes. iEMG is robust against electrode shift (e.g., socket rotation) and change in skin impedance and sweat. Several studies have demonstrated the performance of simultaneous wrist and hand motions (three DOFs) using six to eight iEMG electrodes; Smith & Hargrove (50) showed that iEMG has better decoding performance than sEMG. High decoding performance is reported in real time (105), and in fully implanted setups, the results are stable for several days (106).

On the other hand, Farrell & Weir (51) compared the pattern recognition-based grasp classification performance of iEMG and sEMG on 12 movement classes with eight channels and did not find a statistical difference between electrode types. They concluded that the choice of electrode should be based not on classification accuracy but rather on signal consistency over time and robustness to electrode lift-off. Zia ur Rehman et al. (107) compared a standard linear discriminant analysis with a deep network for grasp classification. They performed a multiday analysis comparing six iEMG and six sEMG electrodes, and their results showed that deep learning had better decoding performance and was more stable over time.

Kamavuako et al. (108) investigated the effect of combining iEMG to target deep muscles with sEMG on myoelectric control. They showed that the combined solution improved offline and real-time control performance compared with sEMG alone.

With 32 iEMG electrodes, Dantas et al. (109) compared different decoding methods for the continuous control of five DOFs corresponding to the flexion and extension of each digit. Using a data set aggregation algorithm, they showed a normalized mean squared error as low as 0.033 with a deep convolutional neural network. They also investigated signal stability during 150 days after training, showing a small degradation during the first month (0.003 normalized mean squared error per day with a convolutional neural network), but that degradation stopped in the next four months.

For transradial amputees, an alternative to using EMG signals to control hand prostheses is decoding from peripheral nerve signals. Different grasp types can be decoded from peripheral nerve signals with high accuracy using different interfaces, both offline and in real time (53, 110–112). Implanted peripheral nerve recordings are more invasive than sEMG but are more stable over time. Indeed, donning and doffing the prosthesis does not move these electrodes as much as it does sEMG electrodes. Recently, Cracchiolo et al. (52) decoded up to 11 class states using TIMEs on an amputee subject and showed that the active sites chosen on the first day could also be used in the following sessions, for up to seven days (80% accuracy, compared with 83% by selecting active sites every session). However, this modality is generally

used to provide sensory feedback (63, 113–115). Therefore the development of new approaches to record neural signals during peripheral stimulation [e.g., artifact removal (116)] is necessary.

Vu et al. (37) recently developed a regenerative peripheral nerve interface to increase signal specificity and long-term stability. They implanted transected peripheral nerves into a free muscle graft. After regeneration, revascularization, and reinnervation, the graft becomes a nerve bioamplifier that creates EMG signals. Using chronically implanted iEMG to record from these grafts, they performed five-class decoding in real-time with up to 98.2% accuracy with two transradial amputees in a virtual hand environment. They also showed results from a Box and Block Test using a robotic hand prosthesis that provided continuous control of two DOFs of thumb motions through their interface combined with a third DOF based on sEMG.

4.4. Perspectives

Motor decoding for RPHs is progressing in two main directions: Noninvasive approaches have seen advances in decoding algorithms using large data sets and increases in the number of recording points, and implanted electrodes (either muscular or intraneural) have seen improvements that enable better recording stability and more robust decoding. There is currently no consensus on which approach is best for transradial amputee patients, as they each have their own strengths and limitations. The need for daily signal and classification recalibration is a weak point of the classic sEMG approach, which is being addressed by several research groups developing, for example, HD-sEMG. And despite iEMG's promising control performance, which is robust to donning and doffing of the prosthesis, its overall performance gain, when compared with sEMG, may not currently be sufficient to justify an invasive surgery. The same reasoning can be applied to intraneural electrodes.

One can imagine a future where both invasive and noninvasive approaches will continue to progress and will target either patients who prefer a stable decoding setup or those who do not want to undergo surgery and will accept the need to calibrate their prosthesis on a regular basis (117). Another scenario can be a parallel development of invasive technologies for both sensory and motor functions. Indeed, as shown in Section 5, the approach using intraneural implanted electrodes has permitted unprecedented levels of somatosensory restoration; it might, therefore, be reasonable to perform a single surgery to restore both motor and sensory functions. For this reason, motor decoding using the intraneural interface can become a viable solution if these interfaces one day permit both providing sensory feedback and recording discriminative signals for motor decoding in parallel, but online artifact removal remains an important challenge.

Power consumption is another critical issue: RPHs should embed small electronics because the size of the prosthesis limits the space available for batteries, but doing so usually comes at the cost of limited processing resources. Also, the electronics for the HD-sEMG remain cumbersome due to the large number of input channels and should be miniaturized and portable. Moreover, decoding model complexity is also limited by portable processing resources. In practice, an increased number of electrodes is already available in wearable

systems (Sessantaquattro, OT Bioelettronica, Italy) and may become available for prostheses in the future.

Finally, low latency is paramount for seamless prosthesis control [<300 ms between user intention and real-time decoding (118)]. Among the studies discussed above, only a few performed analyses to show the feasibility of real-time control (without processing resource limitations), and even fewer included embedded electronics that would translate for home use. One possible solution for real-time decoding with complex models is to bypass embedded electronic limitations; this could be achieved by taking advantage of the computational power of cell phones or by relying on cloud computing and the next generations of wireless cellular networks for low-latency communication.

5. RESTORING SENSORY FEEDBACK

Sensory information plays a critical role in both the exploration of the external environment and in any manipulation task. When an individual interacts with surrounding objects, tactile sensations are used to infer features such as size, compliance, temperature, and texture, while the same sensations are exploited to handle them properly or use them as tools. From this perspective, aiming to restore afferent sensory channels from a hand prosthesis is a critical step in designing a device that ensures two key aspects: dexterous manipulation and embodiment of the prosthetic device.








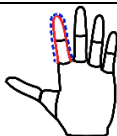

The design of a sensory feedback system that can successfully deliver information relies on three fundamental blocks working together: (a) sensor readings, processed by (b) an encoding strategy capable of translating meaningful information to the user, through (c) an interface. Previous sections have described the different available interfaces; here, we present the encoding techniques and sensors relevant to the design of modern hand prostheses (**Table 1**).


Sensors mounted on a robotic hand should ideally record the whole spectrum of available human sensations, from both external and internal sources. Indeed, sensory information from the human hand covers both interactions with the external world (tactile perception, thermal perception, and nociception, i.e., perception of pain) and internal perception of the positions of the joints and the length and forces exerted by the muscles, together known as proprioception. **Table 2** shows examples of sensor placements on RPHs from recent studies.

5.1. Sensors for Proprioception

Proprioception is not only fundamental for a dexterous hand prosthesis, enabling vision-free manipulation and multitasking, but is also the key to a properly embodied device (63). Usually, kinematic parameters of the robotic hand and (when available) the force exerted are needed to implement low-level control of the actuators, so they are measured with well-established systems, such as rotary encoders or the motor's current draw.

Table 2 Sensor types and encoding strategies used in milestone publications on bidirectional hand prostheses

Reference	RPH model	Mechanical stimulation encoding	Electrical stimulation encoding			Interface	Sensor distribution ^a
			Frequency	Amplitude	Pulse width		
3	Passive	Linear	—	—	—	G10 tactor	
5	IH2 Azzurra	—	Fixed	Linear	Fixed	TIME	
59	IH2 Azzurra	—	Fixed	Fixed	Linear	TENS	
61	IH2 Azzurra	—	Model based	Model based	Fixed	TIME	
36	SensorHand Speed	—	Linear	Fixed	Time variant	FINE	
60	IH2 Azzurra	—	Neuromorphic	Fixed	Fixed	TIME	
128	Various	Discrete events	—	—	—	Vibrators	
135	VariPlus Speed	—	Linear	Fixed	Fixed	FINE	
58	bebionic	—	Neuromorphic	Fixed	Neuromorphic	TENS	
63	IH2 Azzurra	—	Fixed	Fixed	Linear	TIME	
138	DEKA Luke	—	Model based	Fixed	Fixed	Utah Slanted Electrode Array	

137	SensorHand Speed	—	Linear	Fixed	Fixed	Cuff electrode	
-----	---------------------	---	--------	-------	-------	-------------------	---

Abbreviations: FINE, flat interface nerve electrode; RPH, robotic prosthetic hand; TENS, transcutaneous electrical nerve stimulation; TIME; transverse intrafascicular multichannel electrode.

^aThe positions of the pressure sensors are shown in green, the joints where force is measured are shown with solid red lines, and the joints where the position is read are shown with blue dashed lines.

5.2. Tactile Sensors

Despite improvements in sensor miniaturization, computational power, and knowledge of the neurophysiology of somatosensation (tactile sensation and proprioception), the capabilities of sensorized RPHs remain far from those of a natural hand. Overcoming this limitation will require satisfying three conditions: The sensors must match the skin's sensing ability, a sufficient number of sensors must be embedded on the surface of the hand, and it must be possible to reliably read information from them. The first condition can be addressed with current technology, as the resolution of existing force and pressure sensors already matches human skin performance (119). However, fulfilling the second and third conditions is another matter, and we need to push the boundaries of circuit integration in order to create an RPH with many sensors and a way to communicate with them.

The classical solution of using general-purpose sensors developed separately from the signal conditioning circuit and the subsequent signal processing has shown its limit. Instead, efforts are being made to optimize these devices with prosthetics in mind. For example, borrowing the concept of morphological computation from robotics (120), sensors can be optimized for specific tasks by tuning the features of their mechanical structures accordingly. Indeed, exploiting the low-pass filtering effect of a compliant material or surfaces with specific structures can increase texture discrimination (60, 114). Another example comes from Kim et al. (121), who measured forces using sensors embedded in a soft substrate.

5.3. Sensory Architectures

The problem of handling many sensors at the same time has been addressed successfully in the past by using time-sharing (multiplexing) and space-sharing (matrix arrangement) techniques, minimizing wiring complexity while keeping read latency in an acceptable range. Nevertheless, this approach does not scale well in terms of covering the whole hand with a sensor density comparable to that of the human hand. Additionally, the unavoidable increase in the number of electrical connections makes the system highly susceptible to breakage.

Event-based architectures rely on the concept of send-on-delta (122), where each sensor (comprising an analog front end and an analog-to-digital converter), instead of signaling its value at a constant rate, does so only when the value changes by more than a certain threshold. These architectures have many advantages owing to the sparsity of the data

representation. In other words, the communication line does not need to be capable of handling all the sensors simultaneously (as an interaction where all the sensor are triggered in the same moment is unlikely); instead, single sensors are polled at a high rate, which preserves the time structure of the stimulus.

The underlying idea of event-based systems is inspired by how neurons communicate information to each other, sending a train of spikes instead of continuous value. In earlier implementations, data flowed from sensors to the central unit through digital communication lines using well-known protocols such as Universal Asynchronous Transmitter Receiver (UART), Ethernet, and the Controller Area Network (CAN) bus. Some groups have designed communication paradigms by mimicking information encoding by the nerves; using pulses of 20 ns, Bartolozzi et al. (123) showed a 94% improvement in data rate over traditional protocols.

An even more advanced step was made in the work of Lee et al. (124), where the sensors communicate with spikes through the same conductive surface without any flow control, reducing the wires needed to two (data and ground). In this way, at the cost of a decoding stage for sensor value acquisition, the performance of the architecture increased, reaching up to 100,000 sensors sharing the same bus.

5.4. Sensory Feedback

In basic myoelectric or body-powered prostheses, feedback is delivered mainly by visually inspecting the movements of the prosthesis and by the physical interaction between the device and the user (125), as with hook prostheses. Clearly, the goal of a modern, robotic hand prosthesis is to deliver richer information more intuitively.

Sensory feedback strategies are characterized by their precision and the coherence between the evoked sensation and the desired one in terms of timing (synchronicity), position (somatotopy) and modality (i.e., touch, vibration, and temperature). Feedback techniques encode sensor values to stimulation parameters, which in turn are strongly tied to the chosen stimulation interface (**Table 2**). Here, we focus mainly on electrical interfaces for feedback, but we also briefly discuss the mechanical interfaces.

Noninvasive feedback strategies are attractive approaches since they do not necessitate surgical interventions (**Figure 2a**). Starting with the Boston Arm, which Mann & Reimers (126) used to demonstrate that position feedback was needed for precise reaching movements, these techniques have improved in both mechanical and electrical interfaces with the user. Indeed, the intact mechanoreceptors in the skin of the arm can be stimulated with small linear (127) or vibrating (128) motors that vary in their driving amplitude and frequency. On the other hand, mechanical stimulation brings an unavoidable delay of approximately 400 ms in the delivery of the sensation (129), and the integration and miniaturization of mechanoreceptors are challenging. The miniaturization of noninvasive feedback approaches is also challenging.

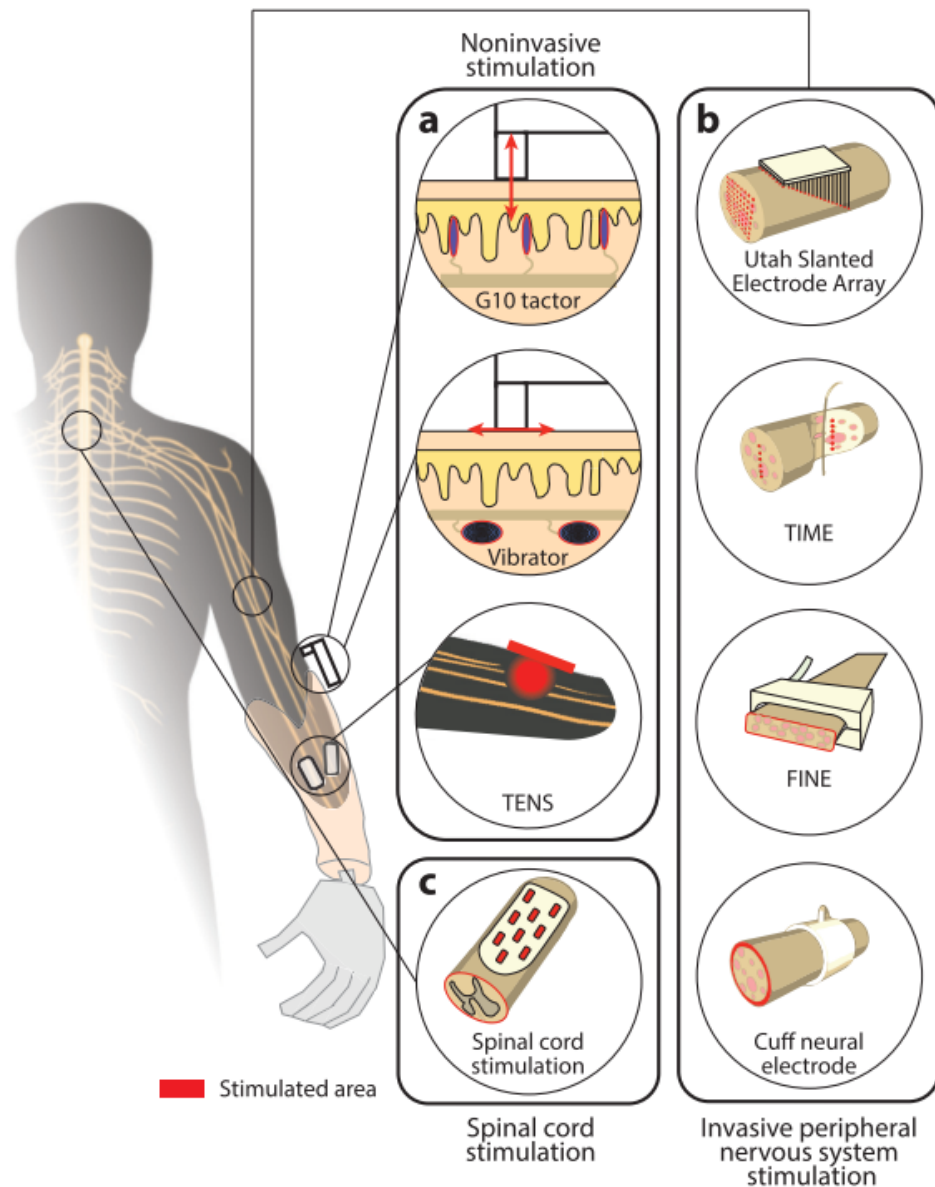


Figure 2 A neural interface and the target area for somatosensory feedback. (a) Noninvasive strategies include tactors targeting Meissner corpuscles and encoding pressure (3), vibrators that activate Pacinian corpuscle mechanoreceptors (128), and TENS (58), which targets the nerve noninvasively. (b) Invasive peripheral nervous system stimulation can be done with cuff electrodes (137) or FINEs (36, 135) that stimulate the nerve from outside the fiber. TIMEs (5, 59, 60, 63, 179) and Utah Slanted Electrode Arrays (180) are more invasive and are inserted through the nerve but stimulate directly from inside the fiber. (c) Epidural stimulation of the lateral spinal cord at the cervical level was able to induce tactile sensation in three upper-arm amputees (139). Abbreviations: FINE, flat interface nerve electrode; TENS, transcutaneous electrical nerve stimulation; TIME, transverse intrafascicular multichannel electrode. Nerve design from panels (a) and (b) adapted with permission from reference (41).

Electrical stimulation is usually delivered as train pulses, of which width, amplitude, and frequency can be independently modulated and can be conveyed noninvasively through the skin; this technique is generally known as electrotactile feedback (130). Single electrotactile electrodes can be assembled in bands and arrays (131) for targeting multiple sites at the same time, encoding information in both the position and amplitude of the stimulation. The main drawbacks of electrotactile stimulation are the dependence of sensory thresholds on the stimulation position (130), which forces a calibration after each mounting, and the artifacts induced in EMG readings, which strongly impair its application in closed-loop RPHs.

Electrocutaneous stimulation tries to overcome electrotactile limitations by implanting subdermally thin electrodes. Geng et al. (132) characterized the sensations evoked and highlighted improvements in the detection threshold, the threshold of noticeable differences, and the general pleasantness compared with traditional electrotactile feedback. Electrocutaneous stimulation still has technical issues in real-world implementations, such as interference with EMG readings and variability in stimulation parameters over time (133), which impair long-term applications.

Feedback through neural electrodes is a promising modality that matches how sensory information is transmitted in the nervous system (**Figure 2b**). These electrodes are implemented at both the cortical (134) and peripheral levels. Here, we focus on techniques targeting the peripheral nervous system.

The three controlled parameters are the frequency, amplitude, and pulse width; the most straightforward approach is proportional modulation according to sensor readings. Studies have shown that this method can be successful even in long-term implants (113, 135–137) and confirmed the improvements brought by sensory feedback through peripheral nervous system interfaces in both performance and embodiment.

Compared with noninvasive approaches, invasive neural stimulation has the advantage of being able to elicit sensations intuitive for the user, as they are delivered through the expected biological route (the peripheral nervous system) for sensory feedback. The focus in this field is currently shifting from basic feedback to evoking complex and natural sensations, feeding high-level features such as texture (60), and in general exploiting the potential of stimulating the nerves directly. Noninvasive feedback strategies are limited in the spatial precision of the evoked sensation in both mechanical and electrical stimulation (59).

The naturalness and information content of the stimulation can be improved by modulating with patterns that go beyond a simple relation with the sensor value. George et al. (138) devised two biomimetic stimulation patterns: one that is proportional to the first derivative of the force and another that is proportional to the aggregated tactile nerve response. Both approaches outperformed standard modulation techniques and were felt to be more informative by the user. Valle et al. (61) started from a model of the response to the touch of human afferent fibers and modulated frequency and amplitude according to a simulated fire rate and fiber recruitment; at the cost of a small reduction in sensitivity, the user reported a consistent increase in the naturalness of the sensation together with an increase in dexterity during functional evaluations. Both of these studies highlighted that the

goal is not only to elicit precise sensations but also to focus on naturalness and intuitiveness. Neuromorphic stimulation patterns have also proven to be rich in information not only about tactile contact but also about the sliding speed and texture of an object (114).

Considering the complex surgical procedure and the effort needed to develop a peripheral nervous system interface, techniques based on spinal cord stimulation are promising, as they rely on devices that have already been tested and approved by the US Food and Drug Administration. Chandrasekaran et al. (139) recently demonstrated a sensory neuroprosthetic for amputee subjects with spinal cord stimulation (**Figure 2c**). The main issue with this approach is the difficulty of eliciting natural sensations; biomimetic stimulation approaches could help address this limitation in the future.

5.5. Perspectives

We believe that sensorization will play a significant role in the next generation of RPHs. Here, we discuss three main directions influenced by sensorization: embedded sensorization, improved stimulation strategies, and new computational architectures.

5.5.1. Embedded sensorization.

Sensorized hands are not yet prevalent in the literature but are starting to draw interest, especially with the improvement of interfaces for bidirectional prostheses (for a list of RPHs with sensorized fingertips, see **Supplemental Tables 1 and 2**). As a recent example, Controzzi et al. (140) developed the Mia hand (Prensilia, Italy), which is integrated with sensors that can measure normal and tangential forces at the fingertips. Sensorization of RPHs is a design requirement that should be considered as important as other functional requirements for hand prostheses, such as weight or dexterity. To improve RPH performance and sensor integration, next-generation RPHs should then be designed with their sensorization in mind. Information about hand state (joint position, forces, and touch) can also be beneficial to increase the dexterity of such hands, enabling automatic adjustments such as catching slipping objects (e.g., the bebionic3 hand) and shared-control strategies (see Section 4).

5.5.2. Improved stimulation strategies.

Biomimicry is one of the strongest trends in nerve stimulation strategies, as it promises to deliver biologically plausible stimulation patterns to evoke more natural sensations. Biomimetic approaches rely on bio-inspired models to compute the stimulation patterns, so new iterations of these models, based on the current experience in stimulation and neural recording, are needed to improve the quality of elicited sensations.

These model-based approaches permit simpler modulation strategies that increase the naturalness of sensations. Tan et al. (36), for example, proved that a sinusoidal modulation of the pulse width improved the naturalness of the sensation. Formento et al. (141) instead designed a strategy to activate asynchronously stimulated fibers, mimicking healthy neural activity; in their work, they replaced classical biphasic stimulation with a high-frequency burst

of pulses that slowly increased in amplitude, and confirmed their hypothesis in ex vivo experiments. Stimulation patterns that try to overcome the physical limits of present neural interfaces (as in 141) while paving the way for more natural evoked sensations also suggest the requirements for the future generation of neural interfaces and stimulators for sensory feedback: increase reaching without losing discrimination.

Biphasic: characterized by a two-phase, bidirectional wave with one positive phase and one negative phase

5.5.3. New computational architectures.

Neuromorphic architectures have the potential to represent a paradigm shift in the design of the control systems for bidirectional hand prostheses, going toward distributed systems and edge computing. Both sensor acquisition and stimulation can benefit from these trends because they lead to more reliable systems that scale well with the increase of sensors and stimulation active sites. If the next generation of neuromorphic hardware promotes portability and lower power consumption, it could lead to broader implementation and adoption of neuromorphic systems in bidirectional hand prostheses.

Many RPHs rely on advanced encoding and decoding algorithms implemented with neural networks (61), which are more computationally demanding than traditional approaches. It is interesting that even deep learning networks can be translated into spiking neural networks (142), possibly enabling full neuromorphic hardware encoding and decoding in future prostheses.

6. PERFORMANCE ASSESSMENT

Given the increasing complexity of RPHs that integrate both sensory and motor functionalities, it is important to have standardized tools to measure the efficacy of novel technologies (143). While designing custom experiments to evaluate a technology might be tempting, there is a crucial need for well-established assessment tools to enable comparisons of different approaches on a common basis.

Caregivers should assess how a technology solves patients' impairments (their body structures or functions), activity limitations (e.g., by improving their ability to grasp), and participation restrictions (e.g., by allowing them to participate in a sport). In addition, the impairment should be viewed not only from a biological perspective but also in terms of its psychosocial consequences; an effective RPH should promote autonomy and support the reintegration of the individual into society. The measurement of patients' health-related quality of life has now become a norm during the rehabilitation process (144). For example, the Disabilities of the Arm, Shoulder, and Head (DASH) questionnaire (145) and its shorter, 11-item version, QuickDASH (146), provide self-administered measurements that focus on patients' symptoms and physical, social, and psychological aspects in populations with

Table 3 Clinical assessments for transradial amputees using robotic prosthetic hands

Name	Reference(s)	Measurement type	Clinically validated	Measurement					
				Quality of life	Embodiment	Grasp	Reach	Fine movement	Somatosensory feedback
QuickDASH	146	Questionnaire	X	X					Implicit
WHOQOL-BREF	147	Questionnaire	X	X					
Orthotics and Prosthetics User's Survey	143, 149	Questionnaire	X	X					Implicit
Box and Block Test	153, 154	Pick and place	X			X	X		Implicit
Nine Hole Peg Test	156, 157	Pick and place	X				X	X	Implicit
Clothespin Relocation Test	158	Pick and place							Implicit
Action Research Arm Test	159	Handling and manipulation of objects	X						Implicit
Southampton Hand Assessment Procedure	160	Handling and manipulation of objects	X						Implicit
Grasping Relative Index of Performance	138	Grasping				X			Explicit
Virtual Egg Test	128	Pick and place				X	X		Explicit
Prosthesis Efficiency and Profitability	138	Pick and place, manipulation				X	X		Explicit
Magnetic table task	163	Pick and place				X	X		Explicit
Cross Congruent Task	181	Psychometric			X				
Peripersonal test	174	Psychometric			X				

Abbreviations: QuickDASH, short version of the Disabilities of the Arm, Shoulder, and Head questionnaire; WHOQOL-BREF, short version of the World Health Organization Quality of Life scale.

upper-extremity musculoskeletal conditions (**Table 3**). More generally, subjects' perception of their quality of life can be measured with the short version of the World Health Organization Quality of Life scale (WHOQOL-BREF) (147) or the Quality of Life Scale (QOLS) (148). The Orthotics and Prosthetics User's Survey (OPUS) (149) has also been used in upper-limb amputees (135). A recent study showed that long-term use of a sensorized prosthetic arm improved subjects' participation (e.g., skiing and fishing) (137); the authors performed semistructured interviews at patients' homes using a phenomenological approach to infer their experience with the prosthetic arm and to investigate the influence of a novel treatment within subjects' social groups (using an emic ethnographic approach) (150).

Another straightforward metric for evaluating the quality of a tool is patients' acceptance of the proposed protocol. Treatment adherence—measured by, for example, the number of sessions carried out by the patients per month, or the average session length—can help the experimenter develop tools that will be effectively used by the patients (150). In a study by Graczyk et al. (135) that compared the use of a prosthetic hand with and without tactile feedback, the subjects used a modified version of the OPUS Upper Extremity Functional Status module to report on a daily basis the difficulty of performing tasks such as brushing teeth or using a key in a lock.

When considering RPHs, assessment of the motor (or sensorimotor) functions is clearly essential. As described above, somatosensory feedback is crucial to performing a dexterous motor task (151); therefore, functional tests for motor tasks also implicitly evaluate the sensory feedback. In other words, high performance in, for example, a pick-and-place task using a bidirectional RPH indicates both an accurate motor decoding and sensory feedback. Other assessments [e.g., the Virtual Egg Test (152)] target the somatosensory feedback more explicitly. Here, we describe both types of measurements.

The Box and Block Test (153) is a common evaluation of unilateral gross manual dexterity (**Figure 3a**), where subjects must transport as many wooden blocks as possible from one compartment of a box to another within one minute. A modified version of this test with motion capture has been proposed (154) to evaluate eventual compensatory strategies of the shoulder or the trunk; a normative version using predefined positions of the blocks inside the box has also been proposed to facilitated kinematic analysis (155). The fine dexterity of fingers can be measured with the Nine Hole Peg Test, which involves the placing of small 1.3-cm-diameter dowels into nine holes (156). Variations of this test with motion tracking have also been proposed (157). The Clothespin Relocation Test (**Figure 3b**) measures both grasping and pronation/supination functions (158).

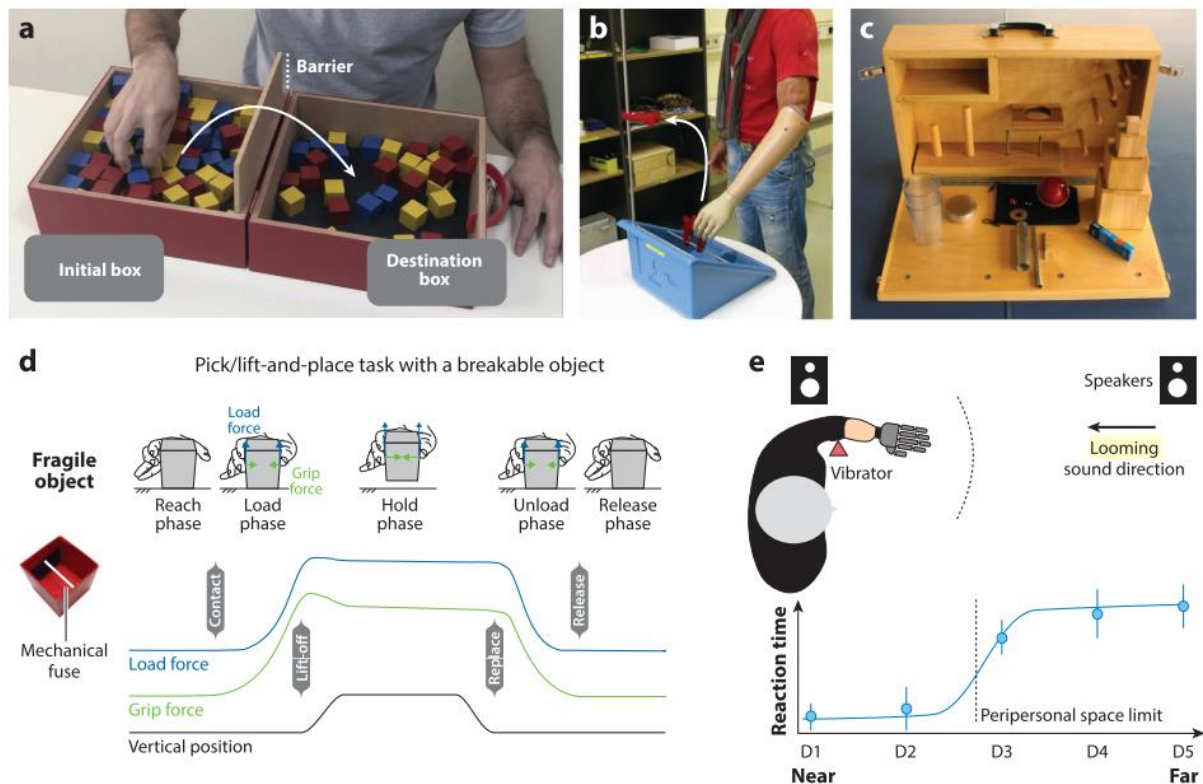


Figure 3 Examples of available assessment tools. (a) The standardized test equipment for the Box and Block Test includes a box with two compartments separated by a barrier and 150 2.5-cm colored blocks. The subject is asked to transfer as many blocks as possible from one from one compartment to the other in one minute. Panel adapted with permission from accsim instrumentos. (b) The Clothespin Relocation Test measures hand function (reaching, grasping, and wrist rotation). The measurement consists of the time it takes for the subject to move three clothespins from a horizontal to a vertical bar and then back (see, e.g., 182). Pannel adapted with permission from reference 182. (c) The Action Research Arm Test standard box is commercially available and contains different objects to assess grasp, grip pinch, and gross movement functions. Pannel reproduced with permission fromArat Kits.. (d) The Virtual Egg Test is a variation of the Box and Block Test where blocks are replaced by breakable objects. In this example, the plastic cubes have a magnetic fuse that breaks if the grasping force exceeds a certain threshold. Panel adapted with permission from Reference 128 (e) An audio–tactile interaction task has been used to measure the brain representation of the peripersonal space (the brain’s presentation of the space immediately around the body) (174). The test consists of a looming sound (perceived as coming from far away and moving toward the amputated hand) and a vibrator placed on the subject’s stump that is triggered when the sound is perceived to be at different distances from the subject (D1 to D5). The position where the presence of the sound facilitates the perception of the vibrator (reaction time) is used a proxy for the peripersonal space limit (*dashed line*).

The Action Research Arm Test (**Figure 3c**) is one of the most widely used measurements for upper-extremity (arm and hand) functions (159). It assesses four basic movements: grasp, grip, pinch, and gross movements of extension and flexion at the elbow and shoulder. Various sized and shaped objects from daily living (a cup, a washer, etc.) are used for the test, which provides a broad overview of patients' improvement in the activity and impairment domains. Finally, the Southampton Hand Assessment Procedure uses a set of abstract objects and activities of daily living with tasks specifically developed to assess the effectiveness of upper-limb prostheses (160).

These evaluations are used in rehabilitation and have been clinically validated (**Table 3**). Most of them were developed for neurological impairments (such as a stroke), multiple sclerosis, or spinal cord injuries and have been adapted for the evaluation of RPHs. While these well-established evaluations are essential, detailed investigation of RPHs—mainly when integrating sensory feedback capabilities—implies specific challenges that have been addressed in a series of tests introduced in recent years. These tests, although not yet clinically validated, are, in our opinion, of great interest.

The Grasping Relative Index of Performance measures the ability to control the desired force during grasping (138) independently from the control and feedback modalities. This measurement is based on the well-known Fitts' law, which states that the difficulty of a reaching task is given by the log of the ratio between the distance to the target and its size; in other words, the farther away and smaller a target is, the harder it is to reach it. Thumser et al. (161) argued that grasping is similar to pointing with the thumb and finger toward selected positions and defined the index of difficulty for grasping as the ratio of the object's weight to its hardness (where grasping a fragile object is analogous to a reaching a small target). Other assessments have been proposed to estimate object stiffness (138) and size discrimination (5); Risso et al. (162) investigated the contribution of vision, tactile feedback via intraneural stimulation, and visuo-tactile integration to estimate the size of a handheld object.

The magnetic table task (163) and the Virtual Egg Test (128) (**Figure 3d**) are variations of the Box and Block Test in which the blocks are replaced by magnetic cubes and breakable objects, respectively. Both have been used to evaluate the efficacy of different sensory encoding strategies (see 135 for the magnetic table task and 61 for the Virtual Egg Test). Finally, Prosthesis Efficiency and Profitability is an ad hoc measurement for prosthetics with sensory feedback to assess searching, reaching, grasping, manipulating, and decision-making during a foraging task (138).

Use of cognitive load during a sensorimotor task can give an indirect evaluation of the intuitiveness of a task: Do patients need to give their full attention to a particular movement, or are they able to perform it as part of a dual task? Subjects might be asked, for example, to perform a task while counting backward, finding words that start with a given letter, or visually following a moving target on a screen (for an example with a Virtual Egg Test, see 62). More direct measurement of the cognitive burden via electroencephalographic event-related potentials during human-machine interactions have also been proposed (164). Here, the subject must perform a specific task (the primary task) while detecting an auditory stimulus

(the secondary task), and the amplitude of the event-related potentials in response to the auditory stimulus then indicates the amount of dedicated attention to the secondary and primary tasks. Simply put, a small response to the auditory cue suggests more extensive attention to the primary task (165) and therefore a greater cognitive load.

The prolonged use of prosthetic limbs can reverse some of the effects of post-traumatic maladaptive plasticity, one of the most debilitating of which is phantom limb pain, a condition present in the majority of subjects with amputation (166). Phantom limb pain has a complex etiology that can be elicited by a multitude of factors, including nociceptive (neuroma hyperactivity), neuropathic (cortical reorganization), or psychogenic mechanisms. Numerous studies have shown that the use of prosthetics with sensory feedback significantly reduces phantom limb pain for upper-limb (36, 111, 113) and lower-limb (165) amputees. Typical measurements of pain are the McGill Pain Questionnaire (167), the Neuropathic Pain Symptom Inventory (168), and the Visual Analog Pain intensity scale, but it can also be measured with the DASH assessment (145) and the physical domain of the WHOQOL test.

Longitudinal experiments with amputee patients have demonstrated changes in body schema representation and embodiment of the prosthetic when tactile (61, 169) or proprioceptive (170) feedback is provided to the subject. A questionnaire-based measurement inspired by the rubber hand illusion (171) is often used. Tools for psychometrical measurement of the embodiment include a visuo-tactile integration task (172) and a cross-modal congruency task (173). A similar protocol using audio-tactile stimuli (174) revealed changes of the peripersonal space around the stump following prolonged use of a prosthetic limb (**Figure 3e**). In the same study, the authors used a tactile distance perception task in subjects' healthy and amputated arms to measure the perceived length of the remaining part of the upper limb and the homologous region of the healthy limb.

There is no single measurement that assesses all aspects of the use of an RPH. To evaluate the validity of novel technology, the experimenter should consider the multifaceted aspects of the impairment and subjects' biopsychosocial welfare, which is possible only via a series of tools, as presented in this section. In the case of prosthetics with sensory feedback, there is a lack of validated and well-established measurements, but several research groups are working to define adapted measurements, which might become the new norm in the future.

7. CONCLUSION

More than 20 years ago, remarkable results by a group of French surgeons for hand transplantation (7) had raised hopes for a future where grafting would be the norm and prosthetics eventually obsolete (175). However, not only has this prediction—unfortunately—not yet come to pass, but also the adoption of new RPH technologies has been slower than expected. As such, RPHs are still a field of active research. Significant efforts have been made to reduce their price and weight, improve their aesthetics and anthropomorphism, increase the robustness and accuracy of their motor intention decoding, and provide natural and

accurate somatosensory feedback. We have proposed here an outline of possible iterations of RPHs for the next few years and for 5–10 years in the future.

In our view, there could soon be a broader integration of simple somatosensory feedback using mature implantable techniques, such as cuff electrodes. Motor decoding using machine learning and shared-control algorithms could permit continuous command of single fingers and broader sets of grasps. Ultimately, the next generation of prosthetics could use more advanced soft implantable electrodes, which could enable more sophisticated sensory encoding (proprioception, temperature perception, touch perception, and nociception) and motor decoding using, for example, deep learning techniques. But to reach this goal, the field must tackle significant challenges related to system integration, electronic miniaturization, computational power, surgical procedure, electrode robustness, the robotic hand itself, and the encoding of somatosensory information.

DISCLOSURE STATEMENT

SM holds shares of Sensars Neurotechnology aiming at developing “bionic” limbs for amputees. The other authors declare no competing interests.

ACKNOWLEDGMENTS

The authors would like to thank Iason Batzianoulis for his valuable help on robotic hand control. The review was partly funded by the Swiss National Science Foundation through the National Centre of Competence in Research (NCCR) Robotics, the CHRONOS project, the Wyss Center for Bio and Neuroengineering and by the Bertarelli Foundation.

LITERATURE CITED

1. Castiello U. 2005. The neuroscience of grasping. *Nat. Rev. Neurosci.* 6:726–36
2. Bicchi A. 2000. Hands for dexterous manipulation and robust grasping: a difficult road toward simplicity. *IEEE Trans. Robot. Autom.* 16:652–62
3. Marasco PD, Kim K, Colgate JE, Peshkin MA, Kuiken TA. 2011. Robotic touch shifts perception of embodiment to a prosthesis in targeted reinnervation amputees. *Brain* 134:747–58
4. Ehrsson HH, Rosen B, Stocksli A, Ragnö C, Kohler P, Lundborg G. 2008. Upper limb amputees can be induced to experience a rubber hand as their own. *Brain* 131:3443–52
5. Raspopovic S, Capogrosso M, Petrini FM, Bonizzato M, Rigosa J, et al. 2014. Restoring natural sensory feedback in real-time bidirectional hand prostheses. *Sci. Transl. Med.* 6:222ra19

6. Kyberd PJ, Hill W. 2011. Survey of upper limb prosthesis users in Sweden, the United Kingdom and Canada. *Prosthet. Orthot. Int.* 35:234–41
7. Dubernard JM, Owen E, Herzberg G, Lanzetta M, Martin X, et al. 1999. Human hand allograft: report on first 6 months. *Lancet* 353:1315–20
8. Piazza C, Catalano MG, Godfrey SG, Rossi M, Grioli G, et al. 2017. The SoftHand Pro-H. *IEEE Robot. Autom. Mag.* 24(4):87–101
9. Smit G, Plettenburg DH, Van Der Helm FCT. 2015. The lightweight Delft Cylinder hand: first multi-articulating hand that meets the basic user requirements. *IEEE Trans. Neural Syst. Rehabil. Eng.* 23:431–40
10. Baril M, Laliberté T, Gosselin C, Routhier F. 2013. On the design of a mechanically programmable underactuated anthropomorphic prosthetic gripper. *J. Mech. Des.* 135:121008
11. Smit G, Plettenburg DH. 2010. Efficiency of voluntary closing hand and hook prostheses. *Prosthet. Orthot. Int.* 34:411–27
12. Biddiss E, Chau T. 2007. Upper limb prosthesis use and abandonment: a survey of the last 25 years. *Prosthet. Orthot. Int.* 31:236–57
13. Lotti F, Tiezzi P, Vassura G, Biagiotti L, Palli G, Melchiorri C. 2005. Development of UB Hand 3: early results. In *Proceedings of the 2005 IEEE International Conference on Robotics and Automation*, pp. 4488–93. Piscataway, NJ: IEEE
14. Honda Y, Miyazaki F, Nishikawa A. 2010. Control of pneumatic five-fingered robot hand using antagonistic muscle ratio and antagonistic muscle activity. In *2010 3rd IEEE RAS and EMBS International Conference on Biomedical Robotics and Biomechatronics*, pp. 337–42. Piscataway, NJ: IEEE
15. Cordella F, Ciancio AL, Sacchetti R, Davalli A, Cutti AG, et al. 2016. Literature review on needs of upper limb prosthesis users. *Front. Neurosci.* 10:209
16. Melchiorri C, Palli G, Berselli G, Vassura G. 2013. Development of the UB Hand IV: overview of design solutions and enabling technologies. *IEEE Robot. Autom. Mag.* 20(3):72–81
17. Pfeifer R, Gomez G. 2009. Morphological computation – connecting brain, body, and environment. In *Creating Brain-Like Intelligence*, ed. B Sendhoff, E Körner, O Sporns, H Ritter, K Doya, pp. 66–83. Berlin: Springer
18. Jing X, Yong X, Jiang Y, Li G, Yokoi H. 2019. Anthropomorphic prosthetic hand with combination of light weight and diversiform motions. *Appl. Sci.* 9:4203
19. Mohammadi A, Lavranos J, Zhou H, Mutlu R, Alici G, et al. 2020. A practical 3D-printed soft robotic prosthetic hand with multi-articulating capabilities. *PLOS ONE* 15:e0232766
20. Chamara RPDD, Gopura RARC. 2019. An under-actuated mechanism for anthropomorphic robotic prosthetic hand. In *2019 5th International Conference on Control, Automation and Robotics*, pp. 162–66. Piscataway, NJ: IEEE
21. Pozzobon LA, Da Silva Guerra R, Librelotto GR. 2019. A low-cost, compliant, underactuated prosthetic hand with custom flex sensors for finger bending estimation. In *2019 19th International Conference on Advanced Robotics*, pp. 69–74. Piscataway, NJ: IEEE

22. Fajardo J, Ferman V, Cardona D, Maldonado G, Lemus A, Rohmer E. 2020. Galileo Hand: an anthropomorphic and affordable upper-limb prosthesis. *IEEE Access* 8:81365–77
23. Abayasiri RAM, Abayasiri RST, Gunawardhana RAGM, Premakumara RMC, Mallikarachchi S, et al. 2020. An under-actuated hand prosthesis with finger abduction and adduction for human like grasps. In *2020 6th International Conference on Control, Automation and Robotics*, pp. 574–80. Piscataway, NJ: IEEE
24. a Yong X, Jing X, Wu X, Jiang J, Yokoi H. 2019. Development of an adaptive prosthetic hand. In *2019 IEEE International Conference on Robotics and Biomimetics*, pp. 2800–5. Piscataway, NJ: IEEE
25. Weiner P, Starke J, Hundhausen F, Beil J, Asfour T. 2018. The KIT prosthetic hand: design and control. In *2018 IEEE/RSJ International Conference on Intelligent Robots and Systems*, pp. 3328–34. Piscataway, NJ: IEEE
26. Nemoto Y, Ogawa K, Yoshikawa M. 2020. F3Hand II: a flexible five-fingered prosthetic hand using curved pneumatic artificial muscles. In *2020 IEEE/SICE International Symposium on System Integration*, pp. 99–104. Piscataway, NJ: IEEE
27. Controzzi M, Cipriani C, Carrozza MC. 2008. Mechatronic design of a transradial cybernetic hand. In *2008 IEEE/RSJ International Conference on Intelligent Robots and Systems*, pp. 576–81. Piscataway, NJ: IEEE
28. Trivedi D, Rahn CD, Kier WM, Walker ID. 2008. Soft robotics: biological inspiration, state of the art, and future research. *Appl. Bionics Biomech.* 5:520417
29. Hirose S, Ma S. 1991. Coupled tendon-driven multijoint manipulator. In *1991 IEEE International Conference on Robotics and Automation*, pp. 1268–75. Piscataway, NJ: IEEE
30. Carrozza MC, Cappiello G, Stellin G, Zaccone F, Vecchi F, et al. 2005. A cosmetic prosthetic hand with tendon driven under-actuated mechanism and compliant joints: ongoing research and preliminary results. In *Proceedings of the 2005 IEEE International Conference on Robotics and Automation*, pp. 2661–66. Piscataway, NJ: IEEE
31. Godfrey SB, Zhao KD, Theuer A, Catalano MG, Bianchi M, et al. 2018. The SoftHand Pro: functional evaluation of a novel, flexible, and robust myoelectric prosthesis. *PLOS ONE* 13:13e0205653.
32. Amend J, Lipson H. 2017. The JamHand: dexterous manipulation with minimal actuation. *Soft Robot.* 4:70–80
33. Yamaguchi A, Takemura K, Yokota S, Edamura K. 2011. A robot hand using electro-conjugate fluid. In *2011 IEEE International Conference on Robotics and Automation*, pp. 5923–28. Piscataway, NJ: IEEE
34. Zhao H, O'Brien K, Li S, Shepherd RF. 2016. Optoelectronically innervated soft prosthetic hand via stretchable optical waveguides. *Sci. Robot.* 1:eaai7529
35. Navarro X, Valderrama E, Stieglitz T, Schüttler M. 2001. Selective fascicular stimulation of the rat sciatic nerve with multipolar polyimide cuff electrodes. *Restor. Neurol. Neurosci.* 18:9–21
36. Tan DW, Schiefer MA, Keith MW, Anderson JR, Tyler J, Tyler DJ. 2014. A neural interface provides long-term stable natural touch perception. *Sci. Transl. Med.* 6:257ra138

37. Vu PP, Vaskov AK, Irwin ZT, Henning PT, Lueders DR, et al. 2020. A regenerative peripheral nerve interface allows real-time control of an artificial hand in upper limb amputees. *Sci. Transl. Med.* 12:eaay2857
38. Raspopovic S, Cimolato A, Panarese A, Vallone F, del Valle J, et al. 2020. Neural signal recording and processing in somatic neuroprosthetic applications. A review. *J. Neurosci. Methods* 337:108653
39. Yoshida K, Bertram MJ, Cox TGH, Riso RR. 2017. Peripheral nerve recording electrodes and techniques. In *Neuroprosthetics: Theory and Practice*, ed. K Yoshida, MJ Bertram, TG Hunter Cox, RR Riso, pp. 377–466. Singapore: World Sci.
40. Navarro X, Krueger TB, Lago N, Micera S, Stieglitz T, Dario P. 2005. A critical review of interfaces with the peripheral nervous system for the control of neuroprostheses and hybrid bionic systems. *J. Peripher. Nerv. Syst.* 258:229–58
41. Boretius T, Badia J, Pascual-Font A, Schuettler M, Navarro X, et al. 2010. A transverse intrafascicular multichannel electrode (TIME) to interface with the peripheral nerve. *Biosens. Bioelectron.* 26:62–69
42. Yoshida K, Pellinen D, Pivin D, Rousche P, Kipke D. 2000. Development of the thin-film longitudinal intra-fascicular electrode. In *Proceedings of the 5th Annual Conference of the International Functional Electrical Stimulation Society*, pp. 279–84. Graz, Austria: Int. Funct. Electr. Stimul. Soc.
43. Badia J, Boretius T, Andreu D, Azevedo-Coste C, Stieglitz T, Navarro X. 2011. Comparative analysis of transverse intrafascicular multichannel, longitudinal intrafascicular and multipolar cuff electrodes for the selective stimulation of nerve fascicles. *J. Neural Eng.* 8:036023
44. Howell B, Grill WM. 2015. Design of electrodes for stimulation and recording. In *Implantable Neuroprostheses for Restoring Function*, ed. K Kilgore, pp. 59–93. Amsterdam: Elsevier
45. Cui X, Wiler J, Dzaman M, Altschuler RA, Martin DC. 2003. In vivo studies of polypyrrole/peptide coated neural probes. *Biomaterials* 24:777–87
46. Kennedy PR, Bakay RAE, Sharpe SM. 1992. Behavioral correlates of action potentials recorded chronically inside the cone electrode. *Neuroreport* 3:605–8
47. Lacour SP, Courtine G, Guck J. 2016. Materials and technologies for soft implantable neuroprostheses. *Nat. Rev. Mater.* 1:16063
48. Kipke DR. 2004. Implantable neural probe systems for cortical neuroprostheses. In *26th Annual International Conference of the IEEE Engineering in Medicine and Biology Society*, pp. 5344–47. Piscataway, NJ: IEEE
49. Merletti R, Holobar A, Farina D. 2008. Analysis of motor units with high-density surface electromyography. *J. Electromyogr. Kinesiol.* 18:879–90
50. Smith LH, Hargrove LJ. 2013. Comparison of surface and intramuscular EMG pattern recognition for simultaneous wrist/hand motion classification. In *2013 35th Annual International Conference of the IEEE Engineering in Medicine and Biology Society*, pp. 4223–6. Piscataway, NJ: IEEE

51. Farrell TR, Weir RF. 2008. A comparison of the effects of electrode implantation and targeting on pattern classification accuracy for prosthesis control. *IEEE Trans. Biomed. Eng.* 55:2198–211
52. Cracchiolo M, Valle G, Petrini F, Strauss I, Granata G, et al. 2020. Decoding of grasping tasks from intraneural recordings in trans-radial amputee. *J. Neural Eng.* 17:026034
53. Wendelken S, Page DM, Davis T, Wark HAC, Kluger DT, et al. 2017. Restoration of motor control and proprioceptive and cutaneous sensation in humans with prior upper-limb amputation via multiple Utah Slanted Electrode Arrays (USEAs) implanted in residual peripheral arm nerves. *J. Neuroeng. Rehabil.* 14:121
54. Cipriani C, Dalonzo M, Carrozza MC. 2012. A miniature vibrotactile sensory substitution device for multifingered hand prosthetics. *IEEE Trans. Biomed. Eng.* 59:400–8
55. Chen B, Feng Y, Wang Q. 2016. Combining vibrotactile feedback with volitional myoelectric control for robotic transtibial prostheses. *Front. Neurobot.* 10:8
56. Antfolk C, D'Alonzo M, Controzzi M, Lundborg G, Rosen B, et al. 2013. Artificial redirection of sensation from prosthetic fingers to the phantom hand map on transradial amputees: vibrotactile versus mechanotactile sensory feedback. *IEEE Trans. Neural Syst. Rehabil. Eng.* 21:112–20
57. Gonzalez J, Soma H, Sekine M, Yu W. 2012. Psycho-physiological assessment of a prosthetic hand sensory feedback system based on an auditory display: a preliminary study. *J. Neuroeng. Rehabil.* 9:33
58. Osborn L, Betthausen J, Kaliki R, Thakor N. 2018. Targeted transcutaneous electrical nerve stimulation for phantom limb sensory feedback. In *2017 IEEE Biomedical Circuits and Systems Conference*. Piscataway, NJ: IEEE. <https://doi.org/10.1109/BIOCAS.2017.8325200>
59. D'Anna E, Petrini FM, Artoni F, Popovic I, Simanić I, et al. 2017. A somatotopic bidirectional hand prosthesis with transcutaneous electrical nerve stimulation based sensory feedback. *Sci Rep.* 7:10930
60. Oddo CM, Raspopovic S, Artoni F, Mazzoni A, Spigler G, et al. 2016. Intraneural stimulation elicits discrimination of textural features by artificial fingertip in intact and amputee humans. *eLife* 5:e09148
61. Valle G, Mazzoni A, Iberite F, D'Anna E, Strauss I, et al. 2018. Biomimetic intraneural sensory feedback enhances sensation naturalness, tactile sensitivity, and manual dexterity in a bidirectional prosthesis. *Neuron* 100:37–45.e7
62. Valle G, D'Anna E, Strauss I, Clemente F, Granata G, et al. 2020. Hand control with invasive feedback is not impaired by increased cognitive load. *Front. Bioeng. Biotechnol.* 8:287
63. D'Anna E, Valle G, Mazzoni A, Strauss I, Iberite F, et al. 2019. A closed-loop hand prosthesis with simultaneous intraneural tactile and position feedback. *Sci. Robot.* 4:eaau8892
64. Shokur S, Gallo S, Moioli RC, Donati ARC, Morya E, et al. 2016. Assimilation of virtual legs and perception of floor texture by complete paraplegic patients receiving artificial tactile feedback. *Sci. Rep.* 6:32293
65. Geethanjali P. 2016. Myoelectric control of prosthetic hands: state-of-the-art review. *Med. Devices Evid. Res.* 9:247–55

66. Farina D, Jiang N, Rehbaum H, Holobar A, Graimann B, et al. 2014. The extraction of neural information from the surface EMG for the control of upper-limb prostheses: emerging avenues and challenges. *IEEE Trans. Neural Syst. Rehabil. Eng.* 22:797–809
67. Ferguson S, Dunlop GR. 2002. Grasp recognition from myoelectric signals. In *Proceedings of the Australasian Conference on Robotics and Automation*, ed. W Friedrich, P Lim, pp. 83–87. Sydney: Aust. Robot. Autom. Assoc.
68. Martelloni C, Carpaneto J, Micera S. 2008. Classification of upper arm EMG signals during object-specific grasp. In *2008 30th Annual International Conference of the IEEE Engineering in Medicine and Biology Society*, pp. 5061–64. Piscataway, NJ: IEEE
69. Kakoty NM, Hazarika SM. 2011. Recognition of grasp types through principal components of DWT based EMG features. In *2011 IEEE International Conference on Rehabilitation Robotics*. Piscataway, NJ: IEEE. <https://doi.org/10.1109/ICORR.2011.5975398>
70. Castellini C, Van Der Smagt P. 2009. Surface EMG in advanced hand prosthetics. *Biol. Cybern.* 100:35–47
71. Atzori M, Cognolato M, Müller H. 2016. Deep learning with convolutional neural networks applied to electromyography data: a resource for the classification of movements for prosthetic hands. *Front. Neurobot.* 10:9
72. Tenore FVG, Ramos A, Fahmy A, Acharya S, Etienne-Cummings R, Thakor NV. 2009. Decoding of individuated finger movements using surface electromyography. *IEEE Trans. Biomed. Eng.* 56:1427–34
73. Bhattachargee CK, Sikder N, Hasan MT, Nahid A. 2019. Finger movement classification based on statistical and frequency features extracted from surface EMG signals. In *2019 International Conference on Computer, Communication, Chemical, Materials and Electronic Engineering*. Piscataway, NJ: IEEE. <https://doi.org/10.1109/IC4ME247184.2019.9036671>
74. Bhagwat S, Mukherji P. 2020. Electromyogram (EMG) based fingers movement recognition using sparse filtering of wavelet packet coefficients. *Sādhanā* 45:3
75. Muceli S, Farina D. 2012. Simultaneous and proportional estimation of hand kinematics from EMG during mirrored movements at multiple degrees-of-freedom. *IEEE Trans. Neural Syst. Rehabil. Eng.* 20:371–78
76. Jiang N, Vest-Nielsen JL, Muceli S, Farina D. 2012. EMG-based simultaneous and proportional estimation of wrist/hand kinematics in uni-lateral trans-radial amputees. *J. Neuroeng. Rehabil.* 9:42
77. Hioki M, Kawasaki H. 2012. Estimation of finger joint angles from sEMG using a neural network including time delay factor and recurrent structure. *ISRN Rehabil.* 2012:604314
78. Zhuang KZ, Sommer N, Mendez V, Aryan S, Formento E, et al. 2019. Shared human-robot proportional control of a dexterous myoelectric prosthesis. *Nat. Mach. Intell.* 1:400–11
79. Mussa-Ivaldi FA, Casadio M, Danziger ZC, Mosier KM, Scheidt RA. 2011. Sensory motor remapping of space in human-machine interfaces. *Prog. Brain Res.* 191:45–64
80. Dyson M, Barnes J, Nazarpour K. 2018. Myoelectric control with abstract decoders. *J. Neural Eng.* 15:056003

81. Dyson M, Dupan S, Jones H, Nazarpour K. 2020. Learning, generalization, and scalability of abstract myoelectric control. *IEEE Trans. Neural Syst. Rehabil. Eng.* 28:1539–47
82. Daley H, Englehart K, Hargrove L, Kuruganti U. 2012. High density electromyography data of normally limbed and transradial amputee subjects for multifunction prosthetic control. *J. Electromyogr. Kinesiol.* 22:478–84
83. Hargrove L, Englehart K, Hudgins B. 2006. The effect of electrode displacements on pattern recognition based myoelectric control. *2006 International Conference of the IEEE Engineering in Medicine and Biology Society*, pp. 2203–6. Piscataway, NJ: IEEE
84. Boschmann A, Platzner M. 2014. Towards robust HD EMG pattern recognition: Reducing electrode displacement effect using structural similarity. In *2014 36th Annual International Conference of the IEEE Engineering in Medicine and Biology Society*, pp. 4547–50. Piscataway, NJ: IEEE
85. Stango A, Negro F, Farina D. 2015. Spatial correlation of high density EMG signals provides features robust to electrode number and shift in pattern recognition for myocontrol. *IEEE Trans. Neural Syst. Rehabil. Eng.* 23:189–98
86. Farina D, Holobar A, Merletti R, Enoka RM. 2010. Decoding the neural drive to muscles from the surface electromyogram. *Clin. Neurophysiol.* 121:1616–23
87. Kapelner T, Negro F, Aszmann OC, Farina D. 2018. Decoding motor unit activity from forearm muscles: perspectives for myoelectric control. *IEEE Trans. Neural Syst. Rehabil. Eng.* 26:244–51
88. Dai C, Hu X. 2020. Finger joint angle estimation based on motoneuron discharge activities. *IEEE J. Biomed. Heal. Inform.* 24:760–67
89. Hu Y, Wong Y, Wei W, Du Y, Kankanhalli M, Geng W. 2018. A novel attention-based hybrid CNN-RNN architecture for sEMG-based gesture recognition. *PLOS ONE* 13:e0206049E
90. Olsson AE, Sager P, Andersson E, Björkman A, Malešević N, Antfolk C. 2019. Extraction of multi-labelled movement information from the raw HD-sEMG image with time-domain depth. *Sci Rep.* 9:7244
91. Ameri A, Akhaee MA, Scheme E, Englehart K. 2019. Regression convolutional neural network for improved simultaneous EMG control. *J. Neural Eng.* 16:036015
92. Xia P, Hu J, Peng Y. 2018. EMG-based estimation of limb movement using deep learning with recurrent convolutional neural networks. *Artif. Organs* 42:E67–77
93. Alom MZ, Taha TM, Yakopcic C, Westberg S, Sidike P, et al. 2018. The history began from AlexNet: a comprehensive survey on deep learning approaches. arXiv:1803.01164 [cs.CV]
94. Patricia N, Caputo B. 2014. Learning to learn, from transfer learning to domain adaptation: a unifying perspective. In *2014 IEEE Conference on Computer Vision and Pattern Recognition*, pp. 1442–49. Piscataway, NJ: IEEE
95. Tommasi T, Orabona F, Castellini C, Caputo B. 2013. Improving control of dexterous hand prostheses using adaptive learning. *IEEE Trans. Robot.* 29:207–19
96. Côté-Allard U, Fall CL, Drouin A, Campeau-Lecours A, Gosselin C, et al. 2019. Deep learning for electromyographic hand gesture signal classification using transfer learning. *IEEE Trans. Neural Syst. Rehabil. Eng.* 27:760–71

97. Du Y, Jin W, Wei W, Hu Y, Geng W. 2017. Surface EMG-based inter-session gesture recognition enhanced by deep domain adaptation. *Sensors* 17:6–9
98. Ameri A, Akhaee MA, Scheme E, Englehart K. 2019. A deep transfer learning approach to reducing the effect of electrode shift in EMG pattern recognition-based control. *IEEE Trans. Neural Syst. Rehabil. Eng.* 28:370–79
99. Phinyomark A, Scheme E. 2018. EMG pattern recognition in the era of big data and deep learning. *Big Data Cogn. Comput.* 2:21
100. Khamparia A, Singh KM. 2019. A systematic review on deep learning architectures and applications. *Expert Syst.* 36:e12400
101. Biddiss E, Chau T. 2007. Upper-limb prosthetics: critical factors in device abandonment. *Am. J. Phys. Med. Rehabil.* 86:977–87
102. Došen S, Cipriani C, Kostić M, Controzzi M, Carrozza MC, Popović DB. 2010. Cognitive vision system for control of dexterous prosthetic hands: Experimental evaluation. *J. Neuroeng. Rehabil.* 7:42
103. Light CM, Chappell PH, Hudgins B, Engelhart K. 2002. Intelligent multifunction myoelectric control of hand prostheses. *J. Med. Eng. Technol.* 26:139–46
104. Fani S, Bianchi M, Jain S, Neto JSP, Boege S, et al. 2016. Assessment of myoelectric controller performance and kinematic behavior of a novel soft synergy-inspired robotic hand for prosthetic applications. *Front. Neurorobot.* 10:11
105. Smith LH, Kuiken TA, Hargrove LJ. 2014. Real-time simultaneous and proportional myoelectric control using intramuscular EMG. *J. Neural Eng.* 11:066013
106. Pasquina PF, Evangelista M, Carvalho AJ, Lockhart J, Griffin S, et al. 2015. First-in-man demonstration of a fully implanted myoelectric sensors system to control an advanced electromechanical prosthetic hand. *J. Neurosci. Methods* 244:85–93
107. Zia ur Rehman M, Gilani S, Waris A, Niazi I, Slabaugh G, et al. 2018. Stacked sparse autoencoders for EMG-based classification of hand motions: a comparative multi day analyses between surface and intramuscular EMG. *Appl. Sci.* 8:1126
108. Kamavuako EN, Scheme EJ, Englehart KB. 2014. Combined surface and intramuscular EMG for improved real-time myoelectric control performance. *Biomed. Signal. Process. Control* 10:102–7
109. Dantas H, Warren DJ, Wendelken SM, Davis TS, Clark GA, Mathews VJ. 2019. Deep learning movement intent decoders trained with dataset aggregation for prosthetic limb control. *IEEE Trans. Biomed. Eng.* 66:3192–203
110. Petrini FM, Mazzoni A, Rigosa J, Giambattistelli F, Granata G, et al. 2019. Microneurography as a tool to develop decoding algorithms for peripheral neuro-controlled hand prostheses. *BioMed. Eng. OnLine* 18:44
111. Rossini PM, Micera S, Benvenuto A, Carpaneto J, Cavallo G, et al. 2010. Double nerve intraneural interface implant on a human amputee for robotic hand control. *Clin. Neurophysiol.* 121:777–83

112. Davis TS, Wark HAC, Hutchinson DT, Warren DJ, O'Neill K, et al. 2016. Restoring motor control and sensory feedback in people with upper extremity amputations using arrays of 96 microelectrodes implanted in the median and ulnar nerves. *J. Neural Eng.* 13:036001
113. Petrini FM, Valle G, Strauss I, Granata G, Di Iorio R, et al. 2019. Six-month assessment of a hand prosthesis with intraneural tactile feedback. *Ann. Neurol.* 85:137–54
114. Mazzoni A, Oddo CM, Valle G, Camboni D, Strauss I, et al. 2020. Morphological neural computation restores discrimination of naturalistic textures in trans-radial amputees. *Sci. Rep.* 10:527
115. Graczyk EL, Schiefer MA, Saal HP, Delhay BP, Bensmaia SJ, Tyler DJ. 2016. The neural basis of perceived intensity in natural and artificial touch. *Sci. Transl. Med.* 8:362ra142
116. Kogler V, Nguyen TAK, Digiovanna J, Micera S. 2011. Recording vestibular evoked potentials induced by electrical stimulation of the horizontal semicircular canal in guinea pig. In *2011 5th International IEEE/EMBS Conference on Neural Engineering*, pp. 261–64. Piscataway, NJ: IEEE
117. Micera S, Carpaneto J, Raspopovic S. 2010. Control of hand prostheses using peripheral information. *IEEE Rev. Biomed. Eng.* 3:48–68
118. Englehart K, Hudgins B. 2003. A robust, real-time control scheme for multifunction myoelectric control. *IEEE Trans. Biomed. Eng.* 50:848–54
119. Park M, Bok BG, Ahn JH, Kim MS. 2018. Recent advances in tactile sensing technology. *Micromachines* 9:321
120. Pfeifer R, Iida F, Gómez G. 2006. Morphological computation for adaptive behavior and cognition. *Int. Congr. Ser.* 1291:22–9
121. Kim Y, Chortos A, Xu W, Liu Y, Oh JY, et al. 2018. A bioinspired flexible organic artificial afferent nerve. *Science* 360:998–1003
122. Wu J, Jia QS, Johansson KH, Shi L. 2013. Event-based sensor data scheduling: trade-off between communication rate and estimation quality. *IEEE Trans. Autom. Control* 58:1041–6
123. Bartolozzi C, Ros PM, Diotalevi F, Jamali N, Natale L, et al. 2017. Event-driven encoding of off-the-shelf tactile sensors for compression and latency optimisation for robotic skin. In *2017 IEEE/RSJ International Conference on Intelligent Robots and Systems*, pp. 166–73. Piscataway, NJ: IEEE
124. Lee WW, Tan YJ, Yao H, Li S, See HH, et al. 2019. A neuro-inspired artificial peripheral nervous system for scalable electronic skins. *Sci. Robot.* 4:eaax2198
125. Antfolk C, D'Alonzo M, Rosén B, Lundborg G, Sebelius F, Cipriani C. 2013. Sensory feedback in upper limb prosthetics. *Expert Rev. Med. Devices* 10:45–54
126. Mann RW, Reimers SD. 1970. Kinesthetic sensing for the EMG controlled “Boston Arm.” *IEEE Trans. Man-Mach. Syst.* 11:110–15
127. Patterson PE, Katz JA. 1992. Design and evaluation of a sensory feedback system that provides grasping pressure in a myoelectric hand. *J. Rehabil. Res. Dev.* 29:1–8
128. Clemente F, D'Alonzo M, Controzzi M, Edin BB, Cipriani C. 2016. Non-invasive, temporally discrete feedback of object contact and release improves grasp control of

- closed-loop myoelectric transradial prostheses. *IEEE Trans. Neural Syst. Rehabil. Eng.* 24:1314–22
129. D'Alonzo M, Clemente F, Cipriani C. 2015. Vibrotactile stimulation promotes embodiment of an Alien hand in amputees with phantom sensations. *IEEE Trans. Neural Syst. Rehabil. Eng.* 23:450–57
 130. Stephens-Fripp B, Alici G, Mutlu R. 2018. A review of non-invasive sensory feedback methods for transradial prosthetic hands. *IEEE Access* 6:6878–99
 131. Dosen S, Markovic M, Strbac M, Belic M, Kojic V, et al. 2017. Multichannel electrotactile feedback with spatial and mixed coding for closed-loop control of grasping force in hand prostheses. *IEEE Trans. Neural Syst. Rehabil. Eng.* 25:183–95
 132. Geng B, Dong J, Jensen W, Dosen S, Farina D, Kamavuako EN. 2018. Psychophysical evaluation of subdermal electrical stimulation in relation to prosthesis sensory feedback. *IEEE Trans. Neural Syst. Rehabil. Eng.* 26:709–15
 133. Dong J, Geng B, Niazi IK, Amjad I, Dosen S, et al. 2020. The variability of psychophysical parameters following surface and subdermal stimulation: a multiday study in amputees. *IEEE Trans. Neural Syst. Rehabil. Eng.* 28:174–80
 134. Flesher SN, Downey JE, Weiss JM, Hughes CL, Herrera AJ, et al. 2019. Restored tactile sensation improves neuroprosthetic arm control. bioRxiv 653428. <https://doi.org/10.1101/653428>
 135. Graczyk EL, Resnik L, Schiefer MA, Schmitt MS, Tyler DJ. 2018. Home use of a neural-connected sensory prosthesis provides the functional and psychosocial experience of having a hand again. *Sci. Rep.* 8:9866
 136. George JA, Page DM, Davis TS, Duncan CC, Hutchinson T, et al. 2020. Long-term performance of Utah Slanted Electrode Arrays and intramuscular electromyographic leads implanted chronically in human arm nerves and muscles. bioRxiv 2020.03.30.016683. <https://doi.org/10.1101/2020.03.30.016683>
 137. Ortiz-Catalan M, Mastinu E, Sassu P, Aszmann O, Brånemark R. 2020. Self-contained neuromusculoskeletal arm prostheses. *N. Engl. J. Med.* 382:1732–38
 138. George JA, Kluger DT, Davis TS, Wendelken SM, Okorokova EV, et al. 2019. Biomimetic sensory feedback through peripheral nerve stimulation improves dexterous use of a bionic hand. *Sci. Robot.* 4:eaax2352
 139. Chandrasekaran S, Nanivadekar AC, McKernan G, Helm ER, Boninger ML, et al. 2020. Sensory restoration by epidural stimulation of the lateral spinal cord in upper-limb amputees. *eLife* 9:e54349
 140. Controzzi M, Clemente F, Barone D, Luciani LB, Pierotti N, et al. 2019. Progress towards the development of the *DeTOP* hand prosthesis: a sensorized transradial prosthesis for clinical use. In *Converging Clinical and Engineering Research on Neurorehabilitation III*, ed. L Masia, S Micera, M Akay, J Pons, pp. 103–6. Cham, Switz.: Springer
 141. Formento E, D'Anna E, Gribi S, Lacour SP, Micera S. 2019. A biomimetic electrical stimulation strategy to induce asynchronous stochastic neural activity. *J. Neural Eng.* 17:046019[**AU: Updated with published version—OK?**]

142. Sengupta A, Ye Y, Wang R, Liu C, Roy K. 2019. Going deeper in spiking neural networks: VGG and residual architectures. *Front Neurosci.* 13:95
143. Lindner HYN, Nätterlund BS, Hermansson LMN. 2010. Upper limb prosthetic outcome measures: review and content comparison based on International Classification of Functioning, Disability and Health. *Prosthet. Orthot. Int.* 34:109–28
144. Hill W, Stavdahl Ø, Hermansson LN, Kyberd P, Swanson S, Hubbard S. 2009. Functional outcomes in the WHO-ICF model: establishment of the upper limb prosthetic outcome measures group. *J. Prosthet. Orthot.* 21:115–19
145. Hudak PL, Amadio PC, Bombardier C. 1996. Development of an upper extremity outcome measure: the DASH (disabilities of the arm, shoulder, and head). *Am. J. Ind. Med.* 29:602–8
146. Beaton DE, Wright JG, Katz JN, Amadio P, Bombardier C, et al. 2005. Development of the QuickDASH: comparison of three item-reduction approaches. *J. Bone Jt. Surg. A* 87:1038–46
147. Harper A, Power M, Orley J, Herrman H, Schofield H, et al. 1998. Development of the World Health Organization WHOQOL-BREF quality of life assessment. *Psychol. Med.* 28:551–58
148. Burckhardt CS, Anderson KL. 2003. The Quality of Life Scale (QOLS): reliability, validity, and utilization. *Health Qual. Life Outcomes* 1:60
149. Heinemann AW, Bode RK, O'Reilly C. 2003. Development and measurement properties of the Orthotics and Prosthetics User's Survey (OPUS): a comprehensive set of clinical outcome instruments. *Prosthet. Orthot. Int.* 27:191–206
150. Lendaro E, Middleton A, Brown S, Ortiz-Catalan M. 2020. Out of the clinic, into the home: the in-home use of phantom motor execution aided by machine learning and augmented reality for the treatment of phantom limb pain. *J. Pain Res.* 13:195–209
151. Johansson RS, Flanagan JR. 2009. Coding and use of tactile signals from the fingertips in object manipulation tasks. *Nat. Rev. Neurosci.* 10:345–59
152. Taub E, Uswatte G, Pidikiti R. 1999. Constraint-induced movement therapy: a new family of techniques with broad application to physical rehabilitation—a clinical review. *J. Rehabil. Res. Dev.* 36:237–51
153. Mathiowetz V, Volland G, Kashman N, Weber K. 1985. Adult norms for the Box and Block Test of manual dexterity. *Am. J. Occup. Ther.* 39:386–91
154. Hebert JS, Lewicke J. 2012. Case report of modified box and blocks test with motion capture to measure prosthetic function. *J. Rehabil. Res. Dev.* 49:1163–74
155. Hebert JS, Lewicke J, Williams TR, Vette AH. 2014. Normative data for modified box and blocks test measuring upper-limb function via motion capture. *J. Rehabil. Res. Dev.* 51:919–31
156. Mathiowetz V, Weber K, Kashman N, Volland G. 1985. Adult norms for the Nine Hole Peg Test of finger dexterity. *Occup. Ther. J. Res.* 5:24–38
157. Lamercy O, Fluét MC, Lamers I, Kerkhofs L, Feys P, Gassert R. 2013. Assessment of upper limb motor function in patients with multiple sclerosis using the Virtual Peg Insertion Test: a pilot study. In *2013 IEEE International Conference on Rehabilitation Robotics*. Piscataway, NJ: IEEE. <https://doi.org/10.1109/ICORR.2013.6650494>.

158. Kyberd P, Hussaini A, Maillet G. 2018. Characterisation of the Clothespin Relocation Test as a functional assessment tool. *J. Rehabil. Assist. Technol. Eng.* 5.
<https://doi.org/10.1177/2055668317750810>
159. Yozbatiran N, Der-Yeghiaian L, Cramer SC. 2008. A standardized approach to performing the action research arm test. *Neurorehabil. Neural Repair* 22:78–90
160. Light CM, Chappell PH, Kyberd PJ. 2002. Establishing a standardized clinical assessment tool of pathologic and prosthetic hand function: normative data, reliability, and validity. *Arch. Phys. Med. Rehabil.* 83:776–83
161. Thumser ZC, Slifkin AB, Beckler DT, Marasco PD. 2018. Fitts' law in the control of isometric grip force with naturalistic targets. *Front. Psychol.* 9:560
162. Risso G, Valle G, Iberite F, Strauss I, Stieglitz T, Controzzi M. 2019. Optimal integration of intraneural somatosensory feedback with visual information: a single-case study. *Sci Rep.* 9:7916
163. Schiefer M, Tan D, Sidek SM, Tyler DJ. 2015. Sensory feedback by peripheral nerve stimulation improves task performance in individuals with upper limb loss using a myoelectric prosthesis. *J. Neural Eng.* 13:016001
164. Deeny S, Chicoine C, Hargrove L, Parrish T, Jayaraman A. 2014. A simple ERP method for quantitative analysis of cognitive workload in myoelectric prosthesis control and human-machine interaction. *PLOS ONE* 9:e112091
165. Petrini FM, Bumbasirevic M, Valle G, Ilic V, Mijović P, et al. 2019. Sensory feedback restoration in leg amputees improves walking speed, metabolic cost and phantom pain. *Nat. Med.* 25:1356–63
166. Ephraim PL, Wegener ST, MacKenzie EJ, Dillingham TR, Pezzin LE. 2005. Phantom pain, residual limb pain, and back pain in amputees: results of a national survey. *Arch. Phys. Med. Rehabil.* 86:1910–19
167. Melzack R. 2005. The McGill Pain Questionnaire: from description to measurement. *Anesthesiology* 103:199–202
168. Bouhassira D, Attal N, Fermanian J, Alchaar H, Gautron M, et al. 2004. Development and validation of the Neuropathic Pain Symptom Inventory. *Pain* 108:248–57
169. Rognini G, Rossini PM, Strauss I, D'Anna E, Mange R, et al. 2018. Multisensory bionic limb to achieve prosthesis embodiment and reduce distorted phantom limb perceptions. *J. Neurol. Neurosurg. Psychiatry* 90:833–36
170. Marasco PD, Hebert JS, Sensinger JW, Shell CE, Schofield JS, et al. 2018. Illusory movement perception improves motor control for prosthetic hands. *Sci. Transl. Med.* 10:eaa06990
171. Botvinick M, Cohen J. 1998. Rubber hands 'feel' touch that eyes see. *Nature* 391:756
172. Di Pino G, Romano D, Spaccasassi C, Mioli A, D'Alonzo M, et al. 2020. Sensory- and action-oriented embodiment of neurally-interfaced robotic hand prostheses. *Front. Neurosci.* 14:389
173. Blustein D, Wilson A, Sensinger J. 2018. Assessing the quality of supplementary sensory feedback using the crossmodal congruency task. *Sci Rep.* 8:6203

174. Canzoneri E, Marzolla M, Amoresano A, Verni G, Serino A. 2013. Amputation and prosthesis implantation shape body and peripersonal space representations. *Sci. Rep.* 3:2844
175. Lundborg G. 2000. A 25-year perspective of peripheral nerve surgery: evolving neuroscientific concepts and clinical significance. *J. Hand. Surg.* 25:391–414
176. Schultz AE, Marasco PD, Kuiken TA. 2009. Vibrotactile detection thresholds for chest skin of amputees following targeted reinnervation surgery. *Brain Res.* 1251:121–29
177. Geng W, Du Y, Jin W, Wei W, Hu Y, Li J. 2016. Gesture recognition by instantaneous surface EMG images. *Sci. Rep.* 6:36571
178. Navarro X, Calvet S, Rodríguez FJ, Stieglitz T, Blau C, et al. 1998. Stimulation and recording from regenerated peripheral nerves through polyimide sieve electrodes. *J. Peripher. Nerv. Syst.* 3:91–101
179. Valle G, Petrini FM, Strauss I, Iberite F, D’Anna E, et al. 2018. Comparison of linear frequency and amplitude modulation for intraneural sensory feedback in bidirectional hand prostheses. *Sci. Rep.* 8:16666
180. George JA, Davis TS, Brinton MR, Clark GA. 2019. Intuitive neuromyoelectric control of a dexterous bionic arm using a modified Kalman filter. *J. Neurosci. Methods* 330:108462
181. Maravita A, Spence C, Driver J. 2003. Multisensory integration and the body schema: close to hand and within reach. *Curr. Biol.* 13:R531–39
182. Hahne JM, Schweisfurth MA, Koppe M, Farina D. 2018. Simultaneous control of multiple functions of bionic hand prostheses: Performance and robustness in end users. *Sci. Robot.* 3:eaat3630

2 EMG Decoding

2.1 Deep Learning with Convolutional Neural Network for Proportional Control of Finger Movements

Deep learning has demonstrated promising potential in electromyography (EMG) decoding, particularly for grasp classification. By employing deep neural network architectures, deep learning (DL) facilitate the extraction of high-dimensional, non-linear patterns within EMG signals. The incorporation of DL techniques in single-finger proportional EMG decoding not only promises to improve the dexterity of prosthetic devices but also allows for more intuitive and natural control, which could significantly enhance the functional capabilities and user experience of advanced prosthetic hands.

The content of this section is the postprint from the conference article Mendez et al., "Deep Learning with Convolutional Neural Network for Proportional Control of Finger Movements from surface EMG Recordings," 2021 10th International IEEE/EMBS Conference on Neural Engineering (NER), Italy, 2021, pp. 1074-1078

Find the published article here: <https://doi.org/10.1109/NER49283.2021.9441095>

Personal contributions as the first author: conceived the experiments, prepared the protocols and the experimental setup (hardware and software), and conducted the experiment in the framework of another article. I also analyzed the results based on a preliminary analysis performed by the second author, prepared the figures, and wrote the manuscript.

Deep Learning with Convolutional Neural Network for Proportional Control of Finger Movements from surface EMG Recordings

V. Mendez, L. Pollina, F. Artoni, S. Micera *Member, IEEE*

Abstract

The control of robotic prosthetic hands (RPHs) for upper limb amputees is far from optimal. Simultaneous and proportional finger control of a RPH based on EMG signals is still challenging. Based on EMG and kinematics recordings of subjects following a pre-defined sequence of single and multi-fingers movements, we aimed at predicting finger flexion and thumb opposition angles. We compared two deep learning (DL) based approaches, the first one using the raw EMG signals and the second one using the spectrogram of the signal as input, with the standard state of the art decoding technique (STD) for finger angle regression. Using a genetic algorithm for hyper-parameter optimization, we obtained an optimized model architecture (and set of features in the case of STD) for each condition on one recording session. Then, we evaluated the best model of each condition on the eleven EMG and finger kinematics recordings available from four subjects. The two DL approaches based on convolutional neural networks predicted finger angles with a similar mean squared error loss but both of them outperformed the standard approach for the regression of simultaneous single-finger angles. This proposed decoding strategy and hyper-parameter optimization framework provides a basis to further improve single finger proportional control for RPHs.

1. Introduction

Controlling the human hand feels simple and intuitive but relies on a sophisticated and robust control strategy that allows for dexterous manipulation of a variety of objects. Hand loss is a traumatic event with not only motor but also psychological consequences (1), resulting in limited ability to perform object manipulation, sensing, as well as non-verbal communication. Robotic Prosthetic Hands (RPHs) aim at restoring hand functionality in trans-radial amputees. In order to capture the user's intention, these RPHs usually rely on electromyographic (EMG) signals recorded from their residual forearm muscle activity. Commercially available RPHs usually use two surface EMG (sEMG) electrodes placed on remaining antagonist muscles (usually wrist flexion/extension). The control of these robotic hands rely on a simple threshold based strategy controlling one degree of freedom (2). The type of grasp can be selected using co-contraction to cycle between pre-defined grasps.

By using more electrodes (~6-8), pattern recognition algorithms are an alternative to this direct control approach. It consists of extracting discriminative features from the EMG signals to decode directly the type of grasp intended by the user. After a calibration phase, the user only has to think to perform the desired grasp with his phantom hand. Results showed 98% accuracy on 4 classes (3) and up to 75% for 50 classes (4). Other groups showed the possibility to decode single finger flexion and extension (5) with performance of 99% accuracy on single and multi-finger movements.

Although this approach is more intuitive, it is still different from the natural way of controlling finger. Indeed, to obtain fingers in a middle position, the user has to contract his muscles until the desired angle is reached then relax to keep the RPH in the same position. In order to obtain an even more natural

control, few groups showed the possibility to perform single finger proportional control performing angle regression instead of movement classification (6–8).

To decode meaningful information from EMG data, it is necessary to transform the signals into informative, discriminating and independent features. It has been now several decades that researchers have been working on the design of the best features to decode motor intentions from EMG signals (9). Since the first example in 2016 (10), the EMG decoding community shifted from this standard feature engineering (STD) approach to feature learning approach using deep learning (DL) and in most cases convolutional neural networks (CNN). The standard deep networks usually consists of several convolutional layers followed by fully-connected layers (11). Convolutional layers can learn discriminative features from the input signal and reduce its dimension. These features are then used as input to the fully connected layers that will make the prediction (see Figure 1). For EMG decoding, the input of CNNs can be either the raw signal (12) or the spectrogram of the signal (13). Several studies showed that deep networks could learn more discriminative features directly from the raw signal to perform grasp classification with higher accuracies than STD (14,15). Few groups showed DL-based regression of motor intention using sEMG for arm (16) and wrist motion (17–19) with promising results. For a more extensive review on RPHs see (20).

The “perfect” motor decoding strategy could be described as one that increases subject dexterity to a level comparable to the healthy hand. In order to be as close as possible to the natural control of the hand, one have to decode fingers angle continuously and simultaneously. Due to the higher performance of DL compared to the STD approach in grasp classification, we aimed at quantifying the performance of single finger proportional control with a DL vs STD approach.

2. Methods

A. EMG Dataset and pre-processing

The detailed protocol for EMG acquisition comes from Zhuang et al. (2019) experiment 3 (21). Briefly, four healthy subjects aged between 20 and 26 were recruited for this experiment. Ethical approval was obtained by the cantonal ethical committee of Vaud. Informed consent was obtained from all participants in the study. The subjects participated to 2 or 3 calibration sessions where EMG signals were recorded using a Noraxon Delsys system connected to a LabJack data acquisition card to record six channels placed around the subject’s forearm on specific muscles corresponding to the flexion of each finger and thumb opposition found with palpation. In this article, we focus only on the offline calibration part of the decoding model. The subjects followed a series of movements on a screen performed in a virtual environment. Hand kinematics were obtained from the finger angles shown on the video. The movements consisted in single and multi-finger movements and the virtual environment was synchronized with the EMG acquisition setup. The sequence of movements was repeated 5 times, each with a hold period of 5 seconds and the total time of the video was 4.5 minutes (see Figure 1). The EMG signals were recorded at 2 kHz and the kinematics at 60 Hz.

From the 15 joint angles recorded during the training phase on the virtual environment, six joint angles were selected: the metacarpophalangeal joint angle of each finger to estimate finger flexion/extension and the carpometacarpal joint angle for thumb opposition. Kinematic data was linearly interpolated and oversampled at 2 kHz to match the EMG signal sampling frequency.

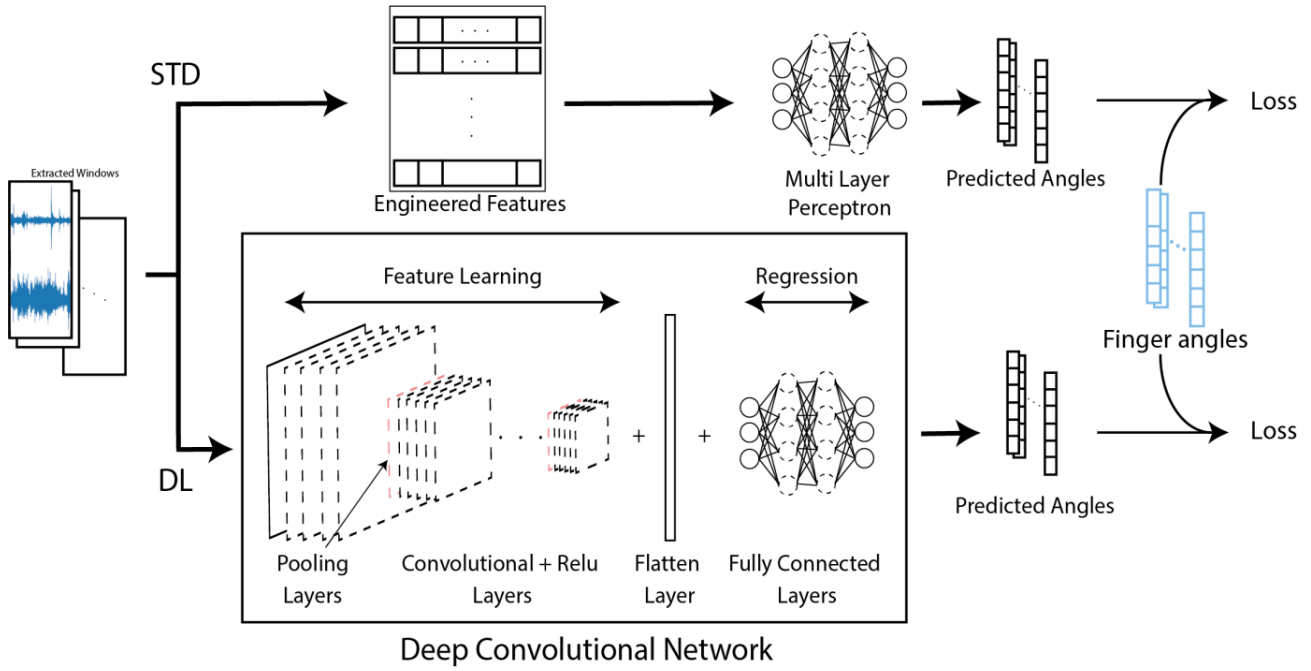


Figure 1. Training paradigm difference between a STD approach and Deep learning (dashed objects represents tunable hyper parameters).

The dataset was then split into train, validation and test set, the three first repetitions were used for the training set, one for the validation set and the last one for testing. This non-random split was done to consider the real-world use case of RPH. Indeed, amputees would use their RPH after this calibration phase and therefore the last repetition for testing is the most suited repetition to evaluate performance of the decoding in real world scenario. For each set, a sliding window of 192ms with a moving step of 40ms (152ms overlap) was used, the angle values of the end of each window were kept as labels and the angles were rescaled between 0 (fully open) and 10 (fully flexed).

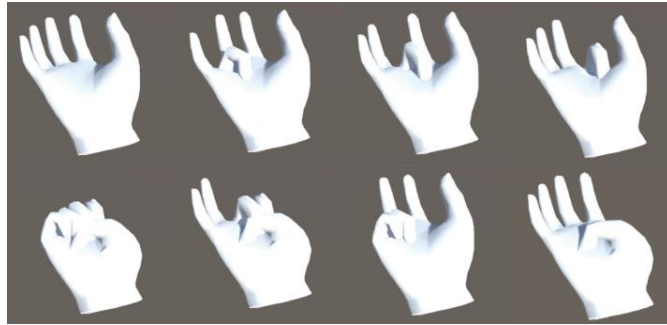


Figure 2. Illustration of the movements present in the EMG recordings.

B. Learning paradigms

In order to quantify the performance of DL vs STD, three learning paradigms are compared: The standard feature engineering approach (STD), a DL approach with the raw signal as input (RAW) and a DL approach with the spectrogram computed with the fast Fourier transform of each individual window (FFT) as input. For the two DL approaches, the input signal window is reshaped as squared images as in (22). In the STD one, EMG signals are processed and features are extracted from each channel. We chose 9 well-explored time and frequency domain features to extract from each time window (23):

1. Mean Absolute Value
2. Wavelength: Cumulative length of waveform over time
3. Maximum Absolute Value
4. Standard Deviation
5. Zero Crossings: Number of times the signal crosses zero
6. Slope sign changes: Number of time that the slope of the EMG signal changes sign
7. Root Mean Square
8. Log detector: $e^{\frac{1}{N} \sum_{i=1}^N \log(|x_i|)}$ where x_i is the EMG amplitude at time bin i .
9. Frequency spectrums in each frequency bin between 7 and 12 Hz, 12-30, 30-50, 50-100, 100-150 and 150-400 Hz from FFT results.

C. Hyper-parameter optimization

There is a high number of hyper-parameters to optimize for each paradigm. Among those, we optimized a set of parameters based on the first session of the first subject due to computational power required to perform a hyper-parameter search for each recording. The hypothesis being that the quantity of information is relatively the same for each recording and therefore, the complexity of the dataset is relatively the same, meaning that the best model architecture for one recording is a good model for the other recordings.

For the two DL approaches (RAW and FFT), we started from a VGG-like architecture (24) and optimized the shape of the network: the number of convolutional layers before each average pooling layer (up to 3), the number of pooling layer (up to 5) and the number of filters for each convolutional layer (16, 32, 64, 128). A batch-normalization layer follows each convolutional layer. Then, the number of fully connected layers (up to two layers) and the number of nodes for each layer (16, 32, 64) were also tuned. Except from the architectural parameter, the drop rate was also optimized (0, 0.2, 0.5) as well as the L_2 regularization rate (0, 1e-3, 0.1), the learning rate (0.1, 0.01, 0.001), the convolutional filter size in x dimension, in y dimension (1, 3, 5) and the padding strategy for image border (with or without). The CNN networks were optimized with a batch gradient descent with a batch size of 32 samples, with 50 epochs, a step decay with a drop of $\frac{1}{2}$ every 10 epochs and an early stopping if the validation loss did not decreased for more than 13 epochs.

For the STD approach, the model was a multi-layer perceptron (MLP) and therefore has less parameters to tune. However, the feature selection is an important process in order not to overfit the data. Therefore the hyper-parameters were the selection or not of a feature, the number of fully connected layers (up to 3 hidden layers), the number of node per layer (16, 32, 64, 128, 256), the drop rate (0, 0.2, 0.5), the L_1 and L_2 regularization terms (0, 1e-3, 0.1), the learning rate (0.1, 0.01, 0.001) and the optimizer (Adam, RMSprop, batch gradient descent). The MLP was optimized with a batch gradient descent with a batch size of 16 samples, with 100 epochs and similarly to the CNN, a step decay with a drop of $\frac{1}{2}$ every 10 epochs with an early stopping if the validation loss did not decreased for more than 13 epochs. All the models were trained with a mean squared error loss (MSE).

Due to the high dimensionality of the hyper-parameter space, a grid search was impossible to perform in a reasonable amount of time. Therefore, we opted for a genetic algorithm (GA) parameter optimization approach (25). The problem was formulated as a genetic representation of the solution domain where each hyper-parameter was encoded as a gene on a chromosome that could take one of the discrete possible values. The fitness function was encoded as the validation loss of the trained model

to evaluate the solution domain. A population of 20 random individual was created and trained for 200 generation using a fitness proportionate (or roulette wheel) offspring selection method. The rate of mutation was set to 0.1 and the selection rate to 0.6.

D. Performance evaluation of each subject

After hyper-parameter optimization on one session, the same pre-processing steps will be applied to all the available recordings in order to train a model on each recording available. For each recording, the model was trained ten times and the model with the lowest validation loss is kept. This step was necessary to reduce the chances of having the model stuck in a local minimum. Then the best model was evaluated on the testing set.

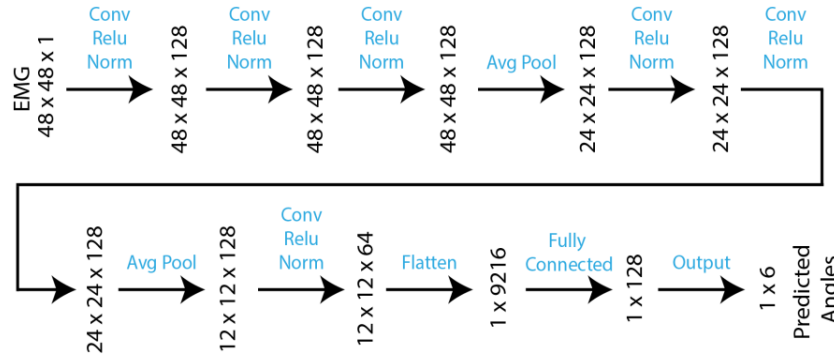


Figure 3. Architecture of the best model

3. Results

The best model for the three paradigms obtained with the genetic algorithms was with RAW condition and had a validation loss of 5.34 and a training loss of 2.20. The model architecture is shown in Figure 3. It is trained with a drop rate of 50%, without L₂ normalization, a learning rate of 0.01 and the shape of the convolutional mask is (3, 1) with 0 padding to keep the same output dimension.

For the FFT condition, the minimum validation loss was 6.41 with a training loss of 4.82 and for STD, the minimum validation loss was 9.14 with a training loss of 9.43. For the STD model, features from all channels were extracted and the final model used all the features except the slope sign change for a total of 46 features.

The average test loss, meaning the performance on unseen data, per condition is shown in Figure 4 for the 11 sessions. The STD test loss is significantly different from the two other conditions (t-test, $p < 0.05$) but the FFT and RAW conditions are not different.

The test loss for each subject is shown in Figure 5, each subject recorded 3 sessions except S2 who did only two calibration sessions. An example of the predicted angles versus the target labels is shown in Figure 6 for the RAW condition on the test set of subject S1. It consists of one repetition of each movement and lasts for 56 seconds. The angles correspond to the sequence: Index Flexion, Middle Finger Flexion, Ring Finger Flexion, Ulnar Grasp, Open, Tridigital Grasp, Power Grasp, Thumb opposition and Thumb opposition + flexion. It corresponds to a loss of 7.36. The baseline loss corresponding to a model outputting only the mean value of the targets was ~19.

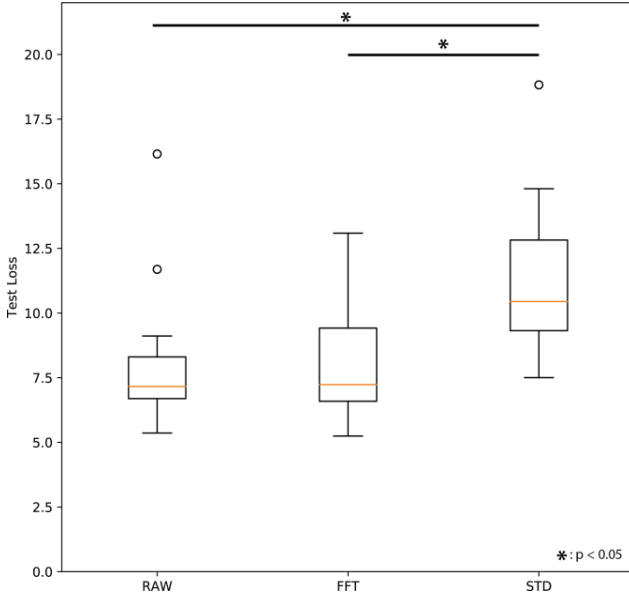


Figure 4. Boxplots of the test loss over all sessions for the best model with RAW, FFT and STD conditions

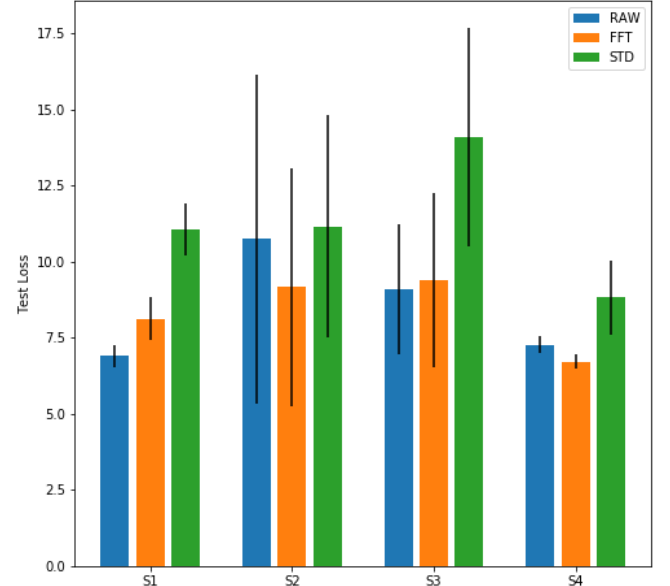


Figure 5. Barplot of the test loss per subject for the best model with RAW, FFT and STD conditions

4. Discussion

This work aimed at quantifying the performance of DL compared to a STD feature extraction approach. The results showed that both DL conditions (RAW and FFT) are performing better than STD. However, it is not possible to conclude on which approach between RAW and FFT is best suited for single finger proportional control. For simplicity, one could argue to keep the RAW condition to avoid computing the FFT and therefore reduce the computational time for real time applications. A possible optimization is the combination of time-frequency information merging the RAW and FFT approaches, increasing the amount of information that inputs the model.

However, the amount of data per session in these experiments is relatively low (3 repetitions for the train set) which create uncertainty during the training of the different models and high differences between the validation and testing losses.

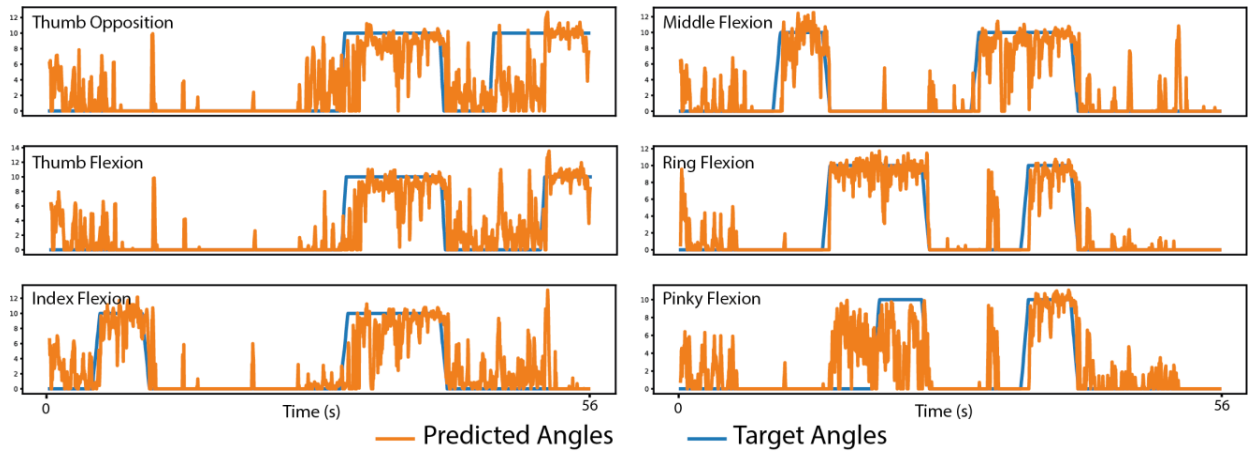


Figure 6. Plot of the predicted angles (orange) vs. target angles of the test set. X-axis is shared across columns

Another limitation to take into account is that the dataset comprised only fully open and closed positions held for several seconds without any real “rest/middle” position or other arbitrary angles. Indeed, when the users follow movements shown on a screen, there are intrinsic delays due to their reaction time that create jitter between expected kinematics and actual finger positions. In the case of single finger proportional control, exact finger position is paramount. Therefore, obtaining synchronized middle values is challenging and may be obtained using a kinematic glove for example.

Deep networks like CNNs need a huge amount of data to reach their maximum accuracy (e.g. ImageNet Challenge (26)) which means that increasing the amount of data could play a significant role in the performances obtained. However, a subject cannot reasonably record tens of hours of data in a single sitting. One possible solution is to leverage the information of several subjects to pre-train a general network that could be fine-tuned for the subject’s specific EMG activity. Several authors (13,27,28) investigated this approach and showed promising results for grasp classification, this strategy could be applied to single finger proportional control.

5. Conclusion

To conclude, we showed that deep learning is a promising approach for proportional EMG decoding. Due to the placement of the electrodes on the forearm, these results obtained on healthy subjects could apply for trans-radial amputees or amputations that are more distal. On the decoding side, we cannot conclude on the best DL approach between raw signals or spectrogram as input since both outperformed the standard state-of-the-art approach but were not statistically different.

For future developments, increasing the amount of data should be the main objective. Leveraging open access EMG databases like NinaPro (29,30) to improve performances of DL for single-finger regression. The feasibility of this DL approach in real time to control a real prosthesis or any microprocessor should also be addressed due to the high computational cost of the models used.

References

1. Meyer TM. Psychological aspects of mutilating hand injuries [Internet]. Vol. 19, Hand Clinics. Hand Clin; 2003 [cited 2020 Dec 15]. p. 41–9. Available from: <https://pubmed.ncbi.nlm.nih.gov/12683445/>
2. Geethanjali P. Myoelectric control of prosthetic hands: State-of-the-art review. Med Devices Evid Res. 2016;9:247–55.
3. Englehart K, Hudgins B. A Robust, Real-Time Control Scheme for Multifunction Myoelectric Control. IEEE Trans Biomed Eng [Internet]. 2003 [cited 2018 Jun 13];50(7). Available from: https://moodle.epfl.ch/pluginfile.php/1733963/mod_resource/content/1/Englehart_myoelectric_features.pdf
4. Atzori M, Gijsberts A, Kuzborskij I, Elsig S, Mittaz Hager AG, Deriaz O, et al. Characterization of a benchmark database for myoelectric movement classification. IEEE Trans Neural Syst Rehabil Eng. 2015 Jan 1;23(1):73–83.
5. Bhagwat S, Mukherji P. Electromyogram (EMG) based fingers movement recognition using sparse filtering of wavelet packet coefficients. Sadhana - Acad Proc Eng Sci. 2020 Dec 1;45(1):1–11.
6. Baldacchino T, Jacobs WR, Anderson SR, Worden K, Rowson J. Simultaneous Force Regression

- and Movement Classification of Fingers via Surface EMG within a Unified Bayesian Framework. *Front Bioeng Biotechnol* [Internet]. 2018 Feb 26 [cited 2020 Dec 15];6:13. Available from: <http://journal.frontiersin.org/article/10.3389/fbioe.2018.00013/full>
7. Muceli S, Farina D. Simultaneous and proportional estimation of hand kinematics from EMG during mirrored movements at multiple degrees-of-freedom. *IEEE Trans Neural Syst Rehabil Eng*. 2012;20(3):371–8.
 8. Hioki M, Kawasaki H. Estimation of Finger Joint Angles from sEMG Using a Neural Network Including Time Delay Factor and Recurrent Structure. *ISRN Rehabil*. 2012;2012:1–13.
 9. Herberts P, Almström C, Kadefors R, Lawrence PD. Hand prosthesis control via myoelectric patterns. *Acta Orthop*. 1973;44(4–5):389–409.
 10. Park KH, Lee SW. Movement intention decoding based on deep learning for multiuser myoelectric interfaces. In: 4th International Winter Conference on Brain-Computer Interface, BCI 2016. Institute of Electrical and Electronics Engineers Inc.; 2016.
 11. Aloysius N, Geetha M. A review on deep convolutional neural networks. In: *Proceedings of the 2017 IEEE International Conference on Communication and Signal Processing, ICCSP 2017*. Institute of Electrical and Electronics Engineers Inc.; 2018. p. 588–92.
 12. Atzori M, Cognolato M, Müller H. Deep Learning with Convolutional Neural Networks Applied to Electromyography Data: A Resource for the Classification of Movements for Prosthetic Hands. *Front Neurorobot* [Internet]. 2016 Sep 7 [cited 2019 Jun 13];10:9. Available from: <http://journal.frontiersin.org/Article/10.3389/fnbot.2016.00009/abstract>
 13. Allard UC, Nougrou F, Fall CL, Gigù P, Gosselin C, Laviolette F, et al. A convolutional neural network for robotic arm guidance using sEMG based frequency-features [Internet]. [cited 2019 Oct 28]. Available from: <http://kinovarobotics.com/>
 14. Phinyomark A, Scheme E. EMG Pattern Recognition in the Era of Big Data and Deep Learning. *Big Data Cogn Comput*. 2018 Aug 1;2(3):21.
 15. Hu Y, Wong Y, Wei W, Du Y, Kankanhalli M, Geng W. A novel attention-based hybrid CNN-RNN architecture for sEMG-based gesture recognition. *PLoS One*. 2018;13(10):1–18.
 16. Xia P, Hu J, Peng Y. EMG-Based Estimation of Limb Movement Using Deep Learning With Recurrent Convolutional Neural Networks. *Artif Organs*. 2018;42(5):E67–77.
 17. Yang W, Yang D, Li J, Liu Y, Liu H. EMG dataset augmentation approaches for improving the multi-DOF wrist movement regression accuracy and robustness. In: *2018 IEEE International Conference on Robotics and Biomimetics, ROBIO 2018*. Institute of Electrical and Electronics Engineers Inc.; 2018. p. 1268–73.
 18. Zhang X, Tang X, Zhu X, Gao X, Chen X, Chen X. A Regression-Based Framework for Quantitative Assessment of Muscle Spasticity Using Combined EMG and Inertial Data From Wearable Sensors. *Front Neurosci* [Internet]. 2019 May 3 [cited 2020 Dec 15];13(MAY):398. Available from: <https://www.frontiersin.org/article/10.3389/fnins.2019.00398/full>
 19. Ameri A, Akhaee MA, Scheme E, Englehart K. Regression convolutional neural network for improved simultaneous EMG control. *J Neural Eng* [Internet]. 2019 Jun 1 [cited 2019 Jun 13];16(3):036015. Available from: <http://stacks.iop.org/1741-2552/16/i=3/a=036015?key=crossref.7403b6aa090d0e9a98378353d6dece0f>
 20. Mendez V, Iberite F, Shokur S, Micera S. Current Solutions and Future Trends for Robotic Prosthetic Hands. <https://doi.org/10.1146/annurev-control-071020-104336> [Internet]. 2021

[cited 2021 Nov 8];4(1):595–627. Available from:

<https://www.annualreviews.org/doi/abs/10.1146/annurev-control-071020-104336>

21. Zhuang KZ, Sommer N, Mendez V, Aryan S, Formento E, D'Anna E, et al. Shared human–robot proportional control of a dexterous myoelectric prosthesis. *Nat Mach Intell*. 2019 Sep;1(9):400–11.
22. Ameri A, Akhaee MA, Scheme E, Englehart K. Regression convolutional neural network for improved simultaneous EMG control. *J Neural Eng*. 2019 Apr 16;16(3).
23. Phinyomark A, Phukpattaranont P, Limsakul C. Feature reduction and selection for EMG signal classification. *Expert Syst Appl [Internet]*. 2012;39(8):7420–31. Available from: <http://dx.doi.org/10.1016/j.eswa.2012.01.102>
24. Shrestha A, Mahmood A. Review of deep learning algorithms and architectures. Vol. 7, IEEE Access. Institute of Electrical and Electronics Engineers Inc.; 2019. p. 53040–65.
25. Johnson F, Valderrama A, Valle C, Crawford B, Soto R, Nanculef R. Automating Configuration of Convolutional Neural Network Hyperparameters Using Genetic Algorithm. *IEEE Access*. 2020;8:156139–52.
26. Alom MZ, Taha TM, Yakopcic C, Westberg S, Sidike P, Nasrin MS, et al. The History Began from AlexNet: A Comprehensive Survey on Deep Learning Approaches. 2018 Mar 3 [cited 2020 May 12]; Available from: <http://arxiv.org/abs/1803.01164>
27. Ameri A, Akhaee MA, Scheme E, Englehart K. A Deep Transfer Learning Approach to Reducing the Effect of Electrode Shift in EMG Pattern Recognition-based Control. *IEEE Trans Neural Syst Rehabil Eng [Internet]*. 2019 [cited 2020 Jan 6];1–1. Available from: <https://ieeexplore.ieee.org/document/8943097/>
28. Du Y, Jin W, Wei W, Hu Y, Geng W. Surface EMG-based inter-session gesture recognition enhanced by deep domain adaptation. *Sensors (Switzerland)*. 2017;17(3):6–9.
29. Atzori M, Gijsberts A, Kuzborskij I, Elsig S, Mittaz Hager AG, Deriaz O, et al. Characterization of a benchmark database for myoelectric movement classification. *IEEE Trans Neural Syst Rehabil Eng*. 2015 Jan 1;23(1):73–83.
30. Atzori M, Gijsberts A, Heynen S, Hager AGM, Deriaz O, Van Der Smagt P, et al. Building the Ninapro database: A resource for the biorobotics community. In: *Proceedings of the IEEE RAS and EMBS International Conference on Biomedical Robotics and Biomechatronics*. 2012. p. 1258–65.

2.2 A novel medium-density EMG system for prosthetic hand control

Traditional EMG systems as seen in the previous chapter have some limitations. Indeed, the electrodes must be placed carefully on muscles of interest and the number of electrodes available limits the amount of information that can be retrieved from the forearm spatiotemporal muscle activity. On the other hand, the high-density EMG approach also presents limitations since the amount of data to process is one order of magnitude higher, and due to the number of electrodes necessary, amplifiers required for such setups cannot be portable. Therefore, we developed a trade-off solution, a medium-density EMG system, which overcomes the limitations of existing approaches by covering the whole forearm with 64 dry monopolar electrodes without the need for expertise in electrode positioning. In this chapter, We characterize its performance for single-finger proportional decoding when compared to a gold-standard gel-based EMG system.

The content of this section is the preprint of the article Mendez et al., "A Novel Medium-Density EMG System for Prosthetic Hand Control" submitted to the Journal of Neural Engineering on the 15th of March 2023.

Personal contributions as the first author: conceived the experiments, prepared the protocols and the experimental setup (hardware and software), recorded the data, analyzed the results, prepared the figures, and wrote the manuscript.

A Novel Medium-Density EMG System for Prosthetic Hand Control

V. Mendez, F. Artoni, S. Micera

Abstract

Objective: Current control strategies for hand prostheses limit the dexterity of persons with upper-limb amputation, making daily tasks burdensome. Although robotic hands are capable of complex single-finger movements, the control available to patients is still rudimentary. New control strategies must be developed to improve the functionality of hand prostheses. To obtain intuitive and dexterous hand prosthesis control, we aimed to decode single-finger motion simultaneously and proportionally with maximum precision. ***Approach:*** We developed a new medium-density EMG system with 64 dry electrodes placed on the forearm. We compared its performance against a gold-standard gel-based EMG system for single-finger proportional decoding. To obtain performant decoding, we optimized the architecture and hyperparameters of deep convolutional networks and multi-layer perceptrons using a genetic algorithm for each recording. Finally, the generalization capability of the optimized model architectures is assessed by training the recording-specific architectures on each of the other recordings. ***Main results:*** Results indicate that the medium-density EMG system outperforms the gel-based system in decoding thumb opposition and flexion. Model architectures and hyperparameters obtained with the genetic algorithm on one recording generalize to other recordings except with the gold-standard EMG system and MLP. Finally, VGG-like CNNs do not improve single-finger proportional decoding compared to MLPs when the models are automatically optimized with a genetic algorithm. ***Significance:*** Our medium-density EMG system improves single-finger proportional decoding without careful electrode placement which is one step forward in the development of intuitive and dexterous control of prosthetic hands. The performances obtained with this system are stable between subjects and therefore avoid the need to optimize models for each new patient. Finally, feature learning using VGG-like CNNs does not outperform engineered features when models are optimized with a genetic algorithm. We suggest scientists designing new model architectures for EMG decoding performance compare their results against algorithms such as optimized MLPs.

Keywords: Optimization, Model Architecture Tuning, Deep Learning, CNN, Proportional Control, MD-EMG, Robotic Prosthetic Hand

1. Introduction

Millions of individuals live their daily life with only one hand or without any hands (1). For a person in this condition, basic daily tasks can become burdensome. Limited options are available to people with upper limb differences to help them regain some dexterity. For decades, researchers worldwide have been working on developing robotic prosthetic hands (RPHs) that now have the same size and weight as the human hand (2). Nowadays, RPHs are capable to perform single-finger motions and recreate grasps used in the majority of situations as well as non-grasp-related motions (2,3). However, despite their increasing complexity, the control strategy has remained unchanged and such RPHs are still perceived as rudimentary tools (4).

In the case of trans-radial amputation, two surface electromyography (EMG) electrodes are placed on the patient's forearm to create a bipolar derivation usually targeting two antagonist muscles.

Patients can modulate their muscle activity such that the EMG amplitude exceeds a threshold on one electrode or the other to move incrementally the RPH in a specific direction. This direct approach allows the control of only one degree of freedom (DoF) at a time and patients have to use a smartphone to select the type of grasp they want to perform from a predefined list.

Alternatively, using pattern recognition algorithms, it is possible to improve the dexterity and intuitiveness of RPHs by decoding directly the type of grasp intended by the user. To obtain high performance, this approach usually requires 6 to 8 bipolar derivations with gel to reduce the impedance between the electrodes and the skin (5). This method requires a calibration phase to map the grasp intended by the user and his specific EMG activity. During calibration, informative and discriminating features are extracted from the EMG signals to train a machine learning model (6–10).

Over the years, features were designed and compared striving to improve motor intention decoding (11). Nowadays, many groups showed the possibility to decode grasp types together with single-finger motion with high accuracy on subjects with two hands and patients with a limb difference (12–15). Some companies^{1,2} brought this solution to the market being able to obtain high performance as well as robust enough decoding over time with dry electrodes that are more convenient for donning and doffing of RPHs but at the price of a noisier recorded signal (16,17).

More complex models such as multi-layer perceptrons (MLPs) with, as input, different sets of extracted features also showed promising results (12). More recently, due to the breakthrough of deep learning (DL) and more precisely convolutional neural networks (CNNs) in computer vision, the scientific community explored the possibility of using different DL approaches to improve performance (18,19) and robustness (20,21) for EMG-based grasp classification. Using CNNs that can learn discriminative features directly from the raw input signal showed great potential. Such models could improve classification accuracy by almost 10% compared to all the other competitors at the ImageNET image classification competition (22). This DL approach was shown to improve EMG-based grasp classification performance when compared to standard machine learning models (23,24) suggesting that features learned by the CNN can provide very promising performance.

However, one limitation of the aforementioned approaches is the need to place electrodes and create bipolar derivations over each muscle of interest. The positioning of such electrodes is usually performed by trained clinicians and can be challenging for some patients who had an amputation after certain types of accidents that can change the position and number of muscles remaining in the stump. The Myo band developed by Thalmic Labs, used mostly in research, is an elastic band consisting of 8 dry electrodes distributed equally around the forearm and showed promising results in the decoding of intended grasps without careful placement of electrodes both with more standard approaches (25) and deep learning (26).

Another approach, High-Density EMG (HD-EMG), uses grids of closely arranged monopolar electrodes in patches of 64, 128 or 256 to overcome this limitation. Such devices require the use of gel but can record spatiotemporal information from muscle activity by creating 2D images at each time instant and do not require precise positioning of the patches (27). The combination of HD-EMG and DL for grasp classification has been shown to outperform feature-based approaches (28,29).

Nevertheless, HD-EMG requires an inter-electrode distance smaller than 10mm to avoid spatial aliasing (30). Therefore, the number of channels necessary to record muscle activity for grasp

¹ <https://coaptengineering.com/>

² https://www.ottobock.com/en-au/Prosthetics/UpperLimb_MyoPlus

classification is high and can go up to 128 or more (28,29,31,32) which cannot be recorded with wearable devices yet.

A trade-off solution consists in using fewer EMG electrodes (32-64 monopolar derivations) with lower density so that it is possible to acquire the signals with compact and wearable devices as well as cover enough portion of the forearm. This Medium Density approach (MD-EMG) does not require careful placement of the electrodes and was used to decode grasps intended by stroke patients with high accuracy (33). MD-EMG also gives the possibility to extract activation maps from the forearm's muscle activity during wrist and finger movements (34). Ting et al. (35) could extract specific areas related to each finger and wrist motion measured during intended movement from a patient with tetraplegia.

Single finger and grasp classification is the most widespread decoding approach with EMG signals. However, using classification to control an RPH is intrinsically different from the natural way humans are controlling their hands. Indeed, fingers are moved continuously and proportionally which is different from a succession of states. One step closer to natural and intuitive control is to try to regress the joint angle of single fingers continuously and independently. Several examples can be found in the literature on this approach with high performance. Using a few bipolar gel electrodes it is possible to regress single finger flexion angle with high accuracy (36). Others showed similar results using HD-EMG (29,37) or dry MD-EMG setups (38), both with standard decoding approaches or deep learning techniques (see (18) for a more thorough literature review).

However, despite the improved performance obtained with DL approaches, most examples using EMG signals for classification or regression with deep models are comparing single model architectures. Indeed, the architecture of deep networks such as MLPs or CNNs plays an important role in the performance obtained and is often defined with trial and error by experts in the field. In the EMG literature, authors usually get inspiration from computer vision models and reduce the size of the models to train on smaller EMG datasets. For instance (39) created a ResNet to perform single finger angle regression from EMG signals recorded with a Myo band. Ameri et al. (40) used a simplified AlexNET-like architecture to perform wrist movement regression with 8 EMG bipolar derivations.

A performing DL model requires both an optimized architecture as well as an optimized set of hyperparameters to train the model. Several algorithms can be used for this purpose, such as grid search, which has been historically used for hyperparameter tuning in EMG-based grasp classification (9,41,42). Random search is another candidate as it avoids running through all the combinations of parameters that grow exponentially (43). However, due to the high dimensionality of parameters, optimizing the architecture and hyperparameters of deep networks such as CNNs cannot be done using grid search in a reasonable amount of time and random search might not find a good solution in such a high dimensional space.

Genetic algorithms (GAs) are a good tradeoff between random and grid searches as GAs are optimization techniques inspired by natural evolution principles. They are commonly used to solve complex problems that are difficult to address using traditional methods.

Aquino-Britez et al. (44) on EEG signals, outperformed baseline approaches by optimizing CNNs with GA. However, GAs also have some hyperparameters (population size, number of generations, mutation rate, selection rate, and selection strategy) and still can fall into a local minimum that results in a non-optimized model architecture and hyperparameter combination.

This work aims to characterize a new MD-EMG system for single-finger proportional control (See Fig. 1). In order to compare its performance against gold-standard bipolar gel derivations, we developed a framework to automatically optimize CNN and MLP architecture as well as hyperparameters. Optimization of the parameters is performed using a GA with both MD-EMG and gold-standard systems. In the case of MLP, a well-explored set of features is extracted and then selected by the GA.



Figure 1: Picture of the MD-EMG system. It consists of 64 monopolar electrodes placed around the forearm of the subjects.

2. Methods

Data recording and signal processing

In this study, two setups to record EMG signals are compared. The first one is a standard Noraxon DTS desk receiver connected to a Labjack data acquisition card used to wirelessly record 6 bipolar surface EMG derivations at 2kHz. Gel electrodes are placed evenly around the proximal part of the subjects' right forearms starting from the extensor digitorum muscle and rotating clockwise with reference electrodes placed distally (See Fig. 2.B left). For clarity, this setup will be called the low-density EMG system (LD-EMG). All channels are notch filtered at 50Hz and bandpass filtered between 15 and 500Hz. The second system is a homemade MD-EMG prototype designed with four elastic bands that attach around the whole forearm. Subjects were asked to place their forearm on the sleeve with their palm facing up. This system records 64 EMG monopolar channels with dry electrodes made of

Ag/AgCl that are connected to a g.HIAMP amplifier with a gel-based reference electrode placed over the elbow (See Fig. 2.B right). Signals are acquired at 2400Hz, notch filtered at 50Hz, and bandpass filtered between 5 and 500Hz.

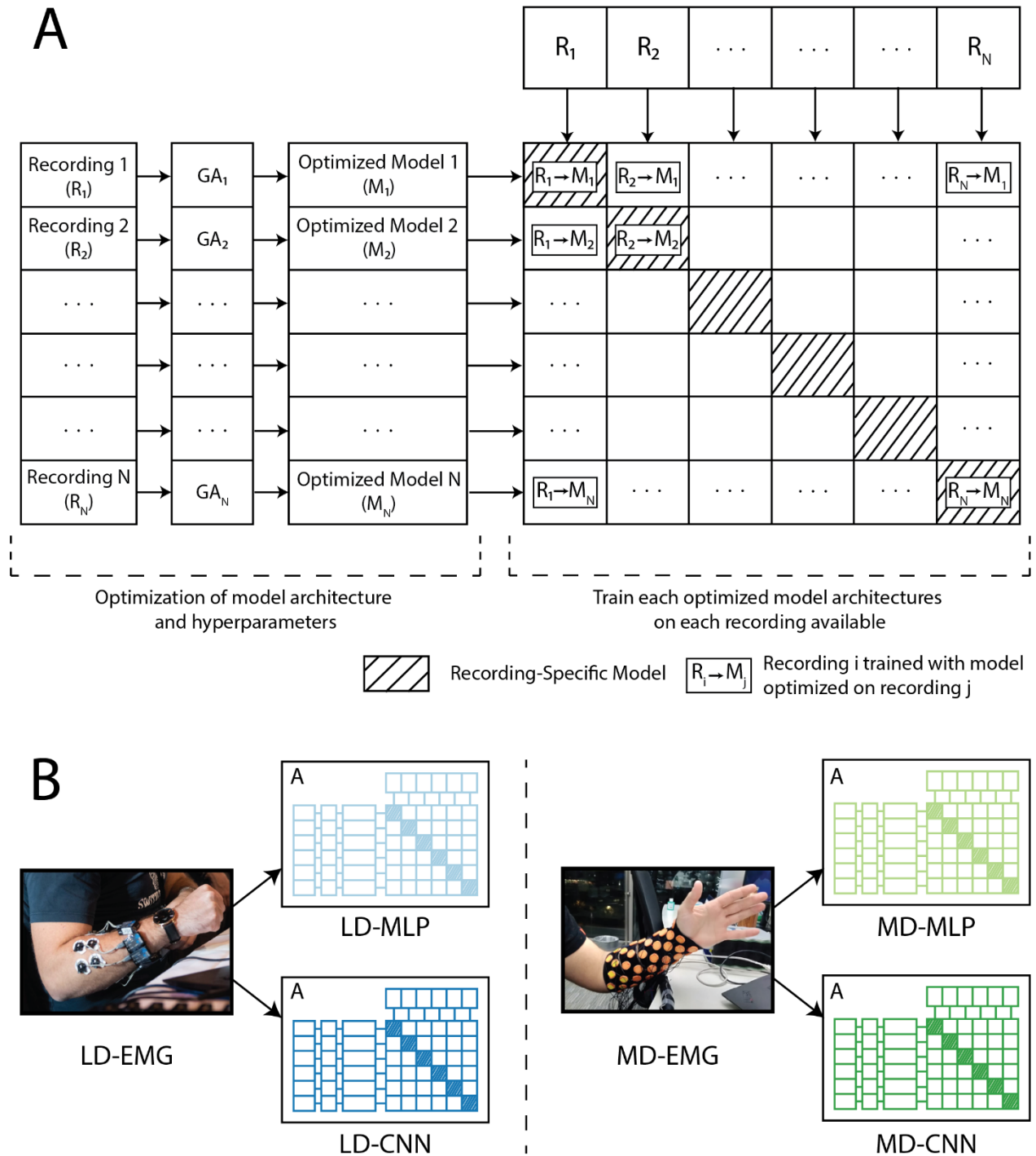


Figure 2: (A) Model optimization pipeline. For each recording, a genetic algorithm (GA) is used to find an optimized model architecture and model hyperparameters. Finally, each optimized model architecture and hyperparameters are trained on each recording. (B) The optimization pipeline described in (A) is performed for each EMG system (LD-EMG and MD-EMG) and each decoding approach (MLP and CNN).

Sixteen subjects were recruited for this experiment (8 Males and 8 Females, aged between 21 and 40 with an average of 25.5 ± 4.6). Nine of them used the LD-EMG system to record one or two sessions and eight were recruited to use the MD-EMG prototype as one subject performed the experiment with both EMG setups. In summary, 9 subjects performed a total of 15 recordings with the LD-EMG setup, and 8 subjects performed 14 recordings with the MD-EMG prototype.

Subjects were comfortably seated in a chair with their arm placed on a table. They are asked to follow a virtual hand shown on a screen performing a series of single and multi-finger opening and closing movements interspersed with resting phases (see Fig. 6 and Fig. 7 for the detailed sequence). Subjects are verbally instructed to slightly force during each movement and relax completely during the resting phases. The goal is to dissociate three main states of the fingers: resting position (when fingers are in a middle position), flexed, and opened positions. Each movement is held for 5 seconds and the resting phase between each movement lasted 3 seconds. The whole sequence was repeated six times and the recording is completed in 9 min and 30 seconds.

To synchronize EMG signals with hand kinematics, finger flexion angles are recorded from the virtual hand at 60Hz. From the 15 joint angles obtained from the virtual hand, six joint angles were selected corresponding to the metacarpophalangeal joint angle of each finger and the thumb's carpometacarpal joint angle for thumb opposition. All joint angles were rescaled between 0 (open) and 10 (close). Each recording is divided into three sets non-randomly. Indeed, the first 4 repetitions are used to train the model, the 5th is used to validate, and the last repetition is the test set. This non-random split was done to consider a real-world use case of an RPH where patients would use their prosthesis right after calibration and therefore the last repetition is the most suited to evaluate decoding performance on unseen data.

For each set, kinematic data is interpolated to match EMG sampling frequency and a sliding window is extracted with a length of 200ms and 150ms overlap which yields a window of shape (time x channels) depending on the sampling frequency and the number of channels. Hand kinematics at the end of each window is retrieved.

Machine learning approaches

In this study, two decoding approaches are compared. The first one is a standard EMG decoding approach with handcrafted features extracted to input an MLP versus a deep learning CNN-based approach that learns the features directly from the signal to regress the 6 finger angles. For the MLP approach with both the LD-EMG (LD_MLP) and the MD-EMG setup (MD_MLP), a set of time domain, as well as frequency domain features, are extracted for each window:

- Mean absolute value (MAV).
- Wavelength (WL): Cumulative length of the waveform over time.
- Maximum Absolute Value (MaxAV).
- Standard Deviation (STD).
- Zero Crossings (ZC): Number of times the signal crosses zero.
- Slope sign changes (SSC): Number of times the slope of the EMG signal changes signs.
- Root Mean Square (RMS).
- Log detector (LOG): $e^{\frac{1}{N} \sum_{i=1}^N \log(|x_i|)}$ where x_i is the EMG amplitude at time bin i .
- Frequency spectrums in each frequency bin between 7 and 12 Hz, 12-30, 30-50, 50-100, 100-150, and 150-400 Hz obtained from fast Fourier transform (7_12, 12_30, 30_50, 50_100, 100_150, 150_400).

In the CNN case with the LD-EMG setup (LD_CNN), similarly to (40), the windows are reshaped from the shape (400,6) to (50,48) to be able to create deeper networks with more pooling layers. On the other hand, with the MD-EMG setup (MD_CNN) the windows are kept in the original shape (480,64).

Model architecture and hyperparameters Optimization

For each recording, the model architecture and features selected (when applicable) are optimized with a GA (Fig. 2).

In the case of the CNN approach, we started from a VGG-like architecture (45), and the network shape is optimized by adjusting various parameters such as the number of convolutional layers before each average pooling layer (up to 3), the number of pooling layer (up to 3 for the LD-EMG system and 2 for the MD-EMG system), the pooling shape ([2,1], [2,2], [3,3] for both EMG systems and [4,4] was also possible for the LD-EMG setup) and the number of filters for each convolutional layer (16, 32, 64, 128). A batch-normalization layer follows each convolutional layer. Then, the number of fully connected layers (up to three layers) and the number of nodes for each layer (16, 32, 64) are also tuned. Apart from the architectural parameter, other hyperparameters are optimized such as the drop rate (0, 0.2, 0.5) as well as the L2 and L1 regularization rates (0, 1e-3, 0.1), the learning rate (0.1, 0.01, 0.001), the convolutional filter shape ([3,3], [5,5]) and the optimizer (Adam, RMSprop, batch gradient descent). The CNN networks are optimized with a batch gradient descent with a batch size of 32 samples, for 50 epochs, a step decay with a drop of $\frac{1}{2}$ every 10 epochs, and an early stopping if the validation loss did not decrease for more than 13 epochs.

For the MLP approach, the model is a multi-layer perceptron and, therefore, has fewer parameters to tune. For the architecture, the number of layers of MLPs is optimized (up to three layers), and the number of nodes for each layer (16,32,64,128,256). Hyperparameter values are the same as with the CNN case tuning only the drop rate, L2 and L1 regulation rates, the optimizer, and the learning rate. However, feature selection is an important process in order not to overfit the data. Therefore, the selection or not of any channel-feature combination was another hyper-parameter. The MLP was trained with a batch gradient descent with a batch size of 64 samples, with 50 epochs, and similarly to the CNN, a step decay with a drop of $\frac{1}{2}$ every 10 epochs with an early stopping if the validation loss did not decrease for more than 13 epochs. All the models were trained with a mean squared error loss (MSE).

To perform the GA, each hyper-parameter is encoded as a gene on a chromosome that could take one of the discrete possible values. The number of possible models for CNN models is approx. 10^6 and higher for MLPs as each combination of feature-channel could be selected or not. The fitness function is encoded as the validation loss of the trained model. A population of 20 random individuals is created and trained for 200 generations using a fitness proportionate (or roulette wheel) offspring selection method. The rate of mutation is set to 0.1 and the selection rate to 0.6. In summary, 4000 models were trained in each condition which equals 16000 models trained for the four conditions for each recording. In total, for the 29 recordings available, 464'000 models are trained. A High-Performance Computing cluster with Nvidia V100 GPUs is used to train all the models. The difference in hyperparameters between conditions is due to the amount of RAM available.

Model selection and generalizability

For each recording, the model with the lowest validation loss was selected. Each optimized model architecture was trained on each recording available 3 times locally on a Lenovo Extreme with an

Nvidia GeForce GTX 1050Ti GPU and the model with the lowest validation loss was selected to avoid falling in a local minimum (See Fig. 2).

After comparing the performance between conditions on recording-specific models (model architectures and hyperparameters optimized on a specific recording, striped models in Fig. 2), we assess the generalization performance of these optimized model architectures on other recordings.

To compare the performance of the different conditions, the coefficient of determination R^2 is extracted for each DoF decoded on the test set and used for the statistical analysis. The normality of variable distributions is assessed with the Shapiro–Wilk test such that parametric or non-parametric tests are used accordingly.

Model architecture and hyperparameters selected

To compare the different optimized models, several parameters are extracted from the architecture. In the CNN case, the number of trainable parameters is extracted before the flattening layer to remove the effect of the input shape and have a fair comparison between the two EMG systems. The number of embeddings is the output shape of the flattening layer and can be interpreted as the features extracted from the EMG signal whereas in the MLP case, the number of selected channel-feature combinations is extracted.

3. Results

Genetic Algorithm

The evolution of the training and validation loss across generations of the GA for each recording is shown in Fig. 3.A. The GA did not converge for one recording in the condition LD_MLP as well as for two recordings in both MD_CNN and MD_MLP. The recordings were therefore removed from the analysis. For the remaining recordings, a plateau in performance is reached at approx. 30-40 generations except in the case of the MD_CNN condition where there is a second drop in validation loss starting at generation 100.

The performance of the models selected (with the lowest validation loss) in each condition is shown in Fig. 3.B. A Kruskal-Wallis test shows a statistical difference between conditions ($H(3)=22.889$, $p<0.001$). Post-hoc tests show a difference between LD_MLP and both MD_MLP and MD_CNN conditions (Mann-Whitney test, $U=129.0$, $p<0.01$ and $U=141.0$, $p<0.001$ respectively) as well as between LD_CNN and both MD_MLP and MD_CNN (Student's T-test, $t(24)=4.19$, $p<0.001$ and $t(24)=4.74$, $p<0.001$ respectively).

In summary, the median validation loss is lower for the MD-EMG setup compared to the standard LD-EMG system. However, there is no statistical difference between the CNN and the MLP approaches.

Performance of selected models

Figure 4 shows the finger-averaged R^2 coefficient of recording-specific models in all conditions on the test set (Fig. 2.A striped models). There is a statistical difference between individual conditions (ANOVA, $F(3,47)=3.034$, $p<0.05$). Post-hoc tests show a significant difference in performance between LD_CNN and MD_MLP (Student's t-test, $t(24)=-2.418$, $p<0.05$) as well as between LD_CNN and MD_CNN (Student's t-test, $t(24)=-2.234$, $p<0.05$).

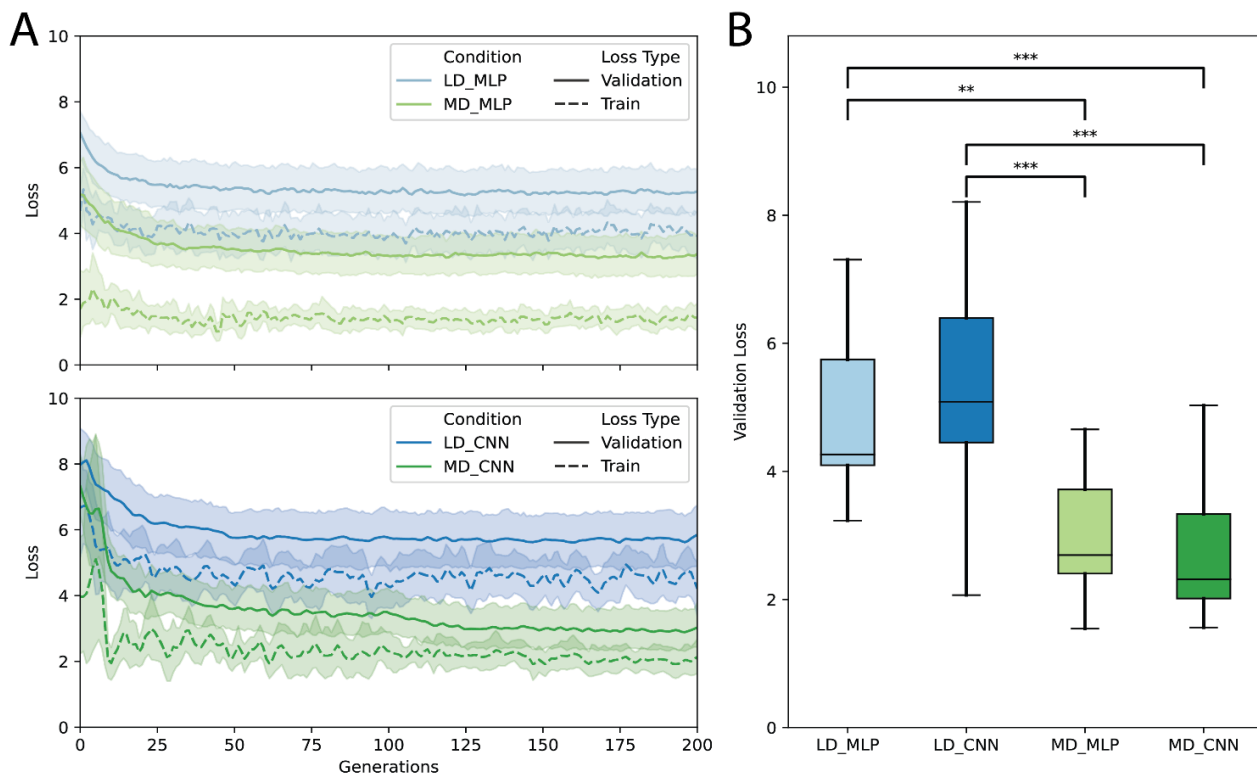


Figure 3: Genetic Algorithm results. (A) Training and Validation loss evolution of the best individual at each generation. Lines represent the average loss of all recordings and shadowed areas the standard deviation. (B) Boxplot of the validation loss obtained from the best-performing model for each condition.

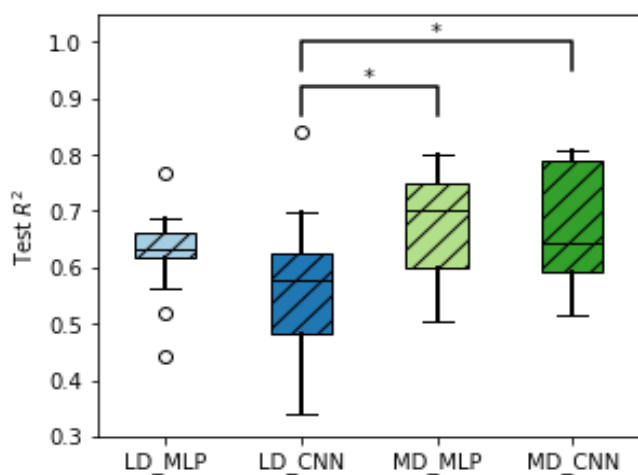


Figure 4: Boxplot of the finger-averaged coefficient of determination (R^2) on the testing set obtained from models with the lowest validation loss.

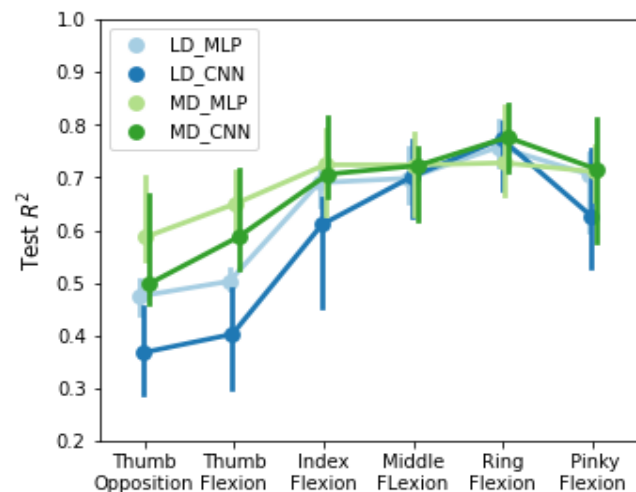


Figure 5: Single-finger performance in each condition. Circles represent medians and error bars represent 25% and 75% percentiles.

Figure 5 shows more precisely the differences between each finger, we observe that both decoding conditions with the MD-EMG setup are in general better at decoding thumb movements and index flexion but there is no difference for the other fingers (see Fig. S1 for detailed results and statistical analyses). Fig. 6 and 7 show the decoded joint flexions on the test set of a representative recording with the LD-EMG and the MD-EMG systems respectively. Heatmaps show the relative amplitude of the EMG envelopes averaged during each movement of the sequence with respect to the average resting activity.

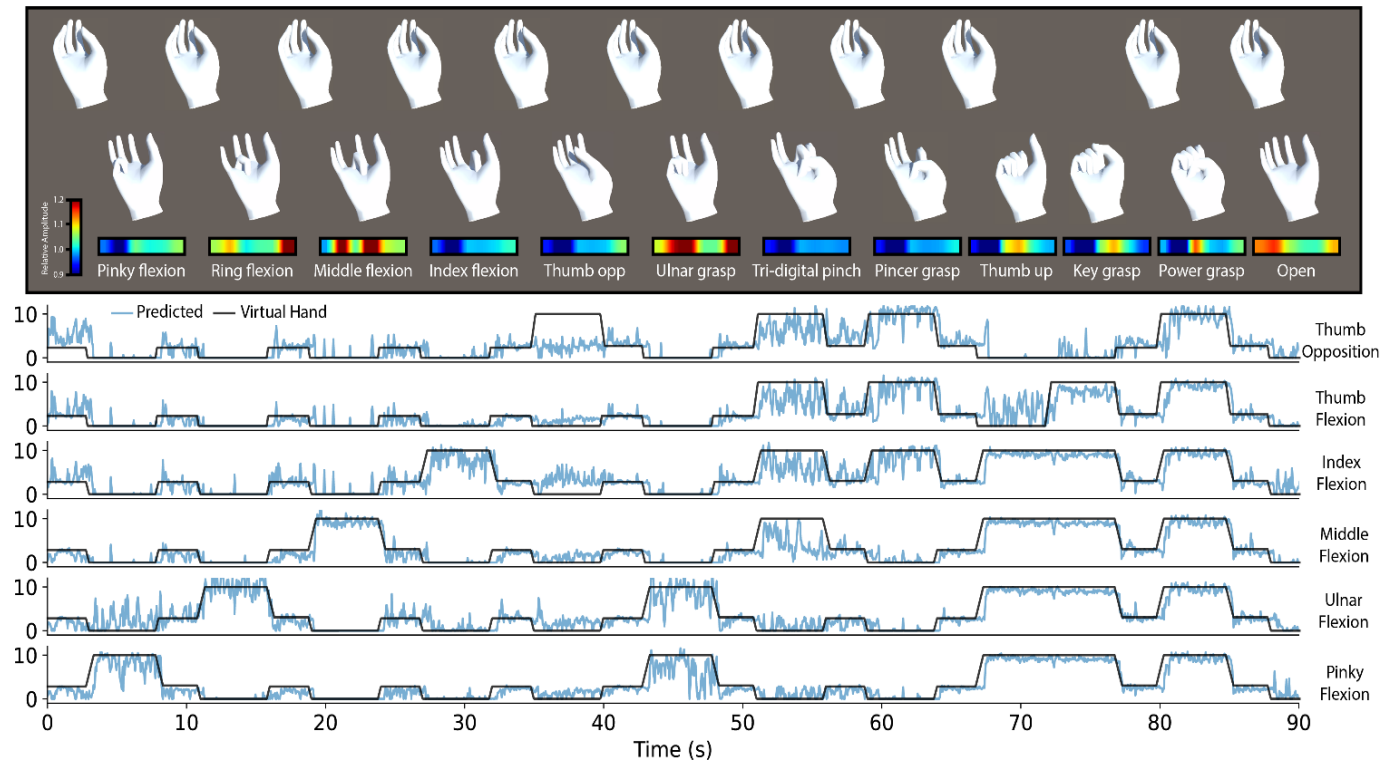


Figure 6: Virtual hand and predicted scaled finger angles on unseen data from a representative LD-EMG recording. Heatmaps are the average EMG signal envelope amplitude for each channel during each movement of the sequence with respect to the average activity during resting phases. The R^2 of this specific recording is equal to 0.71.

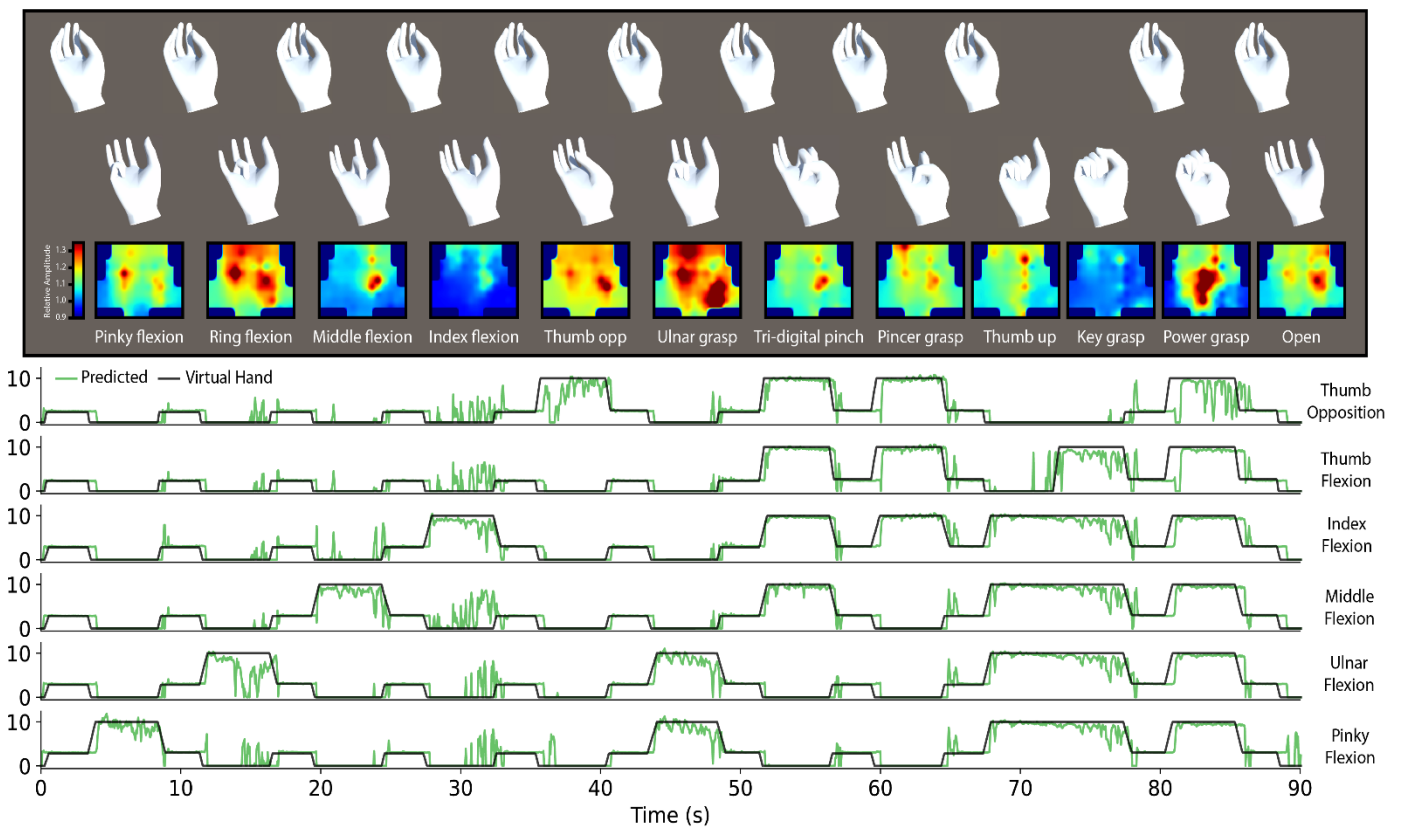


Figure 7: Virtual hand and predicted scaled finger angles on unseen data from a representative MD-EMG recording. Heatmaps are the average EMG signal envelope amplitude for each channel during each movement of the sequence with respect to the average activity during resting phases. The R^2 of this specific recording is equal to 0.79.

Inter-subject model architecture stability

For each recording, the performance of the recording-specific model architecture and hyperparameters is compared with the average of all the other architectures obtained with the GA in the other recordings. Finger averaged R^2 of all the available recordings is shown in Fig. 8. There is a statistical difference for the condition LD_MLP where the R^2 dropped by 0.09 between the GA-selected models and the ones obtained on other recordings. When looking at each recording individually, and comparing the value obtained with the recording-specific model versus all the other architectures obtained on the other recordings, this difference is significant for 13/13 recordings in the condition LD_MLP, 8/14 in the condition LD-CNN, 5/12 for MD_CNN and 3/12 for MD_MLP. The MD_MLP condition has the lowest proportion of recordings that obtained different performances with other optimized architectures and hyperparameters than the recording-specific one.

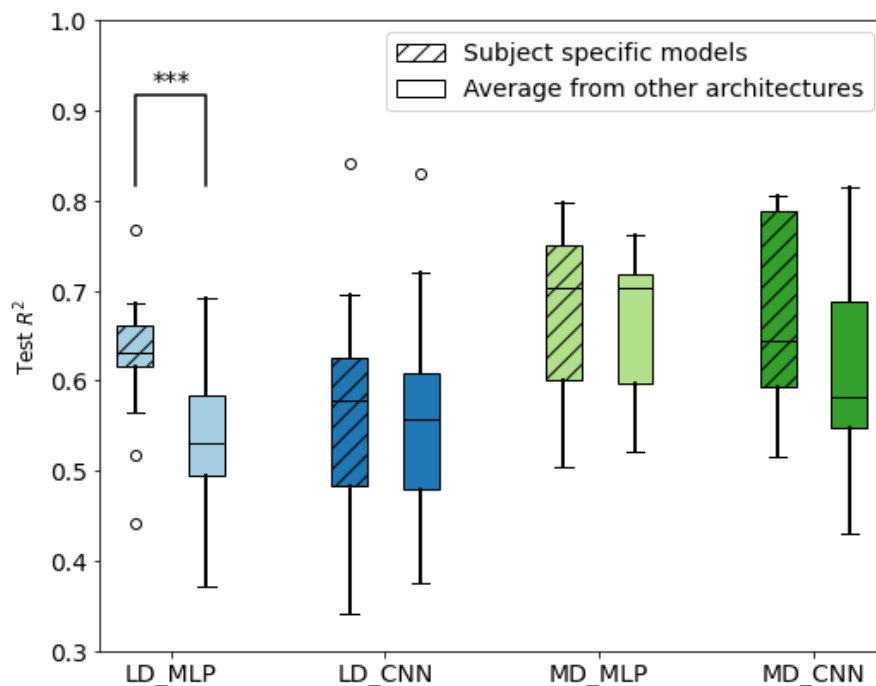


Figure 8: Finger-averaged R^2 between recording-specific model architecture (A) and the average of all other architectures (B).

Selected architectures and hyperparameters

A subset of the hyperparameters selected by the GA is shown in Fig. 9. There is no noticeable difference in CNN architectures between LD and MD EMG systems. Indeed, the number of trainable parameters in the convolutional layers of the CNNs is not different between LD and MD-EMG systems (Fig. 9.C) and the number of embeddings extracted in the CNN-based approach is not different between EMG systems (Fig. 9.A) whereas for the MLP approach the number of channel-feature combination is statistically different between the EMG systems (Fig. 9.B). However, when the ratio of features per channel is compared, there is no statistical difference with an average of 6.95 features selected over 14 possible features per channel. The number of fully connected layers is different between CNNs and MLPs with more layers in the latter case (Fig. 9.D) but the number of embeddings that inputs the fully connected layers in the CNN approach is at least one order of magnitude higher than the channel-features combinations selected. Fig. S2 shows the hyperparameters selected by the GA in each condition.

In the MLP case, features from all channels were selected equally in both EMG systems (Kruskal-Wallis, $H = 8.84$, $p = 0.12$ for LD-EMG and $H = 62.6$, $p = 0.49$ for MD-EMG). Some features were more selected than others for the LD-EMG system (Kruskal-Wallis, $H = 28.41$, $p < 0.01$). Post-Hoc analysis with the Mann-Whitney U test with a significance level of $p=0.01$ showed that WL and ZC features were more selected than SSC, 7_12, 12_30, and 30_50 frequency bins. There is no statistical difference for the MD-EMG system (Kruskal-Wallis, $H = 16.85$, $p = 0.21$). See supplementary Figures S3 and S4 for heatmaps showing the percentage of recording where each feature of each channel was selected.

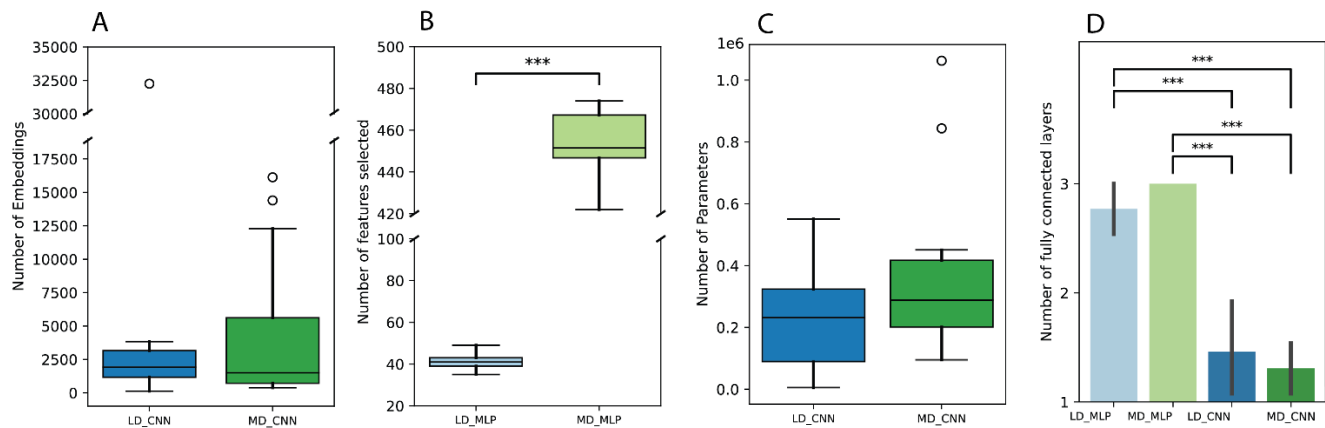


Figure 9: Model architecture overview. (A) shows the number of embeddings obtained after the flattening layer that is the input to the fully connected layers of the CNN. (B) shows the number of channel/features combination selected to input the MLP. (C) Number of trainable parameters in the convolutional part of the CNNs. (D) Number of fully connected layers selected by the genetic algorithm in each condition.

4. Discussion

In this study, we implemented a genetic algorithm to automatically optimize model architecture and hyperparameters for EMG decoding. This pipeline was used to compare the performance of a new MD-EMG system compared to a gold-standard gel-based LD-EMG system for simultaneous and proportional decoding of single-finger motion. We compared the performance obtained with CNNs using the raw signal as input and MLPs using automatically selected features as input for both EMG systems.

The results show that both decoding approaches with the MD-EMG system obtained better results than the LD_CNN condition (Fig. 4) and the difference is coming from thumb opposition, thumb flexion, and index flexion (Fig. S1). When looking at each DoF individually, there is a significant difference between LD_MLP and both MD-EMG conditions for thumb movements whereas the difference in the finger-averaged test loss is not significant.

While this difference could come from the higher forearm coverage, another important aspect is the generalizability of model architecture and hyperparameters as it removes the need to perform a GA for each new patient. Indeed, running a GA for each recording in each condition as it was done in this study is computationally heavy. The models and hyperparameters obtained from the GA could generalize to other recordings without significant performance drops except in the LD_MLP case (Fig. 8). Therefore, for the LD_CNN and both MD-EMG conditions, the GA could have been performed on one recording, and the resulting model used on all other recordings without changing the conclusions.

Therefore, our new MD-EMG system is more suitable for prosthesis control as it can obtain higher performance than LD-EMG systems and optimized architectures are generalizable between

recordings. The design of this MD-EMG system using dry electrodes is easy to wear on the forearm and does not require careful placement of the electrodes. Moreover, by changing the inter-electrode distance, its size can be adapted to different stump lengths in order to obtain maximum performance.

When examining in more detail the model differences between the conditions, we first see that there is no difference in model size (defined by the number of trainable parameters) on the convolutional layers between LD_CNN and MD_CNN conditions. There is a difference in the nature of the features extracted and the ones learned from the convolutional layers. Indeed, while approximately 7 features were selected per channel in both MLP cases, the number of embeddings obtained after the convolutional layers is at least one order of magnitude higher but is not different when the number of channels increases (Fig. 9). This could explain the architecture difference in the number of fully connected layers between CNNs where one fully connected layer is enough to obtain high performance and MLPs where the model has to combine non-trivially the features with 2 or 3 layers to regress finger angles. This result implies that simpler models such as linear discriminant analysis or support vector models might not be able to obtain optimal performance from carefully selected features. Therefore, we suggest that deep model architectures trained on a single recording should be compared with optimized MLPs if the aim is to improve decoding performance.

On the other hand, CNNs are known to require huge amounts of data in order to perform well. As datasets for EMG decoding cannot be recorded over thousands of hours on a single subject, another approach is to use transfer learning. By leveraging data acquired from many subjects, (46,47) showed an improvement in decoding performance with CNNs using transfer learning.

To conclude, we showed that our new MD-EMG system can outperform gold-standard gel-based EMG systems by decoding better thumb movements with a single optimization step and a simple placement of electrodes. In the case of upper limb amputation, this MD-EMG system can be tailored for different stump lengths and extract the maximum information to decode single finger movements proportionally. Finally, for single-finger proportional control, this VGG-like CNN approach is not outperforming more standard feature-based MLPs when model architectures, hyperparameters, and features are selected automatically with a GA.

Data availability statement

The data and code that support the findings of this study are available upon reasonable request.

References

1. McDonald CL, Westcott-McCoy S, Weaver MR, Haagsma J, Kartin D. Global prevalence of traumatic non-fatal limb amputation. <https://doi.org/10.1177/0309364620972258> [Internet]. 2020 Dec 4 [cited 2023 Feb 16]; Available from: <https://journals.sagepub.com/doi/10.1177/0309364620972258>
2. Belter JT, Segil JL, Dollar AM, Weir RF. Mechanical design and performance specifications of anthropomorphic prosthetic hands: a review. *J Rehabil Res Dev* [Internet]. 2013 [cited 2023 Mar 15];50(5):599–618. Available from: <https://pubmed.ncbi.nlm.nih.gov/24013909/>
3. Mendez V, Iberite F, Shokur S, Micera S. Current Solutions and Future Trends for Robotic Prosthetic Hands. <https://doi.org/10.1146/annurev-control-071020-104336> [Internet]. 2021 [cited 2021 Nov 8];4(1):595–627. Available from: <https://www.annualreviews.org/doi/abs/10.1146/annurev-control-071020-104336>
4. Maimon-Mor RO, Makin TR. Is an artificial limb embodied as a hand? Brain decoding in prosthetic limb users. *PLOS Biol* [Internet]. 2020 Jun 1 [cited 2023 Mar 15];18(6):e3000729.

- Available from: <https://journals.plos.org/plosbiology/article?id=10.1371/journal.pbio.3000729>
5. Merletti R, Muceli S. Tutorial. Surface EMG detection in space and time: Best practices. *J Electromyogr Kinesiol*. 2019 Dec 1;49:102363.
 6. Ferguson S, Ferguson S, Dunlop GR. Grasp Recognition from Myoelectric Signals. *Proc Australas Conf Robot Autom* [Internet]. 2002 [cited 2020 May 7]; Available from: <http://citeseerx.ist.psu.edu/viewdoc/summary?doi=10.1.1.227.4953>
 7. Martelloni C, Carpaneto J, Micera S. Classification of upper arm EMG signals during object-specific grasp. In: *Proceedings of the 30th Annual International Conference of the IEEE Engineering in Medicine and Biology Society, EMBS'08 - "Personalized Healthcare through Technology."* 2008. p. 5061–4.
 8. Kakoty NM, Hazarika SM. Recognition of grasp types through principal components of DWT based EMG features. In: *IEEE International Conference on Rehabilitation Robotics*. 2011.
 9. Castellini C, Van Der Smagt P. Surface EMG in advanced hand prosthetics. *Biol Cybern*. 2009 Jan 18;100(1):35–47.
 10. Atzori M, Cognolato M, Müller H. Deep learning with convolutional neural networks applied to electromyography data: A resource for the classification of movements for prosthetic hands. *Front Neurorobot*. 2016;10(SEP).
 11. Zardoshti-Kermani M, Wheeler BC, Badie K, Hashemi RM. EMG Feature Evaluation for Movement Control of Upper Extremity Prostheses. *IEEE Trans Rehabil Eng*. 1995;3(4):324–33.
 12. Tenore FVG, Ramos A, Fahmy A, Acharya S, Etienne-Cummings R, Thakor N V. Decoding of individuated finger movements using surface electromyography. *IEEE Trans Biomed Eng*. 2009;56(5):1427–34.
 13. Bhattachargee CK, Sikder N, Hasan MT, Nahid A Al. Finger Movement Classification Based on Statistical and Frequency Features Extracted from Surface EMG Signals. In: *5th International Conference on Computer, Communication, Chemical, Materials and Electronic Engineering, IC4ME2 2019*. Institute of Electrical and Electronics Engineers Inc.; 2019.
 14. Bhagwat S, Mukherji P. Electromyogram (EMG) based fingers movement recognition using sparse filtering of wavelet packet coefficients. *Sadhana - Acad Proc Eng Sci*. 2020 Dec 1;45(1):1–11.
 15. Atzori M, Gijssberts A, Muller H, Caputo B. Classification of hand movements in amputated subjects by sEMG and accelerometers. 2014 36th Annu Int Conf IEEE Eng Med Biol Soc EMBC 2014. 2014 Nov 2;3545–9.
 16. Jamal MZ, Lee DH, Hyun DJ. Real Time Adaptive Filter based EMG Signal Processing and Instrumentation Scheme for Robust Signal Acquisition Using Dry EMG Electrodes. 2019 16th Int Conf Ubiquitous Robot UR 2019. 2019 Jun 1;683–8.
 17. Searle A, Kirkup L. A direct comparison of wet, dry and insulating bioelectric recording electrodes. *Physiol Meas* [Internet]. 2000 May 1 [cited 2023 Mar 15];21(2):271. Available from: <https://iopscience.iop.org/article/10.1088/0967-3334/21/2/307>
 18. Phinyomark A, Scheme E. EMG Pattern Recognition in the Era of Big Data and Deep Learning. *Big Data Cogn Comput*. 2018 Aug 1;2(3):21.
 19. Hu Y, Wong Y, Wei W, Du Y, Kankanhalli M, Geng W. A novel attention-based hybrid CNN-RNN architecture for sEMG-based gesture recognition. *PLoS One*. 2018;13(10):1–18.
 20. Xia P, Hu J, Peng Y. EMG-Based Estimation of Limb Movement Using Deep Learning With Recurrent Convolutional Neural Networks. *Artif Organs*. 2018;42(5):E67–77.
 21. Dantas H, Warren DJ, Wendelken SM, Davis TS, Clark GA, Mathews VJ. Deep Learning Movement Intent Decoders Trained with Dataset Aggregation for Prosthetic Limb Control. *IEEE Trans Biomed Eng*. 2019 Nov 1;66(11):3192–203.
 22. Russakovsky O, Deng J, Su H, Krause J, Satheesh S, Ma S, et al. ImageNet Large Scale Visual Recognition Challenge. *Int J Comput Vis* [Internet]. 2015 Dec 1 [cited 2023 Mar 15];115(3):211–

52. Available from: <https://link.springer.com/article/10.1007/s11263-015-0816-y>
23. Park KH, Lee SW. Movement intention decoding based on deep learning for multiuser myoelectric interfaces. In: 4th International Winter Conference on Brain-Computer Interface, BCI 2016. Institute of Electrical and Electronics Engineers Inc.; 2016.
24. Du Y, Jin W, Wei W, Hu Y, Geng W. Surface EMG-based inter-session gesture recognition enhanced by deep domain adaptation. *Sensors (Switzerland)*. 2017;17(3):6–9.
25. Pizzolato S, Tagliapietra L, Cognolato M, Reggiani M, Müller H, Atzori M. Comparison of six electromyography acquisition setups on hand movement classification tasks. *PLoS One* [Internet]. 2017 Oct 1 [cited 2023 Mar 5];12(10). Available from: [/pmc/articles/PMC5638457/](https://pubmed.ncbi.nlm.nih.gov/25638457/)
26. Allard UC, Nougrou F, Fall CL, Gigù P, Gosselin C, Laviolette F, et al. A convolutional neural network for robotic arm guidance using sEMG based frequency-features [Internet]. [cited 2019 Oct 28]. Available from: <http://kinovarobotics.com/>
27. Boschmann A, Platzner M. Towards robust HD EMG pattern recognition: Reducing electrode displacement effect using structural similarity. In: 2014 36th Annual International Conference of the IEEE Engineering in Medicine and Biology Society, EMBC 2014. Institute of Electrical and Electronics Engineers Inc.; 2014. p. 4547–50.
28. Geng W, Du Y, Jin W, Wei W, Hu Y, Li J. Gesture recognition by instantaneous surface EMG images. *Sci Rep*. 2016;6(June):6–13.
29. Olsson AE, Sager P, Andersson E, Björkman A, Malešević N, Antfolk C. Extraction of Multi-Labelled Movement Information from the Raw HD-sEMG Image with Time-Domain Depth. *Sci Rep*. 2019;9(1):1–10.
30. Afsharipour B, Ullah K, Merletti R. Amplitude indicators and spatial aliasing in high density surface electromyography recordings. *Biomed Signal Process Control*. 2015 Aug 18;22:170–9.
31. Pan L, Zhang D, Jiang N, Sheng X, Zhu X. Improving robustness against electrode shift of high density EMG for myoelectric control through common spatial patterns. *J Neuroeng Rehabil* [Internet]. 2015 Dec 2 [cited 2023 Mar 4];12(1):1–16. Available from: <https://jneuroengrehab.biomedcentral.com/articles/10.1186/s12984-015-0102-9>
32. Stango A, Negro F, Farina D. Spatial Correlation of High Density EMG Signals Provides Features Robust to Electrode Number and Shift in Pattern Recognition for Myocontrol. *IEEE Trans Neural Syst Rehabil Eng*. 2015;23(2):189–98.
33. Meyers EC, Gabrieli D, Tacca N, Wengerd L, Darrow M, Friedenberg D. Decoding hand and wrist movement intention from chronic stroke survivors with hemiparesis using a user-friendly, wearable EMG-based neural interface. *medRxiv* [Internet]. 2021 Nov 12 [cited 2022 Dec 14];2021.09.07.21262896. Available from: <https://www.medrxiv.org/content/10.1101/2021.09.07.21262896v3>
34. Gazzoni M, Celadon N, Mastrapasqua D, Paleari M, Margaria V, Ariano P. Quantifying forearm muscle activity during wrist and finger movements by means of multi-channel electromyography. *PLoS One*. 2014 Oct 7;9(10).
35. Ting JE, Del Vecchio A, Sarma D, Verma N, Colachis SC, Annetta N V., et al. Sensing and decoding the neural drive to paralyzed muscles during attempted movements of a person with tetraplegia using a sleeve array. *J Neurophysiol* [Internet]. 2021 Dec 1 [cited 2023 Mar 15];127(1):2104–18. Available from: <https://journals.physiology.org/doi/10.1152/jn.00220.2021>
36. Hioki M, Kawasaki H. Estimation of Finger Joint Angles from sEMG Using a Neural Network Including Time Delay Factor and Recurrent Structure. *ISRN Rehabil*. 2012;2012:1–13.
37. Celadon N, Došen S, Binder I, Ariano P, Farina D. Proportional estimation of finger movements from high-density surface electromyography. *J Neuroeng Rehabil*. 2016;13(1):1–19.
38. Stapornchaisit S, Kim Y, Takagi A, Yoshimura N, Koike Y. Finger angle estimation from array EMG system using linear regression model with independent component analysis. *Front Neurorobot*. 2019 Sep 26;13:75.

39. Liu Y, Zhang S, Gowda M. NeuroPose: 3D hand pose tracking using EMG wearables. Web Conf 2021 - Proc World Wide Web Conf WWW 2021 [Internet]. 2021 Apr 19 [cited 2022 Jan 17];1471–82. Available from: <https://doi.org/10.1145/3442381.3449890>
40. Ameri A, Akhaee MA, Scheme E, Englehart K. Regression convolutional neural network for improved simultaneous EMG control. J Neural Eng [Internet]. 2019 Jun 1 [cited 2019 Jun 13];16(3):036015. Available from: <http://stacks.iop.org/1741-2552/16/i=3/a=036015?key=crossref.7403b6aa090d0e9a98378353d6dece0f>
41. Shin S, Tafreshi R, Langari R. A performance comparison of hand motion EMG classification. Middle East Conf Biomed Eng MECBME. 2014;353–6.
42. Kakoty NM, Hazarika SM, Gan JQ. EMG Feature Set Selection Through Linear Relationship for Grasp Recognition. J Med Biol Eng [Internet]. 2016 Dec 1 [cited 2023 Mar 15];36(6):883–90. Available from: <https://link.springer.com/article/10.1007/s40846-016-0188-y>
43. Bergstra J, Yoshua B. Random search for hyper-parameter optimization. J Mach Learn Res [Internet]. 2012 Feb 1 [cited 2023 Mar 15];13:281–305. Available from: <https://dl.acm.org/doi/10.5555/2188385.2188395>
44. Aquino-Brítez D, Ortiz A, Ortega J, León J, Formoso M, Gan J, et al. Optimization of Deep Architectures for EEG Signal Classification: An AutoML Approach Using Evolutionary Algorithms. Sensors 2021, Vol 21, Page 2096 [Internet]. 2021 Mar 17 [cited 2023 Mar 15];21(6):2096. Available from: <https://www.mdpi.com/1424-8220/21/6/2096/htm>
45. Simonyan K, Zisserman A. Very Deep Convolutional Networks for Large-Scale Image Recognition. 3rd Int Conf Learn Represent ICLR 2015 - Conf Track Proc [Internet]. 2014 Sep 4 [cited 2023 Mar 15]; Available from: <https://arxiv.org/abs/1409.1556v6>
46. Lehmler SJ, Saif-Ur-Rehman M, Tobias G, Iossifidis I. Deep transfer learning compared to subject-specific models for sEMG decoders. J Neural Eng [Internet]. 2022 Oct 20 [cited 2022 Nov 1];19(5):056039. Available from: <https://iopscience.iop.org/article/10.1088/1741-2552/ac9860>
47. Côté-Allard U, Fall CL, Drouin A, Campeau-Lecours A, Gosselin C, Glette K, et al. Deep Learning for Electromyographic Hand Gesture Signal Classification Using Transfer Learning. IEEE Trans Neural Syst Rehabil Eng. 2019;27(4):760–71.

2.3 EMG Data Augmentation for Grasp Classification Using Generative Adversarial Networks

Data augmentation techniques can play a crucial role in EMG decoding, particularly when employing DL approaches for more sophisticated, functional, and robust decoding algorithms. As deep models require large amounts of data to learn complex patterns and generalize well to unseen data, a large amount of data is necessary to potentially unlock the full potential of DL approaches. However, in practice, obtaining a sufficient quantity of EMG data can be both challenging and time-consuming. Data augmentation methods enable the generation of new, synthetic data points. This enriched dataset also improves the robustness of the deep learning models by introducing variability and simulating different real-world conditions. Consequently, data augmentation contributes to the enhancement of decoding performance, ultimately leading to more accurate and reliable control strategies for prosthetic hands. In this chapter, we investigate the possibility of using generative adversarial networks to obtain high-quality synthetic EMG data.

The content of this section is the postprint from the conference article Mendez, Lhoste et al., "EMG Data Augmentation for Grasp Classification Using Generative Adversarial Networks," 2022 44th Annual International Conference of the IEEE Engineering in Medicine & Biology Society (EMBC), Glasgow, Scotland, United Kingdom, 2022, pp. 3619-3622

Find the published article here: <https://doi.org/10.1109/EMBC48229.2022.9871625>

Personal contributions as the co-first author: conceived the experiments, prepared the protocols, recorded the data, formatted the figures, and wrote the manuscript

EMG Data Augmentation for Grasp Classification Using Generative Adversarial Networks

V. Mendez*, C. Lhoste*, S. Micera, *Fellow, IEEE*

Abstract

Electromyography (EMG) has been used as an interface for the control of robotic hands for decades but with the improvement of embedded electronics and decoding algorithms, many applications are now envisaged by companies. Deep learning has shown the possibility to increase decoding performance, but it requires large amounts of data to show its full capabilities. However, recording such amounts of EMG signals face several issues since recording hours of data from patients is very time-consuming and can result in muscle fatigue. We explore a deep learning data augmentation strategy using generative adversarial networks (GANs) to create high-quality synthetic data to increase the performance of grasp classification.

Clinical Relevance— This approach can increase the decoding performance of already existing decoding algorithms for patients with an amputation and suggests the possibility to increase the protection of personal data when recorded at a larger scale.

1. Introduction

Electromyography (EMG) has been used for decades for the control of commercial robotic prosthetic hands (RPHs) (1). However, patients were able to control only one degree of freedom (DoF) at the time with non-homologous muscle activity. Patients could cycle between different types of grasps using co-contraction of antagonist muscles or a smartphone app. Since a few years, some companies started to provide faster and more intuitive control of RPHs using pattern recognition methods that allow the patients to perform the intended grasp directly in a homologous way. This method is based on the extraction of discriminative features of the EMG signal that are used to train a classifier and identify the grasp intended by the patient. In the research literature, this approach showed high performance with accuracies up to 95% accuracy on 15 classes (2).

In 2012, deep learning revolutionized the field of image classification in the ImageNET competition beating by more than 10% all the competitors who used a standard approach with feature extraction (3). Therefore, researchers applied similar approaches to EMG signals and showed an increase in decoding performance (4). One of the main limitations of deep learning is the amount of data necessary to outperform standard approaches, for instance, the ImageNet dataset has more than 14M images. However, datasets with hours of patient recordings are not feasible due to sweat that changes electrode impedance and muscle fatigue. Such a dataset cannot be recorded over several days due to subject variability among recordings as well as electrode placement which is crucial for comparable recordings (5).

To tackle this issue, several groups showed the possibility to use transfer learning leveraging data acquired from several subjects to create a model that learns a general mapping of EMG signals which is then fine-tuned with a few repetitions of movements performed by the target subject. For instance, Fan

*Research supported by the Swiss National Competence Center for Research in Robotics, the Bertarelli foundation and CHRONOS project funded by the Swiss National Science Foundation. The first two authors contributed equally to this work.

V.M and S.M are with the Bertarelli Foundation Chair in Translational Neuroengineering, Centre for Neuroprosthetics and Institute of Bioengineering, School of Engineering, École Polytechnique Fédérale de Lausanne, Lausanne, Switzerland (Corresponding author: silvestro.micera@epfl.ch)

C. L. is pursuing his master degree at the École Polytechnique Fédérale de Lausanne, Lausanne, Switzerland

et al. (6) showed an increase in decoding accuracy using transfer learning from a database of healthy subjects to patients with an amputation

Another approach is to augment the dataset with synthetic data. Indeed, the combination of deep learning with data augmentation could increase decoding performances. For EMG signals, several techniques exist to increase the diversity of available data such as Gaussian noise addition, magnitude wrapping, wavelet decomposition or synthetic EMG models and can effectively improve decoding performance (7). To draw a parallel with images, such techniques could be seen as equivalent to classical image data augmentation techniques such as noise addition, flipping, rotation or contrast modification (8). On the other hand, deep learning approaches with generative adversarial networks (GANs) are capable of generating completely new synthetic images such as faces with different emotions to increase classification accuracy on underrepresented classes (9). However, despite the promising results with images, deep learning has not been widely investigated for EMG data augmentation. Only a few groups showed the possibility of improving classification accuracy with deep learning approaches. Bird et al. (10) showed a generative algorithm for EEG and EMG data using GPT-2, a transformer-based generator originally developed for text generation. They show a real-time increase in performance with EMG for a three-class decoding task. Campbell et al. (11) used a sinGAN and improved the classification of a six-class decoding task by creating several models for each repetition of each motion per subject. We focused on the model developed by Zanini et al. (12) for Parkinson's disease EMG data augmentation. The model is a deep convolutional GAN with an architecture that has been modified to capture more relevant features from EMG datasets. The discriminant model consists of four parallel convolutional pipelines that take as input the raw EMG signal, its frequency spectrum using FFT, FFT of the signal envelope as well as wavelet expansion that can extract essential features from EMG signals to perform movement classification.

Another important point has to be taken into consideration. While EMG was mainly used for RPHs, clinicians for diagnostic purposes or research for different robotic applications (1,12), with the improvement of decoding algorithms and power of embedded electronics, companies nowadays consider EMG as a potential interface to interact with computers for games, keyboard typing that could be used by the general public. Personal data anonymization is a key aspect of research and medical environments and should be preserved when such technologies will hit the market. One application of GANs could be the anonymization of biometric data to allow data sharing (13).

In this work, using the same model architecture as in (12), we train a deep convolutional GAN on a simple grasp classification dataset as a first step to create high-quality synthetic EMG data and augmenting a dataset for grasp classification. We report differences in classification accuracy with the addition of synthetic data as well as a close analysis of the amount of generated data necessary. We also investigate whether using only generated data is suitable for this task.

2. Methods

A. EMG recording and pre-processing

EMG signal from one healthy subject (Male, 26 years old) was recorded for this study. Ethical approval was obtained from the cantonal ethical committee of Vaud and the subject signed informed consent. EMG signals were recorded at 2kHz using a Noraxon Delsys system connected to a LabJack data acquisition card to record six bipolar electrode channels placed uniformly around the subject's forearm. During acquisition, the EMG signal is amplified and filtered with a notch filter at 50Hz and a bandpass filter between 15-500Hz. To synchronize EMG signals with hand gestures, the subject was asked to follow a virtual hand performing different finger gestures and hold for five seconds; the sequence of movement was repeated five times. In order to reduce synchronization issues between EMG and kinematics, the first second of each grasp was removed to train the GAN. We focused on three types of movements recruiting different sets of muscles: Power grasp, 2-digit pincer grasp, pinky finger closing and rest. For classification, the three first repetitions were considered as the training set while the fourth repetition was used as the validation set and results are reported on the last repetition which is the test set.

B. Generation of synthetic EMG data

Using the model from (12), trained for each of the 6 channels and each class was evaluated for a total of 24 models trained. Each GAN was trained to generate one second of synthetic data using a sliding window of one second of EMG signal with a moving step of one sample. The GAN models were trained on one, two or three repetitions to detect any change in the quality of the generated samples. When using multiple repetitions of movements that are not continuous in time, the sliding window was computed separately on trials.

The discriminative part of the GAN gave more weight to the frequency domain of the EMG signal than the time domain. Therefore, scaling could be an issue when generating different types of grasps separately, as the different models could not learn their relative range of values. Hence, the synthetic data, once generated, was rescaled in order to obtain the same standard deviation of the train set.

C. Synthetic EMG signal validation

To assess synthetic data quality and to quantify the effect of adding generated data for a grasp classification task, we chose a set of seven well-explored features: Mean Absolute Value (MAV), Waveform Length: Cumulative length of the EMG waveform over time (WL), Maximum Absolute Value (MaxAV), Standard Deviation (STD), Root Mean Square of the EMG signal (RMS), Zero Crossings: Number of times the signal crosses zero (ZC) and Slope Sign Changes: Number of times that the slope of the EMG signal changes sign (SSC).

These features were computed on windows of 250ms with a moving step of 25ms (225ms overlap) to train a multi-layer perceptron (MLP) for grasp classification. The extracted features of the EMG signal and the generated data were standardized based on the train set.

Three conditions were compared: the baseline where the MLP was trained using EMG signal only, the generated condition where the MLP was trained using only synthetic data and the combined condition where a combination of EMG signal and synthetic data was used for training. In the second and third conditions, different amounts of generated data are compared. Then, the classification accuracies of the three conditions are reported on the test set which consists of true EMG signal only. Each training was performed 10 times and mean accuracy is reported with standard deviation.

The MLP is composed of three layers (7 features input per channel, 350 nodes, 50 nodes, 4 classes output). ReLU activation function was used for the first two layers and SoftMax for the last one. Each MLP was trained with a batch size of 16 samples, with 50 epochs, a step decay with a drop of $\frac{1}{2}$ every 10 epochs with an early stopping if the validation loss did not decrease for more than 13 epochs. The models were trained with a cross-entropy loss (categorical cross-entropy), using an Adam optimizer.

3. Results

The first part of the analysis is performed on one GAN only, therefore on one channel, one class and the whole train set (three repetitions of movements) to assess the quality of the generated signals. Then, the analysis is focused on GANs from the same channel for all classes to assess performance differences with the addition of generated data. The quality of generated data is also compared when trained with one, two or three repetitions of movements. Finally, all GANs are used to train a model for grasp classification with the whole train set.

Due to the non-normality of feature distribution (tested with a Shapiro-Wilk test), a Mann-Whitney U test was performed to compare the distribution of features of generated data and true data. Out of the 24 GANs trained, only 5 produced a similar distribution for at least one feature. Altogether, out of 168 feature distributions compared (24 GANs*7 features), the null hypothesis could not be rejected for 10 distributions.

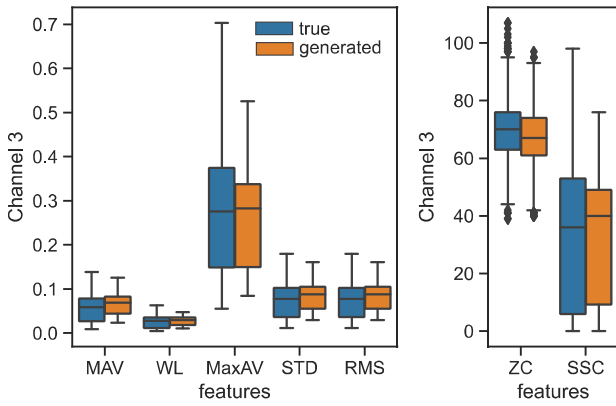


Figure 1. Distribution of features extracted from EMG signal (true) and synthetic data (generated) for one channel and all classes with the whole train set.

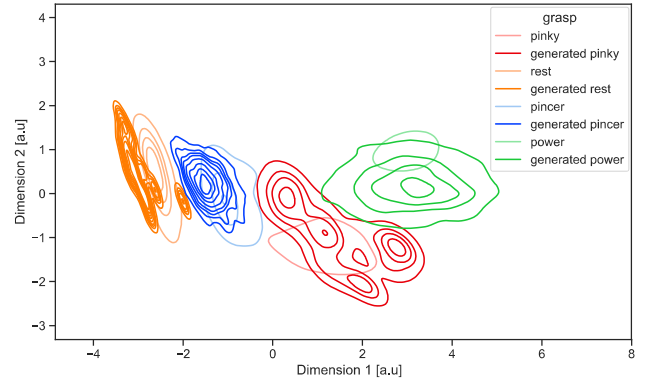


Figure 2. Two first components extracted from PCA on the EMG signal of one channel for all classes with the whole train set. Generated data was transformed with the same covariance matrix used for the true EMG signal. For clarity, Gaussian kernel density estimates are shown.

Figure 1 shows the distribution of the extracted features on EMG signals and synthetic data for all classes. A Mann-Whitney U test was also performed mixing all classes and showed that the distributions of each feature are also different ($p < 0.05$). Therefore, a PCA was performed to visualize the seven features of one EMG channel in 2D for all classes and retained 97% of the variance. Generated data was transformed with the same covariance matrix and is shown in figure 2 together with the true EMG signal.

Regarding the classification task with one EMG channel, as shown in figure 3, the baseline accuracy of the classification task increased from one to two repetitions of movements from 0.56 (std=0.04) to 0.70 (std=0.16) (Welch's test, $p < 0.05$), but not from two to three repetitions (Welch's test, $p = 0.062$). On the other hand, the best classification accuracy obtained with generated data increased when the number of repetitions increased (12000, 1250 and 8000 generated samples respectively, Welch's test, $p < 0.05$). The condition with generated data is higher than baseline when the GAN is trained with three repetitions with an accuracy of 0.76 (Welch's test, $p < 0.05$). With three repetitions, generated data alone has a higher test accuracy than the combined condition (Welch's test, $p < 0.05$).

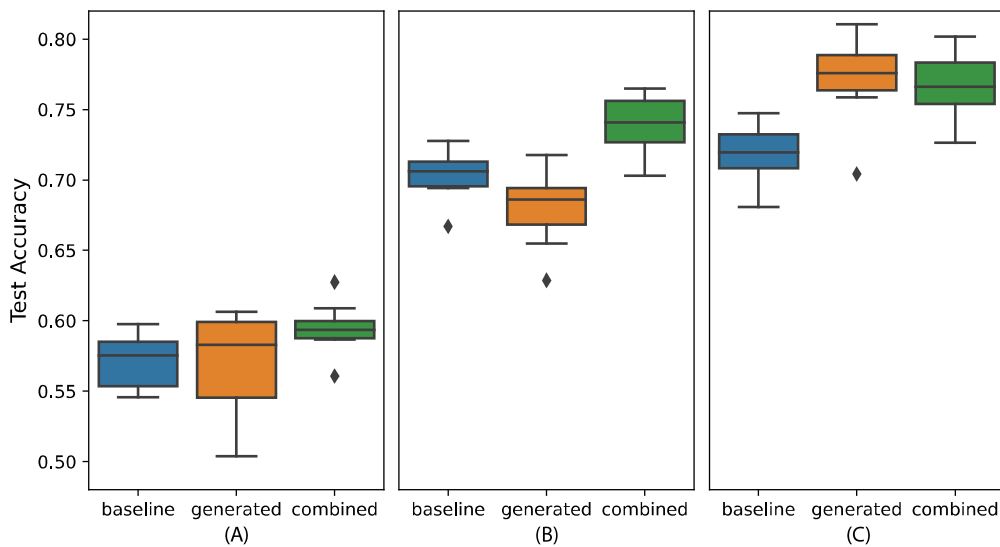


Figure 3. Boxplots of the accuracy obtained for the three conditions with (A) one repetition of the movements, (B) two repetitions and (C) the whole train set. Generated and combined accuracy values are obtained with the optimal amount of generated data.

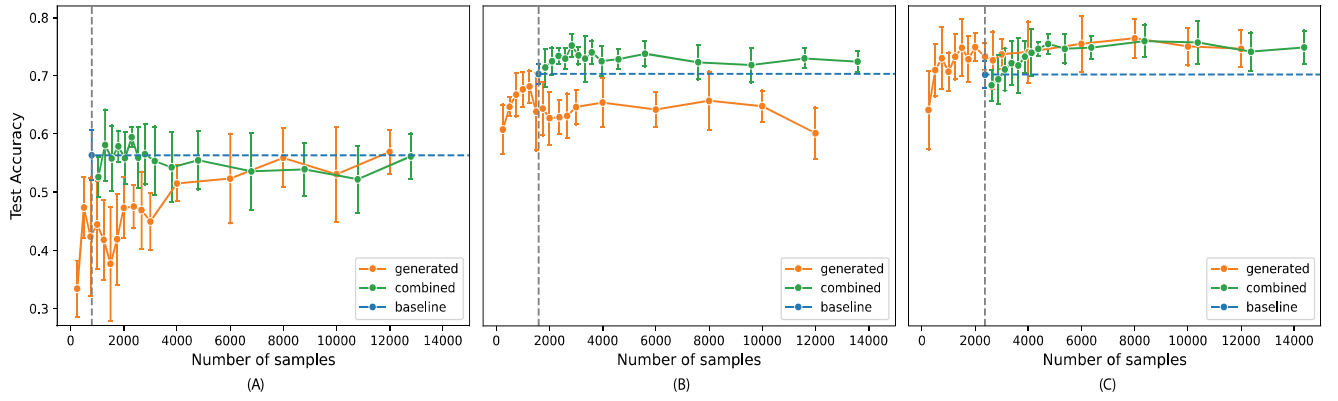


Figure 4. Evolution of the accuracy with respect to the number of samples used during training for the three conditions with (A) one repetition of the movements, (B) two repetitions and (C) the whole train set.

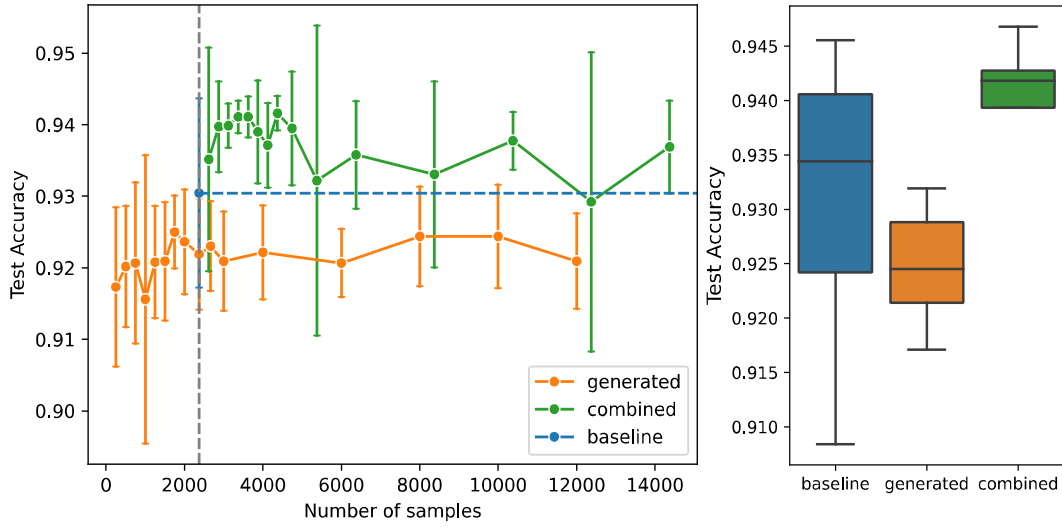


Figure 5. (Left) Evolution of the accuracy with respect to the number of samples used during training for the three conditions with all channels on the whole train set. (Right) Boxplots of the accuracy obtained for the three conditions. Generated and combined accuracy values are obtained with the optimal amount of generated data.

The combination of EMG signal and synthetic data showed an increase between one and two repetitions and between two and three repetitions (Welch's test, $p < 0.05$). The evolution with respect to the amount of generated data added in the train set is shown in figure 4.

With all the channels, the baseline condition has an average accuracy of 0.93 (See figure 5). Nevertheless, with all channels, the condition with generated data only is not different from baseline (1748 generated samples, Welch's test, $p = 0.248$). However, the combined condition (mean = 0.942) with 4400 generated samples is higher than the baseline (Welch's test, $p < 0.05$).

4. Discussion

This work aimed at generating synthetic data to increase performances on a grasp classification task. As highlighted in figure 2, the generated data distribution is different from the true EMG signals. However, new plausible generated data can add additional variability to the input dataset and increase performance on unseen samples.

We show in figure 3 that with enough training data, the combination of true features with the right amount of generated data can increase classification accuracy. While the gain in accuracy with one channel is on average 4.9%, the difference with all channels is relatively smaller (1.1%). This result

could have several explanations. Indeed, the baseline accuracy with all channels is already at 93.5% and the small improvement with generated data could be due to a ceiling effect. The other factor comes from the fact that all GAN models were trained independently for each channel and cannot grasp the relationship between channels when generating new samples.

Therefore, a potential improvement would be to design a new GAN architecture capable of generating several channels at once. Other types of models like RNNs specifically tailored to this application could better catch the time evolution of EMG signals. Moreover, such models could be developed for regression that allows more intuitive control of RPHs (1). However, there are only a few examples of GANs developed for regression problems (14). When trained with one channel and three repetitions, the performance of the generated condition is similar to the combined condition and can therefore be used to train a classifier without using any true EMG data. This result suggests that generated synthetic data could be a solution to legal and ethical issues of biometric data privacy and use by companies at large scale (13).

5. Conclusion

To conclude, this preliminary work showed the possibility to increase the decoding performance of a simple classification task with a focus on the amount of generated data necessary. For future development, more grasps should be added to have a functionally relevant setup for RPH control. Other model architectures (RNNs) should be investigated especially for the generation of synthetic data for regression tasks. Moreover, this approach can be combined with deep convolutional networks to perform classification and transfer learning since deep networks increase greatly their performances with more data. Finally, the results have to be confirmed with patients with amputation in a long-term analysis to assess robustness to electrode shift, sweat or muscle fatigue which are among the main factors that limit the application of such techniques outside of lab settings.

References

1. Mendez V, Iberite F, Shokur S, Micera S. Current Solutions and Future Trends for Robotic Prosthetic Hands. <https://doi.org/10.1146/annurev-control-071020-104336> [Internet]. 2021 [cited 2021 Nov 8];4(1):595–627. Available from: <https://www.annualreviews.org/doi/abs/10.1146/annurev-control-071020-104336>
2. Bhagwat S, Mukherji P. Electromyogram (EMG) based fingers movement recognition using sparse filtering of wavelet packet coefficients. *Sadhana - Acad Proc Eng Sci*. 2020 Dec 1;45(1):1–11.
3. Krizhevsky A, Sutskever I, Hinton GE. ImageNet Classification with Deep Convolutional Neural Networks. *Adv Neural Inf Process Syst* [Internet]. 2012 [cited 2022 Jan 20];25. Available from: <http://code.google.com/p/cuda-convnet/>
4. Xia P, Hu J, Peng Y. EMG-Based Estimation of Limb Movement Using Deep Learning With Recurrent Convolutional Neural Networks. *Artif Organs*. 2018;42(5):E67–77.
5. Ameri A, Akhaee MA, Scheme E, Englehart K. A Deep Transfer Learning Approach to Reducing the Effect of Electrode Shift in EMG Pattern Recognition-based Control. *IEEE Trans Neural Syst Rehabil Eng* [Internet]. 2019 [cited 2020 Jan 6];1–1. Available from: <https://ieeexplore.ieee.org/document/8943097/>
6. Fan J, Jiang M, Lin C, Li G, Fiaidhi J, Ma C, et al. Improving sEMG-based motion intention recognition for upper-limb amputees using transfer learning. *Neural Comput Appl* [Internet]. 2021 Jul 25 [cited 2022 Jan 20];1–11. Available from: <https://link.springer.com/article/10.1007/s00521-021-06292-0>
7. Tsinganos P, Cornelis B, Cornelis J, Jansen B, Skodras A. Data augmentation of surface electromyography for hand gesture recognition. *Sensors (Switzerland)* [Internet]. 2020 Sep 1 [cited 2021 Mar 26];20(17):1–23. Available from: [/pmc/articles/PMC7506981/](https://pubmed.ncbi.nlm.nih.gov/347506981/)

8. Shorten C, Khoshgoftaar TM. A survey on Image Data Augmentation for Deep Learning. *J Big Data* [Internet]. 2019 Dec 1 [cited 2022 Jan 20];6(1):1–48. Available from: <https://link.springer.com/articles/10.1186/s40537-019-0197-0>
9. Zhu X, Liu Y, Li J, Wan T, Qin Z. Emotion Classification with Data Augmentation Using Generative Adversarial Networks. *Lect Notes Comput Sci (including Subser Lect Notes Artif Intell Lect Notes Bioinformatics)* [Internet]. 2018 Jun 3 [cited 2022 Jan 20];10939 LNAI:349–60. Available from: https://link.springer.com/chapter/10.1007/978-3-319-93040-4_28
10. Bird JJ, Pritchard M, Fratini A, Ekart A, Faria DR. Synthetic Biological Signals Machine-Generated by GPT-2 Improve the Classification of EEG and EMG through Data Augmentation. *IEEE Robot Autom Lett*. 2021 Apr 1;6(2):3498–504.
11. Campbell E, Cameron JAD, Scheme E. Feasibility of Data-driven EMG Signal Generation using a Deep Generative Model. *Proc Annu Int Conf IEEE Eng Med Biol Soc EMBS*. 2020 Jul 1;2020-July:3755–8.
12. Zanini RA, Colombini EL. Parkinson's disease EMG data augmentation and simulation with DCGANs and style transfer. *Sensors (Switzerland)*. 2020 May 1;20(9).
13. Yoon J, Drumright LN, Van Der Schaar M. Anonymization through data synthesis using generative adversarial networks (ADS-GAN). *IEEE J Biomed Heal Informatics*. 2020 Aug 1;24(8):2378–88.
14. Rezagholiradeh M, Haidar MA. Reg-Gan: Semi-supervised learning based on generative adversarial networks for regression. *ICASSP, IEEE Int Conf Acoust Speech Signal Process - Proc*. 2018 Sep 10;2018-April:2806–10.

2.4 Optimizing setup and usability for potential home-based applications

The existing dichotomy between cutting-edge EMG decoding research in lab settings and the relatively simple commercially available solutions highlights the need to translate advanced techniques into practical applications for patients' daily use. To bridge this gap, it is essential to develop solutions that are not only effective but also accessible and easy to use for patients at home. This can be achieved by developing more user-friendly calibration procedures and leveraging robust data processing techniques that can account for the variability in real-world conditions.

The following section outlines preliminary results from three approaches aiming to bring single-finger proportional control at home for patients. The first subsection focuses on markerless kinematic tracking, the second subsection explore the use of transfer learning to reduce calibration time, and finally, a real-time training framework is presented for the instantaneous generation of decoding models.

2.4.1 Simple finger angle acquisition with markerless angle extraction

The content of this section is a preliminary analysis adapted from the poster sent to Society for Neuroscience (SfN) in 2022: Mendez et al., "A Framework for Markerless Wrist and Finger Angle Extraction from a single webcam for EMG-based Proportional Control of robotic prosthetic hands", poster, Society for Neuroscience 2022, San Diego, CA, November 12–16, 2022

Personal contributions as the first author: conceived the experiments, prepared the protocols, recorded the data, formatted the figures, prepared and presented the poster.

Up to this section, EMG signals and hand movements were synchronized by asking the participants to mimic the movements of a virtual hand. However, proportional control requires precise calibration data from the recorded subject. In addition to the inherent delay between the virtual hand and the subject's motion, the subject may occasionally become distracted, leading to a non-linear delay throughout the entire recording. This ultimately reduces the quality of the calibration data. As this approach is a good trade-off for persons with a bilateral amputation, for persons amputated on only one arm, we could leverage the synchronous movements of both hands to synchronize EMG signals with intended motions. To achieve the most intuitive control of these sophisticated RPHs, EMG-based proportional control is essential, necessitating precise angle extraction for the calibration of decoding algorithms. Many groups showed the possibility to record hand kinematics on able-bodied subjects as well as amputated patients using kinematic gloves or motion capture systems. However, kinematic gloves are bulky, expensive, and fragile while motion capture systems using markers require a full setup that cannot realistically be used at home by patients due to their complexity and

price. In response to these challenges, recent developments have focused on markerless pose estimation software solutions that leverage one depth camera or multiple cameras to provide a more accessible and cost-effective alternative for angle extraction and calibration of RPHs in real-world settings. Nonetheless, depth cameras or calibrated systems with several cameras are not available everywhere.

In this section, we investigate the performance of MediaPipe, a markerless kinematic tracking library capable of inferring 21 3D landmarks on a hand from a single camera. This approach has the advantage of being usable with a smartphone to re-calibrate the prosthesis anytime, anywhere. From these landmarks, we extracted five finger flexion angles and the thumb opposition angle, resulting in a total of 6 degrees of freedom (DoFs). With a brief 5-second calibration to obtain the orientation of the subject's forearm, wrist flexion and pronation angles were also obtained from MediaPipe (see Figure 1) and compared to accurate angles from two IMU sensors placed on the back of the hand and the elbow for reference. This process allowed us to develop a framework for easily calibrating an EMG-based single-finger proportional decoder using a single webcam, predicting a total of 8 DoFs.

To demonstrate the feasibility of this approach, one able-bodied subject was recruited for the study. Seven wireless bipolar EMG channels were placed uniformly around the subject's forearm. The subject was instructed to follow a video of a person performing grasp and wrist gestures, repeating the sequence of movements six times. The first four repetitions were used to train a multi-layer perceptron (MLP), the fifth repetition as a validation set for early stopping, and the final repetition to evaluate the performance of the model.

Seven well-explored features (MAV, WL, MaxAV, STD, RMS, ZC, and SSC) were extracted using a sliding window of 200ms with a 170ms overlap to train the MLP. The EMG signal features were standardized based on the train set.

Wrist Angle Extraction: IMU vs MediaPipe

The angles obtained from IMUs represent the difference between the angles measured by the hand and elbow IMUs. Overall, wrist angles are accurately approximated using this approach (Figure 2). The pronation angle derived from MediaPipe is found to be more correlated to the IMU angles ($R^2=0.77$) than the flexion angle ($R^2=0.54$). This result suggests that MediaPipe provides a reliable method for approximating wrist angles, particularly for pronation, offering a viable alternative to traditional IMU-based methods.

EMG Decoding

The finger angles were predicted with an average coefficient of determination (R^2) of 0.80 (Figure 3), while the wrist angles achieved an average R^2 of 0.72 (Figure 4). To enhance clarity, the testing set predictions were post-processed using an 11-point moving median filter (330ms). This post-processing technique can be easily applied in real-time settings,

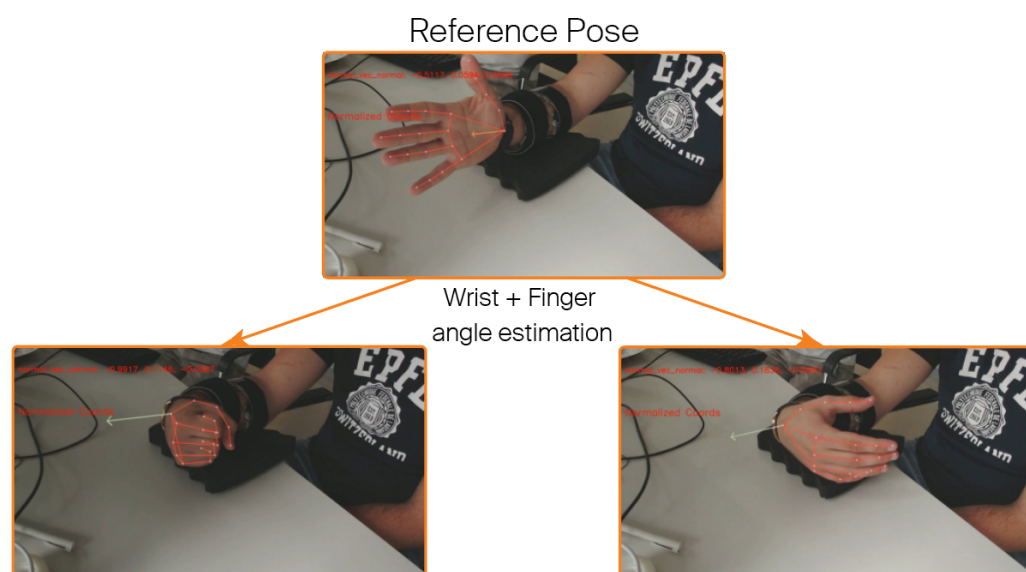


Figure 1. Illustration of the wrist and finger angles obtained from MediaPipe. Finger angles could be obtained from MediaPipe without calibration, as they are defined by hand landmarks. Wrist angles, on the other hand, were determined by the difference in pose relative to a reference pose, requiring the subject to maintain a consistent forearm orientation throughout the session.

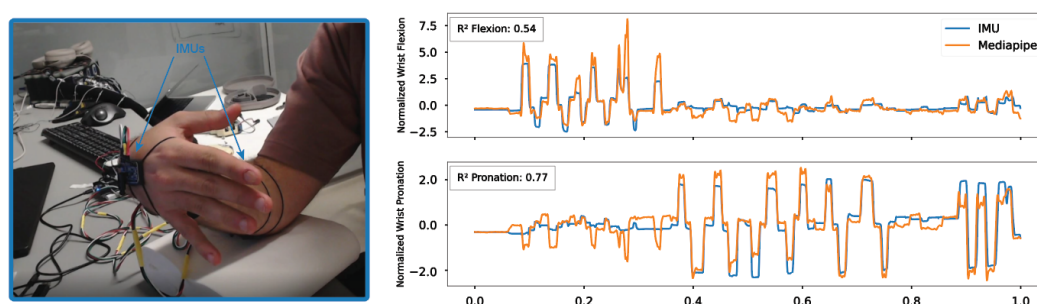


Figure 2. (Left) Position of IMUs to extract the wrist pronation/supination and flexion/extension angles. (Right) Normalized angles extracted from IMUs and MediaPipe.

with the drawback of increased delay. These results suggest that the proposed method offers a reasonably high level of accuracy in predicting both finger and wrist angles, making it a promising approach for EMG-based decoding applications.

The proposed framework demonstrated promising results for simultaneous and proportional decoding of wrist and finger angles, and it could be tested on patients with amputations if they perform synchronized and mirrored movements with their healthy and phantom hands. With the extraction of 21 landmarks on the hand, more degrees of freedom could be determined as RPHs continue to advance in complexity. Although this approach may not be as precise as more complex tracking solutions, it enables high-quality decoding and a straightforward calibration procedure that patients can easily perform daily at home. Ultimately, by gathering data across multiple days and employing deep learning techniques, decoding accuracy could be further improved, enhancing the overall effectiveness of this approach.

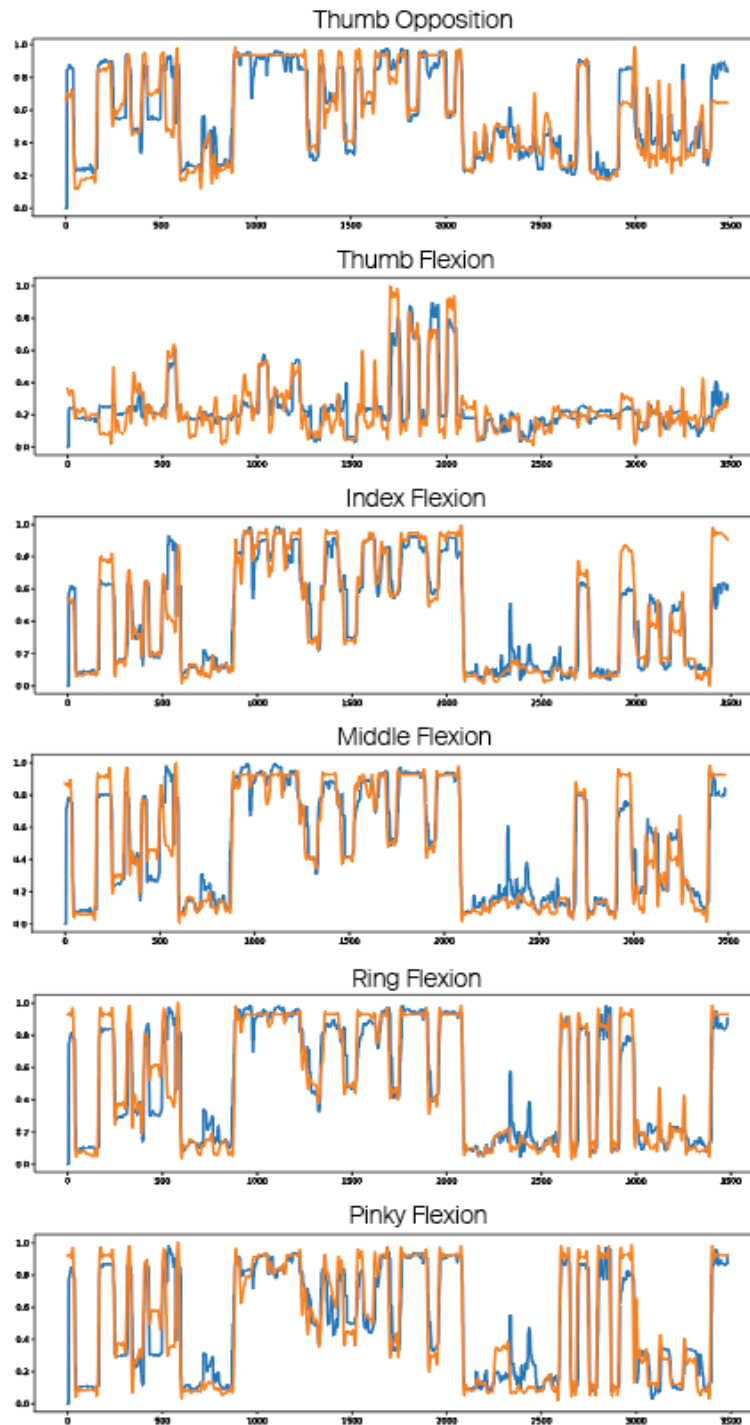


Figure 3. Plot of the predicted finger angles from EMG signals (Blue) vs. target angles obtained from MediaPipe (orange) on the test set. The average R^2 for all the fingers is 0.80.

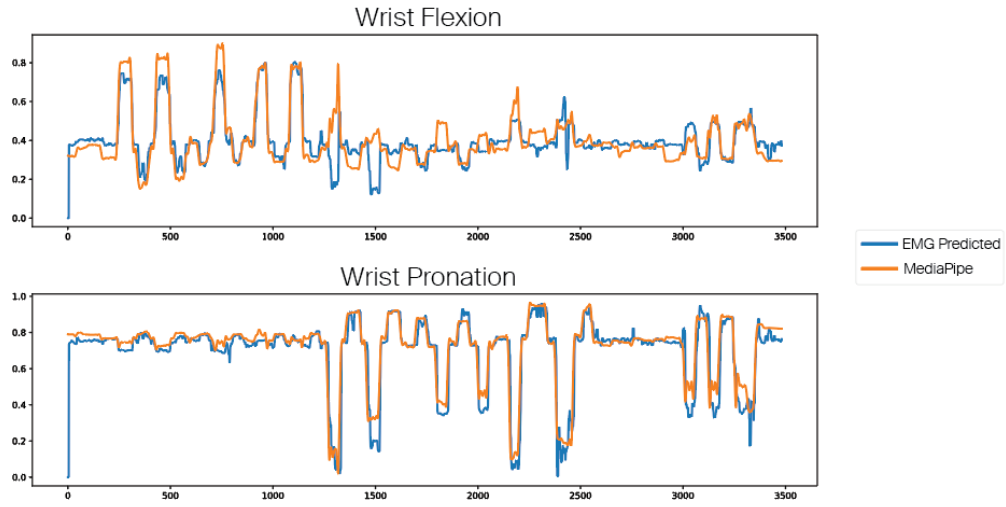


Figure 4. Plot of the predicted wrist angles from EMG signals (Blue) vs. target angles obtained from MediaPipe (orange) on the test set. The average R^2 for the two wrist movements is 0.72.

2.4.2 Transfer Learning to reduce calibration time

In computer vision, transfer learning has shown many advantages with deep learning approaches by improving decoding performance, particularly when dealing with complex tasks and large-scale datasets. Leveraging pre-trained models, several authors showed that it is possible to achieve superior performance with comparatively less training data and reduced computational costs. In the context of EMG, deep learning has the potential to improve decoding performance for single-finger proportional control. Therefore, transfer learning offers significant potential to overcome challenges related to inter-session variability in muscle activation patterns or electrode placement. Indeed, collecting large amounts of EMG data from a specific subject can be challenging as patients with an amputation would not accept to calibrate their prosthesis for one hour every day. This subsection focuses on a transfer learning approach to reduce calibration time for subjects.

In this preliminary study, four able-bodied subjects (3M-1F, 20-27 years old) were recruited. Using the MD-EMG prototype described in section 2.2, EMG signals were recorded from 64 monopolar channels at 2400Hz, bandpass filtered between 5 and 500Hz, notched filtered at 50Hz, and an overlapping sliding window of length 200ms (overlap of 150ms) was extracted. Subjects were asked to follow a 14-minute long video showing a sequence of single and multi-finger movements repeated 6 times. Finger angles were obtained with a webcam using MediaPipe and synchronized with the EMG signals.

To obtain the baseline decoding performance for each subject, a CNN model was trained as in section 2.2 with random initialization, and performance is assessed on the testing set. The CNN model architecture and hyperparameters were optimized on previously acquired data and the validation test was used for early stopping. As performed previously, the first four

repetitions were used for training, the fifth one for validation, and the last one to evaluate the performance of the model.

Next, a model was pre-trained on 10 recordings from subject 1 who recorded the full dataset on 10 different days. This model was then used for fine-tuning on a smaller dataset recorded by all participants consisting of 3 repetitions of movements. During fine-tuning, the training was continued for 20 epochs with all convolutional layers frozen. Two repetitions were used for training and the last one was used to evaluate the model's performance.

Finally, after fine-tuning the model, each subject was asked to control a robotic hand in real-time. The task consisted of grasping an object with the robotic hand with three different grasps (power, tri-digital and ulnar grasp) and maintaining the ball for at least 5 seconds repeated 20 times for each grasp (see Figure 5.).

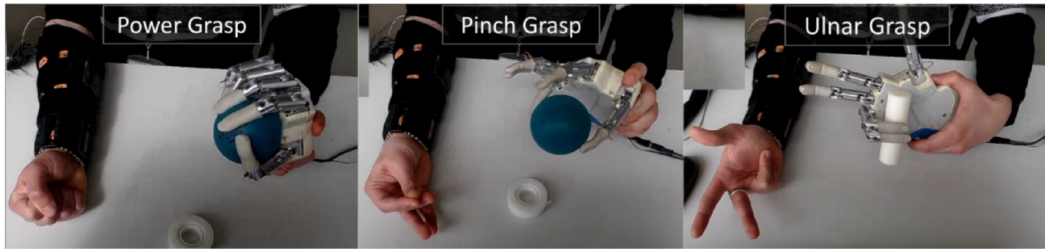


Figure 5. Illustration of the task performed by the subjects with the robotic hand.

Figure 6 shows the offline performance of the models trained from scratch compared to the models pre-trained on 10 recordings before and after fine-tuning. Without fine-tuning the performance is lower than the model trained from scratch and with fine-tuning. The fine-tuned model has on average a lower R^2 than the model trained from scratch.

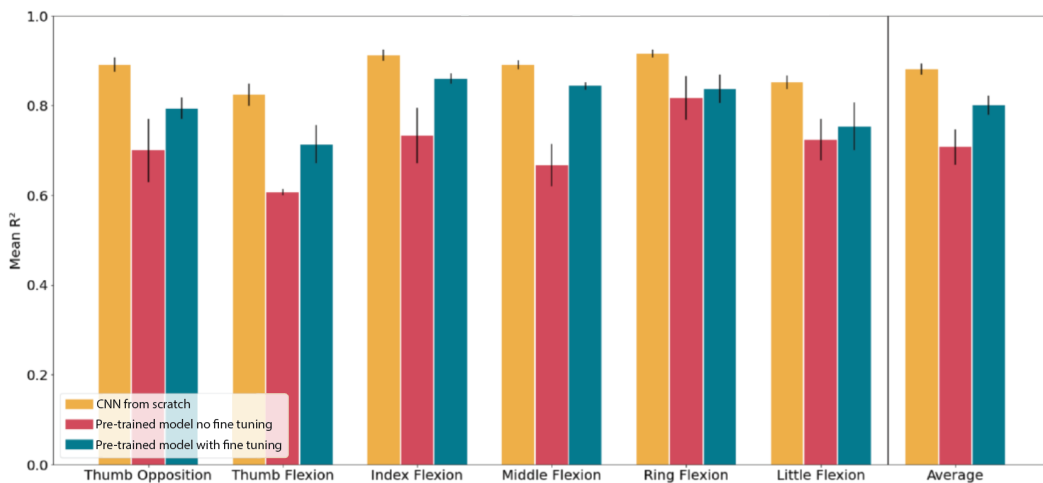


Figure 6. Mean coefficient of determination (R^2) obtained for each degree of freedom decoded.

Table 1 shows the outcome of the functional task. Successful grasp with 5 seconds of holding the object was awarded one full point (✓) while if the grasp was performed but the object was

not grasped for 5 seconds, it counted as 0.5 points (~). Failure to perform the intended grasp resulted in 0 points (×). The average is the number of points obtained divided by the total number of grasps intended. The performance increases with fine-tuning, however, without fine-tuning the performance is relatively poor on subject 1 even after being trained for 10 days.

Grasp Task Experiment													
Pre-trained model no fine tuning													
	Power			Pinch			Ulnar			Power	Pinch	Ulnar	Average
	✓	~	×	✓	~	×	✓	~	×				
Subj1	12	5	3	13	5	2	8	5	7	72.5%	77.5%	52.5%	67.5%
Subj2	0	0	20	15	2	3	1	14	5	0.0%	80.0%	40.0%	40.0%
Subj3	6	9	5	9	8	3	4	1	15	52.5%	65.0%	22.5%	46.6%
Subj4	5	7	8	6	10	4	0	0	20	42.5%	55.0%	0.0%	32.5%
Average	8.38			13.88			5.75			41.9%	69.4%	28.8%	46.7%
Pre-trained model with fine tuning													
	Power			Pinch			Ulnar			Power	Pinch	Ulnar	Average
	✓	~	×	✓	~	×	✓	~	×				
Subj1	18	2	0	17	3	0	20	0	0	95.0%	92.5%	100%	95.8%
Subj2	20	0	0	8	8	4	18	2	0	100%	60.0%	95.0%	85.0%
Subj3	18	2	0	15	2	3	19	1	0	95.0%	80.0%	97.5%	90.8%
Subj4	20	0	0	6	7	7	12	5	3	100%	47.5%	72.5%	73.3%
Average	19.50			14.00			18.25			97.5%	70.0%	91.3%	86.2%

Table 1. Result of the robotic hand task. ✓ refers to a successful grasp, ~ represents a grasp that was not kept for 5 seconds, and × is a trial where the robotic hand didn't move or didn't perform the intended grasp.

This preliminary analysis confirmed the potential of using transfer learning with an MD-EMG system for single-finger proportional control to reduce calibration time. Indeed, with only 7 minutes of recording, the subjects were able to perform the task with high accuracy. However, the results also show that pre-training a network on many recordings on different days is not enough to eliminate the calibration phase on subject 1. One hypothesis is that increasing the amount of data during pre-training could remove the need to perform calibration. However, the high inter-session variability could make the recording of a "sufficient" amount of data impossible. An alternative hypothesis is that pre-training a model on data from multiple subjects could improve its ability to generalize to new data potentially reducing the amount of data required by a single participant to obtain a model performing without calibration for each new session.

This analysis is preliminary and shows several limitations. For instance, the amount of data necessary with transfer learning to obtain the same performance as the model trained from scratch was not assessed. Moreover, the task was not performed in the case of a model trained from scratch. This limitation is due to the time necessary to record the full sequence, extract the finger angles from the video, and train the CNN which can take up to one hour when performed on a laptop equipped with an Nvidia GeForce GTX 1050Ti GPU. With transfer learning the total time to record and obtain a trained model was reduced to 20 minutes.

2.4.3 A framework to train deep models in real-time for wrist and finger proportional control

In this subsection, we discuss the development of a novel framework combined with MD-EMG that has been patented (Application No: EP 23159952.3, Title: A wearable electromyographic device and system and methods for motion decoding of body parts).

Based on the time limitations of the previous subsection, we designed a framework to reduce the computational cost of EMG decoding and leveraged the full power of CPUs and GPUs as extracting the angles from the video using MediaPipe and training a model with transfer learning is still requiring time to be performed. In this subsection, a framework was developed to extract finger angles from the webcam and train models in real-time. The main advantages of real-time training are that it gives instantaneous feedback on the decoding performance of the model to the user such that one can stop training when the model obtained has sufficient performance, the user can also use the instantaneous feedback to emphasize gestures that are not properly trained by the model. Moreover, the user can use the robotic hand as soon as the model gives satisfactory results and does not need to wait for the analysis to be done before knowing if the model is performing well or not.

To reduce the computational cost of training deep models on raw EMG data recorded at 2400Hz, we preprocess each channel of the MD-EMG system to obtain the envelope of the EMG signal and subsample it to 100Hz. This processing is performed in real-time and allows to reduce in 24 the amount of data stored and lowers the size of the input to the CNN with low to no loss in decoding performance. Preprocessing the data simplifies the feature extraction process for the model, ultimately resulting in a shallower architecture.

On the finger angle extraction side, the frames retrieved from the webcam are processed in real-time to extract only the finger angles. Using CPU parallelization, the frames are acquired, and the finger angles are extracted at a steady frequency of 30 Hz. Moreover, the user is able to see the camera view on the screen of the PC with the value of the finger angles to get feedback on the quality of the angles extracted.

Similar to the previous subsection, a model was pre-trained on 10 recordings of a single subject and is used as a basis to reduce the calibration time.

The real-time framework architecture is shown in Figure 7. Briefly, the system is made of two instances. The first one synchronizes and saves the data received from all modalities (EMG, finger angles from the camera, and wrist angles from IMUs) in a folder. Another instance gets all the data available in this folder to fine-tune the pre-trained model and keeps all the data in a buffer. When a model is ready, it is pushed such that the data incoming is also used as input to the model to obtain predictions. When the training is done, the instance adds the new data available in the folder to its buffer and continues fine-tuning the model obtained at the previous step.

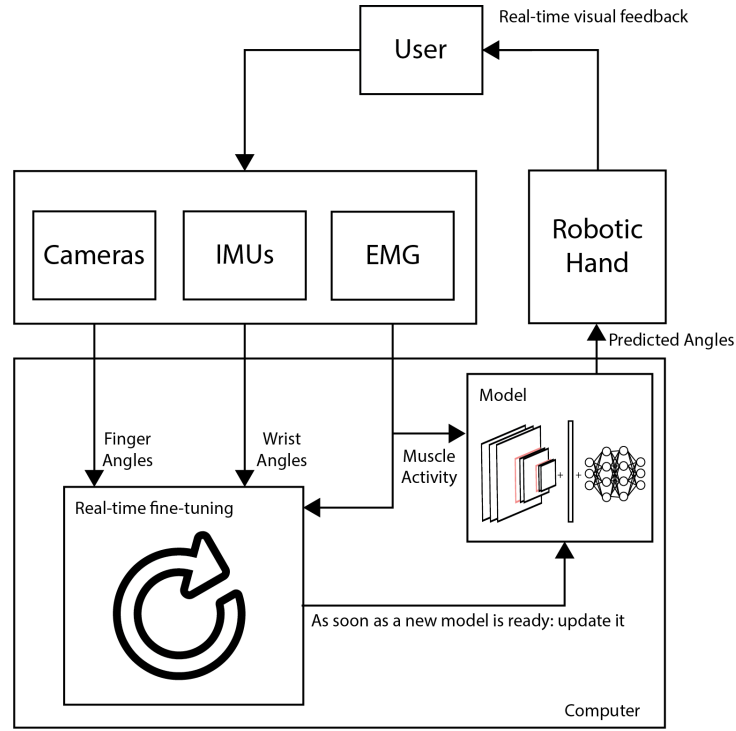


Figure 7. Architecture of the real-time training framework

Two subjects were recruited to control a robotic hand with real-time training and perform the same task as in the previous subsection.

As this work is preliminary, there are only a few results obtained at the time of writing. Table 2 shows the performance of the two subjects on the robotic hand task after roughly 3 minutes and 30 seconds of calibration using the pre-trained model as a basis.

Function Test Using Models Trained from Pre-trained Model

Subjects	Power Grasp			Success rate	Pinch Grasp			Success rate	Ulnar Grasp			Success rate
	✓	~	×		✓	~	×		✓	~	×	
Subject 1	20	0	0	100%	19	1	0	95%	12	5	3	60%
Subject 3	20	0	0	100%	11	5	4	55%	20	0	0	100%

Table 2. Result of the robotic hand task with the real-time framework after 3 minutes and 30 seconds of data acquisition. ✓ refers to a successful grasp, ~ represents a grasp that was not kept for 5 seconds, and × is a trial where the robotic hand didn't move.

This real-time framework opens up many scenarios to be tested with repetitive training of models and to explore different training or transfer learning paradigms to obtain performing models with the lowest amount of calibration data possible. It is important to notice that the training is not exactly the same as what is generally reported in the literature. Indeed, in this

case, the model is trained with all the data available at every step. As the dataset increases in real-time, it implies that the data obtained at the beginning of the recording will be used to train the model more often compared to the latest data. Several strategies need to be compared to obtain the maximum accuracy and long-term robustness of the decoding.

3 Shared Control

EMG decoding will remain limited for some patients due to the number of remaining muscles or movements previously performed by intrinsic muscles of the hand. On the other hand, shared control, or the integration of robotic automation with EMG decoding for robotic hand control, presents several advantages. Dexterity and functionality could be improved by assisting in performing complex tasks such as providing additional stability for instance. This allows the prosthetic user to accomplish tasks with greater ease and precision, enhancing their overall quality of life. This can offload some of the cognitive load required to operate prosthetic hands, as robotic automation can take over certain aspects of the task. It allows the user to focus on higher-level decision-making and less on the intricate details of controlling the prosthesis. Among other potential benefits of shared control, we will show in this chapter two main aspects of adding robotic automation into the decision loop. The first section will cover grasp robustness and potential muscle fatigue reduction while in the second section, we will investigate how robotic automation can increase the dexterity of the user by performing in-hand object manipulation.

3.1 Robotic Automation to Improve Grasp Robustness

The content of this section is the postprint from the article Zhuang et al., "Shared human-robot proportional control of a dexterous myoelectric prosthesis," *Nat Mach Intell* 1, 400–411 (2019).

Find the published article here: <https://doi.org/10.1038/s42256-019-0093-5>

Personal contributions as the co-second author: conceived the third experiment with the physical robot, prepared the protocols and the experimental setup (hardware and software) of the EMG part, and co-conducted the experiment. I analyzed the results from the data recorded with the physical robot, prepared the EMG-related figures, and wrote the manuscript on this part.

Shared human-robot proportional control of a dexterous myoelectric prosthesis

Katie Z. Zhuang, Nicolas Sommer*, Vincent Mendez*, Saurav Aryan*, Emanuele Formento, Edoardo D’Anna, Fiorenzo Artoni, Francesco Petrini, Giuseppe Granata, Giovanni Cannaviello, Wassim Raffoul, Aude Billard[#], and Silvestro Micera[#]

(* Equal contribution as junior authors, [#] Equal contribution as senior authors)

Abstract

Myoelectric prostheses allow users to recover lost functionality by controlling a robotic device with their remaining muscle activity. Such commercial devices can give users a high level of autonomy, but still do not approach the dexterity of the intact human hand. We present here a method to control a robotic hand, shared between user intention and robotic automation. The algorithm allows user-controlled movements when high dexterity is desired, but also assisted grasping when robustness is paramount. This combination of features is currently lacking in commercial prostheses and can greatly improve prosthesis usability. First, we design and test a myoelectric proportional controller that can predict multiple joint angles simultaneously and with high accuracy. We then implement online control with both able-bodied and amputee subjects. Finally, we present a shared control scheme in which robotic automation aids in object grasping by maximizing contact area between hand and object, greatly increasing grasp success and object hold times in both a virtual and a physical environment. Our results present a viable method of prosthesis control implemented in real time, for reliable articulation of multiple simultaneous degrees of freedom.

1. Introduction

In the United States alone, about 1.6 million people live with an amputation, 541,000 of which affect the upper limbs (1). This condition diminishes quality of life, mobility and independence, while also imparting a social stigma (2). Upper limb prostheses controlled using surface electromyographic (sEMG) signals attempt to restore hand and arm functionality by using the amputee’s remaining muscle activity to control movements of a prosthetic device. However, the capabilities of current commercial prostheses are still grossly inferior compared to the dexterity of the human hand. Commercial devices usually use a two-recording-channel system to control a single degree of freedom (DoF), i.e. one sEMG channel for flexion and one for extension (3). While intuitive, the system provides little dexterity. Patients abandon myoelectric prostheses at high rates, in part because they feel that the level of control is insufficient to merit the price and complexity of these devices (4–6). In recent years, various research groups have made significant advances in myoelectric prosthesis control in laboratory and prototype environments. Many groups have demonstrated great success in grasp classification, which is a common approach for prosthesis control, but limits the user to a library of trained hand postures (7–10). However a few groups have now attempted to decode single finger movements (11–13). Despite high decoding accuracy, these studies showed results mainly from able-bodied subjects performing offline tests. With cited

decoding performances of upwards of 90-95% for each method, we see a clear dichotomy between laboratory experiments and clinical viability, a point that is addressed by Jiang et al (14).

The idea of “shared control”, that is, automation of some portion of the motor command, is already a topic of interest within the field of robotics and neuroengineering (15–18). Indeed, shared control approach can play a key role in robotic applications involving human-robot interfacing such as prosthetic body parts. The limited sensory-motor control abilities in this case make the subjects unable to conform their fingers to the shape of the object. This in turn inhibits their ability to secure and adapt their grasp according to the requirement of the task. Shared control can fill this void by stabilizing the grasp, making fine adjustments to the fingers by processing information from the tactile sensors placed on prosthetic hand’s fingers. More generally speaking, shared control strategies aim to bridge the gap between human’s intentions and efficient execution of the intended task by using information from the sensors.

Even if potentially useful, shared control has not yet become prevalent in the area of peripheral nerve interfaces. Došen et al. propose a camera-based approach (19) while Light et al. proposes 1-DoF control with automated grip force adjustment (20). Other methods of automation include automated hand-closing in response to slippage (21) and underactuated systems in which spring-like mechanisms mediate grasp force (22). The only commercial application of shared-control methods to date is the Ottobock Sensorhand Speed which automatically increases thumb flexion during grasping in response to slippage (18). However, it is only capable of binary action choices or 1-DoF proportional velocity control.

The control method presented here attempts to implement a shared-control strategy with a highly-dexterous hand prosthesis by taking advantage of state-of-the art myoelectric decoding as well as an algorithmic controller for grasp optimization. We first propose a kinematic proportional decoder using a multilayer perceptron (MLP), which allows users to simultaneously and continuously control each finger individually. In addition, we propose to integrate and use a shared-control scheme in which a robotic controller aids in stable grasping by maximizing the area of contact between a prosthetic hand and an object (23). The idea behind this scheme is to make object grasping more robust (avoiding accidental drops) while allowing the user to maintain full autonomy over grasping or releasing, grasp preshaping, and non-grasp-related motions. In this way, we achieve both highly dexterous user control when precise positioning is valuable, and partially automated grasp attainment when object droppage avoidance is desirable.

2. Results

We performed three sets of experiments in which we decoded hand movements of subjects using sEMG signals recorded from their forearms. We recruited three subjects with hand/transradial amputations (subjects A1, A2 and A3) and eight able-bodied subjects (subjects B1, B2, B3, B4, S1, S2, S3, S4) for the study. In the first set of experiments, able and amputee subjects performed online control of a virtual prosthetic hand. In the second set of experiments, the same subjects used a virtual hand to grasp and release virtual objects according to visual cues in two conditions: with or without robotic assistance. In the third set of experiments, four able-bodied subjects controlled a physical robotic arm and hand to perform functional object manipulation tasks.

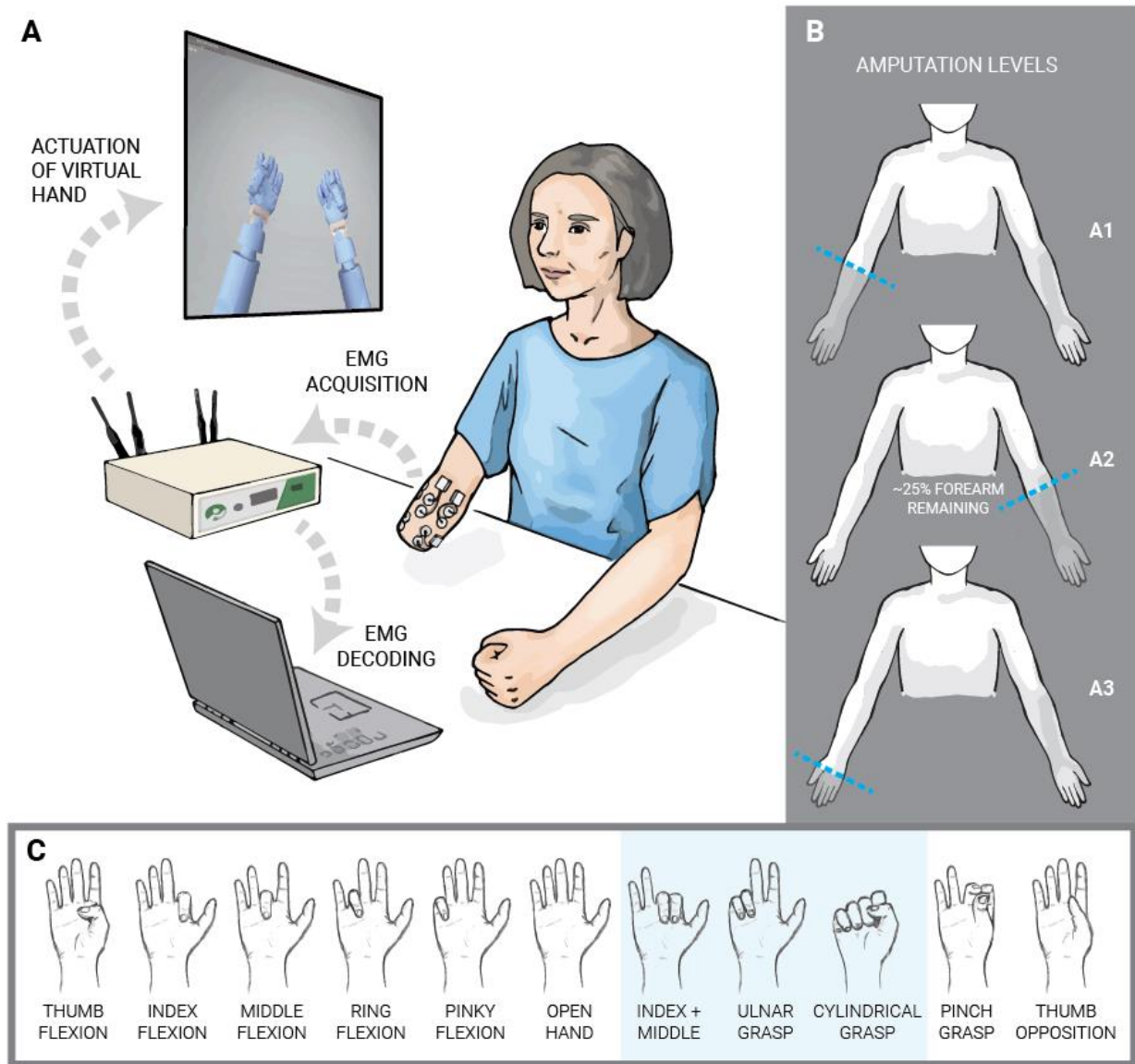


Figure 1. Experimental Setup and Subjects. **a**, In online experiments, four able-bodied subjects and three amputee subjects controlled a virtual robotic hand using their surface EMG signals. The signals were decoded with a multilayer perceptron to obtain predictions of single-digit joint angles. **b**, The three amputee subjects had varying levels of amputation, shown here. **c**, Movements we tested consisted of both single-digit and multi-digit movements. All subjects performed all movements except Subject A2 who did not perform index and middle finger flexion/extension independently.

Experiment 1 (Online Kinematic Decoding). Three amputee subjects (A1, A2 and A3 in Figure 1b) and four able subjects (B1, B2, B3, and B4) performed online control of a virtual prosthetic hand with sEMG decoding. To train the MLP, subjects were asked to mimic the movements of the virtual hand while sEMGs were recorded. We decoded flexion and extension of each digit as well as thumb opposition and reposition. This gave DoFs per subject for all subjects except subject A2 who moved the index and middle fingers concurrently (Figure 1c). The average per-session correlation for all subjects and all sessions was 0.52 and the peak-to-peak normalized mean square error (24) (nMSE) was 15.7%. For all subjects, the MLP successfully predicts the flexion and extension of each finger,

both individually and simultaneously with flexion of other digits. We summarize performance in Supplementary Table 1 for all subjects and sessions.

In order to further analyze the ability of the decoder to predict the desired joint angles and to compare these predictions against chance, we computed the percentage of time of correctly predicted joint angles for each subject (Figure 2a). As a control for this assessment, we selected random angles from the training set range and computed prediction accuracy using the random angle as the instructed one (white sections). This way, we were able to simulate chance accuracy of the MLP predictions. We find that in every degree of freedom for Subject A3, the MLP is able to decode significantly higher than chance (Wilcoxon two-sided signed rank test, $p < 0.01$). The same analysis was performed for all subjects individually with similar results (Supplementary Figure 2) using a non-parametric test due to non-normal data (Kolmogorov-Smirnoff test). We then performed this analysis for all subjects while pooling all of the degrees of freedom to obtain an overall measure of decoding performance (Figure 2b).

To analyze any patterns in prediction error, we calculated a “confusion matrix” for each degree of freedom (Figure 2c). Here, we enforced a threshold (mean prediction angle) to separate joint predictions into either flexion or extension. We also mapped the instructed joint angles into flexion or extension using mean instructed angle for thresholding. Plotting instructed activation on the x-axis and performed action on the y-axis, we color map excessive action (false positive) to orange intensity and lack of action (false negative) to blue intensity. We observed that Subject A3 has trouble controlling thumb flexion; it is excessively flexed during the actions of other fingers. Similarly, Subject A2, who has extensive median nerve damage, has difficulty controlling the thumb, index and middle fingers movements.

These thresholded decoding accuracies are within a similar range as the ones obtained in online classification of finger flexion and extension cited by Cipriani et al. (79% average accuracy for amputees cited vs. our average of 89.5% for a similar number of classes: 7 classes cited vs. our 6 effective classes which are simultaneously considered) (12).

This experiment demonstrates our ability to decode individual finger movements proportionally for multiple simultaneous DoFs and in real time using noninvasive sEMG signals. Performance results are not only above chance level, but robust for all tested movements for both able-bodied subjects as well as amputee subjects.

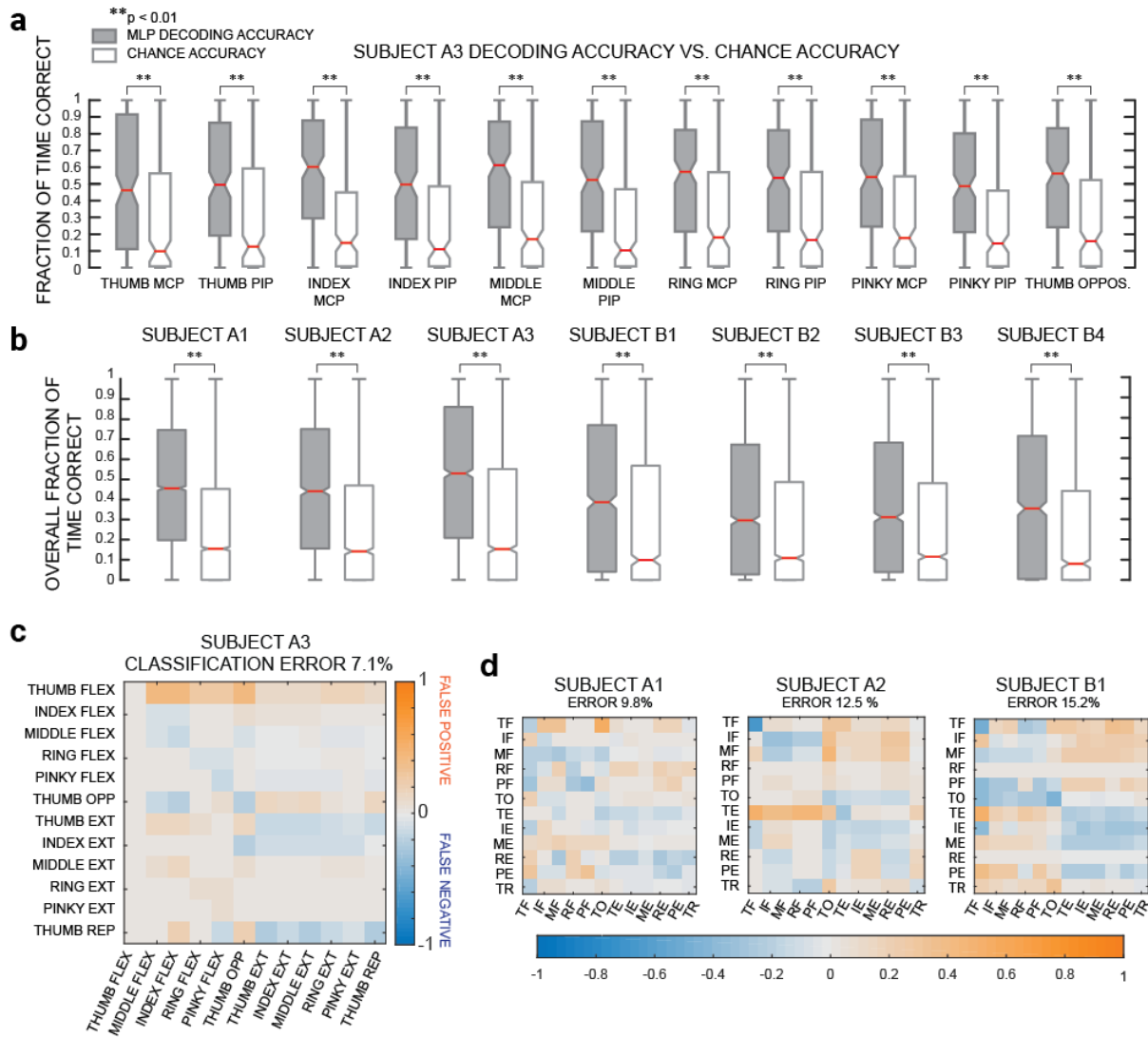


Figure 2. Analysis of online prediction performance of the MLP. **a**, Prediction accuracy of the MLP compared to chance accuracy. Gray boxplots indicate the fraction of time per trial that each predicted DoF is within 15 degrees of the instructed angle. White boxplots indicate the fraction of time per trial that a random angle (within the set of trained angles) is within 15 degrees of the instructed angle. Each degree of freedom was predicted higher than chance level ($p < 0.01$ Wilcoxon two-sided signed rank test). All box plots in this manuscript include a median center line (red), box edges at 25th and 75th percentiles, notches calculated based on interquartile range $\pm \frac{1.57 \cdot IQR}{\sqrt{n}}$. **b**, Overall decoding accuracy versus chance for all subjects. Statistical significance is calculated with the Wilcoxon two-sided signed rank test. **c**, Confusion matrix of each digit's degrees of freedom for one subject. Blue pixels indicate lack of specified movement when instructed (false negatives) while more orange pixels indicate undesired movements (false positives). Overall error is calculated as well as error along the diagonal of the matrix (whether the instructed motion was performed accurately). **d**, Confusion matrices for three other subjects.

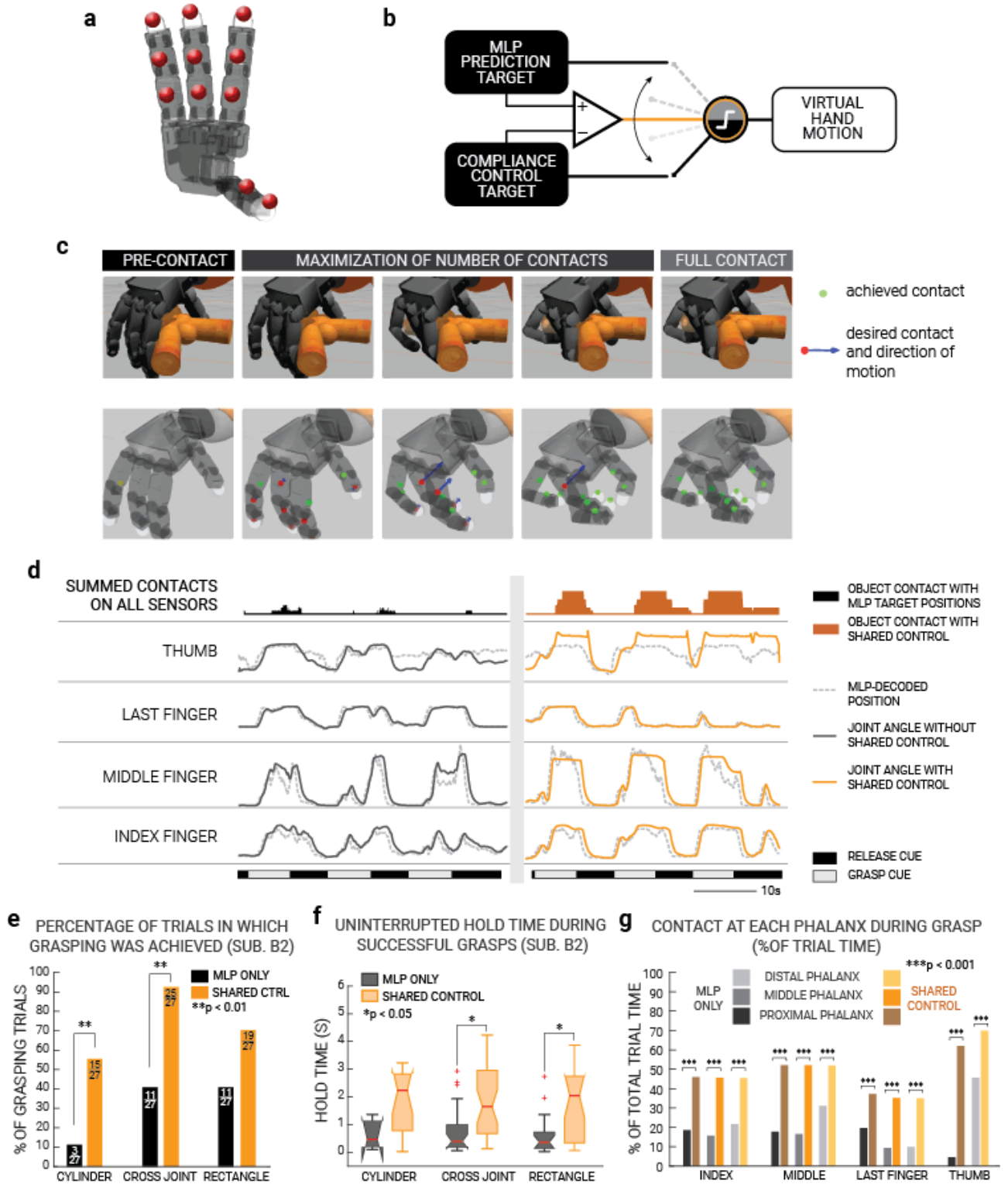


Figure 3. Shared control in virtual environment, setup and results. **a**, Simulator of Allegro Hand **b**, Shared control scheme. Both the MLP decoder and shared controller run simultaneously and the MLP-decoded joint targets prevail before contact. During object contact, the shared control joint targets prevail unless the difference between MLP-only and shared control is above a 50-degree threshold. **c**, Action of the active compliant contact controller. When one contact on a digit touches the object, the direction of motion is computed to bring other contacts of the digit towards the object. Figure adapted from Sommer and Billard et al. (23) **d**, Example traces of shared control (Subject B4). Top row shows total of pressure detected without (left) and with (right) shared control. Traces show the joint angle for each DoF. Dotted lines indicate the MLP

prediction while solid traces indicate the actual position of the virtual robotic hand. Bottom row indicates the cues to grasp or release. **e**, Percentage of trials during which desired contacts are achieved for the three objects by Subject B5 over 3 sessions. (p-values from Fisher's two-tailed exact test). Number of successful trials versus total trials are indicated on each bar. **f**, Duration of hold time for each object out of seven seconds (p-values from Wilcoxon two-sided signed-rank test). **g**, Percentage of grasping trial time during which contacts were touching the objects (p-values from Fisher's two-tailed exact test). Contacts on different phalanges are indicated with different color shades, raw numbers for calculation included in Supplementary Table 1.

Experiment 2 (Shared Control using the virtual environment). In this set of experiments, the user attempted to grasp, hold and then release virtual objects by controlling a sensorized virtual robotic hand implemented in Gazebo and rviz, a ROS package (Figure 3a). The same subjects from Experiment 1 performed this experiment with the exception of subject B1. In addition to the MLP decoding, we tested two conditions: one *with* shared control for partial grasp automation (shared control) and one *without* (MLP only). During the shared control condition, the virtual hand would automatically attempt to maximize contact between the hand and a grasped object by increasing flexion of a finger as soon as a single phalanx touches an object. If, however, the total joint angle difference between MLP predictions and shared control targets of a single digit would differ by more than 50 degrees, the controller would use torque control to achieve MLP-decoded joint angles for that digit (Figure 3b). This threshold was chosen empirically from preliminary testing. In the future, we will strive to make the transition gradual instead using a threshold. The action of the algorithm is shown in Figure 3c under the conditions of pre-contact (MLP joint targets), initial contact (shared control targets in red) and achievement of full contact (in green). Figure 4d shows an example of single-digit flexion and extension with or without shared control for Subject B4 grasping the thin rectangular bar. We see that when shared control is implemented, digits that make initial contact with an object are better able to achieve more contacts and maintain them. The higher number of contacts achieved with shared control reflects this advantage (top row). However, the user is still able to release the object when it is desired (movement instructions at bottom).

In Figures 3e, 4a we show the percentage of trials in which a full grasp is achieved per subject across all sessions with either shared control or only MLP predictions. Full grasp is defined as attaining all possible contacts between the hand and a particular object (see Methods). In the shared control condition, subjects are able to achieve considerably more successful grasp trials for all objects. For each object and for each subject, we also show percentage change in fraction of successful grasp trials between the MLP-only and shared control conditions (Figure 4b).

We also see a difference in grasping performance between objects grasped which is subject-dependent. For example, Subject A2 benefitted the most from shared control for the rectangular bar. This result is consistent with the finding that the same subject has particular difficulty in sustaining muscle activation associated with the thumb, index and middle fingers due to median nerve damage.

In addition to the attainment of grasp, we also assessed how long the subjects were able to maintain holds. Figure 3f, 4c shows the distribution of hold times per object and per subject with or without shared control. We define hold time as the length of continuous time during which the subject could maintain required contacts between the virtual hand and object without any contacts being broken (25). Due to the visual cue, a small percentage of non-hold time is likely due to subject reaction time. For all objects and subjects, hold times are greater with the shared control condition than only MLP, with the exception of the cylinder for subject B2. This may be due to the low number

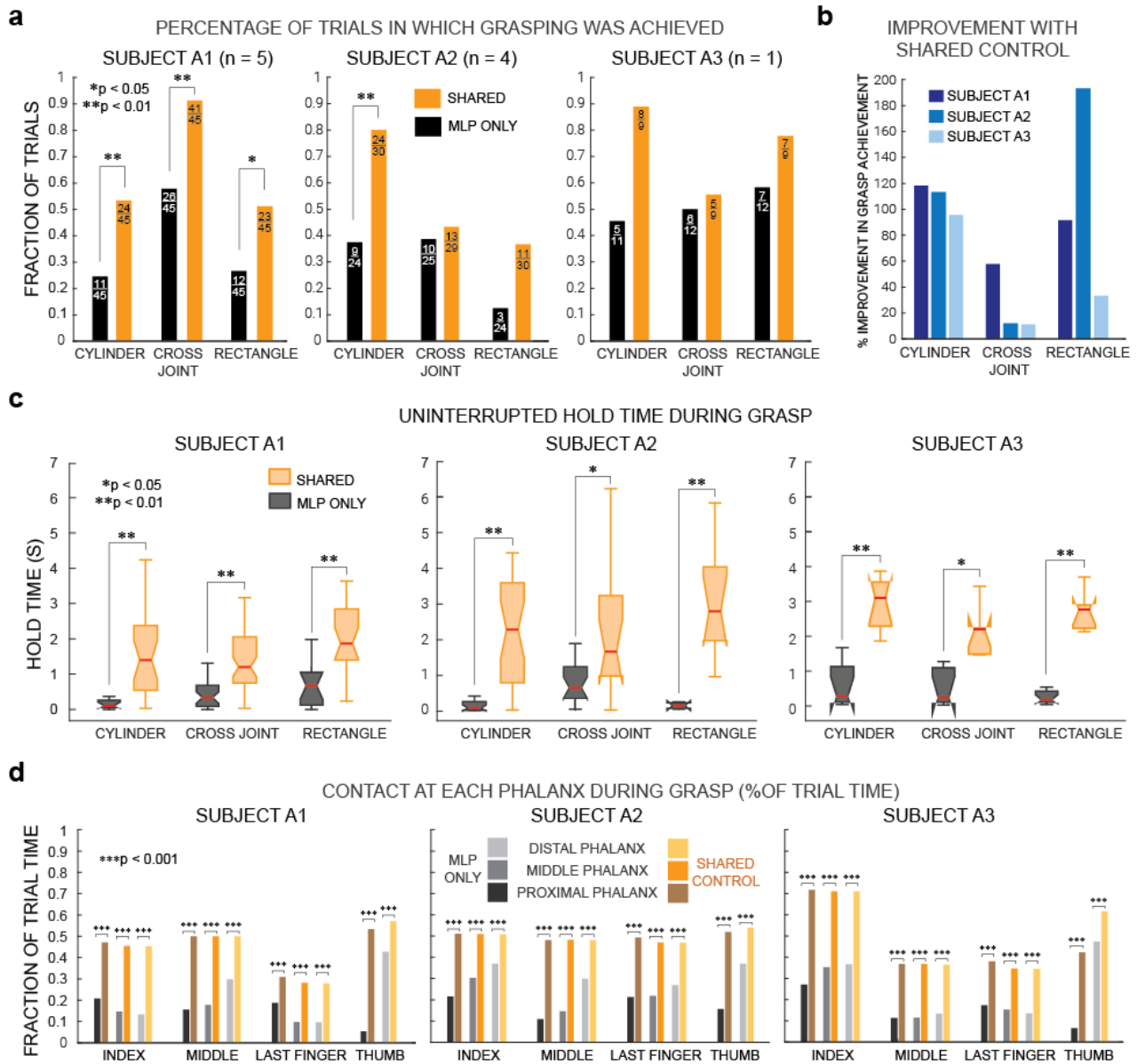


Figure 4. Shared Control results in virtual environment cont'd. **a**, Comparison of fraction of successful grasping trials with (orange) or without (black) shared controller aid for three amputee subjects and all three object types. Data are shown for all sessions of each subject (# of sessions indicated in title). Statistical p-values are computed using Fisher's two-tailed exact test. Number of successful trials versus total trials are indicated on each bar. **b**, Percentage improvement in fraction of correct trials for the three subjects split by object type. Each color indicates a different subject. **c**, Duration of hold time for each object with or without shared control for the three subjects (p-values by Wilcoxon two-sided signed-rank test). Maximum instructed hold time was seven seconds. **d**, Percentage of grasping trial time during which each single contact on each digit made contact with the objects with or without shared control for the three subjects (p-values by Fisher's two-tailed Exact Test). Each plot is for a different subject with the shaded bars indicating contact placement. Lighter color shades indicate more proximal phalanges on the same digit. Data are aggregated over all trials and sessions for a single subject, raw numbers for calculation included in Supplementary Table 2.

of trials subject B2 performed in comparison to Subjects A1-3. .

Finally, we assess the percentage of time that each single sensor contacted the objects to analyze which contacts subjects found more difficult to maintain. For all objects, all subjects were able to maintain longer contacts with all parts of the digits with shared control than with only MLP predictions. Importantly, all subjects were capable of releasing the objects once grasped by relaxing their grasp (Fig. 4d, 6b).

Taken together, these results show that the shared controller aids grasping in multiple ways, namely facilitating longer, more successful grasps and avoiding accidental drops.

Experiment 3 (Shared Control in a physical environment).

This experiment was divided into two sub-experiments. In the first sub-experiment, the subjects performed a variant of the box and block test (26) through teleoperation of a physical robotic hand and arm. The goal was to grasp and move an object (a bottle, half-filled of water) placed on a hard case to another one placed approximately 30cm away. Object droppage was considered a failed trial. The subjects controlled the robotic arm via an optical motion capture system. A robotic hand (the physical analog of the virtual one described in Experiment 2) was mounted onto the robotic arm and controlled with either MLP only or shared control. Four able-bodied subjects participated in this experiment (S1, S2, S3 and S4). After a training phase to train the MLP decoders, the subjects were required to perform 20 trials of the functional task under in each condition (randomized MLP only and shared control) for a total of 40 trials.

Results are shown in Figure 5a (left panel). S3 and S4 performed significantly better with shared control than without whereas S1 and S2 were highly successful at the task in both conditions.

To evaluate whether the shared control improves grasp quality, we defined two metrics based on the pressure sensor data: average number of contacts and the “effective normalized pressure” (see Methods). The results shown in figures 5b and 5c indicate better performance with shared control in terms of both of the two metrics. The p-values, computed using Wilcoxon’s rank-sum test over all trials by all subjects, show statistical significance in case of effective normal pressure ($p < 0.0001$). The same test performed on average number of contacts was not significant for the index finger ($p=0.07$) but showed statistical significance for the other two fingers ($p < 0.05$).

As shared control was notably advantageous for the subject S3, we compared the timeseries plots of a few trials from the subject’s box and block tasks (Figure 5d). In open position (close to zero), the actual position (solid line) closely follows the MLP prediction (dotted line) for each finger. However, the subject cannot close the fingers enough to grasp, leading to insufficient total pressure. With the shared control, the grasps are tightened to achieve the desired pressure. In case of the subjects who performed equally well with and without shared control (S1, S2) the MLP prediction by itself was high enough during grasping to achieve a tight grip and high pressure.

The second sub-experiment used the same training protocol as first, with a slight variation in the behavioral task. The task here consisted of grasping the bottle from the table, bringing it to mouth, tilting it to mimic drinking and then returning the bottle back to a steady position (a few centimeters above the table). Subjects were given less than 10 seconds to complete the movement and then hold the bottle in steady position for at least 10 seconds. The rotation of partially filled bottle leads to the shifting of its moment of inertia due to flow of the water, resulting in a perturbation. Additionally, bottle’s conical shape and smooth surface further adds to sliding of the bottle. Thus, this sub-task can evaluate the potential of shared control in stabilizing the grasp under

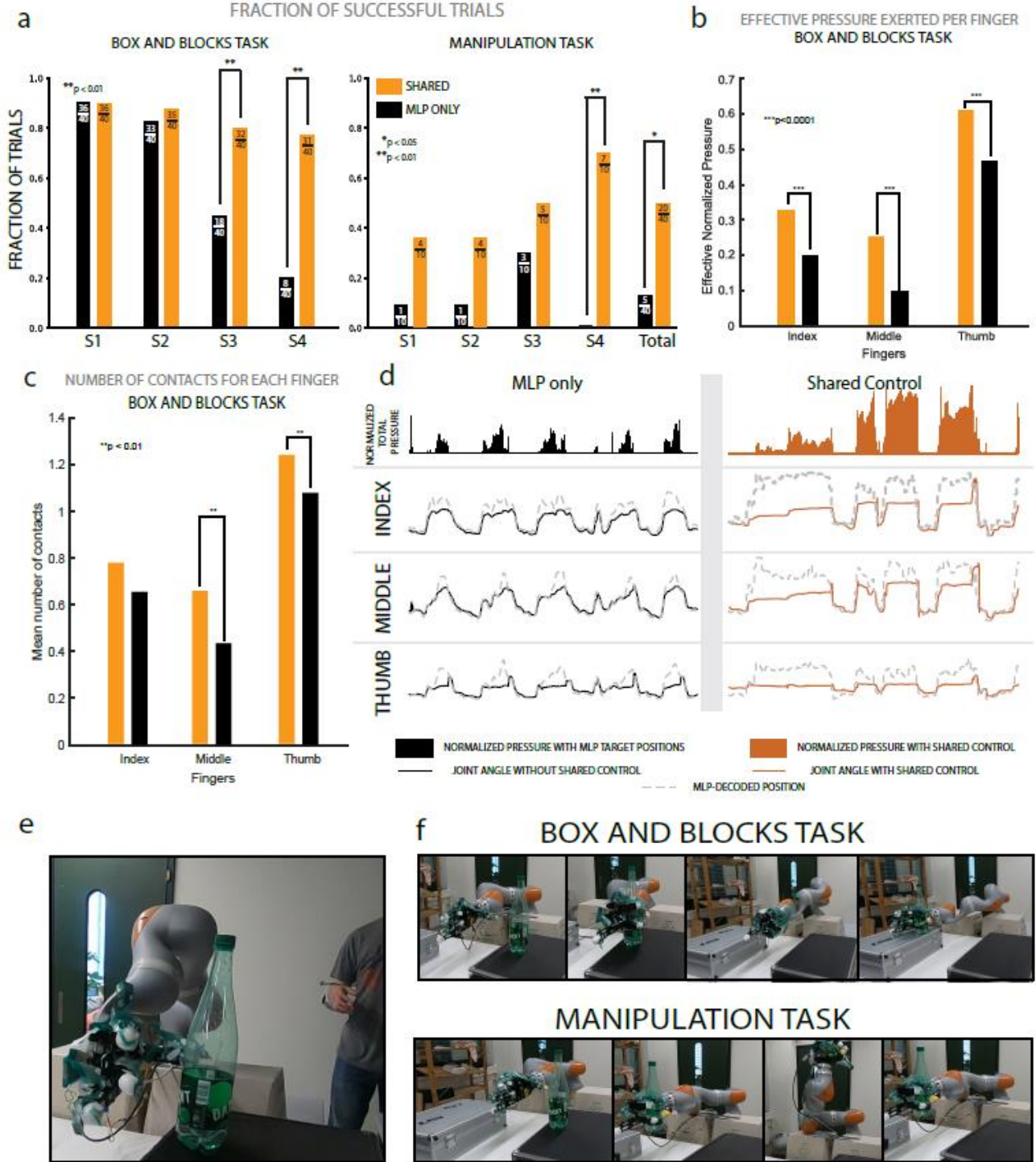


Figure 5. Shared control in physical environment, setup and results. **a**, Comparison of fraction of successful trials for the box and blocks task and the manipulation task with shared control (orange) and without (black). Data are shown for all sessions of each subject. Number of successful trials versus total trials are indicated on each bar when not zero. For the manipulation task (right panel), the total number of successful trials in each condition was summed over all the subjects. Fisher’s two-tailed exact test was used to compute statistical p-values for individual subjects, Wilcoxon rank-sum test was used for total values. **b**, Effective normalized pressure on each finger comparing the trials with and without shared control. The p-values indicated were computed using Wilcoxon’s rank-sum test. **c**, Number of contacts detected by pressure sensors on each finger, averaged over time of each trial. The bars indicate the mean of each trial’s average number of contacts. The p-value is computed using Wilcoxon’s rank-sum test to compare trials of all subjects with and without

shared control. **d**, Time series plots of total pressure, MLP decoded joint positions (dotted) and corresponding actual joint positions of the allegro hand (solid) over few sample grasping trials. The joints on each finger were summed over phalanges. Total pressure was computed by summing over all phalanges after normalization. **e**, Picture of the setup comprising the robotic arm and hand with a subject wearing the EMG acquisition system. **f**, Snapshots of completion of box and blocks task (top) and manipulation task (bottom). For full video see supplementary video 3. One trial of each condition (with and without shared-control) can be seen in supplementary video 4.

object's perturbations, slippery surface and non-uniform shape of object. S1, S2 and S3 performed better with shared control but not significantly (S1 and S3: $p=0.3$, S2: $p=0.65$) while S4 showed statistically significant improvement (Figure 5a right). This is likely due to the limited number of trials. Moreover, S4 was completely unsuccessful at completing the task without shared control but performed relatively well with shared control ($p < 0.01$). The overall advantage of using the shared control becomes evident when we pool together all the subjects (see last histograms in Figure 5b).

3. Discussion

Here we show that we are able to decode single finger kinematics from surface EMGs of both able and amputee subjects. The decoding approach was accurate for both single-finger movements and coordinated, simultaneously activated grasping motions. We also show that decoding is fast enough for real-time applications, with an update rate of 33 Hz. To the best of our knowledge, the work presented here is the first demonstration of a real-time proportional decoder for individual fingers tested with amputee subjects.

One reason commercial prostheses prefer to implement classifier-based decoders instead of proportional ones is the robustness of classifiers in remaining in a particular posture. For grasping, this type of control is ideal to prevent accidental dropping but sacrifices user agency by restricting the number of possible hand postures. Our implementation of shared control allows for both user agency and grasping robustness. In free space, the user has full control over hand movements, which also allows for volitional pre-shaping for grasping.

The tests performed in a physical environment allowed us to show the efficacy of shared control to the improvement of grasp especially when complex tasks are implemented (see Figure 5b). For the first simpler sub-experiment, some subjects (S1 and S2) performed the tasks equally well regardless of the use of shared control while others (S3 and S4) benefitted from shared control significantly. This was because the MLP prediction performance varies across the subjects. These results show that the use of the shared control can be particularly useful for subjects with limited EMG control ability.

Another advantage of shared control is that it requires less energy for the user to maintain a grasp¹⁴. Muscle fatigue is well-documented in sEMG studies (27–31) and is one hurdle for proportionally controlled prostheses. Without the presence of sensory feedback, the simplest solution for a user to be sure of sufficient force is to flex the fingers maximally throughout the duration of the grasp, which can be very fatiguing. In Figure 6b and 6c we show EMG activity of Subject B2 during grasping with shared control or with only MLP predictions. Figure 6b shows averaged EMG activity across all channels and all grasp trials of each object type in a session. As can be seen, for all objects, EMG amplitude is lower with shared control ($p < 0.01$ Wilcoxon two-sided signed rank test). As a control, we also plot averaged EMG during release trials (Fig. 6b right) which

reveals low EMG activity for all objects, after a short peak at the beginning of the trial during which the subject reacts to the visual cue to release. Figure 6c shows the averaged EMG for each individual channel and for each individual object averaged across trials with only MLP predictions (left) or shared control (right). We observe a clear difference in overall muscle activation. This effect on EMG activity was also confirmed during Experiment 3. Figure 6d shows averaged EMG activity across all grasps and all EMG channels for each subject. EMG activity is significantly different for subject S1 and S4 ($p < 0.01$, Wilcoxon two-sided signed rank test), but not for S2 ($p = 0.64$) and S3 ($p = 0.61$). It is interesting to note that even two subjects performed well for the box and blocks test in both conditions (see Fig. 5a), the overall muscle activation is clearly lower during shared control than the MLP-only condition. We find the same result when we analyze each EMG channel separately (Figure 6e).

In our study, inter-subject decoding performance was highly inconsistent. For amputee subjects, many factors can contribute to this heterogeneity, including the level of amputation (Figure 1b), type of injury and time since injury. In Figure 6a we plot the correlation coefficient between the EMG channels we recorded from for each subject. We see that subjects A1 and A3 have relatively uncorrelated EMG channels whereas subject A2 has highly correlated channels. This indicates inability to activate different muscle groups independently. Functionally, this results in subject A2's inability to perform all of the single-digit movements that the other subjects were able to. In addition to a lower number of DoFs independently required for subject A2 (index and middle fingers moved together), we show that shared control can be particularly effective for subjects with few independent muscle groups. We emphasize this point because regardless of the type of decoding algorithm one would implement, the subjects with lower neuromuscular ability will suffer lower decoding accuracy unless they can use some kind of compensation. Such compensation can be surgical, such as in targeted muscle innervation, behavioral, such as learning to contract in an unintuitive way, or it could be algorithmic, as we implemented.

As of now, the compliance controller implemented in our shared control has only one set target force for applying pressure on grasped objects. Future studies should include user-modulated forces, which would be greatly aided with the addition of sensory feedback.

In conclusion, we have explored sEMG-control of individual finger movements in real time with both able-bodied and amputee subjects and show the advantages of a shared-control scheme. In particular, our shared controller leverages the dexterity afforded by user control with the grasp robustness of automation, which can greatly benefit the translation of myoelectric control algorithms into commercial devices. Furthermore, we recognize that amputees and even able users are extremely varied in their ability to modulate their remaining muscle activity. Consequently, some subjects will be less able to control as many DoFs, or as consistently, as others. Shared control can particularly help these users who are less proficient in sEMG modulation and additionally may prevent premature fatigue. Thus, control algorithms should account for user variance and partial automation is one such method that can greatly improve myoelectric prosthesis usability.

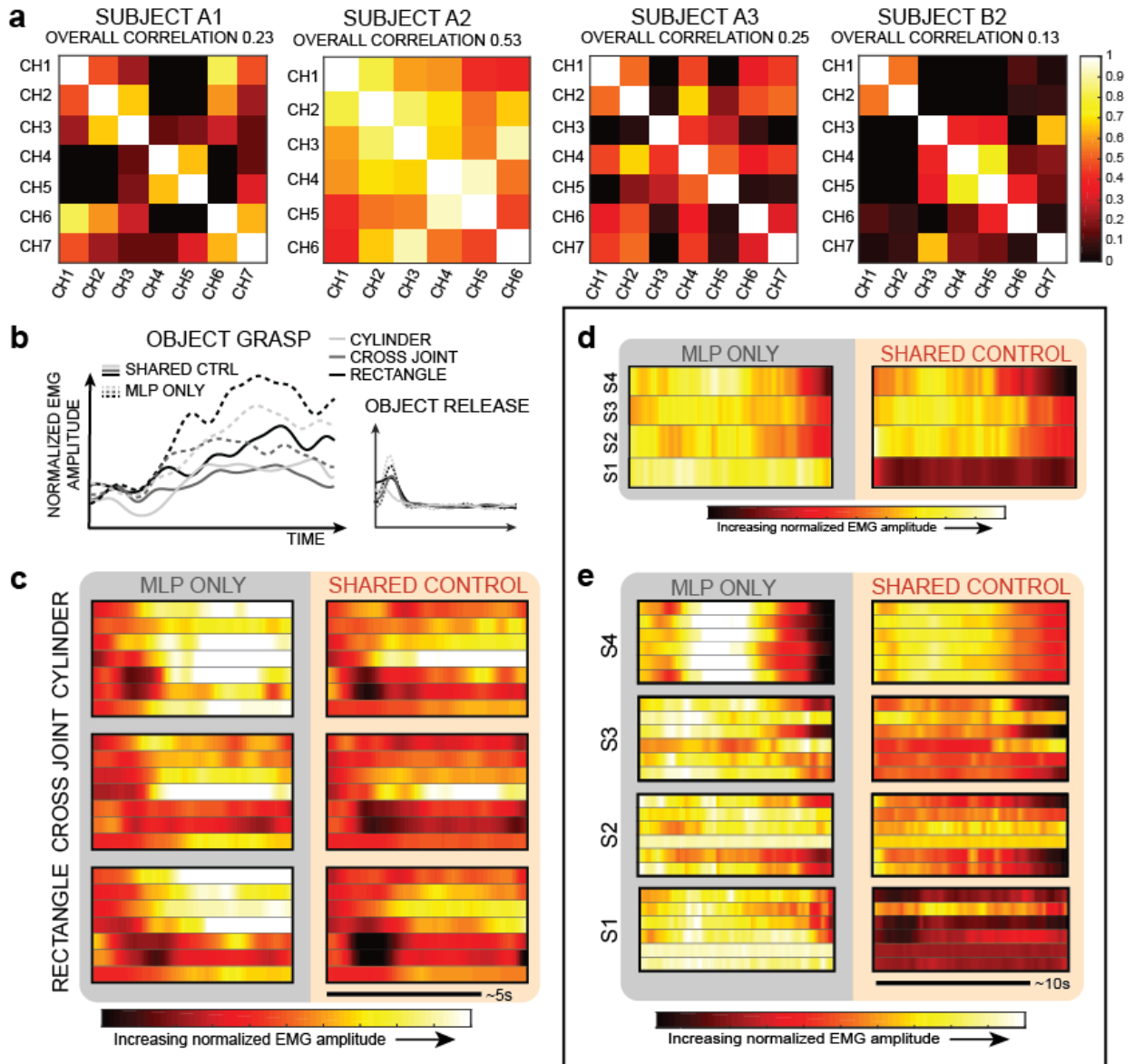


Figure 6. EMG analysis with and without shared control. **a**, Cross-correlation of EMG activity between each of the recorded channels for four subjects during a single session of MLP decoding. Darker pixels indicate lower correlation between pairs of EMG channels while brighter pixels indicate high correlation. High correlation is a proxy for muscle coactivation. **b**, Averaged sEMG amplitude during grasping trials for Subject B2 for the three objects in the virtual environment. Solid lines indicate EMG amplitude during grasp trials of shared control and dashed lines indicate average EMG amplitudes during trials with only MLP control (left). The same plot is shown for release trials: when the subject was instructed to release the object (right). **c**, Per-channel EMG activity during grasp trials of each object for Subject B2. Each row is normalized amplitude of a single EMG channel averaged over all grasping trials for a particular object. **d**, Averaged EMG activity during grasps of the physical box and block task for each subject. Activity is averaged across all grasps and all channels per subject. **e**, Per-channel EMG activity of grasps during one session of the physical box and blocks task for each Subject. Each row is normalized amplitude of a single EMG channel averaged over all trials for a particular subject.

4. Methods

Subjects and EMG recording. Three amputee subjects were recruited for this study, two female (Subjects A2 and A3) aged 53 and 49, respectively, and one male (Subject A1) 69 years of age. Subjects A1 and A2 had proximal transradial amputations while subject A3 had a right hand amputation just distal to the wrist (Figure 1). In addition, seven able bodied subjects were recruited, all of whom were male, between 26 and 30 years of age for experiment 1 and 2. Subject B6 was left-handed and performed all experiments with the left hand. Four additional male subjects aged between 20 and 26 (S1, S2, S3, and S4) were recruited for the third experiment with the physical robot. Ethical approval was obtained by the Institutional Ethics Committees of Policlinic A. Gemelli at the Catholic University, the Italian Ministry of Health, and the cantonical ethical committee of Vaud. Informed consent was obtained from all participants in the study.

In Experiments 1 and 2, we collected data from three able-bodied subjects (subjects B2, B3, and B4) and all three amputee subjects. Subject B1 performed only Experiment 1. For the three experiments, we used the Noraxon Delsys system connected to a LabJack data acquisition card to wirelessly record from five to seven bipolar surface EMG channels at 2kHz from each subject. In general, we tried to use the fewest possible channels that could result in full DoF control in order to show translational potential. Thus, we opted for five channels for subjects A2, B1, B2, B3, B4 and seven channels from A1 and A3 and finally six for S1, S2 and S3. We started with using five EMG channels per subject. For the amputee subjects, we attempted to add more electrodes to improve decoding performance. Subject A2, however, had very limited surface area on the remaining forearm and so we were unable to use any additional electrodes. For the able subjects, the muscles targeted were the extensor digitorum, flexor carpi radialis, palmaris longus, flexor digitorum superficialis and flexor carpi ulnaris, located with palpation. Due to the differences in the cause of amputation (ex. Torsion vs. lacerating), remaining muscles in the forearm differed in placement from non-amputees so palpation of the stump for controllable muscle tone determined electrode placement.

EMG processing and Feature Extraction. We chose eight well-explored time-domain features to extract for both experiments 1 and 2 (32,33):

- Mean absolute value
- Zero crossing: number of time that the amplitude value of the EMG crosses zero
- Slope sign changes: number of times that the slope of the EMG amplitude changes sign
- Waveform length: cumulative length of the EMG waveform
- Log detector: $e^{\frac{1}{N} \sum_{i=1}^N \log(|x_i|)}$ where x_i is the EMG amplitude at time bin i .
- Root mean square of EMG amplitude
- Willison amplitude: number of times the difference between two EMG neighboring samples is greater than a certain threshold. In the implemented code, the threshold has been set to 0.2 times the value of the standard deviation of the global signal.
- Maximum absolute value was used only in Experiment 3.

In Experiment 1, all seven features of all channels became the inputs of the multilayer perceptron model. In experiments 1 and 2, we used a 100ms-sliding window with 50ms of overlap to calculate features, downsampled to 30Hz for the online experiments.

For a preliminary offline experiment (Supplementary Figure 1), we also calculated four autoregressive features. Before fitting the MLP, we performed both channel and feature selection so not all features were included in the network training. In channel selection, one MLP was first trained and tested for each EMG channel. The channel providing the highest estimation performance was chosen as the first optimal channel. In the second fit iteration, the previously selected channel was paired with each of the remaining channels. These pairs were then used to train and test other MLPs. Again, the pair providing the highest estimation performance was chosen as the optimal subset of two channels. This procedure was repeated until either the increase in coefficient of determination (R^2) after adding one channel was less than 0.01 or a limit of 5 channels was reached. For feature selection, the same forward selection algorithm as for channel selection was used, repeating as long as the increase in R^2 after adding one feature was greater than 0.01. For the third experiments, we used a 300ms sliding window with 30ms overlap to extract features offline. Online frequency was kept the same, no feature selection was applied nor channel selection.

Experiments in a virtual environment (Experiments 1 and 2)

Experiment 1 began with a training period lasting approximately 3 minutes. The subject watched a series of movements on a screen performed by a pair of virtual robotic hands (Modular Prosthetic Limb by Johns Hopkins University Advanced Physics laboratory). The subject was instructed to try to copy the movements on the screen with mirrored movement (imagined movement of the phantom hand in the case of amputees). Each movement was repeated three times, each with a hold period of approximately five seconds. sEMG activity from the stump of the amputation (decomposed into features) and the directed movements of the virtual hand served as training signals for the MLP. Thus, we assumed perfect tracking between the subject and the movements presented on the screen. We asked subjects to perform single finger flexions and extensions, thumb opposition, closed hand, three-finger pinch, ulnar grasp, and open hand (Figure 1c). Due to subject A2's lack of residual active muscle, we asked only this subject to perform thumb opposition, index and middle finger combined flexions and extensions, closed hand, three-finger pinch, ulnar grasp and open hand. After the training period, subjects attempted to repeat these movements in random order, using the MLP prediction output. Again, they were cued with the virtual hand movements. Each movement was repeated five times. Either the right or left hand of the virtual hand performed the desired movement, which the subjects attempted to follow, while the other virtual hand showed the MLP-decoded output. The controllable virtual hand was ipsilateral to the amputation for amputee subjects and the dominant hand for able subjects.

During shared control, Experiment 2, the MLP output controlled one virtual hand for grasping objects. Subjects used a color cue (red/green) to signal when to grasp and release each object. Each grasp or release phase lasted seven seconds. The virtual objects presented were a cylinder, a cross-shaped joint, and a thin rectangular bar in one of three different orientations per object (rotations around either the x, y or z axes) presented at random. Subjects controlled the hand with MLP predictions of four digits: thumb, index, middle and either the ring or the pinky finger for the last finger of the Allegro Hand simulation. From the virtual environment, we are able to record data from the hand's contact sensors and hence are able to assess hand-to-object contact as well as hold time. For each object, we defined required contacts for a successful trial based on the contacts that were physically attainable. For the cylinder, required contacts were proximal interphalangeal and metacarpophalangeal contacts on every digit, for the cross-joint, required contacts were distal

and proximal interphalangeal contacts on every digit, and for the rectangular bar, required contacts were the distal phalanges of the index and ring fingers and the thumb. A trial was a success if the subject was able to achieve all required contacts simultaneously.

Experimental Hardware description

The hardware for the final “physical” experiments consists of an Allegro hand mounted on the KUKA IIWA 7 robot, OptiTrack camera system and TEKSCAN pressure sensors. The *right* allegro hand consists of three fingers and a thumb, each with four degrees of freedom. The fingers have four motors, one each at the MCP, PIP and DIP joints while the fourth motor is located just under the finger base, where it is attached to the palm and controls its lateral rotation. The thumb has three motors located at the joint connecting to the palm, controlling rotations along the three axes and one motor located at the joint connecting the two phalanges. Each of the 16 motors can be operated in position control or torque control mode, the later being used in shared control approach. A set of two TEKSCAN tactile sensor GRIP system is mounted on the allegro hand to obtain contact and pressure information at the phalanges. Due to an issue with the third finger, we had to restrain its motion completely and work with the thumb and other two fingers in all our experiments.

The allegro hand is mounted on KUKA arm so that it can be moved around in space by the subject. The subject wears a set of three OptiTrack markers on the wrist, using which the position and orientation of the subject’s hand can be detected by a set of 7 infrared camera. The EE of KUKA is then sent the same to move it in tandem with subject’s hand. KUKA IIWA 7 robot has 7 degrees of freedom, which allows its end-effector (EE) to be moved in desired position and orientation in smooth and continuous manner. An inverse-kinematics solver decodes the EE position and orientation into the individual desired joint positions, and sends them to the KUKA arm’s controller.

Protocols of the “physical” experiments (Experiment 3).

These experiments began with a training period lasting 4 and a half minutes. The subject watched a series of movements on a screen performed by the same virtual environment as experiments 1 and 2. Each movement was repeated five times, each with a hold period of approximately five seconds. sEMG activity from the forearm of the subjects (decomposed into features) and the directed movements of the virtual hand served as training signals for the MLP. Thus, we assumed perfect tracking between the subject and the movements presented on the screen. At the end of this task, the MLP was trained.

For the “box and block” task, two hard cases were placed on a table in front of the robot with a bottle of water placed on one of them. Subjects were instructed to grab a bottle of water (Badoit 1L) and move it from one box to the other. They could grasp it freely and change grip position until they felt confident enough to lift it up. A trial was considered as success if the bottle was moved from one box to the other without droppage before reaching the second box. If the subject knocked over the bottle while trying to grasp it, the experimenter put it back at initial condition and the trial was not considered as fail.

During these experiments, several metrics were used to assess the performance of the subjects:

1. Number of successful trials performed by the subject. A trial was considered as failure if the bottle fell in the gap between the two boxes.
2. Time to perform the overall task
3. Average number of contacts and the “effective normalized pressure”. These two parameters were used to characterize the quality of grasping. Owing to the varying sensitivity of the sensors, pressure of each sensor data was first normalized by dividing by the maximum detected value of the respective sensors. The normalized data were used in rest of the evaluations. The average number of contacts on each finger was computed by summing the number of contacts detected on each finger and averaged over the grasping time of each trial. Whereas, the effective normal pressure is defined as the sum of maximum normalized pressure detected on all phalanges of a finger weighed by the average contact time of the respective phalange during the grasping period of a given trial. Usually, a greater number of contacts on each finger tends to make the grasp more stable against perturbation. Further, higher pressure and duration of contact are expected to improve the grasp in a task such as block test. Therefore, it is reasonable to assume that the two metrics defined here can be used to test shared control’s performance in improving the grasp.

For the manipulation task, the same bottle was placed on a table in front of the robot. Subjects were instructed to grasp and lift the bottle, then tilt their arm as if they were drinking from it. The trial was considered successful if the water flowed to the other side of the bottle (touching the bottle cap). The subject was then required to return the arm to initial position, and then hold the bottle in the air above the table for 10 seconds without any slippage. The experimenter verified that the bottle-tilt movement phase was completed within ten seconds and that the post-movement hold period also lasted 10 seconds. The MLP was retrained between the two behavioral sessions to avoid any loss of performance and the order between the two conditions (MLP only and shared control) was reversed for each subject compared to the first session.

Multilayer perceptron model. We chose to use the multilayer perceptron as the decoding method for decoding finger kinematics due to its extensive use in sEMG applications (34). For experiment 1 and 2, we chose a three-layer network with one input layer, one hidden layer with three neurons and an output layer. The input layer is composed of the different features extracted from sEMG data and the number of nodes is dependent on the number of channels we recorded. Each of the three neurons of the hidden layer exhibit a hyperbolic tangent activation function. The output layer is the decoded output and consists of only one parameter (DoF). Hence, the full decoder incorporates as many MLP networks as desired degrees of freedom. The decoded joints in Experiment 1 were wrist pronation/supination, index and middle finger flexion/extension and ring and little fingers flexion/extension (three DoFs total). The decoded joints in Experiments 2 and 3 were metacarpal-phalangeal joint angle and interphalangeal joint angle of each digit, and thumb opposition/reposition (11 DoFs total). For more robustness, we averaged value of the interphalangeal and metacarpal-phalangeal joints per digit and considered them one DoF for all analyses.

Model training defines the weights of each node’s contribution to the next layer and in an MLP, all nodes of one layer are connected to each of the nodes of the next layer by these weights. Training was accomplished by minimizing a sum-of-squares error function. A training set with

input features x_n where n is the number of time lags ($n = 1, \dots, N$) and desired kinematics t_n has the error function:

$$E(w) = \frac{1}{2} \sum_{n=1}^N \|y(x_n, w) - t_n\|^2$$

Here, w is the array of weights of the neurons and y are the predicted kinematics using the feature input. We chose to use the Levenberg-Marquardt method for fitting the network weights due to its faster convergence time than the more typical gradient descent methods.

In order to fit the MLP weights in Experiment 1, seven movement repetitions were used for the training set, five for the testing set and three for the validation set. We used 10-fold cross-validation in Experiment 1 and 4-fold cross-validation in Experiments 2 and 3, with the training and test sets in order to determine the optimal weights for testing. In Experiment 2, each session began with a 3-minute training phase in order to record a data set of desired movements consisting of three repetitions of each movement, of which 70% of the time was used for training and 30% for validation. We then performed cross-validation in order to choose the optimal weights for online control. The full model-training process lasted a total of less than ten minutes for all of the subjects, with exact duration depending on the number of EMG channels used. Hence, we emphasize the practical implications of such an algorithm for clinical use.

We also performed a preliminary offline experiment in which three able-bodied subjects index and middle finger combined flexion/extension, ulnar grasp/release, and wrist pronation/supination in three different arm positions: arm extended, arm flexed, and arm at rest (supported) shown in Supplementary Figure 1. Subjects performed bilateral volitional alternating movements of each DoF while we optically tracked kinematics of the hand and arm contralateral to the one from which we recorded sEMGs. The MLP decoder was then trained and we performed offline testing of decoder performance. Decoding accuracy of the testing set for one subject is plotted in Figure 2a. With impressive R2 values of 0.82, 0.79 and 0.80 for the index and middle finger flexion/extension, ring and pinky finger flexion/extension, and wrist pronation/supination respectively, the MLP is able to predict movements with high accuracy for each of the DoFs simultaneously. In particular, the decoder adeptly tracks both the sinusoidal flexions and extensions as well as sustained flexion or extension to the full range of motion of the DoFs.

For the final “physical” experiment, the architecture of the MLP was changed slightly from the first two experiments. The MLP was designed using TensorFlow’s (35) premade DNN regressor class and consisted of three fully connected layers as the other experiments but in this case the hidden layer consisted of thirty neurons that exhibited a ReLU activation function ($\max[0, x]$). The output layer is also the decoded output and consists of only one parameter (DoF). Therefore, there was again one MLP per decoded joint. In this case, joint angle values were kept independent. The loss function was the mean squared error as before. The network was trained using adaptive moment estimation (Adam). During training of experiment 3, subjects were required to perform five repetitions of each movement; four were used as the training set and one for validation. No cross-validation was needed since we could directly see the performance in real time with the robot (~test set). The full model-training process lasted approximately ten minutes for each of the three subjects.

Online Control.

Real time software for the MLP was programmed in C++ (Visual Studio 2015)) for experiment 1 and 2, which integrated input from the EMG recording systems and sent decoded joint angles to the Modular Prosthetic Limb and to the Allegro Hand simulator in Gazebo. For experiment 3 the real-time software was programmed in Python 3.6, which received the EMG signals and sent decoded joints to the real Allegro Hand. In the C++ software, matrix functions were implemented using the Armadillo class³⁸ and Scilab (Scilab Enterprises 2012). After fitting of the MLP, we extracted features from EMG signals in real time. Here, we use only the most recent 100ms (or 300ms in the third experiment) of EMG data for feature computation. We first normalize EMG amplitudes with means and standard deviations derived from the training data of the same channels and then made prediction updates at 33Hz (every 30ms). To obtain a smoother signal, we low-pass filtered the MLP output with a 10-frame moving average and in the third experiment, a Kalman filter was added after the moving average filter.

Shared Controller. The autonomous controller for the shared-control condition adapted from the compliant contact approach published by Sommer and Billard for the maximization of “desired contact points” with objects(23). As soon as the hand is in contact with the object, the controller moves the fingers in directions that increase the area in contact. It stops once it has established a contact at all desired contact points. The digits are controlled in torque-mode at all times. The controller’s principle is based on operational space control. That is, it projects the forces/torques in the nullspace of the contact forces. The controller can also modulate the torques in the fingers’ joints to generate the desired forces at the contact point so as to stabilize the object. For a complete mathematical description of the approach, the reader can refer to Sommer and Billard(23).

Depending on the task, different types of contact points and numbers of contacts can be defined. In our implementation, we used a Gazebo simulator of the Allegro Hand, which is a 4-digited robotic hand with simulated contact sensors on the inner, side and top surface of each digit. The hand has three phalanges per digit and joints between the phalanges can all be independently controlled in torque, for a total of 16 actuated degrees of freedom. We defined one desired contact per phalanx of each finger and two for the thumb for a total of 11 desired contacts on the simulator. When the hand is not touching any objects, a proportional-derivative (PD) controller modulates joint torques to achieve the desired joint angle targets. These targets are the angles decoded by the MLP, and streamed to the simulation over UDP. Instead of predefined preshaping as in the previous work, preshaping is left to the user. Indeed, we observed thumb opposition before finger flexion for many subjects (see Supplementary Video 2), which allowed them high grasp stability. In lieu of the drill object tested previously, we presented a thin rectangular bar along with the cylinder and cross joint part (Suppl. Fig. 3a). Each object was tested in one of three random orientations, 30 degrees tilted in either roll, pitch or yaw. This allowed exploration of the full range of object locations with respect to the hand.

In the shared control condition, the algorithm attempts to maximize contact area by applying motor torques in the direction of desired contact points. Once a digit comes in contact with an object at any location, the controller will exert joint torques on the hand in order to achieve more desired contact points with the object. The direction of these joint torques is computed as a summation of the normal vector of the contact point with the object and the direction of the desired contact towards that point (Figure 4c). If there is no contact between a digit and an object, that digit is still PD-controlled to achieve the MLP output’s target angles. As for the contacts already made

between the hand and the object, the shared controller exerts a predefined force, but also permits joint torques in magnitude and direction such that contact force between the desired contact and the object does not change, the contact nullspace. Thus, each digit is allowed to slide along the surface of the object to continue seeking contact with the object at “desired contacts” that have not yet been achieved. Meanwhile, the PD controller continues to compute the joint torques required to achieve MLP-dictated joint angles. The shared controller applies the vector components of these joint torques at already-achieved contacts such that the those contact forces do not change. The result is that the user is still able to move the hand over the object as desired without breaking contact. This feature made object manipulation possible.

The shared controller is designed to optimize for maximum contact between hand and object. However, if the difference in desired joint angle of the active shared controller becomes too different (defined in our case as 50 degrees total difference amongst all joints of a digit) from the decoded MLP output, the PD controller takes over again using MLP-decoded joint angles as target angles. Thus, any contact that may already exist could freely be broken.

Code availability

The MATLAB code used for data analysis and synthesis of results presented in this study are available at <https://github.com/KZizzle/0713.git>. Data collection code is available from the corresponding author on reasonable request.

Data availability

The data that support the findings of this study are available within the paper and its Supplementary Information. All datasets generated for this study are available from the corresponding author upon reasonable request.

Author Contributions

K.Z. and E.F. designed and carried out Experiments 1-2, and performed analysis of data. A.B. and S.M. were responsible for planning and supervising of the work. N.S. provided code and expertise for the shared controller and contributed greatly to experimental setup. V.M. and F. A. developed the decoding algorithm for Experiment 3. V.M., F.A, S.A. performed the system integration. V.M. S.A performed all the trials for Experiment 3. E.D. aided in experimentation, G.G., G.C., and W.R. were clinical liaisons, and F.P. supervised Experiment 1. K.Z., V.M., and S.A. wrote the manuscript and designed figures. N.S., E.F., E.D., A.B., F.A* and S.M. all contributed critical feedback to the manuscript.

Acknowledgements

We wish to acknowledge Brock Wester, Francesco Tenore, and the Johns Hopkins University Applied Physics Laboratory (JHU/APL) for providing the Virtual Integration Environment (VIE), which was developed on the Defense Advanced Research Projects Agency (DARPA) Revolutionizing Prosthetics program under Contract No. N66001-10-C-4056. We would also like to thank Francesco Iberite for his assistance in conducting experiments and Alexis Devillars for the development of the Unity model of the hand.

This project was partly funded by the Swiss National Competence Center for Research (NCCR) in Robotics, by the Bertarelli Foundation, and by the European Union’s Horizon 2020 research and

innovation programme under Marie Skłodowska Curie grant agreement No. 750947 (project BIREHAB).

References

1. Ziegler-Graham K, MacKenzie EJ, Ephraim PL, Travison TG, Brookmeyer R. Estimating the Prevalence of Limb Loss in the United States: 2005 to 2050. *Arch Phys Med Rehabil*. 2008 Mar 1;89(3):422–9.
2. Watve S, Dodd G, MacDonald R, Stoppard ER. Upper limb prosthetic rehabilitation. *Orthop Trauma*. 2011 Apr;25(2):135–142.
3. Geethanjali P. Myoelectric control of prosthetic hands: state-of-the-art review. *Med Devices Auckl NZ*. 2016;9:247.
4. Biddiss E, Chau T. Upper-Limb Prosthetics: Critical Factors in Device Abandonment. *Am J Phys Med Rehabil* [Internet]. 2007;86(12). Available from: http://journals.lww.com/ajpmr/Fulltext/2007/12000/Upper_Limb_Prosthetics__Critical_Factors_in_Device.4.aspx
5. Biddiss EA, Chau TT. Upper limb prosthesis use and abandonment: A survey of the last 25 years. *Prosthet Orthot Int*. 2007 Sep 1;31(3):236–57.
6. Farina D, Jiang N, Rehbaum H, Holobar A, Graimann B, Dietl H, et al. The Extraction of Neural Information from the Surface EMG for the Control of Upper-Limb Prostheses: Emerging Avenues and Challenges. *IEEE Trans Neural Syst Rehabil Eng*. 2014 Jul;22(4):797–809.
7. Hioki M, Kawasaki H. Estimation of Finger Joint Angles from sEMG Using a Neural Network Including Time Delay Factor and Recurrent Structure. 2012 Mar 14;2012.
8. Malešević N, Marković D, Kanitz G, Controzzi M, Cipriani C, Antfolk C. Decoding of individual finger movements from surface EMG signals using vector autoregressive hierarchical hidden Markov models (VARHHMM). In: 2017 International Conference on Rehabilitation Robotics (ICORR). 2017. p. 1518–23.
9. Tenore FVG, Ramos A, Fahmy A, Acharya S, Etienne-Cummings R, Thakor NV. Decoding of Individuated Finger Movements Using Surface Electromyography. *IEEE Trans Biomed Eng*. 2009 May;56(5):1427–34.
10. Smith RJ, Tenore F, Huberdeau D, Etienne-Cummings R, Thakor NV. Continuous decoding of finger position from surface EMG signals for the control of powered prostheses. In: 2008 30th Annual International Conference of the IEEE Engineering in Medicine and Biology Society. 2008. p. 197–200.
11. Ngeo JG, Tamei T, Shibata T. Continuous and simultaneous estimation of finger kinematics using inputs from an EMG-to-muscle activation model. *J NeuroEngineering Rehabil*. 2014;11:122.

12. Krasoulis A, Vijayakumar S, Nazarpour K. Evaluation of regression methods for the continuous decoding of finger movement from surface EMG and accelerometry. In: 2015 7th International IEEE/EMBS Conference on Neural Engineering (NER). 2015. p. 631–4.
13. Cipriani C, Antfolk C, Controzzi M, Lundborg G, Rosén B, Carrozza MC, et al. Online myoelectric control of a dexterous hand prosthesis by transradial amputees. *IEEE Trans Neural Syst Rehabil Eng*. 2011;19(3):260–70.
14. Jiang N, Dosen S, Muller KR, Farina D. Myoelectric Control of Artificial Limbs—Is There a Need to Change Focus? [In the Spotlight]. *IEEE Signal Process Mag*. 2012 Sep;29(5):152–150.
15. Kim HK, Biggs J, Schloerb W, Carmena M, Lebedev MA, Nicolelis MAL, et al. Continuous shared control for stabilizing reaching and grasping with brain-machine interfaces. *IEEE Trans Biomed Eng*. 2006 Jun;53(6):1164–73.
16. Iturrate I, Montesano L, Minguez J. Shared-control brain-computer interface for a two dimensional reaching task using EEG error-related potentials. In: 2013 35th Annual International Conference of the IEEE Engineering in Medicine and Biology Society (EMBC). 2013. p. 5258–62.
17. Chen X, Liao Y, Wang Y, Zhang S, Zhang Q, Zheng X. A shared control policy for center-out movement decoding in motor Brain-machine Interface. 3rd IFAC Conf Intell Control Autom Sci ICONS 2013. 2013 Jan 1;46(20):345–8.
18. Ciancio AL, Cordella F, Barone R, Romeo RA, Bellingegni AD, Sacchetti R, et al. Control of Prosthetic Hands via the Peripheral Nervous System. *Front Neurosci*. 2016;10:116.
19. Došen S, Cipriani C, Kostić M, Controzzi M, Carrozza MC, Popović DB. Cognitive vision system for control of dexterous prosthetic hands: Experimental evaluation. *J NeuroEngineering Rehabil*. 2010;7:42–42.
20. Light CM, Chappell PH, Hudgins B, Engelhart K. Intelligent multifunction myoelectric control of hand prostheses. *J Med Eng Technol*. 2002 Jan 1;26(4):139–46.
21. Tura A, Lamberti C, Davalli A, Sacchetti R. Experimental development of a sensory control system for an upper limb myoelectric prosthesis with cosmetic covering. *J Rehabil Res Dev*. 1998 Jan;35(1):14–26.
22. Fani S, Bianchi M, Jain S, Pimenta Neto JS, Boege S, Grioli G, et al. Assessment of Myoelectric Controller Performance and Kinematic Behavior of a Novel Soft Synergy-Inspired Robotic Hand for Prosthetic Applications. *Front Neurorobotics*. 2016;10:11.
23. Sommer N, Billard A. Multi-contact haptic exploration and grasping with tactile sensors. *Robot Auton Syst*. 2016 Nov 1;85:48–61.

24. Celadon N, Došen S, Binder I, Ariano P, Farina D. Proportional estimation of finger movements from high-density surface electromyography. *J NeuroEngineering Rehabil.* 2016;13:73.
25. Segil JL, Controzzi M, Weir RF ff, Cipriani C. Comparative study of state-of-the-art myoelectric controllers for multigrasp prosthetic hands. *J Rehabil Res Dev.* 2014;51(9):1439–54.
26. Mathiowetz V, Volland G, Kashman N, Weber K. Adult norms for the Box and Block Test of manual dexterity. *Am J Occup Ther.* 1985;39(6):386–91.
27. Park E, Meek SG. Fatigue compensation of the electromyographic signal for prosthetic control and force estimation. *IEEE Trans Biomed Eng.* 1993 Oct;40(10):1019–23.
28. Tkach D, Huang H, Kuiken TA. Study of stability of time-domain features for electromyographic pattern recognition. *J NeuroEngineering Rehabil.* 2010 May 21;7(1):21.
29. Asghari Oskoei M, Hu H. Myoelectric control systems—A survey. *Biomed Signal Process Control.* 2007 Oct 1;2(4):275–94.
30. Micera S, Carpaneto J, Raspopovic S. Control of Hand Prostheses Using Peripheral Information. *IEEE Rev Biomed Eng.* 2010;3:48–68.
31. Wan B, Xu L, Ren Y, Wang L, Qiu S, X. Liu, et al. Study on fatigue feature from forearm SEMG signal based on wavelet analysis. In: 2010 IEEE International Conference on Robotics and Biomimetics. 2010. p. 1229–32.
32. Zardoshti-Kermani M, Wheeler BC, Badie K, Hashemi RM. EMG feature evaluation for movement control of upper extremity prostheses. *IEEE Trans Rehabil Eng.* 1995 Dec;3(4):324–33.
33. Phinyomark A, Phukpattaranont P, Limsakul C. Feature reduction and selection for EMG signal classification. *Expert Syst Appl.* 2012 juin;39(8):7420–31.
34. Chu JU, Moon I, Mun MS. A Real-Time EMG Pattern Recognition System Based on Linear-Nonlinear Feature Projection for a Multifunction Myoelectric Hand. *IEEE Trans Biomed Eng.* 2006 Nov;53(11):2232–9.
35. Abadi M, Barham P, Chen J, Chen Z, Davis A, Dean J, et al. Tensorflow: A system for large-scale machine learning. In 2016. p. 265–83.

3.2 Robotic Automation to Perform In-Hand Object Manipulation

The content of this section is the postprint from the article Khadivar, Mendez et al., "EMG-driven shared human-robot compliant control for in-hand object manipulation in hand prostheses," 2022 J. Neural Eng. 19 066024

Find the published article here: <https://doi.org/10.1088/1741-2552/aca35f>

Personal contributions as the co-first author: conceived the experiments, prepared the protocols and the experimental setup (hardware and software) on the EMG side, co-conducted the experiment, analyzed part of the results, prepared part of the figures, and wrote part of the manuscript.

EMG-Driven Shared Human-Robot Compliant Control for In-Hand Object Manipulation in Hand Prostheses

Farshad Khadivar^{1,5}, Vincent Mendez^{2,5}, Carolina Correia³, Iason Batzianoulis³, Aude Billard^{1,6}, Silvestro Micera^{2,4,6}

¹ LASA Laboratory, Ecole Polytechnique Fédérale de Lausanne, 1015 Laussane, Switzerland

² Neuro X Institute, Ecole Polytechnique Fédérale de Lausanne, 1202 Genève, Switzerland

³ Former member of LASA Laboratory, Ecole Polytechnique Fédérale de Lausanne, 1015 Laussane, Switzerland

⁴ BioRobotics Institute and Department of Excellence in Robotics and AI, 56127 Pisa, Italy

⁵ Equal contribution co-authors.

⁶ Equal contribution senior authors.

Abstract

Objective. The limited functionality of hand prostheses remains one of the main reasons behind the lack of its wide adoption by amputees. Indeed, while commercial prostheses can perform a reasonable number of grasps, they are often inadequate for manipulating the object once in hand. This lack of dexterity drastically restricts the utility of prosthetic hands. We aim at investigating a novel shared control strategy that combines autonomous control of forces exerted by a robotic hand with electromyographic (EMG) decoding to perform robust in-hand object manipulation. **Approach.** We conduct a 3-day long longitudinal study with 8 healthy subjects controlling a 16-degrees-of-freedom robotic hand to insert objects in boxes of various orientations. EMG decoding from forearm muscles enables subjects to move, proportionally and simultaneously, the fingers of the robotic hand. The desired object rotation is inferred using two EMG electrodes placed on the shoulder that record the activity of muscles responsible for elevation and depression. During the object interaction phase, the autonomous controller stabilizes and rotates the object to achieve the desired pose. In this study, we compare an incremental and a proportional shoulder-decoding method in combination with two state machine interfaces offering different levels of assistance. **Main results.** Results indicate that robotic assistance reduces the number of failures by 41% and, when combined with an incremental shoulder EMG decoding, leads to faster task completion time (median=16.9s), compared to other control conditions. Training to use the assistive device is fast. After one session of practice, all subjects managed to achieve tasks with 50% less failures. **Significance.** Shared control approaches that give some authority to an autonomous controller on-board the prosthesis are an alternative to control schemes relying on EMG decoding alone. This may improve the dexterity and versatility of robotic prosthetic hands (RPHs) for people with trans-radial amputation. By delegating control of forces to the prosthesis' on-board control, one speeds up reaction time and improves the precision of force control. Such a shared control mechanism may enable amputees to perform fine insertion tasks solely using their prosthetic hands. This may restore some of the functionality of the disabled arm.

Keywords: In-hand manipulation, EMG decoding, Shared-control, Compliant robot Control

1. Introduction

We rely on our hands and their fine dexterity to perform everyday tasks, from basic manipulations, such as picking up a glass of water, to fine-manipulation skills, such as writing, knitting, and playing an instrument. The human hand owes its dexterity to its individuated control of finger motion and precise sense of touch, and to dedicated brain processes for ensuring fluent control of objects once in hand [Kontoudis2019, Castiello2005].

Being deprived of this dexterity following an amputation affects one's life considerably. Even the simplest chores, such as placing the cap on a bottle or inserting a spoon in a cup, become arduous if not impossible. The lack of tactile perception and the absence of fine finger motions are the predominant hindering factors that render reorienting or repositioning an object impossible. If one could restore some, even if a tenuous part, of this dexterity through the help of automation and robotics, this would have immediate benefits to the persons with an amputation.

While robotics has made vast progress in the control of human-like robotic hands [melchiorri2016robot, okamura2000overview], these advancements have rarely been used to control prostheses. The main reasons are that (i) robotic prosthetic hands (RPHs) remain under-actuated with simple position or speed control, and (ii) we still lack robust decoding strategies to infer and translate the user's intentions into fine and individuated finger motions of an RPH. The latter is a bottleneck that reduces the incentive to develop more complex robotic hands for people with trans-radial amputation.

With a look towards the availability of better and more performing hand prostheses – and while recognizing that individuated finger EMG decoding will remain limited in its accuracy –, we design shared control mechanisms where a robotic controller is in charge of low-level closed-loop control. This controller enables online adaptation of the positioning of fingers and stabilization of the object in hand through forces applied by the fingers. To this end, we build on recent advances in robotic hand control to enable human-like control of the fingers in either individual or coordinated manner [li2016dexterous]. Such enhancements permit the execution of robust grasps with multi-finger robotic hands.

Commercially available RPHs rely on identifying motion intention using EMG. The control of prostheses is usually achieved by placing two electrodes on two remaining antagonist muscles of the forearm. A threshold is set on the EMG amplitude acquired at a fixed frequency to control one degree of freedom (DoF) for closing or opening the fingers by a small increment [mendez2021current]. This is insufficient to capture individuated finger motions and does not allow to provide continuous control of fingers.

Finer EMG-based control can be obtained using single-finger angle regression [1]. With this method, the RPH follows the intended motion of the user in an intuitive manner [Farina2014]. Several groups showed successful use of multi-layer perceptrons (MLPs) for the regression of single finger angles. For instance, one of the first example in 2008, Smith et al. [2] showed the

possibility to regress the metacarpophalangeal (MCP) joint angle of each finger individually and simultaneously with a neural network. Ngeo et al. [Ngeo2014] showed the possibility to regress MCP angle as well as proximal interphalangeal (PIP) and distal interphalangeal (DIP) joint angles of each fingers using a MLP. Finally, Dantas et al. [Dantas2019] obtained similar performance with intramuscular EMG recorded from two amputee patients between convolutional neural network and MLP outperforming polynomial Kalman filters and Long Short-Term Memory networks for single-finger angle regression.

However, continuous control of finger motion from EMG is susceptible to noise. The slightest error in EMG-based intent detecting could lead a finger to inadvertently re-open, letting the object slip. Hence, controlling for a stable and robust grasp when manipulating objects is crucial to restoring the essential dexterity needed for everyday use. This requires ensuring fast and accurate control of finger-object interactions.

Decades of research in robotics have been devoted to devising algorithms for closed-loop control to enable on-the-fly stabilization of a grasp to secure an object in hand when subjected to external disturbances [billard2019trends]. Typically, re-balancing the forces to stabilize the object is performed through impedance control [kao1992quasistatic], whereas repositioning of fingers on the object requires planning algorithms [li2014learning]. In this paper, we consider the task of inserting an object into another object. Such a "peg-in-hole" task can be considered a robotic benchmark. While it has received attention already in the 70's [takeyasu1976precision], it remains a topic of research [tang2015learning]. As simple as it may appear, inserting an object into another one still relies on complex algorithms to determine when the object is jammed and when to correctly adapt the object's orientation so that neither object nor the robot is damaged. Such rapid and compliant control of finger-object interaction requires estimating the force at contact and adapting fingers' motion accordingly. Contact detection is usually done through reading of tactile sensors, sometimes in combination with vision [karayiannidis2016adaptive].

When controlling a prosthesis tasked to insert an object into another one, we must assume that the autonomous controller of the prosthesis has access solely to tactile information. Corrections driven by visual feedback are conveyed implicitly through EMG-based intention detection, driven by the amputee's visual appraisal of the situation. In this paper, we design a shared control framework that uses an autonomous compliant control of fingers to adapt fingers' orientation and exerted forces only based on tactile information.

When integrating users' motor intentions for individuated finger control, a possible solution is to distribute the control by automating some parts of the motor commands and relieving the user from precise modulation [3]. It can ease grasping through preshaping [4], grip force adjustment [3], slip detection [5], and even hand closing using underactuated systems in which spring-like mechanisms mediate grasp force [6]. The Ottobock Sensorhand Speed is a commercial example of shared control in RPHs, which automatically increases thumb flexion during grasping in response to slippage [Ciancio2016]. A more recent study [zhuang2019shared]

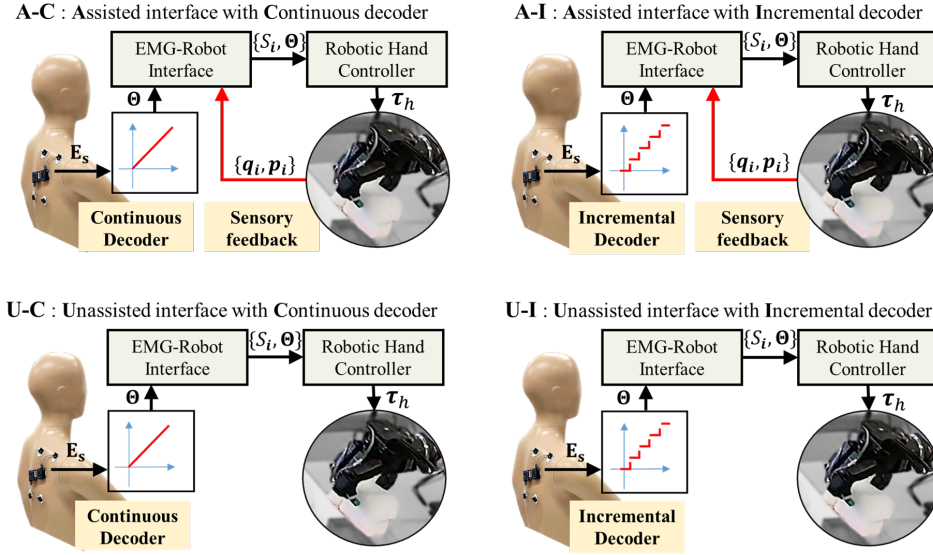


Figure 1. List of shared control conditions. We conduct a 2x2 experimental study with two levels of autonomy in the EMG-Robot interface, (**U**) unassisted and (**A**) assisted, and with two types of EMG shoulder decoding, (**C**) continuous and (**I**) incremental. $E_s \in \mathbb{R}$ is the EMG signal from the shoulder. Θ is a vector of high-level commands determined via EMG decoding (see Figure 3). $S_t \in \mathbb{R}$ denotes the state machine defining the hand's control mode (see Figure 6), and $\tau_h \in \mathbb{R}^{16}$ is the joint torques computed to control the robotic hand. $q_i \in \mathbb{R}^4$ and $p_i \in \mathbb{R}$ are, respectively, the joint positions and tactile sensor feedback for the i -th finger.

showed that an EMG-based shared control strategy could ensure the safe handling of a bottle filled with content. This work leveraged an autonomous robot control that maximized the number of contacts between the robotic hand and an object.

This work evaluates novel shared control strategies to perform EMG-driven object manipulation tasks. We show that these shared control approaches allow subjects to perform a continuum of manipulation: from grasping an object to manipulating it in air and during insertion when in contact with another object. The subject remains in control of deciding when to grasp and release the object and how to preshape the hand. Importantly, our shared control mechanism enables subjects to rotate objects in hand when controlling a dexterous 16-DoF robotic hand. This is achieved thanks to the following:

- i An EMG-based single-finger proportional decoder to infer high-level finger motor intentions from forearm muscles.
- ii A second EMG-based decoder from shoulder muscles to let the user control the in-hand object rotation via elevation or depression of the shoulder.
- iii A virtual object-based compliant controller for low-level robot control. Given the task objective and tactile feedback, the low-level control of the robotic hand employs an autonomous and adaptive compliant controller that regulates online the interaction forces

at contact points.

- iv An interface that uses feedback-based state machines to integrate high-level and low-level robot control. The interface selects which task has to be executed, provided the subject's command and robotic feedback.

In a first experimental protocol, we compare two methods for shoulder decoding, and measure how quickly and precisely healthy participants are able to rotate objects in various orientations. Then, we evaluate our shared control approach with the two shoulder decoding strategies in a longitudinal study, where participants are required to teleoperate a robotic arm to pick, rotate and place an object in boxes with different orientations. The aim of this functional assessment is to evaluate the robustness of our shared control, taking into account the noise induced in finger decoding from forearm motions and interactions between the shoulder decoder and arm motions that would also be present in the case of persons with an amputation.

2. Methods

The first experiment is designed to compare two EMG shoulder decoding strategies, while the robotic hand is locked in place. The first approach is a threshold-based incremental decoding. When the subject elevates or lowers the shoulder and the EMG activity recorded from one electrode exceeds a threshold, the decoder modulates a rotation value that remains constant when the shoulder rests. The second strategy consists of a continuous decoder based on a support vector regression (SVR) algorithm that directly maps the shoulder position to the rotation value (e.g. maximum shoulder movement will result in maximum rotation and rest corresponds to zero rotation). We envision that the continuous decoder would allow subjects to rotate the object faster [Cler2014] as object rotation is proportionally correlated to shoulder movements, whereas the incremental one would be more robust to noise since it does not rely on a non-linear pattern recognition model.

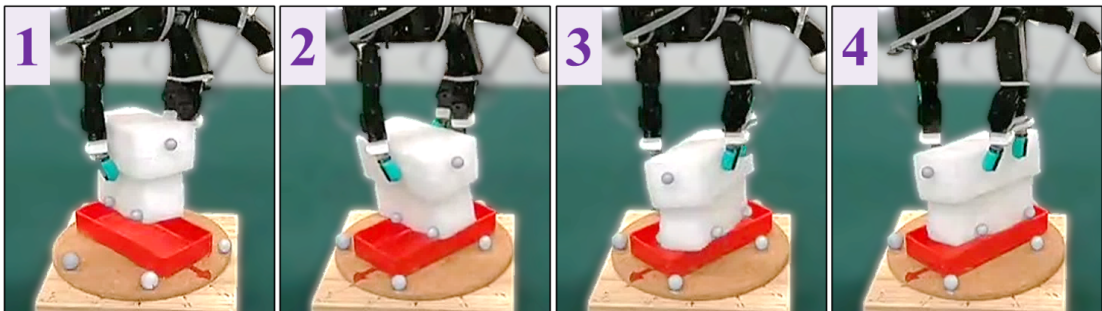


Figure 2. An example of tracking target angle in the first experiment. From left to right: (1) the object and the base are aligned in 60° , (2) target angle is changed to -30° , (3) user is performing in-hand rotation with the robotic hand, and (4) target angle is achieved. All target angles of the rotating base are -60° , -30° , 0° , 30° , and 60° .

In the second experiment, we compare four different shared control schemes; see Figure 1. We

perform a 2x2 experimental study with two levels of autonomy in the state machine interface versus the two types of EMG shoulder decoding, resulting in a total of four types of shared control schemes.

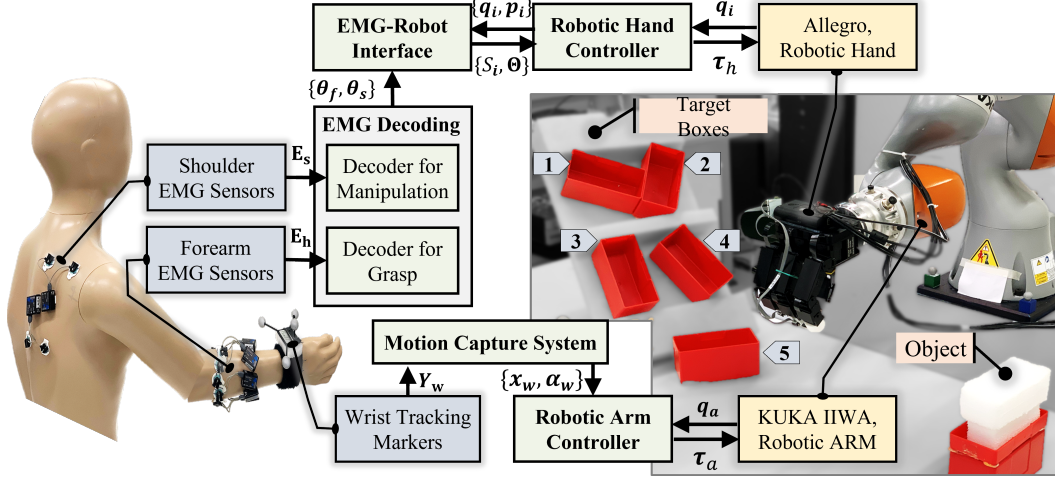


Figure 3. Overview of the experimental setup. The subject is asked to grasp a cuboid and place it in one of the target boxes, differing in position and orientation. The order of all pick and place tasks, as specified from 1 to 5, is fixed throughout the entire recording. A KUKA IIWA 14 robotic arm is set to follow the displacement of the subject’s wrist acquired via the Optitrack capture system (Y_w : markers tracking signals, $x_w \in \mathbb{R}^3$: wrist position, $\alpha_w \in \mathbb{R}^3$: wrist orientation, $q_a \in \mathbb{R}^7$: joint position feedback of the robotic arm, and $\tau_a \in \mathbb{R}^7$: joints torque command send to the robotic arm). A left Allegro robotic hand mounted with BioTac tactile sensors executes grasp and manipulation received from the EMG decoder. The hand is commanded to open or close via processing forearm EMG signals, and to rotate the object within the hand frame through shoulder EMG activation ($E_h \in \mathbb{R}^{200 \times 6}$: forearm EMG signals, $E_s \in \mathbb{R}^{200 \times 2}$: shoulder EMG signals, $\theta_f \in \mathbb{R}^5$: scaled fingers flexion, and $\theta_s \in \mathbb{R}$: scaled shoulder flexion).

The two autonomy modes of the state machine interface are (i) unassisted and (ii) assisted. In the former, the controller relies only on the command and state sequence, whereas the latter also uses feedback from the robotic system. The assisted mode utilizes tactile sensing and finger kinematics for identifying the task and its status. We expect the assistance to reduce trial failures, because it would avoid the unexpected drop of objects coming from noise in the finger EMG decoder.

In order to evaluate the performance of the proposed shared controllers, we adopt the Grooved Peg Test [Wilcox2022], a standard dexterity assessment. The test requires fine motor skills to place grooved pegs in holes with different orientations. This test is performed routinely to quantify the development of dexterity in 6-year-old children [Wilcox2022], and the loss of dexterity in stroke patients [Thompson-Butel2014]. We adapt the Grooved Peg test to the size of the robotic hand at our disposal and design a peg-in-hole task where subjects have to grasp a rectangular object and place it inside boxes with different orientations (Figure 3). An inclined surface is used to prevent subjects from relying on gravity to insert the object in the

box, when the angle of the object does not perfectly match the box's angle.

2.1 Experimental Protocol

Finger and Shoulder Decoders Calibration:

In each session of each experiment, subjects are asked to follow a series of single and multi-finger opening and closing movements performed by a virtual hand on a screen. The sequence of movements is repeated 6 times, and each movement is held for 5 s before the virtual hand goes back to its original resting position for 3 s. The rationale is to dissociate three main states of the fingers: a resting state corresponding to no muscle activation, flexed and opened positions. The total calibration time for the finger movements is 9 minutes and 30 s.

Virtual hand kinematics are recorded at 60 Hz and synchronized with the EMG acquisition system. Six DoFs are recorded from the virtual hand corresponding to each finger's flexion and thumb's opposition. Hand kinematics are rescaled between 0 (opened) and 10 (closed), and the rest position is set to 3 for each DoF to mimic a resting hand pose on the virtual hand. Since there is an intrinsic delay between the movement of the virtual hand and the finger movements of the subject, a visual inspection is performed by the experimenter to time-shift the signals and synchronize virtual hand kinematics and EMG activity (maximum shift of 300 ms).

To calibrate the continuous shoulder controller, the same setup is used, with the virtual hand alternating between closed (target = 10), opened (target = 0) and a middle position (target = 5) to record 1 DoF. The subjects are asked to elevate their shoulder when the hand is flexed, lower their shoulder when the hand is opened, and rest when the virtual hand is in the middle position. Each movement is held for 5 s, alternating with a rest position for 3 s. The sequence is repeated 6 times for a total calibration time of 1 minute and 35 s.

Shoulder Decoders Comparison:

After calibrating all EMG decoders, participants are asked to grasp a cuboid placed by the experimenter in the robotic hand, and to perform a sequence of object in-hand rotation tasks. A rotating base with indicators of the desired rotation angles is placed below the grasped object, see Figure 2. Markers are attached to the cuboid and the base to track their orientations.

The task involves rotating the object 10 times to one of the five target angles. Following instructions from an algorithm creating random integer values between 0 and 5, the experimenter rotates the base randomly between -60° , -30° , 0° , 30° , and 60° .

Before starting the experiment, the participants have a maximum three minutes to familiarize themselves with the shoulder decoders and the direction of rotation. Then, the participants must perform the task with both shoulder decoding strategies starting at random with either decoder. In the case of the cuboid falling from the robotic hand, the experimenter puts it back in the robotic hand, the base resets to the initial configuration without rotation, and the trial

is not considered. The experiment is completed in less than an hour for all subjects.

Longitudinal Functional Assessment:

The experimental protocol is summarized in Figure 5. Subjects enrolled in this experiment participate in 3 sessions consisting of 4 experiment runs. In each run, a specific control condition is selected. Given the control condition, subjects perform 5 tasks of picking and placing a cuboid in different target boxes. In our experimental protocol:

- i. A task consists of grasping a cuboid and inserting it in a target box, see Figure 4. Each experiment run consists of 5 tasks that differ only in position and orientation of target boxes, see Figure 3. Throughout the entire experiment, the order of tasks is fixed.
- ii. There are 4 control conditions specified as the combination of 2 shoulder control conditions (incremental and continuous EMG decoder) and 2 state machine interfaces (assisted and unassisted). Control conditions are listed in Figure 1. To eliminate the effect of factors like fatigue in our analysis, the order of control conditions is chosen randomly for each subject and session.
- iii. Before each session, subjects have to calibrate the finger decoding model and the continuous shoulder controller. The calibration process takes between 12 and 15 minutes.
- iv. After model calibration, subjects are verbally instructed to perform the experiment. Subjects are informed which shoulder decoder is activated but not which control condition is utilized. After each experiment run with a control condition, subjects are given a 2-minute break before starting with the next control condition.
- v. Since acquaintance with the setup can affect performance, all subjects participate in 3 sessions over 3 consecutive days, in order to account for the expected learning effects.
- vi. An experimental session takes between 60 and 100 minutes for all subjects.

2.2 Subjects and EMG Recording

In the first experiment, four male participants aged between 27 and 32, all right-handed are enrolled (average weight: 77kg, average height 177cm). Eight subjects are recruited for the second study, all of whom are males aged between 26 and 30 (average weight: 74kg, average height: 177cm, and two left-handed). A Noraxon DTS system wirelessly records EMG signals at 1 kHz. Six bipolar surface EMG channels are placed on the right forearm to target the extensor digitorum, flexor carpi radialis, palmaris longus, flexor digitorum superficialis, and flexor carpi ulnaris muscles, located with palpation. Two other bipolar surface EMG channels are placed on the right shoulder and the back of the subjects to target the upper and lower fibers of the trapezius that allow, respectively, elevation and depression of the shoulder joint.

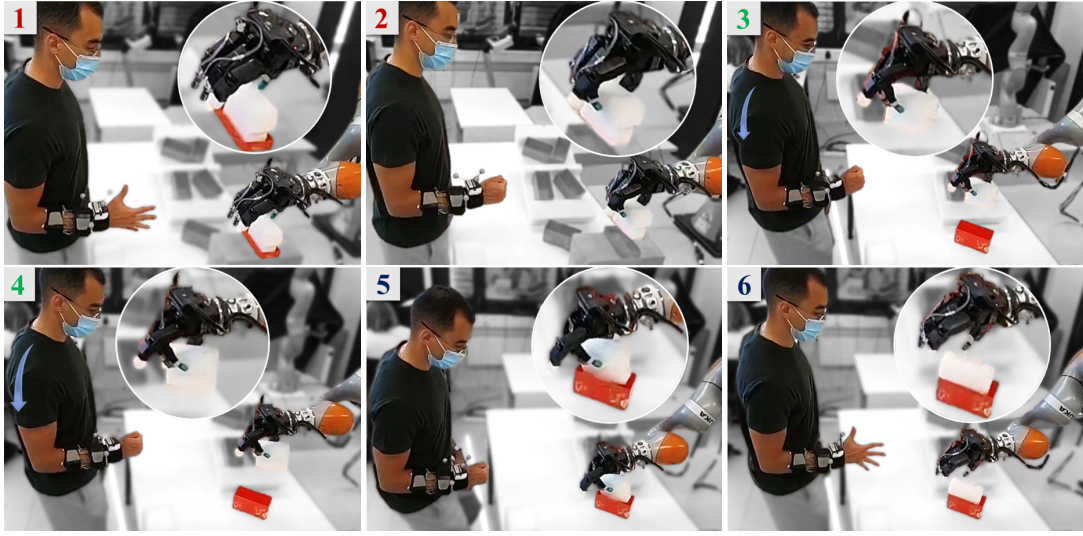


Figure 4. An example of one experiment run. The subject first grasps the object (red numbers), then rotates it within the robotic hand (green numbers), and finally inserts it in the target box (blue numbers). (1) the subject needs to bring the robotic hand to the picking position. The robotic hand is in *open hand* mode given the fingers' EMG decoding. (2) the user commands the robotic hand to grasp the object by closing his fingers. Then, he lifts the object and moves the robotic arm near the target box. The robotic hand is autonomously holding the object. (3) Through shoulder movement, the subject tries to align the orientation of the object and the target box. (4) the subject aligns the orientations by rotating the object within the robotic hand frame. (5) the object is placed in the target box and then released (6).

2.3 Finger and Shoulder Decoders Training

For both decoders, a sliding window of 200 *ms* is used with a moving step of 30 *ms* (170 *ms* overlap). To evaluate the offline performance of the decoders, the last repetition of the sequence of movements is used as a validation set. In total, 5 features are extracted to serve as input for the decoders [Boostani2003]: (i) mean absolute value, (ii) waveform length (cumulative length of the EMG waveform over time), (iii) maximum absolute value, (iv) zero crossings (number of times the signal crosses zero), and (v) slope sign change (number of times the slope of the signal changes sign).

For the EMG finger decoder, a MLP regressor is used to decode simultaneously the 6 DoFs. The model is designed in Keras¹ with Tensorflow² backend. It has 1 hidden layer with 32 nodes (ReLU activation function). The MLP is trained using gradient descent with a batch size of 16 during 50 epochs. The learning rate is set to 0.01 and divided by 2 every 10 epochs. Early stopping is set if the validation loss is not decreasing for more than 13 epochs. A dropout is set to 0.2 during training.

The shoulder continuous decoder is an SVR algorithm with a radial basis function kernel from

¹<https://github.com/fchollet/keras>

²<https://www.tensorflow.org/>

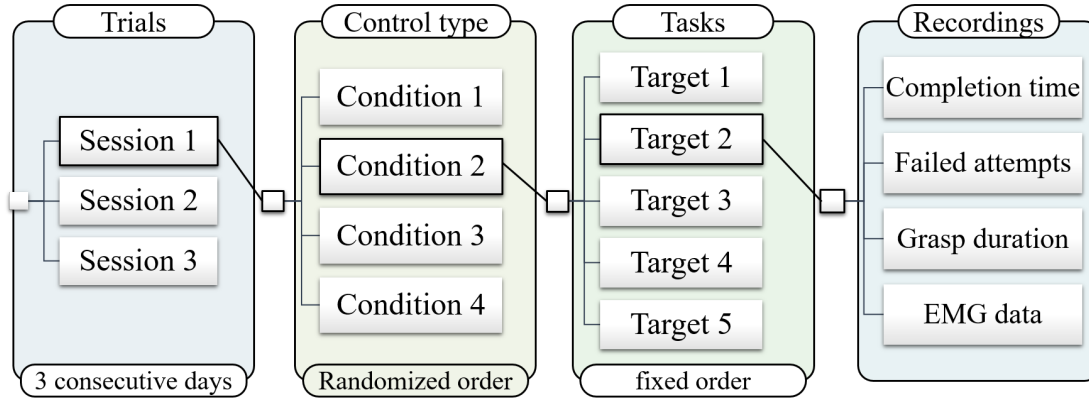


Figure 5. Summary of the experimental protocol. In 3 consecutive days, a subject participates in 3 sessions of 4 experiment runs. In each run, a specific control condition among 4 others is selected. The order of control conditions is randomized in every session and for all subjects. After setting the control condition, subjects complete 5 pick-and-place tasks, differing in the target positions. The task order is fixed from the top left box to the bottom right one in Figure 3. During task execution, we record completion time, the number of failed attempts, the grasping time duration, and EMG signals.

sklearn [**scikit-learn**]. This model is chosen instead of an MLP to avoid overfitting due to the lower amount of calibration data, since the decoding task was simpler.

To maximize real-time performance, decoded values from the MLP are smoothed using a 3-point median filter. Moreover, to reduce noise when subjects are performing the tasks, predicted values are set to 0 if the decoded value is below 2, and set to 10 if the decoded value is higher than 7. Similar post-processing is applied on the SVR shoulder decoder with a median filter and value clipping, if the decoded values are out of bound.

2.4 Data Analysis

To compare the shoulder decoders, the task was divided in rotations between target angles. We quantified the angle difference over time between the target angle obtained from the base and the angle of the object. For each new target angle, the error was computed as the difference between the object and the base angle. We also quantified the time taken to perform each rotation.

For the functional assessment, we measured the completion time and number of failed attempts for each of the 5 different tasks within an experiment run. To better follow the results, the key terms and main outcome variables (completion time and the number of failures) are listed below, following control conditions in Figure 1.

- *Control condition:* There are 4 control conditions differing in the type of employed state machine interface and EMG decoder.

- *Session (Trial)*: A series of 4 experiment runs where the subject completes all tasks with all control conditions. Each subject participates in three sessions over three days.
- *Target*: A box (hole) in a specific pose where the object (cuboid) is placed. In each experiment, there are five fixed targets placed in different positions and orientations.
- *Task Completion Time (success time)*: The time duration in a successful trial that it takes to lift the object from grasp position and place it in the target box. In other words, the time to finish a manipulation/insertion of a peg in a hole. This time duration starts from the moment that the subject lifts the object.
- *Number of Failed Attempts*: The number of failed manipulation attempts. An attempt is counted as a failure if the object is not fully placed in the specific target.

For the first experiment, statistical analysis was performed to test for significant differences in performance between the two shoulder control strategies, in terms of rotation time. In the second experiment, we conducted statistical tests to assess for significant changes in performance (in terms of the number of failures and completion time) across the different sessions, control conditions, and targets. To check if the variables were normally distributed, we used the Shapiro-Wilk test and used parametric or non-parametric tests accordingly.

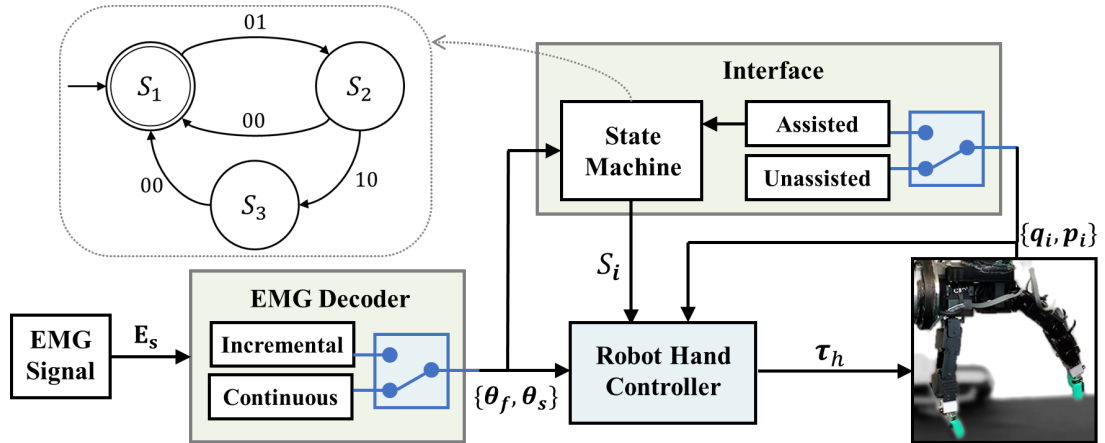


Figure 6. Block diagram of robot hand control with state machines of the (shoulder) EMG-robot interface. S_1 , S_2 , and S_3 represent *preshape*, *grasp*, and *manipulate* modes respectively. We assess 4 control conditions for controlling the robotic hand. Control conditions are the combination of 2 EMG decoders (incremental/ continuous) and 2 interface modes (assisted/ unassisted); see Figures 1 and 3.

2.5 EMG-Robot Interface

The robotic hand operates in three modes:

- Preshape*: robot opens and closes each finger individually.

- ii. *Grasp*: robot grasps the object by closing the fingers and securing contacts by using tactile sensors.
- iii. *Manipulate*: robotic fingers manipulate the object while holding it in the hand frame. Fingers move in a coordinated object-centered fashion to rotate the object.

We model each of these modes via a set of state machines, $S = \{S_1, S_2, S_3\}$, see Figure 6 where S_1, S_2 , and S_3 represent *preshape*, *grasp*, and *manipulate*, respectively. Transitions from S_2 to S_3 , and from S_3 to S_1 are unidirectional. However, the switch from S_1 to S_2 is bi-directional, meaning that if the grasp is not sound, the subject can re-open the hand and attempt a new grasping. The bi-directional transition between these two states allows the subject to open/close fingers several times to find the seemingly fine grasp.

We define and evaluate two state transition functions for our interface. One takes only the EMG command as input (unassisted interface), and the second one uses robotic feedback in addition to the EMG command (assisted interface), see Figure 6. More precisely, in the assisted interface, we benefit from tactile feedback to verify contact with the object and grasp realization, used in the transition from S_2 state to S_3 state. Moreover, from finger kinematics and the joint angles, we estimate object angular displacement. This estimation is then used to confirm the attainment of the desired motion. Once the desired manipulation is achieved, the robotic hand releases the object only if the command from the subject is received consistently over a time window of 4 s, i.e. the subject insists on opening the hand.

2.6 Experimental Hardware

The hardware for experiments consists of an Allegro left hand¹ mounted on a KUKA LBR IIWA 14² robotic arm, OptiTrack motion capture system, and BioTac tactile sensors, see Figure 3. The Allegro hand has four fingers (thumb included), each with four active DoFs. Each DoF is actuated with a motor: three motors at the MCP, PIP, and DIP joints, and the fourth motor is located just under the finger base, attached to the palm and controlling the lateral rotation. The thumb has three motors at the joint connecting to the palm, controlling rotations along the three axes, and one motor at the joint connecting the two phalanges. The Allegro hand can be operated either in position or torque control mode, which is used in our shared control approach. A set of three BioTac sensors are used as fingertips to obtain tactile information at contact points during grasp and manipulation. The robotic hand is mounted on the end-effector (EE) of the KUKA IIWA 14 robotic arm. The KUKA IIWA 14 robot has 7 DoFs that allow its EE to be moved to a desired position and orientation smoothly and continuously. The redundancy in joint space, the extra DoF of KUKA, is exploited to minimize the acceleration in a trajectory, resulting in smooth robot motion.

In the first experiment, 3D markers are placed on the cuboid as well as the rotating base to

¹http://wiki.wonikrobotics.com/AllegroHandWiki/index.php/Allegro_Hand

²<https://www.kuka.com/en-ch/products/robotics-systems/industrial-robots/lbr-iiwa>

record the difference in orientation over time with the OptiTrack camera system; see Figure 2. In the second experiment, the subject wears a set of 3D markers positioned explicitly on the wrist (see Figure 3) to detect the position and orientation of the subject's hand through the OptiTrack camera system. The acquired position and orientation of the subject's wrist are then sent to the control interface and used to teleoperate the KUKA's end-effector. Target boxes and the object's initial place are fixed to specific positions within reach of the robotic arm. During recording, to avoid inconsistency in actuators and sensors performance due to overheating and friction drift during active times, the entire system is shut down for 30 minutes after each experiment run.

2.7 Autonomous Robot Controller

We control both the robotic arm and the robotic hand in the torque mode, maintaining joint compliance. Compliant controllers enable the robot to adapt to perception uncertainties and provide safer human-robot interaction compared to position controllers. We introduced an additional safety layer on top of the controller, a user-robot collision avoidance that enhances the safety of human-robot interaction. Our autonomous compliant controller has two sub-modules: (a) a controller to imitate the subject's wrist displacement in position and orientation with the robotic arm EE, and (b) a controller that computes the joint torques of the robotic hand to perform tasks like grasp and manipulation.

Robotic Arm Control:

The desired position and orientation of the robotic arm EE are computed based on the measured subject's wrist motion. From the OptiTrack system, we obtain the 3D position (x , y , and z axes) and orientation (roll, pitch, and yaw) of the subject's wrist with respect to the world frame. In our tracking strategy, the EE must mimic the subject's wrist displacement in 4 coordinates, 3D position, and the angle in the roll axis. Since the subject and the robot are facing each other in our setup, the robot EE is commanded to mirror the displacement in the pitch axis of the subject's wrist. To restrict the object rotation only to in-hand manipulation in our control scenario, the robot EE is indifferent to the displacement in the yaw axis of the subject's wrist achieved with Rodrigues' rotation formula [belongie1999rodrigues]. We found that mirroring the pitch orientation and not tracking the yaw rotation is more intuitive for subjects and simultaneously results in more accurate tracking. Then, the desired pose of the robot EE is passed to a predefined linear dynamical system (DS) [khadivar2021learning] to find the desired translational and angular velocities. These velocities serve as the inputs for our underlying compliant and passive controller [kronander2015passive, khadivar2021efficient] that outputs a set of joint torques for the robotic arm. Thanks to the dynamical system approach, our controller is robust to perturbations and disturbances and safe for human-robot interactions due to compliant passivity. The redundant DoF of the robotic arm is constantly optimized to decrease robot acceleration while traversing from one point to another.

Robotic Hand Control:

Similar to the robotic arm control, this controller also requires a set of desired fingertip positions/ velocities as inputs. The computation of these inputs depends on the task state and whether or not a finger is in contact with the object. In the pre-grasp state, the desired position is computed based on the angle from the EMG decoder. In this state, each finger of the Allegro hand is separately commanded by the EMG decoder. The object's relative position with respect to the robotic hand is computed by tracking the subject's wrist motion. Once the object is within the hand frame, subjects changing hand posture from open hand to fist is equivalent to a robotic hand attempting to grasp. From tactile feedback, the control state changes from pre-grasp to grasp if three fingers make contact with the object. In this state, the fingers establish a force-closure [prattichizzo2016grasping] around the object. In other words, in case the subject feels a higher grip force is needed to obtain a firm grasp and lift the object, it can be achieved by clenching the fist tighter.

In the manipulation state, where the fingertips are in contact with the object, the control inputs are determined based on the object's desired position. In the grasp state, the object's desired position is fixed. When the subject intends to rotate the object within the robotic hand, in the manipulation state, the object's desired position changes, given the input from the EMG shoulder decoder. This desired pose is relative to the palm frame (a frame attached to the base of the robotic hand) and is used to find the desired object velocity through a linear DS. Translating an object-centric desired velocity to individual in-contact fingers' desired velocities is realized through grasp matrix transformation [prattichizzo2016grasping], grasp stability metric, and the estimated contact mechanical properties. More precisely, we obtain the desired velocity of all fingers from the desired object velocity commanded by the shoulder EMG decoder. Similar to robotic arm control, these velocities are sent to our underlying compliant and passive controller to compute the corresponding joint torques [li2016dexterous].

3. Results

3.1 Shoulder Controllers Comparison

The results of the first experiment are depicted in Figure 7, where we compare the control performance of the incremental and continuous EMG decoders. From Figure 7 (left), we observe that with the incremental decoder, the rotation error decreases more uniformly and to a lower value (0.18rad less) compared to the continuous decoder ($Z=2.07$, $p < 0.05$). On the other hand, Figure 7 (right) shows that the continuous decoder is significantly faster than the incremental one (Wilcoxon test, $Z=133.5$, $p < 0.01$). Therefore, the incremental decoder leads to a slower but more precise control due to smooth error decay compared to the continuous decoder.

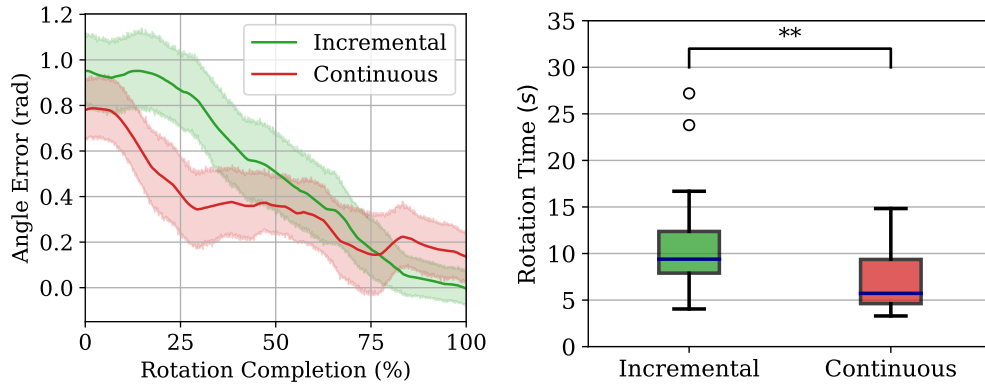


Figure 7. Performance of two shoulder decoders with the robotic hand fixed. Left: Angle error between the grasped object and the desired base orientation for two shoulder decoders. The solid line depicts the mean, and the shaded area shows one standard deviation over all subjects and all target angles. Difference at 100% completion time is statistically different ($Z=2.07$, $p < 0.05$). Right: Boxplots of rotation time to achieve the desired angle. Statistical difference regarding completion time can be seen between the two shoulder decoders. **: $p < 0.01$.

3.2 EMG Decoder

During EMG calibration, subjects were asked to follow a virtual hand doing a sequence of movements 6 times. The first 5 repetitions were used for training the model, and the last one as a validation set, to evaluate the decoding quality and stop the training when the validation loss was not decreasing. The validation losses of the finger decoder for the 3 sessions of the second experiment are shown in Figure 8. The three sessions were compared using Friedman's ANOVA ($\chi^2(2) = 4.75$, $p = 0.093$) and are not statistically different with a significance level of 5%.

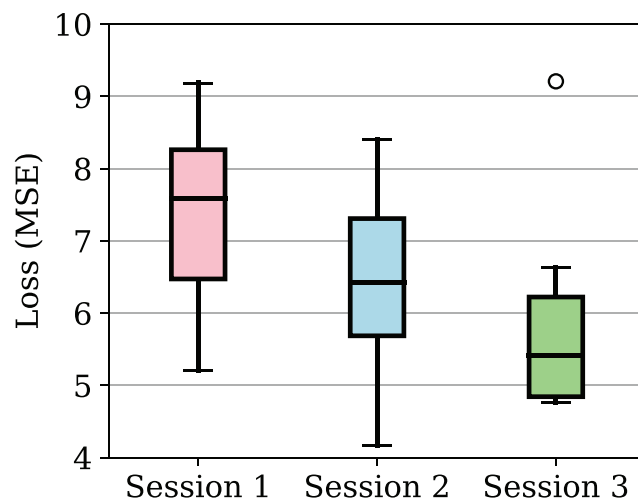


Figure 8. Average EMG validation loss during calibration of the finger decoder across subjects ($N = 8$), throughout the three experimental sessions.

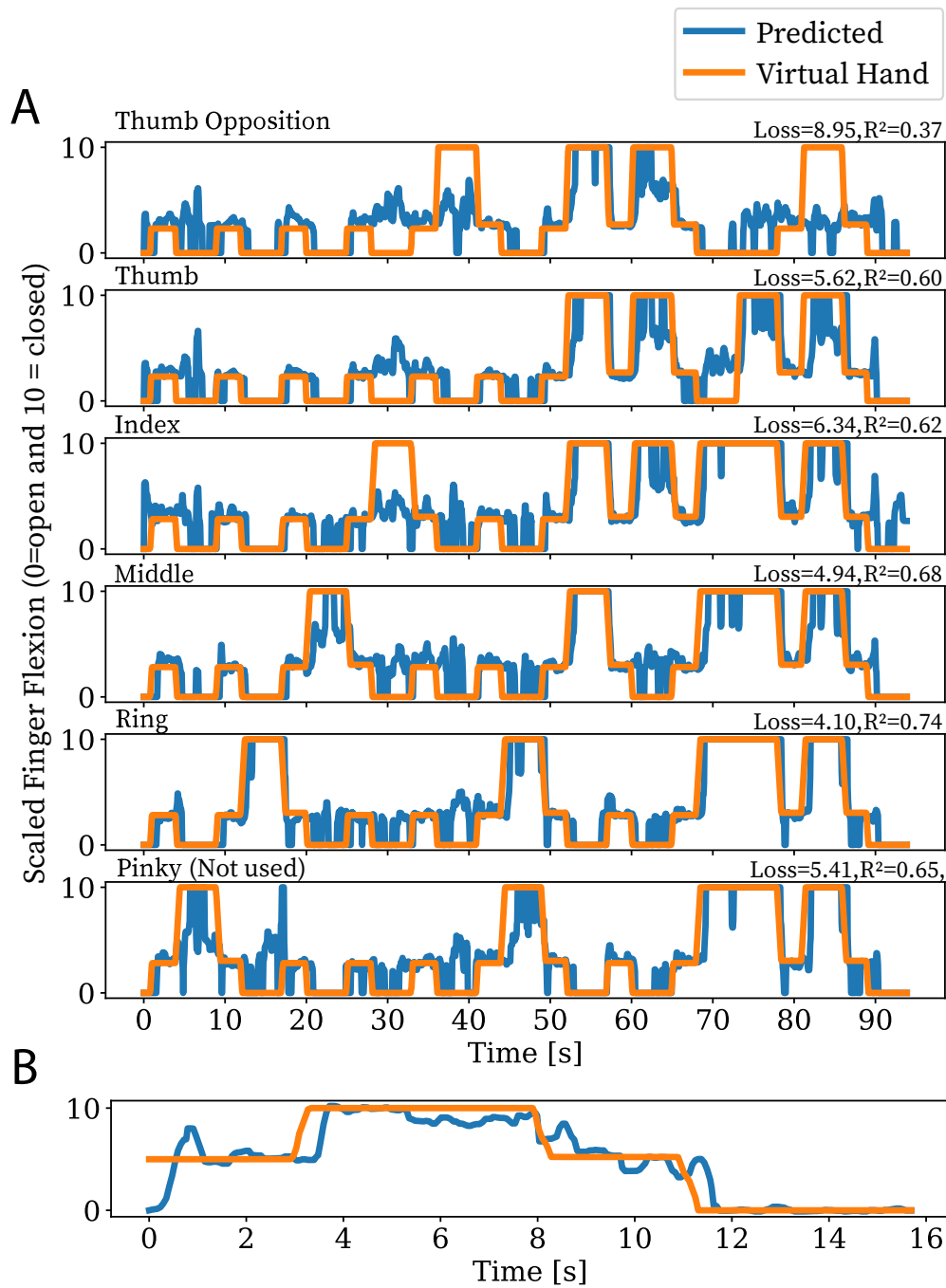


Figure 9. Virtual hand and predicted scaled joint flexion on the validation set of a representative recording for fingers and shoulder.

Predicted values were post-processed as in real-time. A) Finger decoding, the recording corresponds to a loss of 5.90. High values represent flexed fingers. B) Shoulder decoding, the recording corresponds to a loss of 2.18. Maximum value represents shoulder elevation, five corresponds to resting position and zero for shoulder depression (R^2 : coefficient of determination, Loss: Mean Squared Error).

Figure 9 shows a representative example of the EMG decoder accuracy for predicting both finger flexion and shoulder movements. The virtual hand provides the ground truth finger flexion in this example. In contrast, the predicted flexion values are computed from the validation dataset of one subject after performing the EMG calibration. Note that the virtual hand finger values were shifted by 0.150 s to account for the delay between the virtual hand and the subject. A Mean Squared Error loss of 5.90 was obtained before post-processing the predicted angles. For clarity, the data shown in Figure 9 was post-processed using the same methods applied during real-time decoding (smoothed and clipped). In Figure 9 some movements are not completely synchronized even if the general delay between the subject and the virtual hand was taken into account. The model generally performs better on the last fingers than the first ones. Regarding continuous shoulder decoding, all subjects obtained high offline accuracy (average loss: 3.22 ± 1.44 and average R^2 : 0.78 ± 0.1 , see Figure 9 for an example). In real-time, when the subject was moving the object in space, some noise could arise due to arm motion that activated shoulder muscles.

3.3 Shared Control Functional Assessment

On average, one session for a subject took 75 minutes. Approximately 30 minutes were used at the beginning to place the EMG electrodes and calibrate the finger and the shoulder decoders. Then, performing the 5 pick and place tasks took, on average, 6 minutes and 11 s for each condition. Figure 10 provides an overview of the collected data for all participants and conditions.

Task Performance Across Sessions:

Figure 11 shows the mean number of failed attempts and mean completion time for the 8 subjects, across the 3 sessions. Using the Friedman's ANOVA test, we observe a statistically significant difference in task completion time across the 3 sessions, $\chi^2(2) = 31.962$, $p < 0.001$. Post hoc analysis with Wilcoxon signed-rank tests was conducted by using a Bonferroni correction, setting the significance level at $p < 0.05/3 = 0.017$. We observe no significant differences between Session 1 and Session 2 ($Z = -1.943$, $p = 0.052$), whereas there are significant changes in completion time between Session 1 and Session 3 ($Z = -4.996$, $p < 0.001$) and Session 2 and Session 3 ($Z = -4.281$, $p < 0.001$). In fact, from Session 2 (median = 18.0s, $IQR = 11.3$) to Session 3 (median = 15.2s, $IQR = 10.2$) there is a significant decrease of 2.8s in median completion time, and from Session 1 (median = 19.6s, $IQR = 13.4$) to Session 3 the decrease is of 4.4s.

For the number of failures, we also verify a statistically significant difference between the 3 sessions using the Friedman's ANOVA, $\chi^2(2) = 11.494$, $p = 0.003$. Using the Wilcoxon signed-rank test we see, (also in Figure 11), that only from Session 1 (mean = 0.96, standard deviation (SD) = 1.5) to Session 3 (mean = 0.41, SD = 0.68) the mean number of failures decreases significantly ($Z = -3.639$, $p < 0.001$) by an average of 12.1 failures. From Session 1 to Session 2 ($Z = -2.321$, $p = 0.020$) and from Session 2 to Session 3 ($Z = -1.509$, $p = 0.131$) there are no

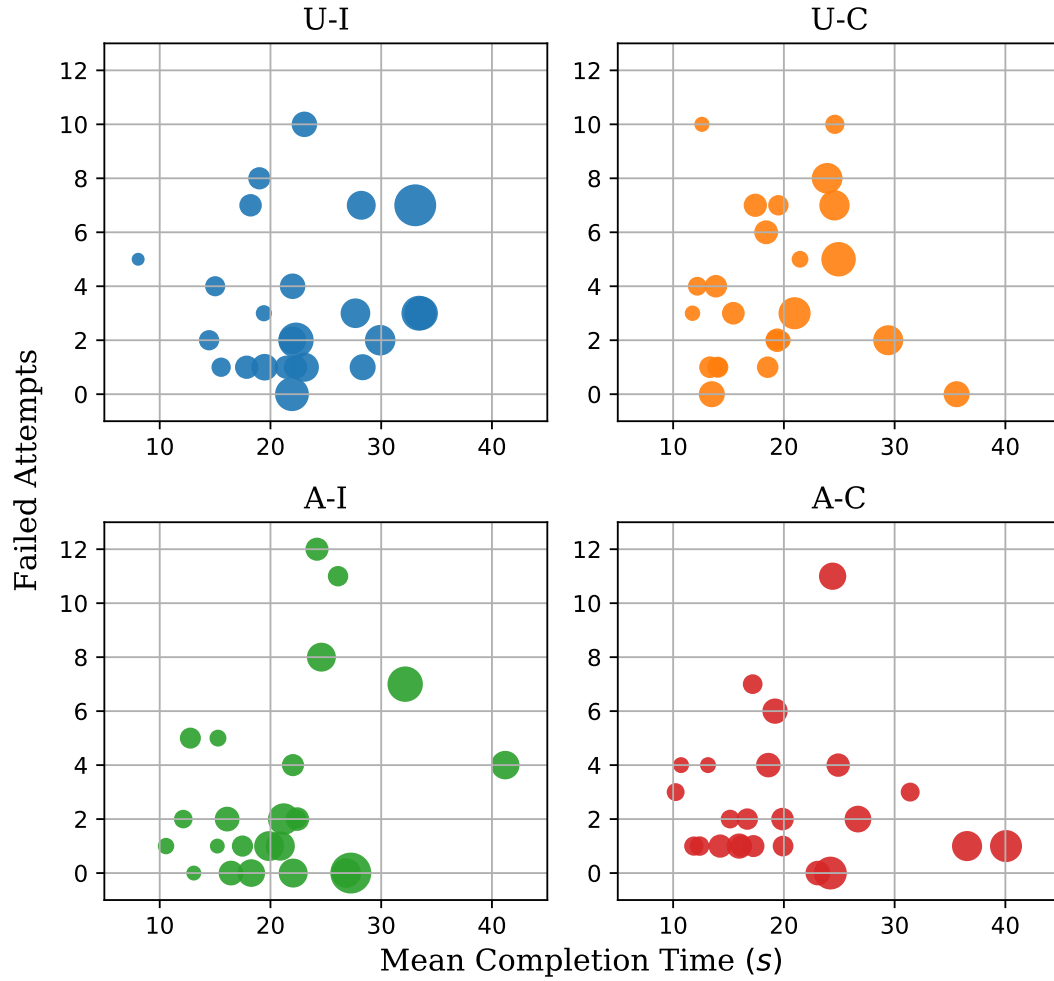


Figure 10. All collected data from all 8 participants. Each subject tried 4 different shared control conditions (see Figure 1) in 3 sessions over three days. Thus, for each control condition, there are 24 data points (8 subjects \times 3 sessions). In each experiment run, subjects were asked to complete five sub-task in a specific order (Figure 3), placing a cuboid in five different target boxes. We recorded the number of failed attempts and the completion of each sub-task. The x -axis for each plot is the mean completion time of these five sub-tasks, the y -axis is the corresponding sum of the failed attempts, and the size of the marker indicates the relative variance in completion time over.

statistically significant changes.

Comparison between Shared Control Conditions:

We investigated the performance of four shared control schemes, which combined two state transition modes (assisted vs. unassisted) with two EMG decoding approaches (continuous vs. incremental). The mean task completion time and mean number of failures were obtained and analyzed for each of the control conditions, for all subjects and experimental sessions (see Figure 12).

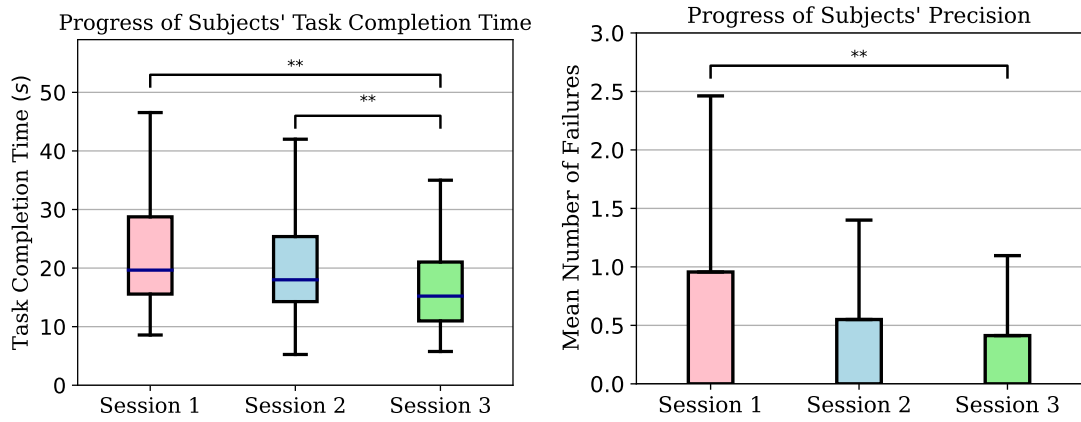


Figure 11. Performance progress of all subjects and all control conditions over 3 sessions (3 days). Left: boxplot of task completion time per session; mid-lines indicate the median. Right: barplot of mean number of failed attempts for each session. Statistically significant differences regarding mean completion time can be seen between sessions 1 and 2, and sessions 2 and 3. For the mean number of failures, only the first and third sessions differ significantly. Error bars: +SD, **: $p < 0.01$.

Using again the Friedman's ANOVA test with $\alpha = 0.05$, we observe a statistically significant difference in task completion time between the 4 experimental conditions, $\chi^2(3) = 11.325$, $p = 0.010$. The same is verified for the number of failures, $\chi^2(3) = 10.305$, $p = 0.016$. By running the Wilcoxon signed-rank test with $p = 0.05/4 = 0.0125$, we find that the task completion time in condition U-I (median = 19.0s, IQR = 11.9) was significantly longer than the completion time in U-C (median = 17.4s, IQR = 10.4), $Z = -2.803$, $p = 0.005$. That is, without assistance, subjects were significantly faster by an average of 3.36s using the continuous controller, when compared to incremental control. Between U-I and A-I (median = 16.9s, IQR = 12.2) – i.e, the two assistance modes using the incremental EMG decoding –, we observe that the assisted robotic interface led to a significantly faster performance ($Z = -2.71$, $p = 0.005$), by an average of 2.48s.

Regarding the number of failures, we see statistically significant changes between U-I (mean 6.125) and A-I (mean 2.625), $Z = -3.046$, $p = 0.002$, and between conditions U-C (mean 6.0) and A-I ($Z = -2.549$, $p = 0.011$). In fact, the number of failed attempts for both control schemes that used an unassisted interface significantly improved with the assisted interface, when combined with the incremental control modality (by 3.5 and 1.5 difference, respectively).

Overall, comparing the two state transition modes (unassisted vs. assisted), the assisted interface was significantly better than the unassisted counterpart, in terms of resulting in lower number of failed attempts (41% more precise) (Wilcoxon test, $Z = 3431.5$, $p < 0.05$). Regarding completion time, no significant difference were observed between the two methods. On the other hand, the two EMG decoding approaches (incremental vs. continuous) performed similarly in terms of both completion time, regardless of the assistance mode.

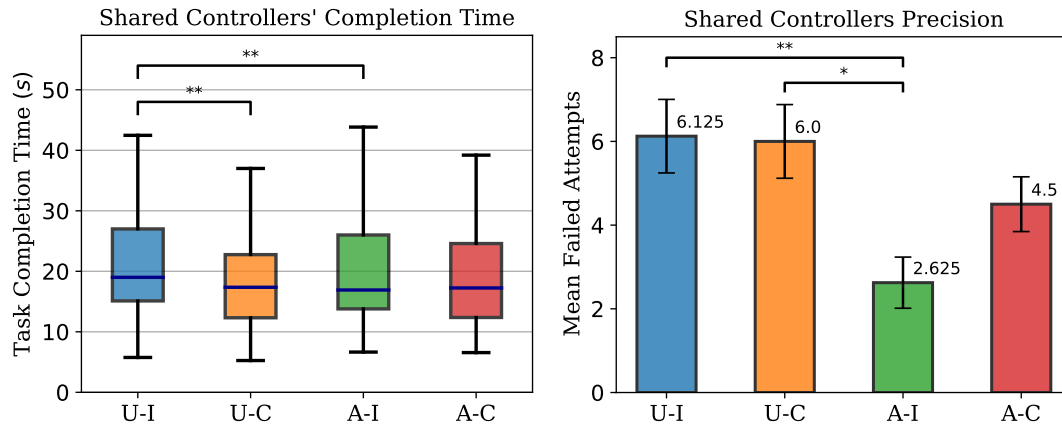


Figure 12. Performance of all shared controller conditions across all subjects and sessions. Left: boxplot of task completion time across control conditions. Right: barplot of subject's mean number of failed attempts per control condition. Error bars: $\pm SD$, * : $p < 0.05$, ** : $p < 0.01$.

Taking a closer look at the performance for each of the 5 targets, Figure 13 shows that the assisted mode resulted in lower failures, especially for those that require large change in wrist orientation and large in-hand rotation (tasks 1,2, and 4 where the necessary angle is higher). The first two tasks are considered to be the most difficult ones, since the subject needs to adjust the orientation of the robot's EE (palm being parallel to the target box inclination) and rotate the object in hand simultaneously.

3.4 Results Summary

In summary, the assisted control mode improved the performance significantly in terms of lowering the number of failed attempts. The assisted state transition mode, when in combination with EMG incremental control condition, *A-I*, outperformed the others as it has the lowest completion time and significantly lower number of failures (higher precision). On the contrary, the incremental EMG decoding without assistance (*U-I*) proved to be the least efficient among control conditions. Comparing the control condition *U-C* with lowest robot autonomy with the condition *A-I* with highest robot autonomy shows that increasing the autonomy of the robot controller improved the precision (reduced number of failures) more significantly (by 41%) than the efficiency (by 2.4s task completion time).

4. Discussion

We first compared two shoulder decoders in a controlled object rotation task, then, to assess the performance of subjects in a functional task, we used a robotic hand to pick, manipulate and place an object in various target boxes. We examined four shared control conditions based on a compliant controller in conjunction with EMG decoding to teleoperate a robotic arm, while maintaining full autonomy over high-level commands. Given the experimental results, we propose the shared control strategy with assisted state machine interface and incremental

Target Specific Performance of Each Shared Control Scenario

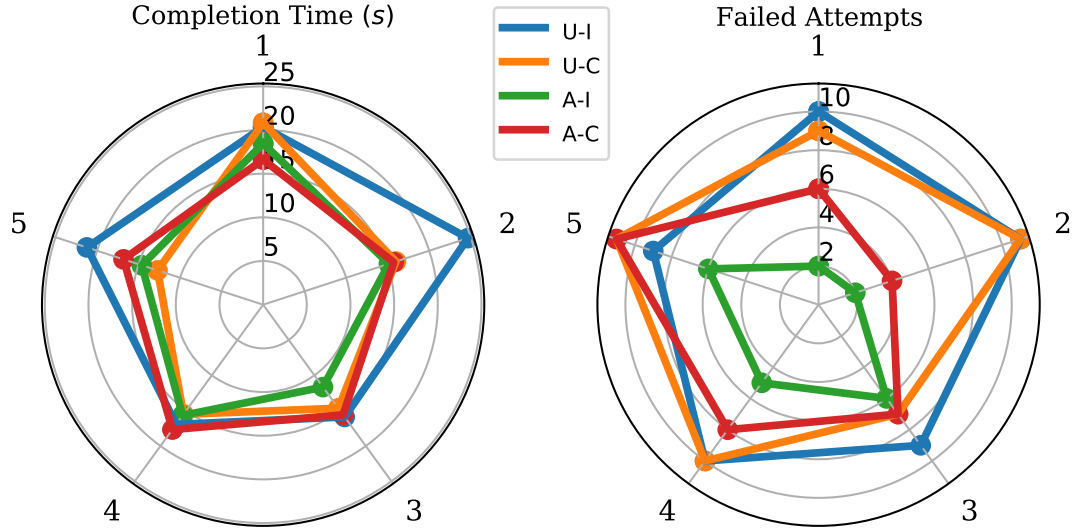


Figure 13. Median completion time (left) and mean failed attempts (right) for each pair of sub-tasks and shared control condition. In each experiment run with a set shared control condition, subjects had to place a cuboid in five different boxes. Here is shown the overall performance of each control condition in accomplishing a specific sub-task.

shoulder EMG decoder.

The participants' grasping motor commands were interpreted individually, simultaneously, and proportionally for each finger. Proportional decoding is intuitive [Farina2014]; it enabled the subjects to effectively complete the task while keeping full control over the fingers when not grasping. However, complex decoding strategies inevitably increased the noise in the predicted output, reducing the system's reliability. The presence of noise in the predicted output and disparities in performance between fingers are highlighted in Figure 9. The anatomy of the forearm is an essential factor, as superficial electrodes do not allow for selective recordings from deep muscles. However, multiple studies demonstrated that deep learning could improve decoding accuracy [Mendez2021, Ameri2019, Hu2018].

The first experiment showed that the incremental decoder was significantly slower than the continuous one when the robotic hand was locked in place. However, this strategy was more stable and precise based on the smoother and lower tracking error (0.18rad less).

In the second experiment, subjects had to reach target boxes on an inclined surface, requiring the subjects to move their arms and to rotate their wrist. Although forearm orientation is a major source of noise for real-time applications [KyungYou2010], the control technique developed in this study was robust enough for the subjects to complete the task. Calibrating the model in the various arm and wrist orientations could improve the robustness to wrist rotation, and arm orientation [Park2016], but this would imply a substantially longer calibration time. Using a virtual hand to synchronize EMG and hand kinematics was also a limitation. Indeed,

unreliable samples were introduced during training due to a non-constant latency between the virtual hand and the subject's movement. Furthermore, because muscle synergies can cause finger co-flexion [Aji2009], the movements expected by the virtual hand were not always natural and, in some situations, deviated from the actual movements of the individuals. Kinematic tracking of real finger motions (on the contralateral hand in the case of unilateral amputation) by using a glove [Atzori2012], or cameras [1] could more precisely track intended movements.

To accomplish in-hand object rotation with a robotic hand, precise finger motions in association with sensory input are necessary [li2016dexterous]. In this study, information such as object position, displacement, and grasp position is obtained directly from the subjects. Computing such variables and states is challenging when approaching complex manipulation tasks. The controller had to remain reactive to the user's commands with a minimal execution time delay to increase intuitiveness and sense of agency [rognini2013visuo]. At the same time, the controller had to be robust to inconsistencies coming from the EMG decoder due to the variability of the signals. Although there was no statistical difference in EMG validation loss between days, we observed that the number of failed attempts and the completion time decreased over test sessions across all tasks and subjects. This confirmed that subjects learned how to improve their performance on this modified grooved peg test and did not rely on an increase in EMG decoding accuracy. In this control approach, we estimated the object's pose relative to the robotic hand from the forward kinematic and the fingers' joint position. This estimation proved helpful in these tasks with a cuboid object; on the contrary, for more complex object shapes and to obtain higher accuracy, more sophisticated object pose estimation methods like vision-based [doosti2020hope] or tactile images [sodhi2021learning] are required. From Figure 13, target tasks that required larger in-hand rotation foreseeably took more time to be completed. To reach human-level performance, reducing delay in user command execution and increasing the decoding precision [Xia2018] are instrumental for future enhancement. Furthermore, we can use the information from the robotic hand to provide sensory feedback to the users. For instance, contact, force, and finger angle information gathered from the robotic hand can be given to users with trans-radial amputation through invasive [DAnna2019] or non-invasive channels [Stephens-Fripp2018]. Sensory feedback can help users to send more accurate high-level commands to the robotic hands, improve embodiment [Bensmaia2020], and reduce cognitive load [Valle2020].

Numerous strategies could have been employed to control object rotation indirectly. However, the chosen strategy cannot interfere with other motor functions when used by individuals with a trans-radial amputation in a real-world scenario. Redundancy in the DoFs of the human body can be used. The shoulder elevation and depression movements are not essential for many activities of daily living and could therefore be leveraged. A widely available portable solution to record such movement is EMG. This solution could alter muscle activity when patients wear their RPH. However, we hypothesize that this shoulder muscle activity would not be that different from a healthy subject moving his arm in space as prosthetic hands weight is now similar to natural hands. Another limitation would then appear when a patient lifts heavy

objects. Nevertheless, heavy objects are rarely manipulated with one hand. Therefore, we investigated two decoding strategies based on shoulder muscle EMG. The continuous decoder was proportional to the shoulder motion but in the first experiment, this decoder showed a noisier behavior with slightly more oscillations in tracking the target angle. Moreover, due to the cross-talk with the arm motion in the functional assessment, we observed noisy behaviors in real-time during the task execution. For instance, when subjects had to lower their arm to reach the fifth target (placed directly on the table), they had to lift their shoulder upwards to rotate the object in the right direction, which increased the number of failed attempts with the continuous shoulder decoder. On the contrary, when activity thresholds were set, the incremental shoulder decoder did not show this unwanted behavior partly because subjects could modulate their shoulder activity to rotate the object before placing it in the correct box. The increments' value determined the objects' desired rotation and allowed the subjects to regulate the rotation accurately. This highlighted the robustness of the incremental decoder for such a task.

In the first experiment (in-hand rotation only), subjects were more accurate (0.18rad less tracking error) but slower in task completion with the incremental decoder compared to the continuous decoder. We observed the same behavior in the functional assessment experiment when both decoders were used without the assisted interface. However, when using the assisted interface, there was no statistical difference between the two shoulder decoders in task completion time. Overall, the assistance reduced the mean number of failures by 41% compared to unassisted.

Indeed, the continuous shoulder decoder was expected to rotate objects faster since it is directly linked to the shoulder angle. On the other hand, in some cases, a too fast rotation could cause the object to slip and fall, increasing the number of failed attempts compared to the incremental decoder. As a result, subjects developed a strategy to overcome this issue. They reduced the shoulder motion speed, which can explain the results obtained. This was valid only in the case of the assisted transition mode as, without assistance, the number of failed attempts was large both with and without assistance. Finally, assistance from the robotic state became greatly beneficial for targets 1 and 2, where decoding the subject's intention and encoding the desired command was more convoluted. Indeed, the two inclined targets had a high angle and elevation. For these targets, the assisted state transition mode significantly decreased the number of failures compared to the unassisted interface.

5. Conclusion

We showed that combining a shared control condition with EMG decoding for finger motions and object rotation could be a realistic alternative for users with trans-radial amputation to improve the dexterity and versatility of RPHs. The shared control created in this study could allow users with an amputation to manipulate objects in their prosthetic hand, which is practical in numerous daily tasks. In our teleoperated system, subjects maintained complete

control over the robotic hand. The condition that obtained the best results was the incremental shoulder EMG decoder with the assisted state transition mode. Surely, integration of an RPH and validation on people with trans-radial amputation with an amputation would be necessary to quantify functional improvements. Another future direction of this work includes the implementation of fine-scale force modulation on objects to allow patients to grasp and manipulate fragile objects. Nonetheless, this study took one step toward more advanced control systems, implying that future RPH development in the direction of sensorized hands with compliant controllers would benefit people with trans-radial amputation.

Data availability statement

The data that support the findings of this study are available upon reasonable request from the authors.

Code availability

The code used in the current study is available from the corresponding author on reasonable request.

Acknowledgments

The authors would like to acknowledge all subjects who participated in the experiments and Dr Ahalya Prabhakar for their help proofreading the manuscript.

Funding sources

This work was supported as a part of NCCR Robotics, a National Centre of Competence in Research, funded by the Swiss National Science Foundation (grant number 51NF40_185543), by the Bertarelli Foundation.

Conflict of interest

S.M. is co-founder of Sensars Neuroprosthetics, a small company working on the commercialization of bidirectional hand prostheses

Ethical statement

This study including the experimental procedures was approved by the cantonal ethical committee of Vaud. Informed consent was obtained from all participants in the study. The

authors have confirmed that any identifiable participants in this study have given their consent for publication.

References

- [1] Yilin Liu, Shijia Zhang, and Mahanth Gowda. “NeuroPose: 3D hand pose tracking using EMG wearables”. In: *The Web Conference 2021 - Proceedings of the World Wide Web Conference, WWW 2021* (Apr. 2021), pp. 1471–1482. DOI: 10.1145/3442381.3449890.
- [2] Ryan J. Smith et al. “Continuous decoding of finger position from surface EMG signals for the control of powered prostheses”. In: *Proceedings of the 30th Annual International Conference of the IEEE Engineering in Medicine and Biology Society, EMBS’08 - “Personalized Healthcare through Technology”* (2008), pp. 197–200.
- [3] Light C.M. et al. “Intelligent multifunction myoelectric control of hand prostheses”. In: *Journal of Medical Engineering and Technology* 26.4 (2002), pp. 139–146. ISSN: 0309-1902. DOI: 10.1080/03091900210142459.
- [4] Strahinja Došen et al. “Cognitive vision system for control of dexterous prosthetic hands: Experimental evaluation”. In: *Journal of NeuroEngineering and Rehabilitation* 7.1 (2010), pp. 1–14. ISSN: 17430003. DOI: 10.1186/1743-0003-7-42.
- [5] Tura A. et al. “Experimental development of a sensory control system for an upper limb myoelectric prosthesis with cosmetic covering”. In: *Journal of rehabilitation research and development* 35.1 (1998).
- [6] Simone Fani et al. “Assessment of myoelectric controller performance and kinematic behavior of a novel soft synergy-inspired robotic hand for prosthetic applications”. In: *Frontiers in Neurorobotics* 10.October (2016), pp. 1–15. ISSN: 16625218. DOI: 10.3389/fnbot.2016.00011.
- [7] Raul C. Sîmpetru et al. “Accurate Continuous Prediction of 14 Degrees of Freedom of the Hand from Myoelectrical Signals through Convolutional Deep Learning”. In: (2022), pp. 702–706. DOI: 10.1109/EMBC48229.2022.9870937.
- [8] Stephan Johann Lehmler et al. “Deep transfer learning compared to subject-specific models for sEMG decoders”. In: *Journal of Neural Engineering* 19.5 (Oct. 2022), p. 056039. ISSN: 1741-2552. DOI: 10.1088/1741-2552/AC9860. URL: <https://iopscience.iop.org/article/10.1088/1741-2552/ac9860%20https://iopscience.iop.org/article/10.1088/1741-2552/ac9860/meta>.
- [9] Rebecca J. Greene et al. “Functionally adaptive myosite selection using high-density sEMG for upper limb myoelectric prostheses”. In: *IEEE Transactions on Biomedical Engineering* (2023), pp. 1–11. DOI: 10.1109/TBME.2023.3274053.
- [10] Caggiano Vittorio et al. “MyoSuite – A contact-rich simulation suite for musculoskeletal motor control”. In: (2022). DOI: 10.48550/ARXIV.2205.13600. URL: <https://arxiv.org/abs/2205.13600>.

- [11] Seonghyeon Hwang and Steven Euijong Whang. “MixRL: Data Mixing Augmentation for Regression using Reinforcement Learning”. In: *CoRR* abs/2106.03374 (2021). arXiv: 2106.03374. URL: <https://arxiv.org/abs/2106.03374>.
- [12] Florian Dubost et al. “Hydranet: Data Augmentation for Regression Neural Networks”. In: *CoRR* abs/1807.04798 (2018). arXiv: 1807.04798. URL: <http://arxiv.org/abs/1807.04798>.
- [13] Hiroshi Ohno. “Auto-encoder-based generative models for data augmentation on regression problems”. In: *Soft Computing* 24.11 (June 2020), pp. 7999–8009. ISSN: 14337479. DOI: 10.1007/S00500-019-04094-0/TABLES/13. URL: <https://link.springer.com/article/10.1007/s00500-019-04094-0>.
- [14] Sumeyra Demir et al. “Data augmentation for time series regression: Applying transformations, autoencoders and adversarial networks to electricity price forecasting”. In: *Applied Energy* 304 (2021), p. 117695. ISSN: 0306-2619. DOI: <https://doi.org/10.1016/j.apenergy.2021.117695>. URL: <https://www.sciencedirect.com/science/article/pii/S0306261921010527>.
- [15] Rafael Anicet Zanini and Esther Luna Colombini. “Parkinson’s disease EMG data augmentation and simulation with DCGANs and style transfer”. In: *Sensors (Switzerland)* 20.9 (May 2020). ISSN: 14248220. DOI: 10.3390/S20092605.
- [16] Hyun K. Kim et al. “Continuous shared control for stabilizing reaching and grasping with brain-machine interfaces”. In: *IEEE Transactions on Biomedical Engineering* 53.6 (2006), pp. 1164–1173. ISSN: 00189294. DOI: 10.1109/TBME.2006.870235.
- [17] Inaki Iturrate, Luis Montesano, and Javier Minguez. “Shared-control brain-computer interface for a two dimensional reaching task using EEG error-related potentials”. In: *Proceedings of the Annual International Conference of the IEEE Engineering in Medicine and Biology Society, EMBS* (2013), pp. 5258–5262. ISSN: 1557170X. DOI: 10.1109/EMBC.2013.6610735.
- [18] Xi Chen et al. *A shared control policy for center-out movement decoding in motor brain-machine interface*. Vol. 3. PART 1. IFAC, 2013, pp. 345–348. ISBN: 9783902823458. DOI: 10.3182/20130902-3-CN-3020.00132.
- [19] Roni O. Maimon-Mor and Tamar R. Makin. “Is an artificial limb embodied as a hand? Brain decoding in prosthetic limb users”. In: *PLOS Biology* 18.6 (June 2020), e3000729. ISSN: 1545-7885. DOI: 10.1371/JOURNAL.PBIO.3000729. URL: <https://journals.plos.org/plosbiology/article?id=10.1371/journal.pbio.3000729>.
- [20] M. Laffranchi et al. “The Hannes hand prosthesis replicates the key biological properties of the human hand”. In: *Science Robotics* 5.46 (2020), eabb0467. DOI: 10.1126/scirobotics.abb0467. eprint: <https://www.science.org/doi/pdf/10.1126/scirobotics.abb0467>. URL: <https://www.science.org/doi/abs/10.1126/scirobotics.abb0467>.
- [21] Giacomo Valle et al. “Hand Control With Invasive Feedback Is Not Impaired by Increased Cognitive Load”. In: *Frontiers in Bioengineering and Biotechnology* 8 (2020). ISSN: 2296-4185. DOI: 10.3389/fbioe.2020.00287. URL: <https://www.frontiersin.org/articles/10.3389/fbioe.2020.00287>.

4 Future Perspectives for the Control of RPHs

Based on the body of work presented in this thesis, the aim of this section is to put into perspective the two main axes. From what was achieved, what are the next steps in order to bring these solutions to the patients? On the EMG decoding and on the shared control side several open questions remain and should be investigated in the future.

4.1 EMG Decoding: Increase performance and reduce computational cost

Deep learning for EMG decoding is a hot topic in the field with recent advances on the proportional decoding of several DoFs [1, 7] with the main hypothesis that learned features are more informative than engineered features. However, as highlighted by the difference in results obtained between sections 2.1 and 2.2, we can see that the benefits of deep learning are not as straightforward. Indeed, we could see that a recording-specific model architecture could yield different outcomes compared to one model architecture applied to all available recordings. Some articles on proportional control are reporting results with only one DL approach which make it impossible to compare with other approaches [1, 2]. But also in articles comparing deep learning with more standard approaches, the reader should be careful about the complexity of models compared and whether model architecture and hyperparameters were optimized only once or for each recording.

In section 2.2, no difference was found between the CNN and the MLP approaches implying that the features learned were not more informative than engineered features. However, other model architectures such as transformers or recurrent neural networks could potentially learn more informative features from the raw EMG signal with sufficient data during training. Indeed, the amount of data necessary to obtain robust and high-quality decoding for a patient with an amputation is still unclear from the literature as only a few studies have shown long-term results with single-finger proportional decoding.

As stated in section 2.4.2, transfer learning has the potential to reduce the amount of data

necessary from a patient. However, the pre-training and fine-tuning best practices are still unclear. Pre-training from several subjects has shown potential [8] but also in section 2.4.2 when pre-training from many recordings of only one subject. The number of different subjects and/or recordings for pre-training should be assessed to see if depending on the machine learning model used, there is a plateau in performance or if hundreds of individuals and recordings will be necessary to obtain a performing model from a few repetitions of a new prosthesis user. Finally, one should investigate how this translates to patients with amputation as muscles can be missing or atrophied.

On the other hand, such models will be used on embedded electronics and therefore, model size as well as energy consumption are important parameters to take into account. New state-of-the-art hardware-accelerated systems are being developed especially in the domain of brain implants. Such technology should also be leveraged for hand prostheses to increase decoding capabilities and maintain battery life.

One way to reduce energy consumption is to decrease the input size. One approach was explored in section 2.4.3 by extracting only the envelope of the signal and subsampling it at 100Hz. However, the performance of models at several sampling frequencies, from raw input or envelope should be compared to find the optimal trade-off.

Another approach consists in selectively choosing electrodes used as input. As MD-EMG covers the full stump, not all electrodes are recording qualitative signals or are highly correlated to other electrodes and therefore are just adding noise to the model. Electrode selection [9] should be performed after placement of the prosthesis as it may fluctuate between recordings, however, this step should be relatively fast as the user cannot wait for the optimization algorithm to run for a long time before each use.

Electrode selection opens up the question of the number of electrodes that are necessary to obtain high-quality decoding. Starting from healthy individuals and assessing patients with trans-radial amputation at different levels, it remains an open question for single-finger proportional decoding and MD-EMG. Nevertheless, the number of electrodes selected, the type of machine learning model, and the number of DoFs decoded is an intertwined question and should be answered for each combination to find the best combination.

Next steps involve the investigation of whether it is possible to decode more than single-finger angles. Section 2.4.1, shows preliminary results of single-finger proportional decoding together with 2-DoFs wrist proportional motions. However, the complexity of the human hand goes beyond position control. The interactions between different joints, the varying degrees of applied force, and the dynamic control of stiffness based on task requirements all add to this intricacy. Therefore, the challenge lies in replicating this sophisticated coordination in prosthetic hands.

Future investigations should consider including additional features beyond positional data in the decoding process. This could encompass the forearm position, the force applied by

each finger, the modulation of joint stiffness based on the type of object being manipulated, or even the torque exerted at each joint. The inclusion of these parameters would require investigation in signal processing techniques, as well as improvements in machine learning algorithms to handle the augmented data complexity. The development of such intricate control systems could indeed push the boundaries of current robotic prosthetic hands, bringing them closer to the sophistication and versatility of the natural human hand. Investigations in that direction might require leveraging musculoskeletal models that can translate muscle activity into motions (see for instance [10]).

Increasing complexity in decoding will imply an increase in the amount of data necessary. To this end, data augmentation could play a crucial role to obtain performant models. In this work, I investigated the potential of GANs to create high-quality synthetic data to improve decoding performance. However, GANs might not be the best model architecture to replicate EMG signals, especially for regression purposes. Some examples [11–13] showed potential model architecture for regression tasks but should be investigated for EMG signals. Moreover, [14] showed that combining different augmentation methods could yield increased performance compared to a single augmentation technique. Therefore, future steps include comparing standard EMG data augmentation techniques with deep learning approaches (GANs, Auto-encoders...) and a combination of all approaches. Finally, to apply these potential results to patients with an amputation, it could be possible to leverage style-transfer as shown in [15] to adapt the EMG signals from healthy individuals to mimic the muscle activity of a specific patient.

4.2 Shared Control: Robotic automation for an improved tool or towards hand replacement?

The use of robotic automation and shared control in the context of prosthetic hands presents a promising avenue for enhancing both functionality and user experience. Shared control was explored in many examples for BCI applications [16–18], but also for hand prosthesis applications [3–6]. The two examples shown in this work could be divided into two distinct objectives. The first example aims at improving grasp robustness and helping the user to perform daily activities without being disturbed about the possibility of releasing the grasped object. On the other hand, the second example doesn't show grasp assistance but rather automatic grasp execution with an extra DoF (in this case shoulder motion). The second example is far less biomimetic and the prosthesis could be seen more as a sophisticated tool.

Robotic automation in prostheses has two sides and is intrinsically linked to the control method. With single-finger proportional control, adding too much robotic automation could lower the user's agency. In my opinion, there are two objectives that should be followed in parallel. Indeed, the first one is to give prosthetic hands to patients that are functional and could help them in activities of daily living. The prosthesis remains a tool (as already the case [19], but will very efficiently help the user. In this case, any robotic automation added to

help the user to perform different tasks is beneficial. EMG decoding and other non-invasive decoding approaches are and will remain limited due to anatomical constraints. Indeed, some movements usually performed by intrinsic muscles of the hand cannot be decoded and robotic automation could increase the user's dexterity. In-hand object manipulation is an example where EMG decoding from the forearm alone will not be possible even by considering perfect decoding and perfect information about the object's properties. In this case, robotic automation has the potential to increase the quality of life of patients by giving them the possibility to perform actions that were not possible before such as grasping objects and replacing them in the hand for firm grasping is an action performed every day.

However, by automatizing a large part of the motor command, the user might lose the sense of agency and ownership. The second objective is the long-term goal of scientists working in this field: replacing the human hand. The extent to which robotic automation and shared control are perceived as a tool or an extension of the body may vary depending on the level of control retained by the user, the transparency of the control interface, and how well the automated actions align with the user's intentions. The goal should be to strike a balance between providing high levels of functionality and maintaining user agency. In this direction, robotic automation could help in grasping to reduce cognitive load, and simplify motor commands sent but should remain transparent in the sense that it should remove the noise in the decoded output to keep the intention of the user. In this case, the extent to which it is possible to add movements without using other DoFs should be investigated. It could be possible that synergies between intrinsic muscles and extrinsic muscles could be identified and leveraged to decode more complex movements such as in-hand object manipulation and performed using robotic automation.

Additionally, shared control integration into these devices requires the development of sufficiently sophisticated prostheses that can incorporate complex robotic controllers and have enough degrees of actuation for task execution. However, the prosthetic hand field is towards underactuated designs due to weight and size considerations [20]. Incorporating robotic automation to perform more complex movements demands the creation of devices that are lightweight, compact, and possess high dexterity. In parallel, another essential feature of these devices is the incorporation of compliant controllers. Such additions make the devices safer, more adaptable, and robust, enhancing the user experience. Compliant controllers mitigate the complexity of necessary control and offer better performance across diverse tasks and environments.

4.3 Integration of a complete system for long-term use

Finally, in order to validate the various hypotheses discussed above, complete systems should be provided to patients for long-term evaluation. The rich feedback obtained from these users will guide future developments, highlighting the primary user requirements. This would also provide a better understanding of the behavior and performance evolution of machine

learning models during extended use. For instance, one could examine whether recalibration of deep models would be required after six months of daily use. Additionally, it would be valuable to explore whether users develop certain strategies over time to enhance dexterity, and if single-finger proportional control offers any everyday life advantages compared to grasp classification. These questions, and more, could be addressed by providing patients with a fully integrated, user-friendly, and easily calibrated system.

Such a comprehensive system necessitates a prosthetic hand capable of complex task execution, potentially with the incorporation of robotic automation. Given that complex manipulation with robotic hands require data about the object being manipulated and the state of the robotic hand, sensorization of the prosthetic hand becomes essential. The subject-specific socket should incorporate medium-density derivations throughout the available area. Furthermore, the system should house the necessary electronics to acquire data, such as EMG signals and sensory information, process inferences from deep learning models, integrate signals, operate the robotic controller, and control the movement of the robotic hand. All these processes should occur in real-time with minimal latency, leading to a highly efficient and responsive prosthetic system.

In the pursuit of comprehensive, user-centered systems, seamless integration for long-term use is a crucial focus of future research directions. This necessitates the creation of a calibration setup that emphasizes accessibility and user-friendliness. Envisioned as an anytime, anywhere solution, the calibration process could be managed through an application on the user's smartphone. This involves the user executing a sequence of predefined movements in front of their mobile device. Subsequently, the smartphone utilizes the kinematic data generated in conjunction with the captured EMG signals to train a deep learning model. Once trained, this model is deployed directly onto the prosthetic hand's integrated electronics. This approach ensures a streamlined, user-controlled calibration process that effectively combines the flexibility and accessibility of smartphone technology with the computational prowess of deep learning models, ultimately facilitating an optimized, real-time performance of the prosthetic hand.

The introduction of a fully integrated, easy-to-use system opens the door for the utilization of sensory information collected by the prosthetic hand, augmenting the user's experience with sensory feedback. This feedback provides the user with valuable information regarding the prosthetic hand's state - including applied force, proprioceptive feedback, and contact points. Sensory feedback can significantly reduce the cognitive load for users by providing them with an intuitive understanding of the prosthetic hand's actions, thereby increasing the ease and efficiency of use [21].

The synergy between shared control and sensory feedback promises to offer a user-friendly and engaging experience. Shared control handles a portion of the manipulative complexity, while sensory feedback offers a sensory link to the prosthetic hand's state, creating a more immersive interaction. The resulting experience is expected to be not only straightforward

and pleasant but also more akin to natural hand usage. It can enable users to focus less on the tool (prosthetic hand) and more on the task at hand, providing a natural and efficient user interface.

In light of these considerations, it is crucial to underscore the importance of ecological settings in testing and refining these comprehensive prosthetic systems. The simulated or laboratory conditions, while useful for preliminary studies, may not entirely reflect the complex realities of day-to-day use. Consequently, long-term assessments in realistic settings, such as a user's own kitchen or a lab-simulated household environment, would provide more insightful data.

Current standard tests may offer a comparative measure of performance between different control methods, but their limited scope might not capture all the nuances that could inform about potential improvements. For instance, observing and tracking users' movements during everyday tasks over extended periods could reveal subtleties in usage patterns that might otherwise be overlooked. This could highlight potential areas of advancement, from improving individual dexterity to refining the shared control and feedback integration.

It is the interplay between these multidimensional factors - advanced prosthetic design, shared control, sensory feedback, user-friendly calibration, and comprehensive assessment methodology - that would truly push the boundaries of what is achievable in prosthetics. The prospect of providing users with a highly functional and intuitive prosthetic solution is more tangible than ever, and the progress in this direction will undoubtedly continue to make significant strides toward recreating a natural hand experience for users.

5 General Conclusion

This thesis has presented a body of work focused on the control of robotic prosthetic hands (RPHs) with single-finger proportional control. I have articulated this work into two distinct, yet complementary goals: investigating deep learning for EMG decoding and the integration of robotic automation for increased RPH dexterity.

I started by introducing the current solutions available to patients suffering from trans-radial amputation and reviewed the state of the art of scientific literature in the multi-faceted field of RPHs. Indeed, RPHs will feel like a natural hand only when significant efforts will be put into both the robotic hand itself and the sensorimotor interface. RPHs should be enhanced in terms of dexterity, and designed with soft and compliant controllers. On the other hand, proficient control of movements relies on the integration of motor commands and sensory information. Therefore we will be able to provide patients the ability to perform complex tasks only when the interfaces will have sufficient bandwidth to allow dexterous control and rich sensory feedback. Although significant progress has been made in the tactile modality, other modalities such as proprioception have been explored only through nonhomologous approaches. Due to the biomimetic nature of single-finger proportional control, it has the potential to partly provide some proprioceptive information to the user, as this approach leverages the natural manner in which we control our fingers.

In the second chapter, I presented my work focused on the motor control of RPHs through surface EMG decoding. I started by investigating the potential of deep learning for single-finger proportional control comparing two CNN approaches with the more standard feature-based approach. In section 2.1 I introduced the genetic algorithm that was used for model parameter optimization. The preliminary results shown in this section suggest that deep learning is a promising approach to improve EMG decoding performance. In section 2.2, I presented a new medium-density EMG system and compared its performance against a gold-standard gel-based EMG system. While the MD-EMG system showed improved performance compared to the low-density system, there was no clear advantage in using deep learning compared to the feature-based approach. The main difference with the results presented in section 2.1 may come from the model optimization strategy. Indeed, in the previous work, only one

optimized model architecture was obtained and generalized to the other recordings while here, the models were optimized for each recording. However, it is well known that CNNs require a substantial amount of training data to show superior performance compared to other machine learning techniques. For this reason, I explored data augmentations techniques with GANs to provide high-quality synthetic data and improve decoding performance, as reported in section 2.3. However, further improvements are necessary to create synthetic data for regression tasks. Section 2.4 explored three approaches to bridge the gap between lab environments and home use of the proposed decoding approach. First, using a single camera to simplify model calibration, second, leveraging transfer learning to reduce the amount of data necessary to train a model and finally performing all the steps in real-time such that the user gets instantaneous feedback on the progression of the training. However, the results presented in this section are still very preliminary and would require a more rigorous examination to quantify the potential advantages of such approaches.

Finally, I explored the advantages of implementing a shared control approach that combines proportional single-finger decoding and robotic automation to control RPHs. Indeed, some movements cannot be decoded due to limitations in the performance of surface EMG decoding and the fact that some motions are performed by intrinsic muscles of the hand. The first section focused on a compliant robotic controller to improve grasp robustness by increasing the number of contacts between the robotic hand and the object. The real-time shared control developed in this section allows for both high dexterity and robust grasping. We showed improvements in different tasks with the shared controller as well as a reduced EMG activity which reflects an increase in confidence and potentially prevents muscle fatigue over long-term use. The objective of the second shared control approach was to enable subjects to perform in-hand object manipulation, a non-trivial task in robotics that cannot be performed with EMG decoding alone. Similarly to the previous section, we combined single-finger proportional decoding with an autonomous controller enabling in-hand object rotation controlled by the subject with shoulder motion. In a pick-and-place task, two types of shoulder controllers and two robotic assistance levels were compared. Results showed that the combination of robotic assistance and an incremental shoulder controller yielded the best performance. This autonomous controller could potentially be integrated with the one discussed in the previous section resulting in both robust grasping and increased dexterity for the users. It is important to notice that both approaches provide full agency on finger movements when the user is not manipulating an object. However, the main limitation of such shared control strategies is the need for highly dexterous robotic hands with compliant actuators which are not yet available in current RPHs due to their size, weight, and battery life constraints.

In conclusion, RPH control could be enhanced with machine learning by improving decoding performance, reduction of calibration time, and increasing intra and inter-session robustness. Many approaches are still to be investigated such as cutting-edge deep models like transformers which have demonstrated remarkable results in natural language processing or combining musculoskeletal models with machine learning to decode not just finger angles but also force

and stiffness.

Ultimately, the advancements presented in this thesis contribute to the ongoing efforts to improve the functionality, dexterity, and adoption of RPHs for individuals with trans-radial amputation. It is hoped that these upcoming solutions will become more accessible, effective, and user-friendly, enabling amputees to regain independence and improve their quality of life.

A Supplementary Material

This section includes the supplementary material of the articles in the thesis.

Supplemental Material: Current Solutions and Future Trends of Robotic Prosthetic Hands

Vincent Mendez^{1,*}, Francesco Iberite^{2,*}, Solaiman Shokur^{1,#}, Silvestro Micera^{1,2,#}

¹Bertarelli Foundation Chair in Translational Neuroengineering, Center for Neuroprosthetics and Institute of Bioengineering, Ecole Polytechnique Federale de Lausanne, Lausanne, Switzerland

²The BioRobotics Institute and Department of Excellence in Robotics and AI, Scuola Superiore Sant'Anna, Pisa, Italy

*equal contribution as junior author

#equal contribution as senior author

Supplemental Table 1. Commercially available robotic prosthetic hands (RPHs)

HAND MODEL	COMPANY	DOFS	DOAS	DOAS/DOFS	SENSORIZED (ON FINGERTIP)	RPH TYPE
I-LIMB	Össur, Reykjavík, Iceland	10	5	0.50	No	Hand
AZZURRA HAND	Prensilia, Pontedera, Italy	16	4	0.25	No	Hand
MICHELANGELO HAND	Ottobock, Berlin, Germany	10	4	0.40	No	Hand
BEBIONIC HAND	Ottobock, Berlin, Germany	11	6	0.55	No	Hand
VINCENT HAND	Vincent Systems, Karlsruhe Germany	10	6	0.60	No	Hand
TASKA HAND	Taska, Christchurch, New Zealand	9	6	0.67	No	Hand
MIA HAND	Prensilia, Pontedera, Italy	6	3	0.50	No	Hand
HERO ARM	Openbionics, Bristol, UK	10	4	0.40	No	Hand
LUKE ARM (RADIAL CONFIGURATION)	Mobiusbionics, USA	13	4	0.31	No	Hand
AXONHOOK	Ottobock, Berlin, Germany	1	1	1.00	No	Hook
SENSORHAND SPEED	Ottobock, Berlin, Germany	1	1	1.00	Yes	3 Fingers
SYSTEM ELECTRIC GREIFER	Ottobock, Berlin, Germany	1	1	1.00	No	Hook
MOTION CONTROL PROPLUS	Fillauer, Chattanooga, TN, USA	1	1	1.00	No	Hand
MOTION CONTROL PROPLUS ETD2	Fillauer, Chattanooga, TN, USA	1	1	1.00	No	Hook
ABILITY HAND	Psyonic, USA	10	4	0.40	No	Hand
HANNES HAND	IIT Lab, Genova, Italy	10	1	0.1	No	Hand

Supplemental Table 2. RPHs found in research papers from 2005 to 2020

	YEAR	HAND MODEL	REFERENCE	DOFS	DOAS	DOAS/DOFS	SENSORIZED (ON FINGERTIP)	RPH TYPE	MATURITY
1	2005	SoftHand	(1)	10	1	0.1	No	Hand	On socket Lab
2	2005	UB Hand III	(2)	16	16	1	No	Hand	Bench Test
3	2006	HIT/DLR Prosth. Hand	(3)	13	3	0.23	No	Hand	Bench Test
4	2007	Biomechatronic hand	(4)	10	4	0.4	No	3 Fingers	Bench Test
5	2011	SmartHand	(5)	16	4	0.25	Yes	Hand	On socket Lab
6	2011	DART Hand	(6)	19	19	1	Yes	Hand	Bench Test
7	2011	ECF Robot Hand	(7)	5	10	2	No	Hand	Bench Test
8	2012	Prosthetic gripper	(8)	16	3	0.19	No	Hand	On socket Lab
9	2012	E-Nable	enablingthefuture.org	10	1	0.1	No	Hand	Open Source
10	2013	Dextrus Hand	openhandproject.org	11	5	0.45	No	Hand	Open Source
11	2013	UB Hand 4	(9)	20	20	1	Yes	Hand	Bench Test
12	2013	ACT Hand	(10)	11	30	2.72	No	Hand	Bench Test
13	2014	ISR-SoftHand	(11)	10	4	0.4	No	Hand	Bench Test
14	2015	Open Bionics Hand	(12)	15	1	0.07	No	Hand	Bench Test, Open Source
15	2015	Delft Hand	(13)	7	1	0.14	No	Hand	Bench Test (with user)
16	2015	SoftHand 2	(14)	19	2	0.11	No	Hand	Bench Test
17	2015	Anthropomorphic Hand	(15)	15	2	0.13	No	Hand	Bench Test
18	2015	SMA Gripper	(16)	6	3	0.5	No	3 Fingers	Bench Test
19	2015	Touch Hand	(17)	15	5	0.33	No	Hand	On socket Lab
20	2015	Soft Bionic Hand	(18)	11	2	0.18	Yes	Hand	Bench Test
21	2015	HACKberry Hand	exiii-hackberry.com	10	3	0.3	No	Hand	Open Source
22	2016	Biomimetic Hand	(19)	21	10	0.48	No	Hand	Bench Test
23	2016	Yale Multigrasp Hand	(20)	11	2	0.18	No	Hand	Patent
24	2016	SoftHand-D	(21)	19	1	0.05	No	Hand	Bench Test
25	2016	SoftHand Pro	(22)	19	1	0.05	No	Hand	On socket Lab
26	2016	ADA Robotic Hand	www.openbionics.com	10	5	0.5	No	Hand	Open Source
27	2016	Soft Prosthetic Hand	(23)	5	5	1	Yes	Hand	Bench Test
28	2016	Bionic Hand	(24)	15	11	0.73	No	Hand	Bench Test
29	2016	Soft Robotic Hand II	(25)	5	10	2	No	Hand	Bench Test
30	2017	Underactuated hand	(26)	10	2	0.2	No	Hand	Bench Test
31	2017	SSSA-MyHand	(27)	3	3	1	No	Hand	On socket Lab
32	2017	MORA Hap-2	(28)	15	4	0.26	No	Hand	Bench Test
33	2017	SCCA Hand	(29)	11	5	0.45	No	Hand	Bench Test
34	2017	SoftHand Pro-H	(30)	19	1	0.05	No	Hand	On socket Lab
35	2017	Robotic Hand II	(31)	10	5	0.5	No	Hand	Bench Test
36	2017	Compliant Prosthetic Hand	(32)	6	6	1	Yes	Hand	On socket Lab
37	2018	HR-Hand	(33)	NA	NA	NA	No	Hand	Bench Test
38	2018	DeTOP Hand	(34)	6	3	0.5	Yes	Hand	On Socket Lab
39	2018	F3Hand	(35)	15	1	0.07	No	Hand	On Socket Lab (with controller)

40	2018	Soft Pneumatic Hand	(36)	6	6	1	No	Hand	Bench Test
41	2018	KIT Prosthetic Hand	(37)	10	2	0.2	No	Hand	Bench Test
42	2019	Low-Cost prosthetic hand	(38)	14	2	0.14	No	Hand	Open Source
43	2019	AstoHand	(39)	10	5	0.5	No	Hand	On socket Lab
44	2019	Low-Cost sEMG Prosthetics	(40)	14	5	0.36	Yes (temperature)	Hand	Bench Test
45	2019	anthropomorphic prosthetic hand	(41)	10	3	0.3	No	Hand	Bench Test
46	2019	Rehand II	(42)	10	1	0.1	No	Hand	on socket lab
47	2019	DUFAB Hand	(43)	13	5	0.38	No	Hand	Bench Test
48	2019	Adaptive Prosthetic Hand	(44)	18	3	0.17	No	Hand	On Socket Lab (healthy subject)
49	2019	Lightweight 10-DOF Robotic Hand	(45)	10	1	0.1	No	Hand	Bench Test
50	2019	Highly compliant prosthetic hand	(46)	15	3	0.2	Yes	Hand	Bench Test
51	2019	Gear-Driven Hand for Toddlers	(47)	1	1	1	No	Hand	On Socket Lab
52	2019	low-cost compliant prosthetic hand	(48)	15	5	0.33	No	Hand	Bench Test
53	2019	thermoregulated lightweight hand prosthesis	(49)	14	1	0.07	No	Hand	On Socket Lab
54	2019	Multi-Fingered Prosthetic Hand	(50)	15	6	0.4	No	Hand	Bench Test
55	2019	Prosthetic hand	(51)	16	3	0.19	No	Hand	On Socket Lab (healthy subject)
56	2020	Under-Actuated Hand Prosthesis	(52)	15	7	0.47	No	Hand	Bench Test
57	2020	Galileo Hand	(53)	15	6	0.4	No	Hand	Bench Test
58	2020	X-Limb	(54)	13	5	0.38	No	Hand	On Socket Lab
59	2020	F3Hand II	(55)	15	1	0.07	No	Hand	On Socket Lab (with controller)

Literature Cited

1. Carrozza MC, Cappiello G, Stellin G, Zaccone F, Vecchi F, Micera S, et al. A cosmetic prosthetic hand with tendon driven under-actuated mechanism and compliant joints: Ongoing research and preliminary results. In: Proceedings - IEEE International Conference on Robotics and Automation. 2005. p. 2661–6.
2. Lotti F, Tiezzi P, Vassura G, Biagiotti L, Palli G, Melchiorri C. Development of UB Hand 3: Early results. In: Proceedings - IEEE International Conference on Robotics and Automation. 2005. p. 4488–93.
3. Zhao DW, Jiang L, Huang H, Jin MH, Cai HG, Liu H. Development of a multi-DOF anthropomorphic prosthetic hand. In: 2006 IEEE International Conference on Robotics and Biomimetics, ROBIO 2006. 2006. p. 878–83.
4. Zollo L, Roccella S, Guglielmelli E, Carrozza MC, Dario P. Biomechatronic design and control of an anthropomorphic artificial hand for prosthetic and robotic applications. IEEE/ASME Trans Mechatronics. 2007 Aug 1;12(4):418–29.
5. Cipriani C, Controzzi M, Carrozza MC. The SmartHand transradial prosthesis. J Neuroeng Rehabil [Internet]. 2011 May 22 [cited 2020 Jun 4];8(1):29. Available from: <http://jneuroengrehab.biomedcentral.com/articles/10.1186/1743-0003-8-29>
6. Thayer N, Priya S. Design and implementation of a dexterous anthropomorphic robotic typing (DART) hand. Smart Mater Struct. 2011 Feb 9;20(3):035010.
7. Yamaguchi A, Takemura K, Yokota S, Edamura K. A robot hand using electro-conjugate fluid. In: 2011 IEEE International Conference on Robotics and Automation. IEEE; 2011. p. 5923–8.
8. Baril M, Laliberté T, Gosselin C, Routhier F. On the design of a mechanically programmable underactuated anthropomorphic prosthetic gripper. J Mech Des Trans ASME. 2013 Dec 1;135(12).
9. Melchiorri C, Palli G, Berselli G, Vassura G. Development of the UB Hand IV: Overview of Design Solutions and Enabling Technologies. IEEE Robot Autom Mag. 2013 Sep;20(3):72–81.
10. Deshpande AD, Xu Z, Weghe MJV, Brown BH, Ko J, Chang LY, et al. Mechanisms of the anatomically correct testbed hand. IEEE/ASME Trans Mechatronics. 2013;18(1):238–50.
11. Tavakoli M, De Almeida AT. Adaptive under-actuated anthropomorphic hand: ISR-SoftHand. In: IEEE International Conference on Intelligent Robots and Systems. Institute of Electrical and Electronics Engineers Inc.; 2014. p. 1629–34.
12. Kontoudis GP, Liarokapis M V., Zisimatos AG, Mavrogiannis CI, Kyriakopoulos KJ. Open-source, anthropomorphic, underactuated robot hands with a selectively lockable differential mechanism: Towards affordable prostheses. In: IEEE International Conference on Intelligent Robots and Systems. Institute of Electrical and Electronics Engineers Inc.; 2015. p. 5857–62.
13. Smit G, Plettenburg DH, Van Der Helm FCT. The lightweight Delft Cylinder hand: First multi-articulating hand that meets the basic user requirements. IEEE Trans Neural Syst Rehabil Eng. 2015 May 1;23(3):431–40.
14. Santina CD, Grioli G, Catalano M, Brando A, Bicchi A. Dexterity augmentation on a synergistic hand: The Pisa/IIT SoftHand+. In: IEEE-RAS International Conference on Humanoid Robots. IEEE Computer Society; 2015. p. 497–503.

15. Chen W, Xiong C, Yue S. Mechanical implementation of kinematic synergy for continual grasping generation of anthropomorphic hand. *IEEE/ASME Trans Mechatronics*. 2015 Jun 1;20(3):1249–63.
16. Simone F, York A, Seelecke S. Design and fabrication of a three-finger prosthetic hand using SMA muscle wires. In: *Bioinspiration, Biomimetics, and Bioreplication 2015*. SPIE; 2015. p. 94290T.
17. Stopforth R, Bright G, Diegel O, van der Riet D. A Low Cost Design of a 3D Printed Multi-fingered Myoelectric Prosthetic Hand SLA Prototyping View project Radar Signal Error View project THE LOW COST DESIGN OF A 3D PRINTED MULTI-FINGERED MYOELECTRIC PROSTHETIC HAND [Internet]. 2015 [cited 2020 Jun 2]. Available from: <https://www.researchgate.net/publication/282818559>
18. Tavakoli M, Lopes P, Lourenço J, Rocha RP, Giliberto L, De Almeida AT, et al. Autonomous Selection of Closing Posture of a Robotic Hand Through Embodied Soft Matter Capacitive Sensors. *IEEE Sens J*. 2017 Sep 1;17(17):5669–77.
19. Xu Z, Todorov E. Design of a highly biomimetic anthropomorphic robotic hand towards artificial limb regeneration. In: *Proceedings - IEEE International Conference on Robotics and Automation*. Institute of Electrical and Electronics Engineers Inc.; 2016. p. 3485–92.
20. Belter. (12) United States Patent. 2016 Aug.
21. Piazza C, Santina C Della, Catalano M, Grioli G, Garabini M, Bicchi A. SoftHand Pro-D: Matching dynamic content of natural user commands with hand embodiment for enhanced prosthesis control. In: *Proceedings - IEEE International Conference on Robotics and Automation*. Institute of Electrical and Electronics Engineers Inc.; 2016. p. 3516–23.
22. Godfrey SB, Bianchi M, Zhao K, Catalano M, Breighner R, Theuer A, et al. The softhand pro: Translation from robotic hand to prosthetic prototype. In: *Biosystems and Biorobotics*. Springer International Publishing; 2017. p. 469–73.
23. Zhao H, O'Brien K, Li S, Shepherd RF. Optoelectronically innervated soft prosthetic hand via stretchable optical waveguides. *Sci Robot*. 2016 Dec 6;1(1).
24. Atasoy A, Kaya E, Toptas E, Kuchimov S, Kaplanoglu E, Ozkan M. 24 DOF EMG controlled hybrid actuated prosthetic hand. In: *Proceedings of the Annual International Conference of the IEEE Engineering in Medicine and Biology Society, EMBS*. Institute of Electrical and Electronics Engineers Inc.; 2016. p. 5059–62.
25. She Y, Chen J, Shi H, Su H-J. Modeling and Validation of a Novel Bending Actuator for Soft Robotics Applications. *Soft Robot* [Internet]. 2016 Jun 1 [cited 2020 Jun 2];3(2):71–81. Available from: <https://www.liebertpub.com/doi/10.1089/soro.2015.0022>
26. Mottard A, Laliberté T, Gosselin C. Underactuated tendon-driven robotic/prosthetic hands: Design issues. In: *Robotics: Science and Systems*. MIT Press Journals; 2017.
27. Controzzi M, Clemente F, Barone D, Ghionzoli A, Cipriani C. The SSSA-MyHand: A dexterous lightweight myoelectric hand prosthesis. *IEEE Trans Neural Syst Rehabil Eng*. 2017 May 1;25(5):459–68.
28. Gopura RARC, Bandara DSV, Gunasekera NPA, Hapuarachchi VH, Ariyaratna BS. A prosthetic hand with self-adaptive fingers. In: *2017 3rd International Conference on Control, Automation and Robotics, ICCAR 2017*. Institute of Electrical and Electronics Engineers Inc.; 2017. p. 269–74.

29. Wiste T, Goldfarb M. Design of a simplified compliant anthropomorphic robot hand. In: Proceedings - IEEE International Conference on Robotics and Automation. Institute of Electrical and Electronics Engineers Inc.; 2017. p. 3433–8.
30. Piazza C, Catalano MG, Godfrey SB, Rossi M, Grioli G, Bianchi M, et al. The SoftHand Pro-H: A Hybrid Body-Controlled, Electrically Powered Hand Prosthesis for Daily Living and Working. *IEEE Robot Autom Mag*. 2017 Dec 1;24(4):87–101.
31. Liu Y, Jiang L, Fan S, Yang D, Zhao J, Liu H. A novel actuation configuration of robotic hand and the mechanical implementation via postural synergies. In: Proceedings - IEEE International Conference on Robotics and Automation. Institute of Electrical and Electronics Engineers Inc.; 2017. p. 2215–22.
32. Choi KY, Akhtar A, Bretl T. A compliant four-bar linkage mechanism that makes the fingers of a prosthetic hand more impact resistant. In: Proceedings - IEEE International Conference on Robotics and Automation. Institute of Electrical and Electronics Engineers Inc.; 2017. p. 6694–9.
33. Faudzi AAM, Ooga J, Goto T, Takeichi M, Suzumori K. Index Finger of a Human-Like Robotic Hand Using Thin Soft Muscles. *IEEE Robot Autom Lett*. 2018 Jan 1;3(1):92–9.
34. Controzzi M, Clemente F, Barone D, Luciani LB, Pierotti N, Bacchereti M, et al. Progress towards the development of the detop hand prosthesis: A sensorized transradial prosthesis for clinical use. In: *Biosystems and Biorobotics* [Internet]. Springer International Publishing; 2019 [cited 2020 Jun 22]. p. 103–6. Available from: https://link.springer.com/chapter/10.1007/978-3-030-01845-0_20
35. Nemoto Y, Ogawa K, Yoshikawa M. F3Hand: A Five-Fingered Prosthetic Hand Driven with Curved Pneumatic Artificial Muscles. In: Proceedings of the Annual International Conference of the IEEE Engineering in Medicine and Biology Society, EMBS. Institute of Electrical and Electronics Engineers Inc.; 2018. p. 1668–71.
36. Fras J, Althoefer K. Soft Biomimetic Prosthetic Hand: Design, Manufacturing and Preliminary Examination. In: IEEE International Conference on Intelligent Robots and Systems. Institute of Electrical and Electronics Engineers Inc.; 2018. p. 6998–7003.
37. Weiner P, Starke J, Hundhausen F, Beil J, Asfour T. The KIT Prosthetic Hand: Design and Control. In: IEEE International Conference on Intelligent Robots and Systems. Institute of Electrical and Electronics Engineers Inc.; 2018. p. 3328–34.
38. Triwiyanto, Hamzah T, Luthfiyah S, Pawana IPA, Utomo B. A low cost and open-source anthropomorphic prosthetics hand for transradial amputee. In: AIP Conference Proceedings [Internet]. American Institute of Physics Inc.; 2019 [cited 2020 Jun 25]. p. 020086. Available from: <http://aip.scitation.org/doi/abs/10.1063/1.5141699>
39. Ariyanto M, Ismail R, Setiawan JD, Yuandi EP. Anthropomorphic transradial myoelectric hand using tendon-spring mechanism. *Telkomnika (Telecommunication Comput Electron Control*. 2019 Feb 1;17(1):537–48.
40. Rehman M-. Design and development of sEMG Prosthetics for recovering amputation of the human hand. *Pure Appl Biol*. 2019 Sep 10;8(3).
41. Chamara RPDD, Gopura RARC. An Under-Actuated Mechanism for Anthropomorphic Robotic Prosthetic Hand. In: 2019 5th International Conference on Control, Automation and Robotics, ICCAR 2019. Institute of Electrical and Electronics Engineers Inc.; 2019. p. 162–6.
42. Odagaki N, Yoshikawa M, Tanaka Y, Kawashima N. Rehand II: Wire-Driven Five-Fingered

- Electric Prosthetic Hand Utilizing Elasticity of a Cosmetic Glove. In: Proceedings of the Annual International Conference of the IEEE Engineering in Medicine and Biology Society, EMBS. Institute of Electrical and Electronics Engineers Inc.; 2019. p. 6661–4.
43. Nahid N, Rahman A, Das TK, Khabir KM, Islam A, Alam MS. Design and implementation of DUFAB Hand, a low-cost myoelectric prosthetic hand. In: 2019 Joint 8th International Conference on Informatics, Electronics and Vision, ICIEV 2019 and 3rd International Conference on Imaging, Vision and Pattern Recognition, icIVPR 2019 with International Conference on Activity and Behavior Computing, ABC 2019. Institute of Electrical and Electronics Engineers Inc.; 2019. p. 206–11.
 44. Yong X, Jing X, Wu X, Jiang J, Yokoi H. Development of an adaptive prosthetic hand. In: IEEE International Conference on Robotics and Biomimetics, ROBIO 2019. Institute of Electrical and Electronics Engineers Inc.; 2019. p. 2800–5.
 45. Shimura T, Murai Y, Togo S, Yinlai J, Yokoi H. Lightweight 10-DOF robotic hand with built-in wire-driven mechanism. In: IEEE International Conference on Robotics and Biomimetics, ROBIO 2019. Institute of Electrical and Electronics Engineers Inc.; 2019. p. 492–6.
 46. Cheng M, Fan S, Jiang L. Design of a highly compliant underactuated prosthetic hand. In: IEEE International Conference on Robotics and Biomimetics, ROBIO 2019. Institute of Electrical and Electronics Engineers Inc.; 2019. p. 2833–8.
 47. Jingl X, Yongl X, Shi Y, Yabiki Y, Jiang Y, Yokoi H, et al. A Gear-Driven Prosthetic Hand with Major Grasp Functions for Toddlers. In: IEEE International Conference on Intelligent Robots and Systems. Institute of Electrical and Electronics Engineers Inc.; 2019. p. 7321–6.
 48. Pozzobon LA, Da Silva Guerra R, Librelotto GR. A low-cost, compliant, underactuated prosthetic hand with custom flex sensors for finger bending estimation. In: 2019 19th International Conference on Advanced Robotics, ICAR 2019. Institute of Electrical and Electronics Engineers Inc.; 2019. p. 69–74.
 49. Sureshbabu AV, Rass D, Zimmermann M. A lightweight transradial hand prosthesis with a variable position thumb and thermoregulation. In: 2019 19th International Conference on Advanced Robotics, ICAR 2019. Institute of Electrical and Electronics Engineers Inc.; 2019. p. 61–8.
 50. Mohanta N, Mishra R, Sharma AK, Raj M. Design and Control Dynamics of Multi-Fingered Prosthetic Hand. In: 2019 4th International Conference on Information Systems and Computer Networks, ISCON 2019. Institute of Electrical and Electronics Engineers Inc.; 2019. p. 405–9.
 51. Jing X, Yong X, Jiang Y, Li G, Yokoi H. Anthropomorphic Prosthetic Hand with Combination of Light Weight and Diversiform Motions. *Appl Sci* [Internet]. 2019 Oct 9 [cited 2020 Jun 25];9(20):4203. Available from: <https://www.mdpi.com/2076-3417/9/20/4203>
 52. Abayasiri RAM, Abayasiri RST, Gunawardhana RAGM, Premakumara RMC, Mallikarachchi S, Gopura RARC, et al. An Under-Actuated Hand Prosthesis with Finger Abduction and Adduction for Human Like Grasps. In Institute of Electrical and Electronics Engineers (IEEE); 2020. p. 574–80.
 53. Fajardo J, Ferman V, Cardona D, Maldonado G, Lemus A, Rohmer E. Galileo hand: An anthropomorphic and affordable upper-limb prosthesis. *IEEE Access*. 2020;8:81365–77.
 54. Mohammadi A, Lavranos J, Zhou H, Mutlu R, Alici G, Tan Y, et al. A practical 3D-printed soft robotic prosthetic hand with multi-articulating capabilities. Connal L, editor. *PLoS One*

[Internet]. 2020 May 14 [cited 2020 Jun 22];15(5):e0232766. Available from:
<https://dx.plos.org/10.1371/journal.pone.0232766>

55. Nemoto Y, Ogawa K, Yoshikawa M. F3Hand II: A Flexible Five-Fingered Prosthetic Hand Using Curved Pneumatic Artificial Muscles. In: Proceedings of the 2020 IEEE/SICE International Symposium on System Integration, SII 2020. Institute of Electrical and Electronics Engineers Inc.; 2020. p. 99–104.

Supplementary Material: A Novel Medium-Density EMG System for Prosthetic Hand Control

V. Mendez, F. Artoni, S. Micera

Supplementary Figures

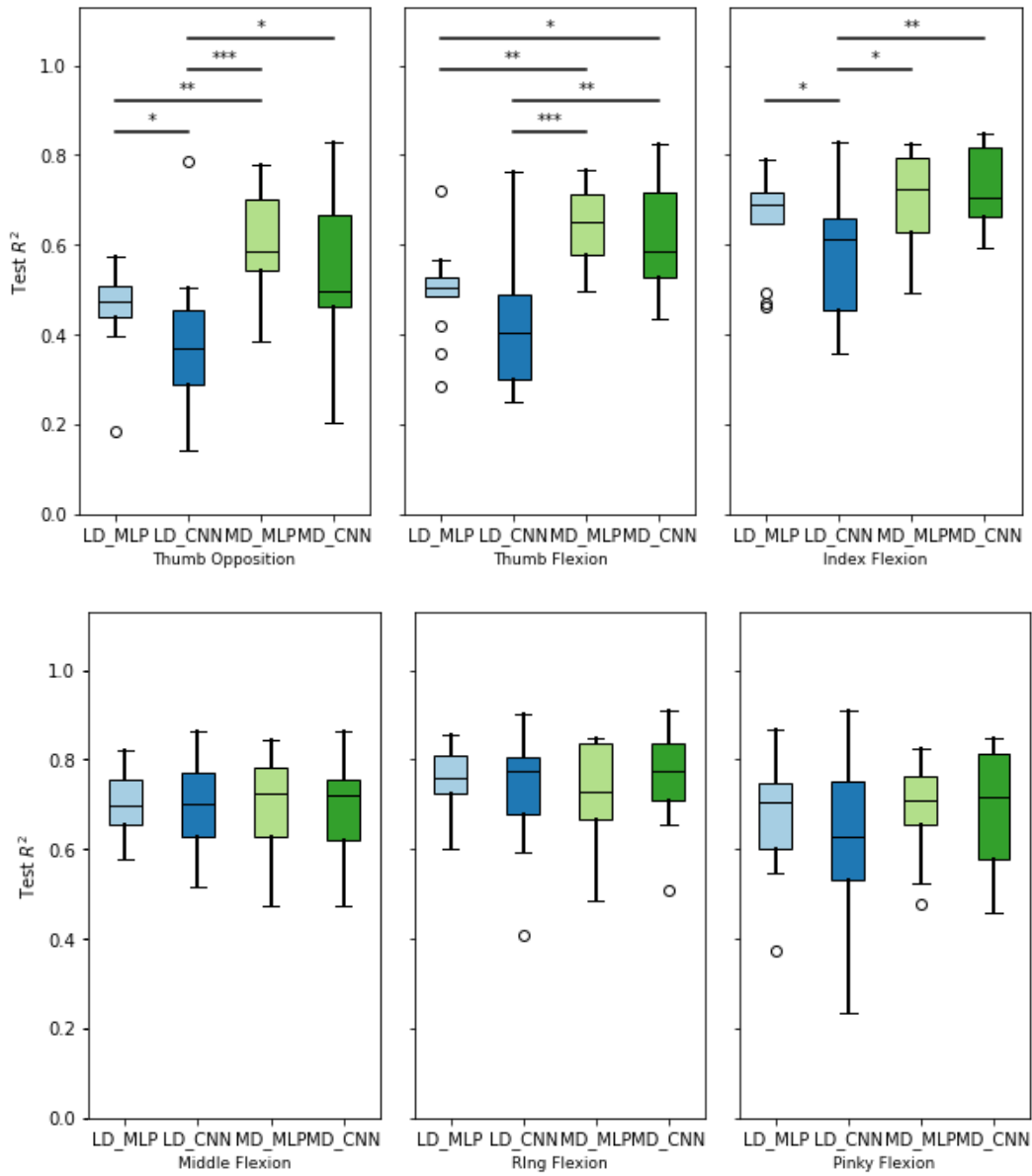


Figure S1: Boxplot of the performance in each condition for each finger (as shown in Fig. 4). The difference between conditions is significant for thumb opposition, thumb flexion, and index flexion (respectively: Kruskal-Wallis $H(3)=16.56$, $p<0.001$, ANOVA $F(3, 47)=9.56$, $p<0.001$ and Kruskal-Wallis $H(3)=9.74$, $p<0.05$). For thumb opposition, there are statistical differences between LD_MLP and LD_CNN (Mann-Whitney test, $U=136.0$, $n_1=n_2=14$, $p<0.05$), LD_MLP and MD_MLP (Mann-Whitney test, $U=24.0$, $n_1=14$, $n_2=12$, $p<0.01$), LD_CNN and MD_MLP (Student's T-test, $t(24)=-4.10$, $p<0.001$) and between LD_CNN and MD_CNN (Student's T-test, $t(24)=-2.28$, $p<0.05$). For thumb flexion, there are differences between LD_MLP and MD_MLP (Student's T-test, $t(23)=3.63$, $p<0.01$), LD_MLP and MD_CNN (Student's T-test, $t(23)=-2.56$, $p<0.05$), LD_CNN and MD_MLP (Student's T-test, $t(24)=-4.52$, $p<0.001$), and between LD_CNN and MD_CNN (Student's T-test, $t(24)=-3.61$, $p<0.01$). Finally for index flexion the significant differences are between LD_MLP and LD_CNN (Mann-Whitney test, $U=135.0$, $n_1=13$, $n_2=12$, $p<0.05$), LD_CNN and MD_MLP (Student's T-test, $t(24)=-2.56$, $p<0.05$) and between LD_CNN and MD_CNN (Student's T-test, $t(24)=-3.20$, $p<0.01$).

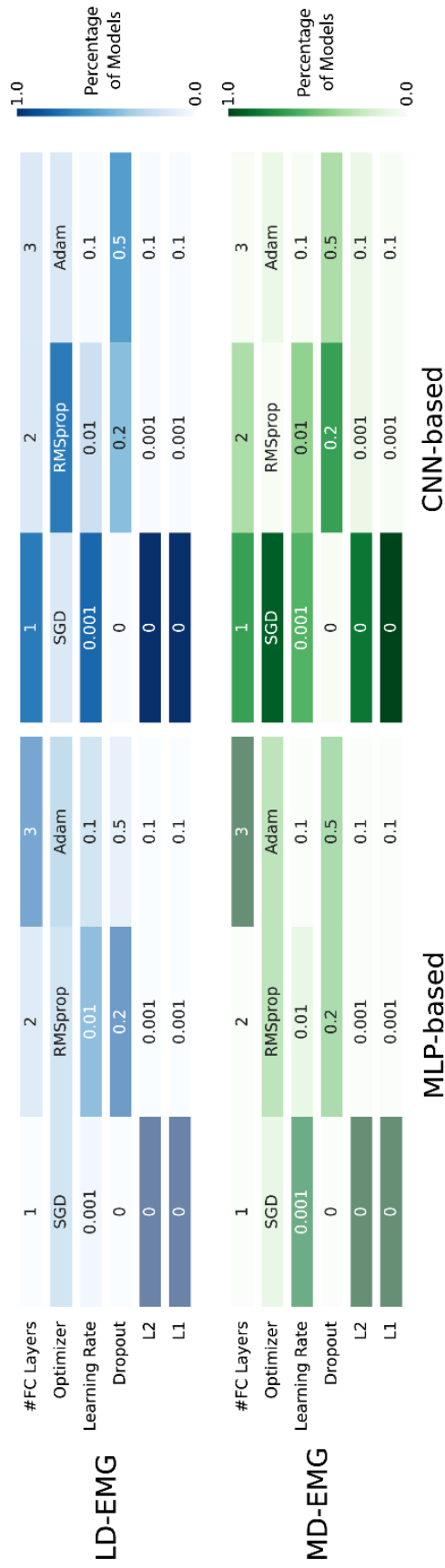


Figure S2: Hyperparameters selected by GA in each condition. Darker colors represent a higher proportion of model that selected a specific hyperparameter.

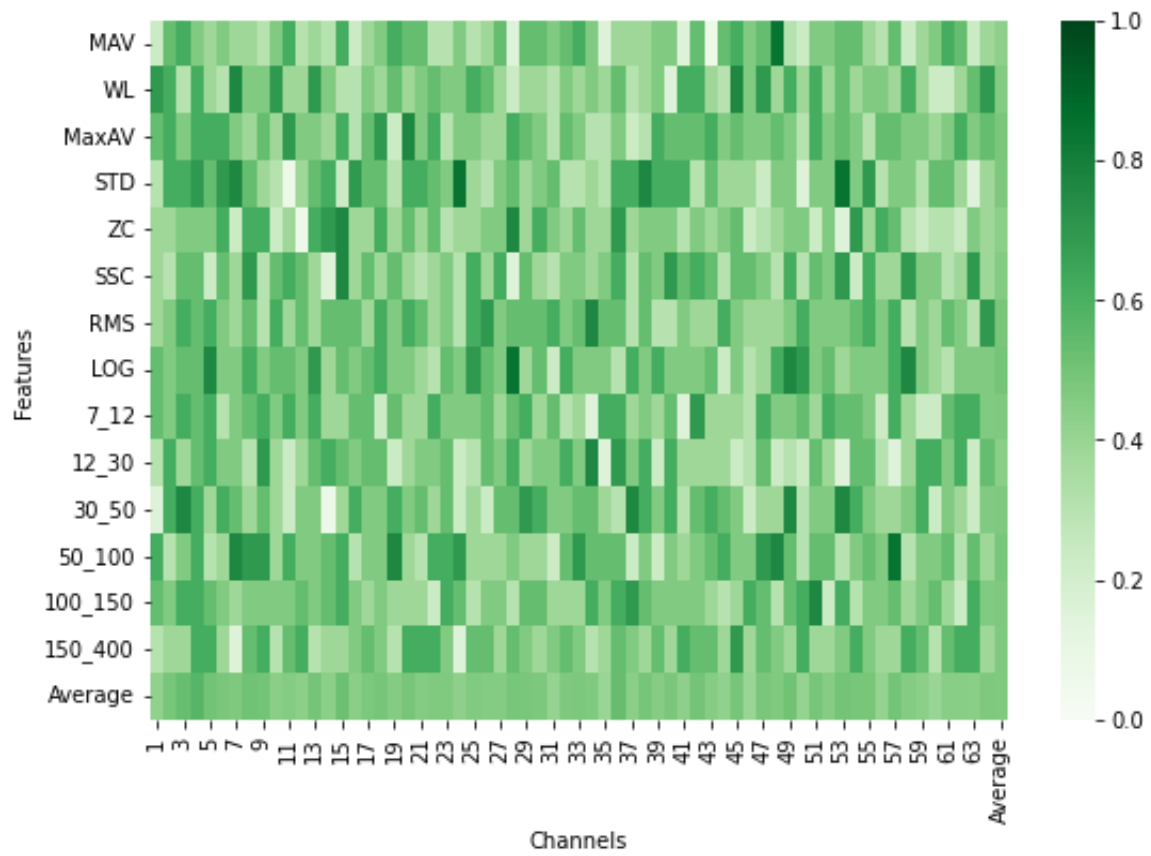


Figure S3: Heatmap showing the percentage of recordings where each feature-channel combination was selected with the MD-EMG system.

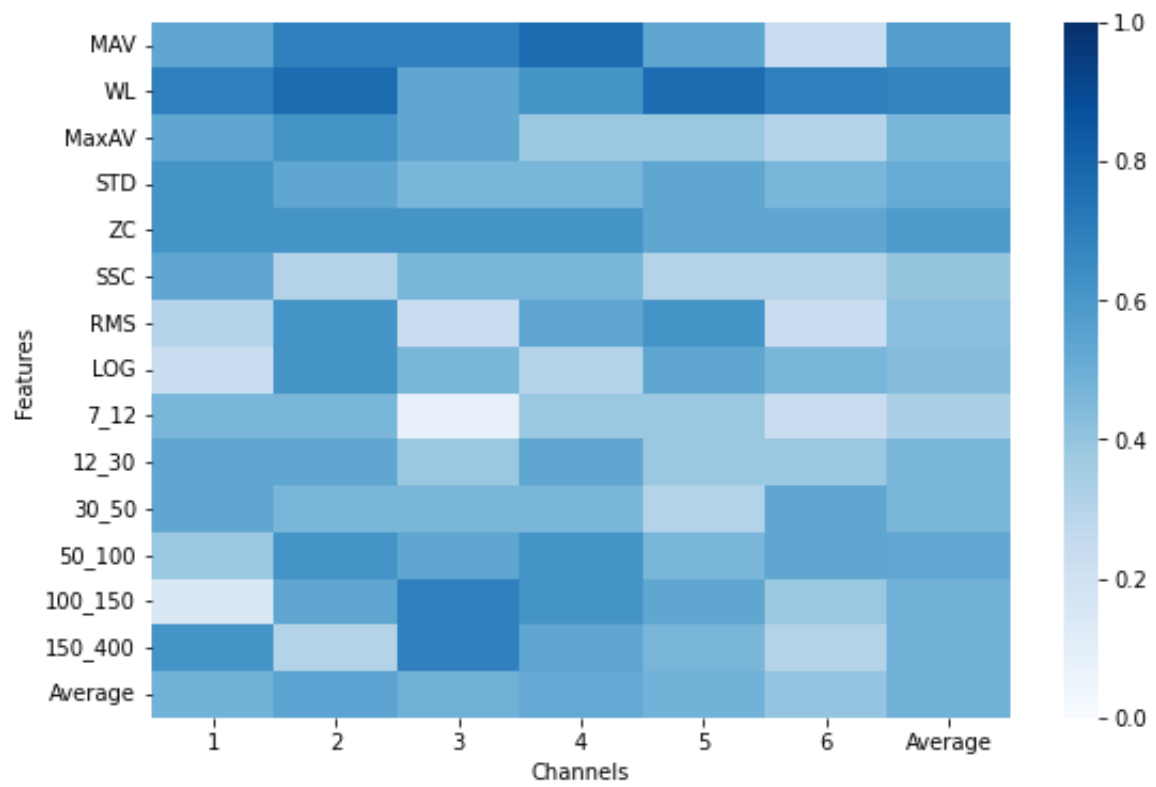


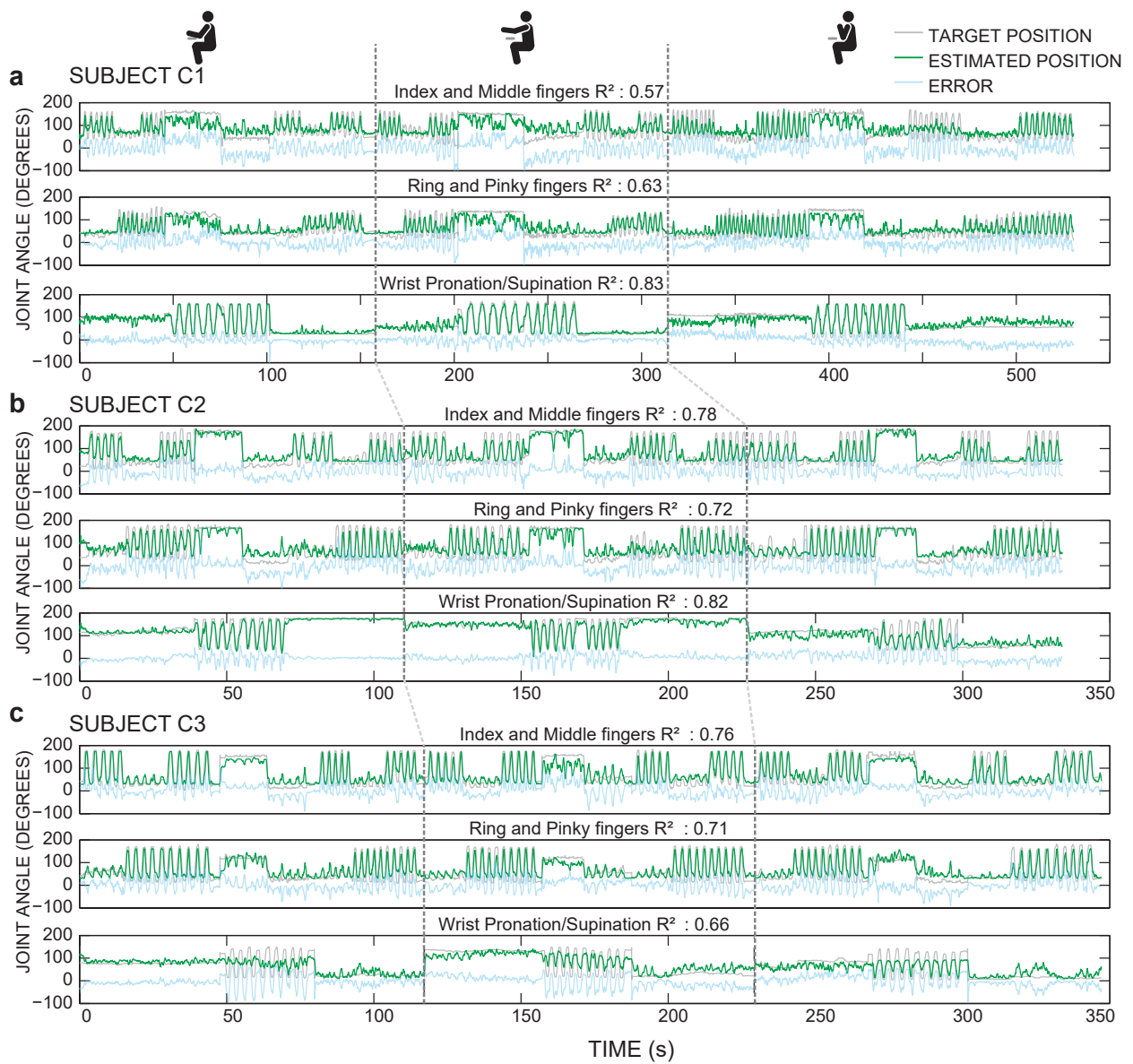
Figure S4: Heatmap showing the percentage of recordings where each feature-channel combination was selected with the LD-EMG system.

In the format provided by the authors and unedited.

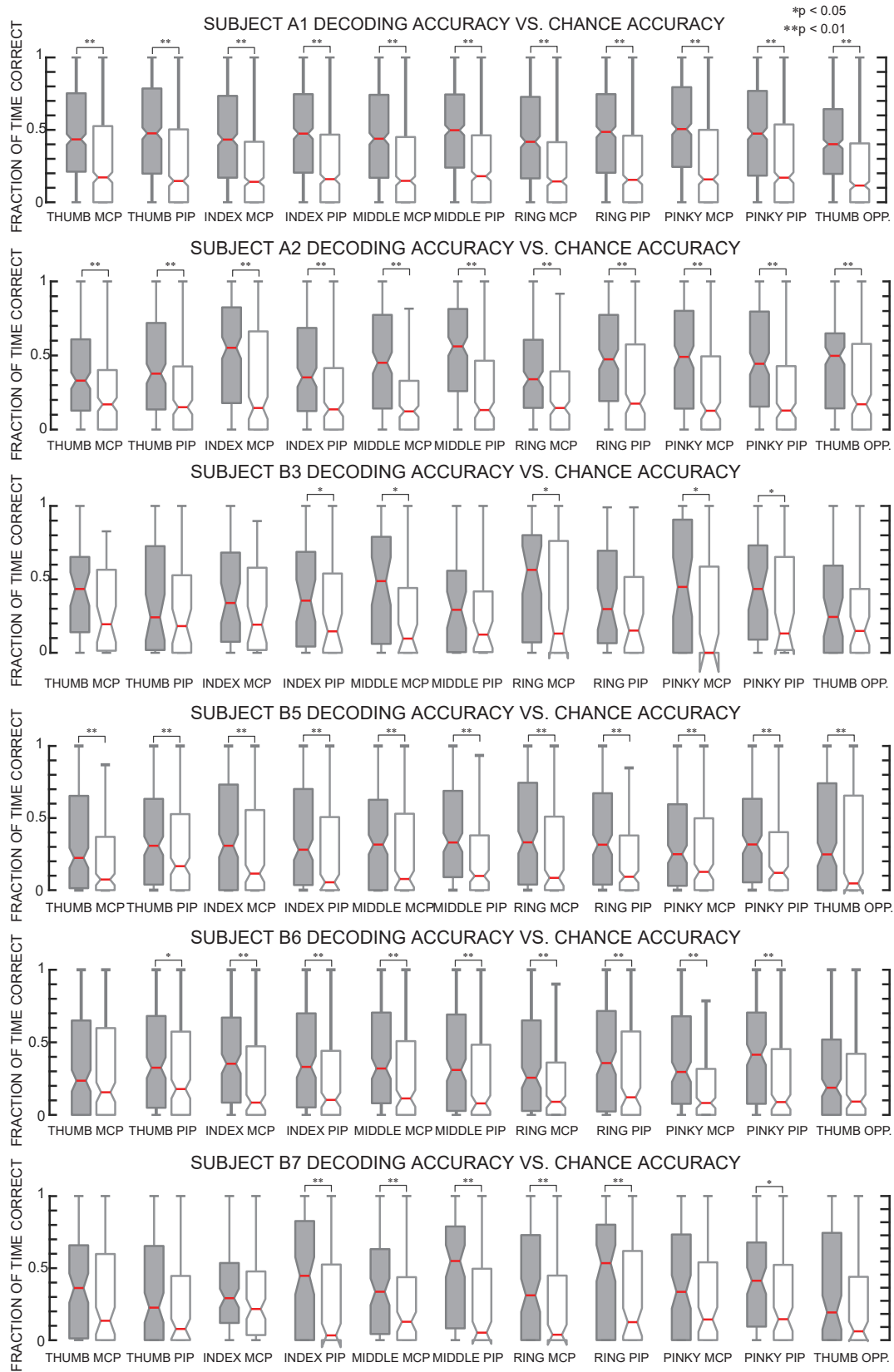
Shared human–robot proportional control of a dexterous myoelectric prosthesis

Katie Z. Zhuang¹, Nicolas Sommer^{2,7}, Vincent Mendez^{1,7}, Saurav Aryan^{2,7}, Emanuele Formento¹, Edoardo D'Anna¹, Fiorenzo Artoni¹, Francesco Petrini¹, Giuseppe Granata³, Giovanni Cannaviello⁴, Wassim Raffoul⁵, Aude Billard^{2,8} and Silvestro Micera^{1,6,8*}

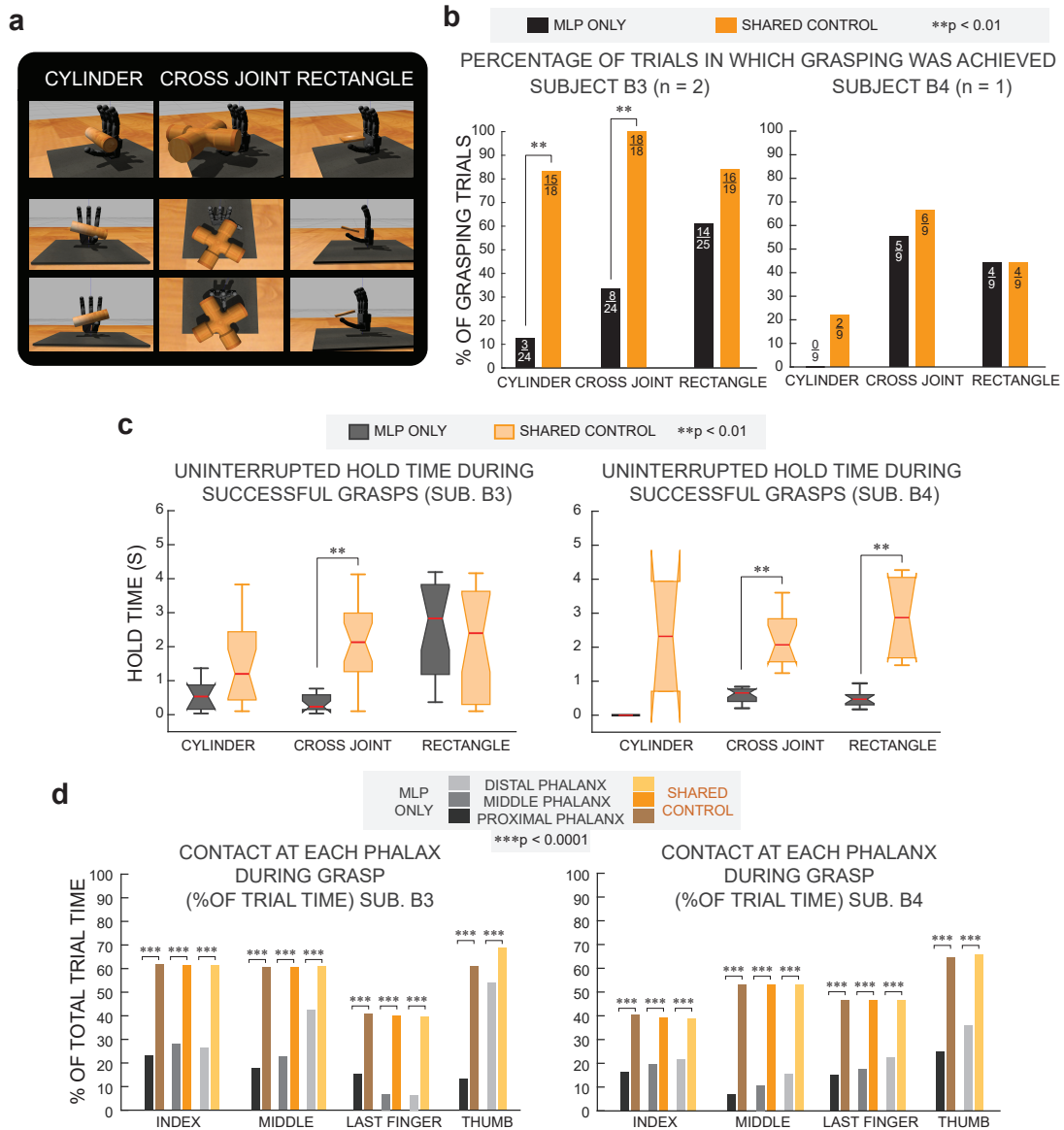
¹Bertarelli Foundation Chair in Translational Neuroengineering, Centre for Neuroprosthetics and Institute of Bioengineering, School of Engineering, École Polytechnique Fédérale de Lausanne, Lausanne, Switzerland. ²Learning Algorithms and Systems Laboratory, Institute of Microengineering, École Polytechnique Fédérale de Lausanne, Lausanne, Switzerland. ³Istituto di Ricovero e Cura a Carattere Scientifico, Fondazione Policlinico Universitario Agostino Gemelli, Rome, Italy. ⁴Villa Beretta Rehabilitation Center, Ospedale Valduce, Costa Masnaga, Italy. ⁵Service of Plastic and Reconstructive Surgery, Lausanne University Hospital and University of Lausanne, Lausanne, Switzerland. ⁶The BioRobotics Institute, Scuola Superiore Sant'Anna, Pisa, Italy. ⁷These authors contributed equally: Nicolas Sommer, Vincent Mendez, Saurav Aryan. ⁸These authors jointly supervised this work: Aude Billard, Silvestro Micera. *e-mail: silvestro.micera@epfl.ch



Supplementary Figure 1. Preliminary offline experiment setup and results for three able-bodied subjects, performing 5 repetitions of each movement. Optical tracking was performed for the arm contralateral to the one from which sEMGs were recorded **a**, Offline prediction results of Subject C1 with target and predicted joint angles of the three DoFs for three different arm positions. **b**, Offline prediction results of Subject C2 in same format as for Subject C1. **c**, Offline prediction results of Subject C3 in same format as for Subjects C1 and C2.



Supplementary Figure 2. Online MLP prediction performance against chance level for Subjects A1, A2, B3, B5, B6, and B7. Gray boxplots indicate the fraction of time per trial that each predicted DoF is within 15 degrees of the instructed angle. White boxplots indicate the fraction of time per trial that a random angle (within the set of trained angles) is within 15 degrees of the instructed angle. DoFs that perform significantly better than chance are marked (assessed by the Wilcoxon two-sided signed rank test). Data are aggregated over all sessions per subject (number of sessions performed are found on Table 1).



Supplementary Figure 3. Shared Control objects and results for Subjects B6 and B7. **a**, Objects tested during grasping: cylinder, cross joint part and rectangular piece. Objects were presented in three different orientations with respect to the robotic hand. **b**, Percentage of trials during which desired contacts are achieved for the three objects with or without shared for able subject B6 (left) and B7 (right). p-values determined with Fisher's two-tailed exact test. Number of successful trials versus total trials are indicated on each bar, number of sessions are indicated in the title. **c**, Duration of hold time for each object out of seven seconds of instructed hold with or without shared control (p-values determined with Wilcoxon two-sided signed-rank test). **d**, Percentage of grasping trial time during which contacts were touching the objects with or without shared control (p-values determined with Fisher's two-tailed Exact Test). Contacts on different phalanges are indicated with different shades – lighter shades indicate more distal phalanges while darker shades indicated more proximal phalanges. Raw data corresponding to these bar plots are shown in Supplementary Table 1.

Supplementary Tables

SUBJECT	METRIC	THUMB	INDEX	MIDDLE	RING	PINKY	THUMB OPP.
A1 (n = 10)	<i>correlation</i>	0.49 +/- 0.16 (0.77)	0.62 +/- 0.06 (0.74)	0.58 +/- 0.07 (0.72)	0.47 +/- 0.07 (0.64)	0.54 +/- 0.06 (0.64)	0.62 +/- 0.07 (0.71)
	<i>nMSE (%)</i>	8.2 +/- 3.1 (3.8)	12.2 +/- 4.5 (6.9)	12.5 +/- 3.0 (7.5)	16.9 +/- 3.0 (13.2)	13.8 +/- 2.2 (10.6)	12.4 +/- 2.5 (7.9)
A2 (n = 8)	<i>correlation</i>	0.26 +/- 0.18 (0.55)	0.53 +/- 0.02 (0.58)	0.51 +/- 0.07 (0.56)	0.70 +/- 0.10 (0.82)	0.71 +/- 0.11 (0.82)	0.52 +/- 0.09 (0.70)
	<i>nMSE (%)</i>	15.3 +/- 5.3 (7.5)	14.5 +/- 1.1 (13.2)	15.0 +/- 2.0 (13.0)	11.1 +/- 5.2 (6.8)	11.0 +/- 6.1 (6.1)	19.0 +/- 7.0 (10.8)
A3 (n = 4)	<i>correlation</i>	0.59 +/- 0.06 (0.64)	0.54 +/- 0.15 (0.68)	0.59 +/- 0.18 (0.78)	0.62 +/- 0.11 (0.74)	0.51 +/- 0.27 (0.79)	0.35 +/- 0.16 (0.47)
	<i>nMSE (%)</i>	10.4 +/- 2.4 (7.2)	11.5 +/- 2.1 (10.0)	9.7 +/- 3.4 (6.2)	10.7 +/- 1.8 (9.0)	15.5 +/- 9.6 (6.8)	21.2 +/- 2.5 (17.5)
B2 (n = 4)	<i>correlation</i>	0.31 +/- 0.20 (0.49)	0.33 +/- 0.23 (0.59)	0.56 +/- 0.24 (0.75)	0.57 +/- 0.15 (0.76)	0.35 +/- 0.21 (0.51)	0.39 +/- 0.16 (0.48)
	<i>nMSE (%)</i>	20.0 +/- 6.3 (14.3)	25.7 +/- 13.4 (10.4)	14.9 +/- 11.2 (6.4)	23.0 +/- 12.7 (10.6)	19.9 +/- 6.7 (14.3)	23.4 +/- 1.3 (22.0)
B3 (n = 4)	<i>correlation</i>	0.21 +/- 0.13 (0.39)	0.39 +/- 0.14 (0.60)	0.53 +/- 0.17 (0.78)	0.70 +/- 0.13 (0.83)	0.58 +/- 0.17 (0.77)	0.39 +/- 0.15 (0.57)
	<i>nMSE (%)</i>	33.1 +/- 18.7 (12.3)	21.1 +/- 7.9 (14.7)	19.9 +/- 7.5 (9.2)	8.3 +/- 2.1 (5.3)	16.5 +/- 8.8 (6.0)	17.8 +/- 3.5 (15.0)
B4 (n = 2)	<i>correlation</i>	0.31 +/- 0.05 (0.35)	0.54 +/- 0.08 (0.60)	0.63 +/- 0.06 (0.67)	0.55 +/- 0.02 (0.59)	0.65 +/- 0.01 (0.66)	0.37 +/- 0.04 (0.40)
	<i>nMSE (%)</i>	35.7 +/- 0.1 (35.6)	13.2 +/- 4.1 (10.3)	9.7 +/- 1.7 (8.5)	26.4 +/- 5.1 (22.8)	21.0 +/- 1.1 (20.2)	20.9 +/- 0.5 (20.6)
B1 (n = 1)	<i>correlation</i>	0.21	0.45	0.38	0.77	0.61	0.52
	<i>nMSE (%)</i>	32.3	32.0	23.2	9.0	10.3	13.0

Supplementary Table 1. Performance metrics of MLP decoder for all subjects and each degree of freedom tested. Correlation coefficient and normalized Mean Squared Error are presented. Under each subject ID, we cite the number of sessions that the subject performed.

		SUBJECT A1 (n=5)		SUBJECT A2 (n=4)		SUBJECT A3 (n=1)		SUBJECT B5 (n=3)		SUBJECT B6 (n=2)		SUBJECT B7 (n=1)	
		SHARED CONTROL	MLP ONLY	SHARED CONTROL	MLP ONLY	SHARED CONTROL	MLP ONLY	SHARED CONTROL	MLP ONLY	SHARED CONTROL	MLP ONLY	SHARED CONTROL	MLP ONLY
INDEX	PROXIMAL PHALANX	11831 25156	5277 25369	8457 16580	3006 13966	3787 5285	1876 6951	6960 15150	2882 15509	6104 9878	3142 13509	2077 5153	855 5276
	MIDDLE PHALANX	11438 25156	3692 25369	8444 16580	4222 13966	3753 5285	2449 6951	6898 15150	2428 15509	6093 9878	3796 13509	2014 5153	1033 5276
	DISTAL PHALANX	11382 25156	3374 25369	8421 16580	5155 13966	3751 5285	2546 6951	6869 15150	3357 15509	6088 9878	3595 13509	2009 5153	1150 5276
MIDDLE	PROXIMAL PHALANX	12570 25156	3958 25369	7974 16580	1505 13966	1944 5285	781 6951	7887 15150	2754 15509	6012 9878	2430 13509	2738 5153	374 5276
	MIDDLE PHALANX	12572 25156	4501 25369	7979 16580	2037 13966	1942 5285	797 6951	7878 15150	2559 15509	6013 9878	3081 13509	2738 5153	570 5276
	DISTAL PHALANX	12554 25156	7538 25369	7960 16580	4168 13966	1922 5285	929 6951	7873 15150	4814 15509	6104 9878	5752 13509	2738 5153	814 5276
LAST FINGER	PROXIMAL PHALANX	7744 25156	4755 25369	8166 16580	2971 13966	2008 5285	1201 5285	5630 15150	3041 15509	4042 9878	2078 13509	2404 5153	796 5276
	MIDDLE PHALANX	7063 25156	2463 25369	7780 16580	3034 13966	1826 5285	1064 6951	5317 15150	1449 15509	3950 9878	932 13509	2397 5153	917 5276
	DISTAL PHALANX	7011 25156	2423 25369	7757 16580	3752 13966	1821 5285	937 6951	5313 15150	1534 15509	3935 9878	853 13509	2391 5153	1195 5276
THUMB	PROXIMAL PHALANX	13409 25156	1359 25369	8606 16580	2186 13966	2231 5285	448 6951	9382 15150	715 15509	6020 9878	1780 13509	3331 5153	1321 5276
	DISTAL PHALANX	14356 25156	10829 25369	8933 16580	5159 13966	3250 5285	3285 6951	10571 15150	7062 15509	6806 9878	7302 13509	3385 5153	1896 5276

Supplementary Table 2. Fraction of trial time during which contact with object exists, per phalanx. Data correspond to bar plots in Fig. 4g, 5d, and Supplementary Fig. 3d. Entries indicate successful contact between sensors on a single phalanx with an object during grasping with shared control (gray shaded) or MLP only control (white shaded) as a fraction of total time steps. Data are aggregated over all object types and sessions for a single subject. Number of sessions are indicated for each subject.

For supplementary videos of section 3.1 refer to: <https://doi.org/10.1038/s42256-019-0093-5>

For supplementary video of section 3.2 refer to: <https://doi.org/10.1088/1741-2552/aca35f>

Bibliography

- [1] Yilin Liu, Shijia Zhang, and Mahanth Gowda. “NeuroPose: 3D hand pose tracking using EMG wearables”. In: *The Web Conference 2021 - Proceedings of the World Wide Web Conference, WWW 2021* (Apr. 2021), pp. 1471–1482. DOI: 10.1145/3442381.3449890.
- [2] Ryan J. Smith et al. “Continuous decoding of finger position from surface EMG signals for the control of powered prostheses”. In: *Proceedings of the 30th Annual International Conference of the IEEE Engineering in Medicine and Biology Society, EMBS'08 - "Personalized Healthcare through Technology"* (2008), pp. 197–200.
- [3] Light C.M. et al. “Intelligent multifunction myoelectric control of hand prostheses”. In: *Journal of Medical Engineering and Technology* 26.4 (2002), pp. 139–146. ISSN: 0309-1902. DOI: 10.1080/03091900210142459.
- [4] Strahinja Došen et al. “Cognitive vision system for control of dexterous prosthetic hands: Experimental evaluation”. In: *Journal of NeuroEngineering and Rehabilitation* 7.1 (2010), pp. 1–14. ISSN: 17430003. DOI: 10.1186/1743-0003-7-42.
- [5] Tura A. et al. “Experimental development of a sensory control system for an upper limb myoelectric prosthesis with cosmetic covering”. In: *Journal of rehabilitation research and development* 35.1 (1998).
- [6] Simone Fani et al. “Assessment of myoelectric controller performance and kinematic behavior of a novel soft synergy-inspired robotic hand for prosthetic applications”. In: *Frontiers in Neurorobotics* 10.October (2016), pp. 1–15. ISSN: 16625218. DOI: 10.3389/fnbot.2016.00011.
- [7] Raul C. Sîmpetru et al. “Accurate Continuous Prediction of 14 Degrees of Freedom of the Hand from Myoelectrical Signals through Convolutional Deep Learning”. In: (2022), pp. 702–706. DOI: 10.1109/EMBC48229.2022.9870937.
- [8] Stephan Johann Lehmle et al. “Deep transfer learning compared to subject-specific models for sEMG decoders”. In: *Journal of Neural Engineering* 19.5 (Oct. 2022), p. 056039. ISSN: 1741-2552. DOI: 10.1088/1741-2552/AC9860. URL: <https://iopscience.iop.org/article/10.1088/1741-2552/ac9860%20https://iopscience.iop.org/article/10.1088/1741-2552/ac9860/meta>.

- [9] Rebecca J. Greene et al. “Functionally adaptive myosite selection using high-density sEMG for upper limb myoelectric prostheses”. In: *IEEE Transactions on Biomedical Engineering* (2023), pp. 1–11. DOI: 10.1109/TBME.2023.3274053.
- [10] Caggiano Vittorio et al. “MyoSuite – A contact-rich simulation suite for musculoskeletal motor control”. In: (2022). DOI: 10.48550/ARXIV.2205.13600. URL: <https://arxiv.org/abs/2205.13600>.
- [11] Seonghyeon Hwang and Steven Euijong Whang. “MixRL: Data Mixing Augmentation for Regression using Reinforcement Learning”. In: *CoRR* abs/2106.03374 (2021). arXiv: 2106.03374. URL: <https://arxiv.org/abs/2106.03374>.
- [12] Florian Dubost et al. “Hydranet: Data Augmentation for Regression Neural Networks”. In: *CoRR* abs/1807.04798 (2018). arXiv: 1807.04798. URL: <http://arxiv.org/abs/1807.04798>.
- [13] Hiroshi Ohno. “Auto-encoder-based generative models for data augmentation on regression problems”. In: *Soft Computing* 24.11 (June 2020), pp. 7999–8009. ISSN: 14337479. DOI: 10.1007/S00500-019-04094-0/TABLES/13. URL: <https://link.springer.com/article/10.1007/s00500-019-04094-0>.
- [14] Sumeyra Demir et al. “Data augmentation for time series regression: Applying transformations, autoencoders and adversarial networks to electricity price forecasting”. In: *Applied Energy* 304 (2021), p. 117695. ISSN: 0306-2619. DOI: <https://doi.org/10.1016/j.apenergy.2021.117695>. URL: <https://www.sciencedirect.com/science/article/pii/S0306261921010527>.
- [15] Rafael Anicet Zanini and Esther Luna Colombini. “Parkinson’s disease EMG data augmentation and simulation with DCGANs and style transfer”. In: *Sensors (Switzerland)* 20.9 (May 2020). ISSN: 14248220. DOI: 10.3390/S20092605.
- [16] Hyun K. Kim et al. “Continuous shared control for stabilizing reaching and grasping with brain-machine interfaces”. In: *IEEE Transactions on Biomedical Engineering* 53.6 (2006), pp. 1164–1173. ISSN: 00189294. DOI: 10.1109/TBME.2006.870235.
- [17] Inaki Iturrate, Luis Montesano, and Javier Minguez. “Shared-control brain-computer interface for a two dimensional reaching task using EEG error-related potentials”. In: *Proceedings of the Annual International Conference of the IEEE Engineering in Medicine and Biology Society, EMBS* (2013), pp. 5258–5262. ISSN: 1557170X. DOI: 10.1109/EMBC.2013.6610735.
- [18] Xi Chen et al. *A shared control policy for center-out movement decoding in motor brain-machine interface*. Vol. 3. PART 1. IFAC, 2013, pp. 345–348. ISBN: 9783902823458. DOI: 10.3182/20130902-3-CN-3020.00132.
- [19] Roni O. Maimon-Mor and Tamar R. Makin. “Is an artificial limb embodied as a hand? Brain decoding in prosthetic limb users”. In: *PLOS Biology* 18.6 (June 2020), e3000729. ISSN: 1545-7885. DOI: 10.1371/JOURNAL.PBIO.3000729. URL: <https://journals.plos.org/plosbiology/article?id=10.1371/journal.pbio.3000729>.

- [20] M. Laffranchi et al. "The Hannes hand prosthesis replicates the key biological properties of the human hand". In: *Science Robotics* 5.46 (2020), eabb0467. DOI: 10.1126/scirobotics.abb0467. eprint: <https://www.science.org/doi/pdf/10.1126/scirobotics.abb0467>. URL: <https://www.science.org/doi/abs/10.1126/scirobotics.abb0467>.
- [21] Giacomo Valle et al. "Hand Control With Invasive Feedback Is Not Impaired by Increased Cognitive Load". In: *Frontiers in Bioengineering and Biotechnology* 8 (2020). ISSN: 2296-4185. DOI: 10.3389/fbioe.2020.00287. URL: <https://www.frontiersin.org/articles/10.3389/fbioe.2020.00287>.

VINCENT MENDEZ

PhD Student

@ vincent.mendez@epfl.ch

+336.15.74.40.30

Campus Biotech B3, Ch. des Mines 9

1202 Geneva, Switzerland

EXPERIENCE

PhD Student

Translational Neural Engineering Lab, Prof. Micera, EPFL

December 2018 – Ongoing

Geneva, Switzerland

- Single finger proportional EMG decoding for prosthetic use
- Deep learning with medium density EMG combined with robotic automation and sensory feedback

Intern

Translational Neural Engineering Lab, Prof. Micera, EPFL

September 2018 – December 2018

Geneva, Switzerland

- Learning state-of-the-art of Neuroprosthetics
- Decoding grasping type and muscle synergies based on EEG
- Explain past work to broad audience in context of open days of EPFL

Master Thesis

Translational Neural Engineering Lab, Prof. Micera, EPFL

February 2018 – July 2018

Geneva, Switzerland

- Design of a deep learning platform with graphic user interface to facilitate mobility intention decoding
- Real time decoding and feedback to subject

Semester Project

Translational Neural Engineering Lab, Prof. Micera, EPFL

September 2017 – January 2018

Geneva, Switzerland

- Computational time comparison between Matlab and TensorFlow to train Neural Networks to decode gait cycles based on intracranial stereo-EEG data

Summer Internship

Ri.MED Foundation

June 2017 – September 2017

Palermo, Italy

- 3D reconstruction of ascending aorta of patients suffering from ascending aortic aneurysm
- Study of patient specific aneurysmal wall elasticity to determine parameters of clinical importance to quantify surgery complication risks
- Motion of the aorta was simulated with FEA and CFD and compared to 2-way FSI

Bachelor Project

Laboratory of Cognitive Neuroscience, Prof. Blanke

February 2016 – July 2016

Geneva, Switzerland

- Experiment design to alter self-consciousness and create feeling of a presence to subjects
- Processing of data and result extraction using Matlab

EDUCATION

Ph.D. in Electrical Engineering

Swiss Institute of Technology (EPFL)

Dec 2018 – Ongoing

Thesis title: Decoding hand and finger movements from muscular activities: towards a more natural hand prosthesis control

M.Sc. in Bioengineering

Swiss Institute of Technology (EPFL)

Sept 2016 – July 2018

B.Sc. in Life Sciences and Technologies

Swiss Institute of Technology (EPFL)

Sept 2013 – July 2016

RELEVANT SKILLS

- Signal Processing and Machine Learning (Neural Networks, Deep Learning)
- Real Time processing of multi-modal bio-signals (EMG, EEG, kinematics,...)
- Fast rate online decoding of finger movement

PROGRAMMING

Python

Matlab

C++

PostgreSQL & Timescale

Relevant python libraries:

TensorFlow

Keras

LSL

Dash

LANGUAGES

French

Mother Tongue

●●●●●

English

Level B2-C1

●●●●●

Spanish

Level A2

●●●●●

Italian

Level A1

●●●●●

PUBLICATIONS

- Chappuis, Christel, Eliot Walt, **Vincent Mendez**, Sylvain Lobry, Bertrand Le Saux, and Devis Tuia (2023). "The curse of language biases in remote sensing VQA: the role of Transformers, fine-tuning and the need for more diverse language". In: *Press*.
- **Mendez, Vincent**, Fiorenzo Artoni, and Silvestro Micera (2023). "A novel medium-density EMG system and model optimization pipeline for the control of prosthetic hands". In: *Preparation*.
- Chappuis, Christel, **Vincent Mendez**, Eliot Walt, Sylvain Lobry, Bertrand Le Saux, and Devis Tuia (2022). "Language Transformers for Remote Sensing Visual Question Answering". In: *International Geoscience and Remote Sensing Symposium (IGARSS) 2022-July*, pp. 4855–4858.
- Khadivar, Farshad, **Vincent Mendez**, Carolina Correia, Iason Batzianoulis, Aude Billard, and Silvestro Micera (2022). "EMG-driven shared human-robot compliant control for in-hand object manipulation in hand prostheses". In: *Journal of Neural Engineering* 19.6, p. 066024.
- **Mendez, Vincent**, Clément Lhoste, and Silvestro Micera (2022). "EMG Data Augmentation for Grasp Classification Using Generative Adversarial Networks". In: *Proceedings of the Annual International Conference of the IEEE Engineering in Medicine and Biology Society, EMBS 2022-July*, pp. 3619–3622.
- Iberite, Francesco, **Vincent Mendez**, Alberto Mazzoni, Solaiman Shokur, and Silvestro Micera (2021). "Biomimetic bidirectional hand neuroprostheses for restoring somatosensory and motor functions". In: *Somatosensory Feedback for Neuroprosthetics*, pp. 321–345.
- **Mendez, Vincent**, Francesco Iberite, Solaiman Shokur, and Silvestro Micera (2021). "Current Solutions and Future Trends for Robotic Prosthetic Hands". In: *Annual Review of Control, Robotics, and Autonomous Systems* 4.1, pp. 595–627.
- **Mendez, Vincent**, Leonardo Pollina, Fiorenzo Artoni, and Silvestro Micera (2021). "Deep learning with convolutional neural network for proportional control of finger movements from surface EMG recordings". In: *International IEEE/EMBS Conference on Neural Engineering, NER 2021-May*, pp. 1074–1078.
- Zhuang, Katie Z., Nicolas Sommer, **Vincent Mendez**, Saurav Aryan, Emanuele Formento, Edoardo D'Anna, Fiorenzo Artoni, Francesco Petrini, Giuseppe Granata, Giovanni Cannaviello, Wassim Raffoul, Aude Billard, and Silvestro Micera (2019). "Shared human-robot proportional control of a dexterous myoelectric prosthesis". In: *Nature Machine Intelligence* 1.9, pp. 400–411.
- **Mendez, Vincent**, Marzio Di Giuseppe, and Salvatore Pasta (2018). "Comparison of hemodynamic and structural indices of ascending thoracic aortic aneurysm as predicted by 2-way FSI, CFD rigid wall simulation and patient-specific displacement-based FEA". in: *Computers in Biology and Medicine* 100.

SOCIAL INITIATIVE

Participation to HackaHealth. It is a community where designers and engineers help people with disabilities in designing artefacts that can solve their specific—often neglected—daily challenges

ABSTRACTS

- **Vincent Mendez**, Xiangyu Xu, Silvestro Micera (2022). A Framework for Markerless Wrist and Finger Angle extraction from a single webcam for EMG-based Proportional Control of robotic prosthetic hands. In the Society for Neuroscience Meeting, San Diego, CA

PATENTS

- **Vincent Mendez**, Fiorenzo Artoni, Silvestro Micera. In preparation. Wearable electromyographic device and system and methods for motion decoding of body parts

PERSONAL INTERESTS

- Backpack Travelling around the world
- Sports: Table Tennis, Badminton. In winter: skiing
- Music: In a band for 5 years as a drummer
- Cooking and more particularly, making pastries. Level to re-create recipes of world class chefs.
- Fun fact: I have been contacted by the TV program "Le meilleur Pâtissier" which is a contest between amateurs who compete at making pastries and are judged by a jury of professionals.

REFeree

Prof. Silvestro Micera

@ Swiss Institute of Technology (EPFL),
Scuola Superiore Sant'Anna

✉ silvestro.micera@epfl.ch
silvestro.micera@santannapisa.it

Campus Biotech - Ch. des Mines 9 CH-1202
Genève - Switzerland
P.za Martiri della Libertà, 33 - 56127 Pisa -
Italy,